Bending of a Circular Beam Resting on an Elastic Foundation

By ENRICO VOLTERRA,[1] CHICAGO, ILL.

Saint Venant's equations (1)[2] for a circular beam, bent out of its plane of initial curvature, are applied to the study of the deflections of beams resting on elastic foundations and loaded by concentrated symmetric forces. The solution of the problem is given in explicit form, and tables for the deflections, angles of twist, bending and twisting moments are presented.

Nomenclature

The following nomenclature is used in the paper:

- M_x = bending moment
- M_z = twisting moment
- v = displacement of axis of beam in direction perpendicular to plane of beam
- β = angle of twist
- $1/R$ = initial curvature of center line of beam
- I_x = moment of inertia of cross section of beam with respect to x-axis
- C = torsional rigidity of beam
- E = Young's modulus of beam
- $y = v/R$
- $\mu = C/(EI_x)$
- $\alpha = EI_x/R^3$
- P = concentrated force
- K = elastic constant of the foundation
- 2γ = angular distance between points of application of external forces
- $\lambda = (KR^4)/(EI_x)$
- $p = (R^2P/EI_x)$

Introduction

The object of the paper is to analyze the deflections of circular beams resting on elastic foundations and loaded by symmetric concentrated forces acting in a plane perpendicular to the plane of the original curvature of the beam and at an angular distance 2γ (see Figs. 1 and 2).

The foundation is supposed to react following the classical Winkler and Zimmerman hypothesis, i.e., the reaction forces due to the foundation are proportional at every point to the deflection of the beam at that point (2, 3, 4).

The author is unaware that this problem has been so far dealt with in previous technical papers, although it occurs very often in

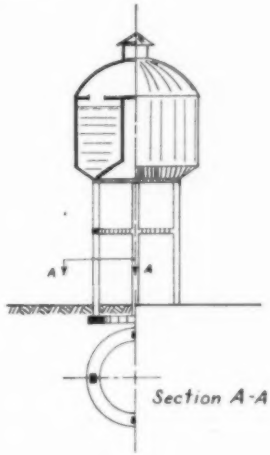

Fig. 1

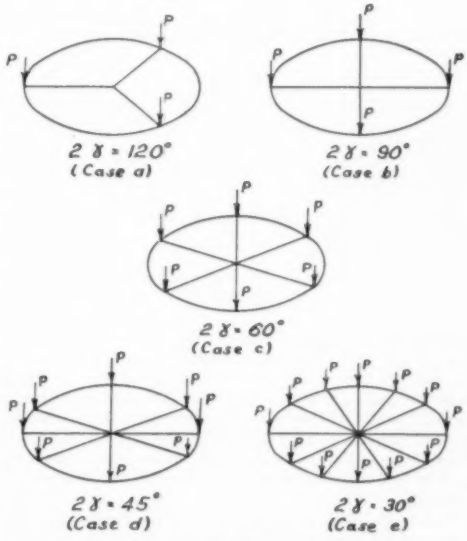

Fig. 2

[1] Associate Professor, Illinois Institute of Technology. Mem. ASME.

[2] Numbers in parentheses refer to the Bibliography at the end of the paper.

Contributed by the Applied Mechanics Division and presented at the Annual Meeting, Atlantic City, N. J., November 25–30, 1951, of The American Society of Mechanical Engineers.

Discussion of this paper should be addressed to the Secretary, ASME, 29 West 39th Street, New York, N. Y., and will be accepted until April 10, 1952, for publication at a later date. Discussion received after the closing date will be returned.

Note: Statements and opinions advanced in papers are to be understood as individual expressions of their authors and not those of the Society. Manuscript received by ASME Applied Mechanics Division, April 27, 1951. Paper No. 51—A-18.

practice, its most common application being the case of circular beams used as foundations of reinforced-concrete water tanks, Fig. 1. The present paper was originated by the study of a practical problem of this type.

The following assumptions will be made:

The beam has constant inertia characteristics EI_z and its axis is a circle of radius R. At equidistant points equal concentrated forces P are applied, the angular distance between the forces being indicated by 2γ, Fig. 2. By using Saint Venant's equations for a curved beam bent out of its plane of initial curvature (1, 5, 6, 7), it is possible to solve the problem in explicit form, i.e., to express the deflections, angles of twist, bending and twisting moments of the beam at each point as functions of the external applied forces P, of the inertia characteristics EI_z of the beam, of the elastic constant K of the foundation, and of the angle 2γ. The solution in explicit form is worked out in the Appendix of the paper. For particular values of the angles 2γ, namely, $2\gamma = 120°, 90°, 60°, 45°, 30°$, tables giving the values of the deflections, angles of twist, bending and twisting moments are presented.

Bending of a Curved Beam Out of Its Plane of Initial Curvature

Let us consider a curved beam, built in at one end, having constant inertia characteristics, Fig. 3. The beam will be referred to

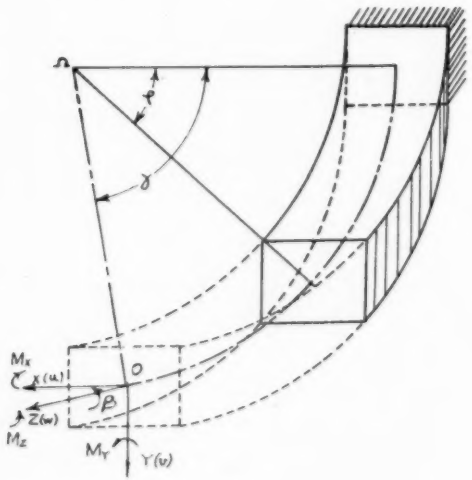

Fig. 3

a system of rectangular co-ordinates $OXYZ$ with the origin O at the centroid of the cross section, the axes X and Y coinciding with the principal axes of inertia of the cross section, and the axis Z with the tangent to the center line at O. The plane XZ coincides with the horizontal plane of the initial curvature of the beam, the positive direction of X being toward the center of curvature, Y is directed positive downward, Z is taken positive away from the built-in end, and the arc s of the center line is measured from the built-in end.

The displacement of the centroid O during bending is resolved into three components, u, v, w in the directions of the X, Y, and Z-axes, respectively. The angle of twist β of the cross section about the Z-axis is taken positive when the rotation is counterclockwise with respect to the Z-axis. The deformation of an element of the curved bar cut out by two adjacent cross sections consists of two bendings in the principal planes XZ and YZ, and of a twist about the Z-axis. If M_x, M_y, M_z are the moments on the cross section at O about the X, Y, Z-axes, respectively (their positive directions are shown in Fig. 3), EI_x, EI_y the two principal flexural rigidities, C the torsional rigidity, $1/R$ the initial curvature of the center line of the bar, the equations for calculating the changes in curvature $(1/R_1;\ 1/R_2)$ and the twist θ are (7)

$$\left.\begin{aligned} \frac{EI_x}{R_1} &= M_x \\ EI_y\left(\frac{1}{R_2} - \frac{1}{R}\right) &= M_y \\ C\theta &= M_z \end{aligned}\right\} \quad \ldots\ldots\ldots\ldots [1]$$

The expressions for the curvatures and twist as functions of u, v, w, and β are (7)

$$\left.\begin{aligned} \frac{1}{R_1} &= \frac{\beta}{R} - \frac{d^2v}{ds^2} \\ \frac{1}{R_2} &= \frac{1}{R} - \frac{u}{R^2} + \frac{d^2u}{ds^2} \\ \theta &= \frac{d\beta}{ds} + \frac{1}{R}\frac{dv}{ds} \end{aligned}\right\} \quad \ldots\ldots\ldots\ldots [2]$$

The condition that during bending and twist the length of the axis of the bar remains unchanged is expressed by (7)

$$\frac{dw}{ds} - \frac{u}{R} = 0 \quad \ldots\ldots\ldots\ldots [3]$$

By the use of Equations [1], [2], and [3] the displacements u, v, w, and the angle β can be determined in the case of small deflections of curved beams.

Circular Beam Resting on an Elastic Foundation

In the case of a circular beam resting on an elastic foundation, the displacements u and w can be neglected and Equations [1] and [2] reduce to the two equations

$$\left.\begin{aligned} EI_x\left(\frac{\beta}{R} - \frac{d^2v}{ds^2}\right) &= M_x \\ C\theta = C\left(\frac{d\beta}{ds} + \frac{1}{R}\frac{dv}{ds}\right) &= M_z \end{aligned}\right\} \quad \ldots\ldots\ldots [4]$$

If K is the elastic constant of the foundation, P, the external concentrated force, 2γ, the angular distance between the points of application of the external forces (see Figs. 2 and 4)

$$y = \frac{v}{R},\ \alpha = \frac{EI_x}{R},\ \mu = \frac{C}{EI_x},\ \nu = \frac{PR^3}{EI_x},\ \lambda = \frac{KR^4}{EI_x}$$

Equations [4] become

$$\left.\begin{aligned} \alpha\left(\beta - \frac{d^2y}{d\varphi^2}\right) &= M_x \\ \mu\alpha\left(\frac{d\beta}{d\varphi} + \frac{dy}{d\varphi}\right) &= M_z \end{aligned}\right\} \quad \ldots\ldots\ldots [5]$$

while for equilibrium, the following equations must be verified

$$\left.\begin{aligned} &\frac{dM_z}{d\varphi} - M_x = 0 \\ &\frac{d^2M_x}{d\varphi^2} + \frac{dM_z}{d\varphi} - a\lambda y = 0 \end{aligned}\right\} \quad \ldots\ldots\ldots\ldots [6]$$

with the boundary conditions

$$\left.\begin{aligned} &\beta(\gamma) = \beta(-\gamma);\ y(\gamma) = y(-\gamma);\ \frac{d^2y(\gamma)}{d\varphi^2} = \frac{d^2y(-\gamma)}{d\varphi^2} \\ &\frac{d\beta(\gamma)}{d\varphi} = \frac{d\beta(-\gamma)}{d\varphi};\ \frac{dy(\gamma)}{d\varphi} = \frac{dy(-\gamma)}{d\varphi}; \\ &\frac{dM_z(\gamma)}{d\varphi} - \frac{dM_z(-\gamma)}{d\varphi} = a\nu \end{aligned}\right\} \quad \ldots [7]$$

The angle φ is measured from the center between the points where the external forces are applied, Fig. 4.

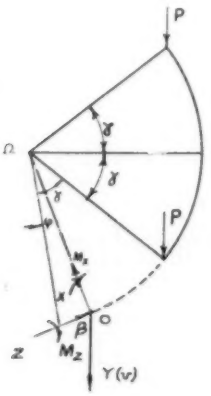

FIG. 4

The values of the functions β, v, M_z, and M_x, are given in Tables 1, 2, 3, 4, and 5 for the following values of the parameters $\lambda = 60$; $\mu = 0.7$; $\lambda = 100$; $\mu = 1$.

NUMERICAL EXAMPLE

Suppose a circular beam of radius $R = 25$ ft, in reinforced concrete [$E = 3(10^6)$ psi] of square cross section (depth 30 in., width 30 in.) with eight concentrated loads $P = 75$ tons each ($2\gamma = 45°$). The constant of the foundation is supposed to be $K = 1500$ lb per in. per in.

TABLE 1 $2\gamma = 120°$ (Case a)

	λ=60			μ=0.7	λ=100			μ=1
φ	$\frac{\beta}{\gamma}$	$\frac{\gamma}{\gamma}$	$\frac{M_x}{Q\gamma}$	$\frac{M_z}{Q\gamma}$	$\frac{\beta}{\gamma}$	$\frac{\gamma}{\gamma}$	$\frac{M_x}{Q\gamma}$	$\frac{M_z}{Q\gamma}$
0°	.001584	.00°326	-.003856	0	.00°969	-.00°660	-.002610	0
10°	.001417	.00°115	-.003794	-.00°674	.00°875	-.00°116	-.002657	-.00°459
20°	.00°929	.00°355	-.003343	-.001305	.00°593	.00°150	-.002631	-.00°924
30°	.00°171	.00°723	-.002123	-.001797	.00°136	.00°408	-.002045	-.001345
40°	-.00074	.001156	.00°489	-.001965	-.00°443	.00°728	-.00°143	-.001361
50°	-.001581	.001547	.005188	-.001505	-.001006	.001034	.005973	-.001266
60°	-.001974	.001726	.012517	0	-.001282	.001181	.011070	0

TABLE 2 $2\gamma = 90°$ (Case b)

	λ=60			μ=0.7	λ=100			μ=1
φ	$\frac{\beta}{\gamma}$	$\frac{\gamma}{\gamma}$	$\frac{M_x}{Q\gamma}$	$\frac{M_z}{Q\gamma}$	$\frac{\beta}{\gamma}$	$\frac{\gamma}{\gamma}$	$\frac{M_x}{Q\gamma}$	$\frac{M_z}{Q\gamma}$
0°	.001000	.00°611	-.005167	0	.00°776	.00°255	-.004373	0
10°	.00°798	.00°703	-.004571	-.00°864	.00°574	.00°331	-.003890	-.00°736
20°	.00°247	.00°952	-.002425	-.001493	.00°184	.00°540	-.002267	-.001294
30°	-.00°479	.001277	.001488	-.001605	-.00°340	.00°818	.001093	-.001427
40°	-.001066	.001537	.007676	-.000841	-.00°776	.001047	.006896	-.00°770
45°	-.001166	.001381	.011717	0	-.00°851	.001087	.010883	0

TABLE 3 $2\gamma = 60°$ (Case c)

	λ=60			μ=0.7	λ=100			μ=1
φ	$\frac{\beta}{\gamma}$	$\frac{\gamma}{\gamma}$	$\frac{M_x}{Q\gamma}$	$\frac{M_z}{Q\gamma}$	$\frac{\beta}{\gamma}$	$\frac{\gamma}{\gamma}$	$\frac{M_x}{Q\gamma}$	$\frac{M_z}{Q\gamma}$
0°	.00°341	.001445	-.004246	0	.00°272	.00°815	-.004091	0
5°	.00°301	.001463	.003899	-.00°360	.00°240	.00°831	-.003764	-.00°347
10°	.00°188	.001511	.002854	-.00°660	.00°150	.00°878	-.002774	-.00°638
15°	.00°214	.001583	.001096	-.00°836	.00°176	.00°946	-.001093	-.00°812
20°	.00°164	.001662	.001394	-.00°830	.00°131	.001022	.001316	-.00°807
25°	-.00°322	.001729	.004631	-.00°575	-.00°257	.001087	.004493	-.00°559
30°	-.00°390	.001758	.008622	0	-.00°312	.001115	.008461	0

TABLE 4 $2\gamma = 45°$ (Case d)

	λ=60			μ=0.7	λ=100			μ=1
φ	$\frac{\beta}{\gamma}$	$\frac{\gamma}{\gamma}$	$\frac{M_x}{Q\gamma}$	$\frac{M_z}{Q\gamma}$	$\frac{\beta}{\gamma}$	$\frac{\gamma}{\gamma}$	$\frac{M_x}{Q\gamma}$	$\frac{M_z}{Q\gamma}$
0°	.00°145	.002061	.003272	0	.00°118	.001213	.003233	0
5°	.00°115	.002073	.002788	.00°271	.00°940	.001225	.002758	.00°268
10°	.00°344	.002108	.001336	.00°458	.00°281	.001259	.001329	.00°454
15°	.00°700	.002152	.001089	-.00°476	.00°571	.001302	.001070	-.00°472
20°	.00°152	.002186	.004489	.00°240	.00°124	.001316	.004451	-.00°238
22°30′	-.00°166	.002192	.006551	0	-.00°135	.001342	.006511	0

TABLE 5 $2\gamma = 30°$ (Case e)

	λ=60			μ=0.7	λ=100			μ=1
φ	$\frac{\beta}{\gamma}$	$\frac{\gamma}{\gamma}$	$\frac{M_x}{Q\gamma}$	$\frac{M_z}{Q\gamma}$	$\frac{\beta}{\gamma}$	$\frac{\gamma}{\gamma}$	$\frac{M_x}{Q\gamma}$	$\frac{M_z}{Q\gamma}$
0°	.00°429	.003165	-.002191	0	.00°352	.001892	-.002186	0
5°	.00°236	.003173	-.001460	-.00°170	.00°194	.001900	-.001457	-.00°170
10°	-.00°206	.003192	.00°732	-.00°212	-.00°170	.001918	.00°729	-.00°212
15°	-.00°489	.003203	.004375	0	-.00°402	.001930	.004370	0

It follows:

$I_x = 6.75(10^4)$ in.^{4}, $\lambda = 60$, $\mu = 0.7$, $\nu = 0.0666$, $a = 28{,}125$ ft-tons, $a\nu = 1873.12$ ft-tons.

In Table 6 the results obtained for this particular case from Table 4 are given

TABLE 6 RESULTS OF NUMERICAL EXAMPLE

φ (deg-min)	β (radians)	v (inches)	M_x (ft-tons)	M_z (ft-tons)
0	0.0°0	0.4122	−61.288	0
5	0.0°766	0.4146	−52.222	−5.076
10	0.0°229	0.4216	−25.025	−8.579
15	−0.0°466	0.4304	20.398	−8.916
20	−0.0°1033	0.4372	84.084	−4.495
22-30	−0.0°1106	0.4384	122.708	0

BIBLIOGRAPHY

1 "Mémoire sur le calcul de la resistance et de la flexion des pièces solides à simple ou à double courbure, en prenant simultanément en considération les divers efforts auxquels elles peuvent être soumises dans tous les sens," by Barré de Saint Venant, Comptes Rendus de l'Académie des Sciences de Paris, France, vol. 17, 1843, pp. 942 and 1020–1031.

2 "Die Lehre von der Elastizität und Festigkeit," by E. Winkler, Prague, Czechoslovakia, 1867, p. 182.

3 "Die Berechnung des Eisenbahnoberbaues," by H. Zimmermann, second edition, Berlin, Germany, 1888, 1930.

4 "Beams on Elastic Foundation—Ann Arbor," by M. Hetényi, The University of Michigan Press, Ann Arbor, Mich., 1946.

5 "De la déformation qu' éprouve une pièce à simple ou à double courbure sous l'action de forces qui lui font subir en même temps une flexion et une torsion," by H. Resal, *Journal de Mathématiques Pures et Appliquées Tome Troisième*, 1877, pp. 307–322.

6 "The Mathematical Theory of Elasticity," by A. E. H. Love, fourth edition, Dover Publications, New York, N. Y., October, 1944.

7 "Strength of Materials—Part II. Advanced Theory and Problems," by S. Timoshenko, The Macmillan Company, New York, N. Y., 1936, pp. 467–473.

Appendix

The solution of Equations [5] and [6] with the boundary conditions expressed by Equations [7] gives the following expressions for the functions y, β, M_x and M_z

$$y = A\cosh(m\varphi) + B_1\cosh(r\varphi)\cos(s\varphi) + B_2\sinh(r\varphi)\sin(s\varphi) \quad \ldots\ldots [8]$$

$$\beta = C\cosh(m\varphi) + D_1\cosh(r\varphi)\cos(s\varphi) + D_2\sinh(r\varphi)\sin(s\varphi) \quad \ldots\ldots [9]$$

$$M_x = aE\cosh(m\varphi) + aF_1\cosh(r\varphi)\cos(s\varphi) + aF_2\sinh(r\varphi)\sin(s\varphi) \quad \ldots\ldots [10]$$

$$M_z = aG\sinh(m\varphi) + aH_1\sinh(r\varphi)\cos(s\varphi) + aH_2\cosh(r\varphi)\sin(s\varphi) \quad \ldots\ldots [11]$$

where m, r, s are determined from the formulas

$$m = \sqrt{-\frac{2}{3} + \frac{1}{3}(u - v)}$$

$$r = \frac{1}{2}\sqrt{\frac{2}{m}\sqrt{\frac{\lambda}{\mu}} - m^2 - 2}$$

$$s = \frac{1}{2}\sqrt{\frac{2}{m}\sqrt{\frac{\lambda}{\mu}} + m^2 + 2}$$

with

$$u^3 = 9\lambda + 1 + \frac{27}{2}\frac{\lambda}{\mu} + \sqrt{27\lambda\left[(\lambda+1)^2 + \frac{9\lambda+1}{\mu} + \frac{27}{4}\frac{\lambda}{\mu^2}\right]}$$

$$v^3 = -9\lambda - 1 - \frac{27}{2}\frac{\lambda}{\mu} + \sqrt{27\lambda\left[(\lambda+1)^2 + \frac{9\lambda+1}{\mu} + \frac{27}{4}\frac{\lambda}{\mu^2}\right]}$$

The constants $A \ldots\ldots H$ are calculated from the following formulas

$$A = \frac{\nu}{2mT\sinh(m\gamma)}\left(-m^2 + \frac{1}{\mu}\right)$$

$$B_1 = \nu\left\{\left[m^2(m^2+2) + \frac{2}{m^2}\frac{\lambda}{\mu} + \frac{1}{\mu}(3m^2+2)\right]R + \left(-m^2 + \frac{1}{\mu}\right)4rsS\right\}$$

$$B_2 = \nu\left\{\left[m^2(m^2+2) + \frac{2}{m^2}\frac{\lambda}{\mu} + \frac{1}{\mu}(3m^2+2)\right]S + \left(m^2 - \frac{1}{\mu}\right)4rsR\right\}$$

$$C = \frac{A}{\mu+1}\left(m^2 + \frac{\lambda}{\mu^2} - \mu\right)$$

$$D_1 = -\frac{\mu}{\mu+1}\left\{\left[\frac{1}{2}\left(m^2 + \frac{1}{\mu}\right)(m^2+2) + 1\right]B_1 + \left(m^2 - \frac{1}{\mu}\right)2rsB_2\right\}$$

$$D_2 = \frac{\mu}{\mu+1}\left\{-\left[\frac{1}{2}\left(m^2 + \frac{1}{\mu}\right)(m^2+2) + 1\right]B_2 + \left(m^2 - \frac{1}{\mu}\right)2rsB_1\right\}$$

$$E = \frac{A\mu}{\mu+1}\left(\frac{\lambda}{\mu m^2} - m^2 - 1\right)$$

$$F_1 = -\frac{\mu}{2(\mu+1)}(m^2+1)(m^2B_1 + 4rsB_2)$$

$$F_2 = \frac{\mu}{2(\mu+1)}(m^2+1)(-m^2B_2 + 4rsB_1)$$

$$G = \frac{E}{m}$$

$$H_1 = m\sqrt{\frac{\mu}{\lambda}}(rF_1 - sF_2) \qquad H_2 = m\sqrt{\frac{\mu}{\lambda}}(rF_2 + sF_1)$$

with

$$T = 3m^4 + 4m^2 + 1 + \lambda$$

$$R = \frac{m}{4rsT}\sqrt{\frac{\mu}{\lambda}}\frac{s\sinh(r\gamma)\cos(s\gamma) + r\cosh(r\gamma)\sin(s\gamma)}{\cosh(2r\gamma) - \cos(2s\gamma)}$$

$$S = \frac{m}{4rsT}\sqrt{\frac{\mu}{\lambda}}\frac{s\cosh(r\gamma)\sin(s\gamma) - r\sinh(r\gamma)\cos(s\gamma)}{\cosh(2r\gamma) - \cos(2s\gamma)}$$

Acknowledgment

The author wishes to express his appreciation and thanks to the "Istituto per le Applicazioni del Calcolo" of the Italian "Consiglio Nazionale delle Ricerche" in Rome, Italy, and particularly to its Director, Professor Mauro Picone, for having checked the formulas and the numerical tables in the paper.

The Bending of Uniformly Loaded Sectorial Plates With Clamped Edges

By H. D. CONWAY[1] and M. K. HUANG,[2] ITHACA, N. Y.

This paper analyzes the bending of a sectorial plate, clamped on all edges and subjected to uniformly distributed load, by using two different methods of superposition on the elementary solution for a uniformly loaded circular plate with a clamped edge.

Nomenclature

The following nomenclature is used in the paper:

a = radius of plate
(r, θ) = polar co-ordinates of a point on plate
w = deflection
E = Young's modulus
h = thickness of plate
ν = Poisson's ratio
D = flexural rigidity of plate = $\dfrac{Eh^3}{12(1-\nu^2)}$

Introduction

Two methods of superposition on the elementary solution for a uniformly loaded circular plate with a clamped edge have been investigated. In the first method, a line distribution of loading in the form of a cosine series is applied normally to a diameter of the plate. By superimposing this solution on that for a uniformly loaded plate, the unknown coefficients of the series are determined such that the resultant deflections of several points along the diameter under the line loading are made equal to zero. The maximum deflection and bending moment in a semicircular plate are thus found.

In the second method, a number of concentrated loads are applied normally to a diameter of the plate, the magnitudes of the loads being adjusted so that the resultant deflections at their points of application are zero. The resultant surface is then approximately the same as that for two semicircular plates having clamped edges and placed with their straight sides in contact. The method of superposition is then used to calculate the maximum deflection. The effect on the maximum deflection of varying the location of the concentrated loads is studied, and it is found that, within certain limits, this is quite small. The method, which may be used to analyze any sectorial plate, is then applied to the case of a quadrant of a circle, and the maximum deflection is again obtained.

Previous Investigations

The problem of analyzing the deflections in a uniformly loaded and clamped sectorial plate resolves itself into finding a solution of the Lagrange differential equation $\nabla^4 w = q/D$, subject to the conditions of zero slope and deflection on the boundary. This problem has been the subject of a few investigations.

The first investigation appears to be that of R. Kuno (1)[3] who treated the case of the semicircular plate. Taking the co-ordinate origin at the center of the straight edge of the plate and measuring the angle θ from a line bisecting the plate, Kuno observed that the equation

$$w = \frac{qa^4}{64D}\left(\frac{r^4}{a^4} - 2\,\frac{r^2}{a^2}\right)(1 + \cos 2\theta) \qquad [1]$$

satisfies the differential equation, together with the conditions of zero slope and deflection on the straight edge and zero slope on the curved edge. The condition of zero deflection on the the curved edge is satisfied by superimposing a solution of the equation $\nabla^4 w = 0$ to eliminate the deflection left by Equation [1] without violating the other boundary conditions. It is observed that the maximum deflection of $0.002016\ qa^4/D$ occurs on a line bisecting the plate and at a radius of $0.485a$. The maximum bending moment of $0.0734\ qa^2$ is radial and occurs at the center of the straight edge.

The more general problem of the uniformly loaded and clamped plate bounded by two radii and two circular arcs has been discussed by Carrier (2). Carrier solves the problem by superimposing two solutions of the differential equation $\nabla^4 w = 0$ on the solution for the simply supported plate. Plots of the bending moment along the circular and straight edges are given for three cases, in each of which the angle of the sector is 60 deg. The solution is very tedious to obtain by this method.

In a recent paper, Hassé (3) has discussed the problem of the uniformly loaded and clamped semicircular plate using a method proposed by Weinstein (4) and later applied to the bending of a square plate by Weinstein and Rock (5). By taking six terms of the series involved in the calculations, the maximum deflection is found to be $0.002022\ qa^4/D$ on a line bisecting the plate and at a radius of $0.48594a$ while, for seven terms, the maximum deflection is $0.002023\ qa^4/D$ at a radius of $0.48587a$. It may be mentioned that Weinstein's method has been used by Stiles (6) in his analysis of clamped rectangular plates.

In a recent paper, Carrier and Shaw (7) have shown how the use of eigenfunctions can facilitate the analysis of clamped-plate problems. They consider the case of a uniformly loaded sectorial plate in which the angle between the radii is 60 deg.

The First Method

Analysis. Consider the case of a clamped circular plate along a diameter of which a line distribution of loading in the form

$$E_i \cos\frac{i\pi r}{2a} \qquad i = 1, 3, 5 \ldots$$

is applied, Fig. 1. The intensity of the load q in the Lagrange differential equation may be represented by the series

---

[1] Professor of Mechanics, Cornell University Jun. ASME.

[2] Instructor in Mechanics, Cornell University.

Contributed by the Applied Mechanics Division and presented at the Annual Meeting, Atlantic City, N. J., November 25–30, 1951, of The American Society of Mechanical Engineers.

Discussion of this paper should be addressed to the Secretary, ASME, 29 West 39th Street, New York, N. Y., and will be accepted until April 10, 1952, for publication at a later date. Discussion received after the closing date will be returned.

Note: Statements and opinions advanced in papers are to be understood as individual expressions of their authors, and not those of the Society. Manuscript received by ASME Applied Mechanics Division, June 4, 1951. Paper No. 51—A-24.

[3] Numbers in parentheses refer to the Bibliography at the end of the paper.

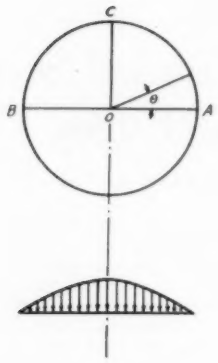

FIG. 1

$$q = \frac{2}{\pi}\frac{E_i}{r}\cos\frac{i\pi r}{2a}\left(\frac{1}{2} + \sum_{m=2,4,6\ldots}^{\infty}\cos m\theta\right) \quad \ldots\ldots [2]$$

and the differential equation is

$$\nabla^4 w = \frac{2}{\pi D}\frac{E_i}{r}\cos\frac{i\pi r}{2a}\left(\frac{1}{2} + \sum_{m=2,4,6\ldots}^{\infty}\cos m\theta\right) \quad \ldots [3]$$

For the first term on the right side of Equation [3] the deflection w_0 may be found by direct integration, and the constants of integration can be determined from the boundary conditions at the clamped edge and from the condition that the deflection, the slope, and the bending moment must be finite at the center of the circular plate. Thus

$$w_0 = \frac{A_i a^3}{2i\pi}\left[\left(\frac{x^2}{2} - \frac{4}{i^2\pi^2}\right)Si\left(\frac{i\pi x}{2}\right) + \frac{2}{i^2\pi^2}\sin\left(\frac{i\pi x}{2}\right) + \frac{x}{i\pi}\cos\left(\frac{i\pi x}{2}\right)\right] - \frac{A_i a^3}{4i\pi}\left[Si\left(\frac{i\pi}{2}\right) - (-1)^{\frac{i-1}{2}}\frac{4}{i^2\pi^2}\right]x^2 + \frac{2A_i a^3}{i^2\pi^3}\left[S_i\left(\frac{i\pi}{2}\right) - (-1)^{\frac{i-1}{2}}\right] \quad \ldots\ldots [4]$$

where

$$x = r/a, \quad A_i = 2E_i/D\pi, \quad \text{and} \quad Si(x) = \int_0^x \frac{\sin y\, dy}{y}^*$$

For the general term on the right side of Equation [3] the solution w_m is obtained by the method of variation of parameters. The constants of integration are also determined from the conditions at the boundary and at the center of the plate. It follows that

$$w_m = \frac{A_i a^3}{8}\left[\frac{1}{m(m-1)}x^{-m+2}\int_0^x y^m\cos\frac{i\pi y}{2}\,dy - \frac{1}{m(m+1)}x^{-m}\int_0^x y^{m+2}\cos\frac{i\pi y}{2}\,dy + \frac{1}{m(m+1)}x^{m+2}\int_1^x \frac{\cos\frac{i\pi y}{2}}{y^m}\,dy - \frac{1}{m(m-1)}x^m\int_1^x \frac{\cos\frac{i\pi y}{2}}{y^{m-2}}\,dy + C_m x^m + D_m x^{m+2}\right]\cos m\theta \quad \ldots\ldots [5]$$

* The integral $Si(x)$ is the so-called sine integral and is a tabulated function; see, for instance, "Tables of Sine, Cosine, and Exponential Integrals," by A. N. Lowan, vols. I and II, 1940, Washington, D. C.

where

$$C_m = -\frac{1}{m-1}\int_0^1 y^m\cos\frac{i\pi y}{2}\,dy + \frac{1}{m}\int_0^1 y^{m+2}\cos\frac{i\pi y}{2}\,dy$$

$$D_m = \frac{1}{m}\int_0^1 y^m\cos\frac{i\pi y}{2}\,dy - \frac{1}{m+1}\int_0^1 y^{m+2}\cos\frac{i\pi y}{2}\,dy$$

Consequently, the complete solution of Equation [3] is

$$w = w_0 + \sum_{m=2,4,6\ldots}^{\infty} w_m \quad \ldots\ldots [6]$$

Along the radius OA (or OB), $\theta = 0$ (or $\theta = \pi$), the expression for the deflection is, after rearranging terms

$$(w)_{\theta=0,\pi} = w_0 + \frac{A_i a^3}{8}\left[\frac{1}{2}\int_0^x y^2\cos\frac{i\pi y}{2}\,dy - 2\sum_{m=2,4,6\ldots}^{\infty}\frac{x^{-m}}{m(m+1)(m+2)}\int_0^x y^{m+2}\cos\frac{i\pi y}{2}\,dy - \frac{x^2}{2}\int_1^x \cos\frac{i\pi y}{2}\,dy + 2\sum_{m=2,4,6\ldots}^{\infty}\frac{x^{m+2}}{m(m+1)(m+2)}\int_1^x y^{-m}\cos\frac{i\pi y}{2}\,dy - x^2\left(\int_0^1 y^2\cos\frac{i\pi y}{2}\,dy - \frac{1}{2}\int_0^1 y^4\cos\frac{i\pi y}{2}\,dy\right) + \sum_{m=2,4,6\ldots}^{\infty}x^{m+2}\left(\frac{1}{m}\int_0^1 y^m\cos\frac{i\pi y}{2}\,dy - \frac{2}{m+1}\int_0^1 y^{m+2}\cos\frac{i\pi y}{2}\,dy + \frac{1}{m+2}\int_0^1 y^{m+4}\cos\frac{i\pi y}{2}\,dy\right)\right] \quad \ldots\ldots [7]$$

Along the radius OC, $\theta = \pi/2$ and

$$(w)_{\theta=\frac{\pi}{2}} = w_0 + \frac{A_i a^3}{8}\left[-\frac{1}{2}\int_0^x y^2\cos\frac{i\pi y}{2}\,dy + 2\sum_{m=2,4,6\ldots}^{\infty}(-1)^{\frac{m}{2}-1}\frac{x^{-m}}{m(m+2)}\int_0^x y^{m+2}\cos\frac{i\pi y}{2}\,dy + \frac{x^2}{2}\int_1^x \cos\frac{i\pi y}{2}\,dy - 2\sum_{m=2,4,6\ldots}^{\infty}(-1)^{\frac{m}{2}-1}\frac{x^{m+2}}{m(m+2)}\int_1^x y^{-m}\cos\frac{i\pi y}{2}\,dy + x^2\left(\int_0^1 y^2\cos\frac{i\pi y}{2}\,dy - \frac{1}{2}\int_0^1 y^4\cos\frac{i\pi y}{2}\,dy\right) + \sum_{m=2,4,6\ldots}^{\infty}(-1)^{\frac{m}{2}}x^{m+2}\left(\frac{1}{m}\int_0^1 y^m\cos\frac{i\pi y}{2}\,dy - \frac{1}{m+2}\int_0^1 y^{m+4}\cos\frac{i\pi y}{2}\,dy\right)\right] \quad \ldots\ldots [8]$$

At the center of the plate, $w = w_0$.

If the line distribution of loading is represented by a cosine series

$$\sum_{i=1,3,5\ldots}^{\infty} E_i\cos\frac{i\pi r}{2a} \quad \ldots\ldots [9]$$

the expression for the deflection is simply, from Equations [4], [5], and [6]

$$w = \sum_{i=1,3,5\ldots}^{\infty} \left(w_{ia} + \sum_{m=2,4,6\ldots}^{\infty} w_{im} \right) \ldots\ldots [10]$$

The solution of a clamped semicircular plate can then be obtained by superimposing Equation [10] on the elementary solution for a uniformly loaded, clamped circular plate in such a way that the resultant deflections along the radius OA (and OB) are zero. Although it would be possible to expand Equation [7] into a Fourier cosine series and then obtain an infinite number of equations containing infinite number of unknowns A_i, the procedure to get the Fourier coefficients would be long and tedious. A simpler procedure is to determine a certain number of unknowns from the condition that the resultant deflections are zero at an equal number of points of equal distance apart along the radius OA (or OB). By taking three terms in Equation [9], the values of A_i necessary to produce zero deflections at $x = 0$, $x = 1/3$, and $x = 2/3$ are

$$A_1 = 0.67528\ qa/D,\ A_3 = -0.08701\ qa/D,\ A_5 = 0.06140\ qa/D.$$

Substituting these values in Equations [8] and [10] and using the deflection equation for a uniformly loaded clamped circular plate

$$w = \frac{q}{64D}(a^2 - r^2)^2 \ldots\ldots [11]$$

the resultant deflection for the semicircular plate is found by superposition. At the point $x = 0.485$ on the bisector of the plate, the deflection is $0.0020202\ qa^4/D$ which agrees very closely with the previous results.

Along the straight edge, where $\theta = 0$ (or $\theta = \pi$), the bending moment in the tangential direction is

$$(M_t)_{\theta=0} = -D\left(\frac{1}{r}\frac{\partial w}{\partial r} + \frac{1}{r^2}\frac{\partial^2 w}{\partial \theta^2} + \nu\frac{\partial^2 w}{\partial r^2}\right)_{\theta=0}$$

Assuming that the resultant deflections along the straight edge of the semicircular plate are made exactly zero by the superposition, the bending moment $(M_t)_{\theta=0}$ at the middle of the edge is

$$(M_t)_{\substack{\theta=0\\ x=0}} = \frac{qa^2}{16} - \sum_{i=1,3,5\ldots}^{\infty} \left\{ \frac{A_i aD}{2i\pi}\left[Si\left(\frac{i\pi}{2}\right) - (-1)^{\frac{i-1}{2}}\frac{4}{i^2\pi^2}\right] + \frac{A_i aD}{8}\left[\int_0^1 \cos\frac{i\pi y}{2}\,dy - 2\int_0^1 y^2\cos\frac{i\pi y}{2}\,dy + \int_0^1 y^4\cos\frac{i\pi y}{2}\,dy\right]\right\} \ldots\ldots [12]$$

By using three terms, this value is found to be $-0.07341\ qa^2$ which is in very good agreement with Kuno's result.

The Second Method

Analysis. The second method proposed here begins with the elementary solution to the uniformly loaded and clamped circular plate. By superimposing a line distribution of loading normal to a diameter of the plate, the deflection at every point on the diameter could be made zero and the resulting case of the clamped semicircular plate could be analyzed. For computing the deflections produced by the line distribution of loading, use could be made of the Michell (8) solution for the clamped circular plate carrying a concentrated load.

However, since the approximate location of the maximum deflection in a clamped semicircular plate may be found by inspection, the foregoing procedure can be simplified greatly. Instead of applying a line distribution of loading, several concentrated loads may be applied to a diameter of the circular plate and the magnitudes of these loads adjusted so that the resultant deflections under their points of application are zero. Since it is apparent that the maximum deflection occurs on a line bisecting the semicircular plate and at a radius of about $r = a/2$, the concentrated loads should be located fairly near the center of the circular plate to obtain the most accurate results.

The deflection at a radius r on a uniformly loaded and clamped circular plate of radius a is

$$w = \frac{q}{64D}(a^2 - r^2)^2 \ldots\ldots [11]$$

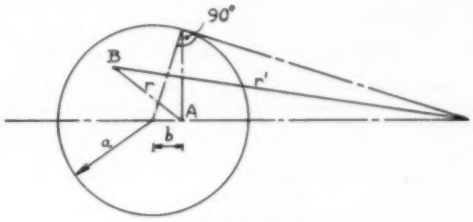

Fig. 2

Referring to Fig. 2, the deflection at point B due to a concentrated load W at A is, according to Michell

$$w = \frac{Wr^2}{8\pi D}\left[\frac{1}{2}\left(\frac{b^2r'^2}{a^2r^2} - 1\right) - \log_e\frac{br'}{ar}\right] \ldots\ldots [13]$$

These are the only basic formulas required in the discussion.

Five concentrated loads were applied to a diameter of the circular plate, one being located at the center, and two on each side of the center at radii of $a/6$ and $a/3$, respectively. The load at the center is denoted P and those at radii $a/6$ and $a/3$ are denoted Q and R, respectively. By the use of Equations [11] and [13], the values of the concentrated loads necessary to produce zero resultant deflections at their points of application are

$$P = 0.175330\ qa^2;\quad Q = 0.095087\ qa^2;\quad R = 0.344401\ qa^2$$

The resultant deflection at a point on the bisector of the semicircle and at radius r is then

$$w = \frac{q}{64D}(a^2 - r^2)^2 - \frac{P}{16\pi D}\left[(a^2 - r^2) - r^2\log\frac{a^2}{r^2}\right] - \frac{Q}{288\pi D}\left[35(a^2 - r^2) - (a^2 + 36r^2)\log\frac{36a^2 + r^2}{a^2 + 36r^2}\right] - \frac{R}{72\pi D}\left[8(a^2 - r^2) - (a^2 + 9r^2)\log\frac{9a^2 + r^2}{a^2 + 9r^2}\right] \ldots [14]$$

From Equation [14], and using interpolation methods, the maximum deflection was found to be $0.0020203\ qa^4/D$ at a radius $r = 0.486a$. This is in exceptionally good agreement with the results of Kuno and Hassé which have already been quoted.

In order to observe the effect of using a smaller number of concentrated loads at increased radii, it was decided to apply three loads, P at the center and Q at radii $a/2$ on each side of the center. It is obvious that such a procedure will produce less accurate results than the previous five loads.

The loads necessary to produce zero deflections at their points of application are, in this case,

$$P = 0.499997\ qa^2; \quad Q = 0.353723\ qa^2$$

The deflection at a radius $r = 0.486a$ for this case was found to be $0.0021732\ qa^4/D$ or about 7 per cent too large. It is therefore apparent that if the number and position of the concentrated loads are carefully chosen, very accurate results will be obtained.

The present method was next applied to the solution of a clamped plate in the form of a quadrant of a circle. In this case, nine concentrated loads were applied to two diameters, at right angles, of the uniformly loaded and clamped plate, one load being at the center, four at radii $a/4$ and four at radii $a/2$. Denoting the load at the center by P, the loads at radii $a/4$ by Q and those at radii $a/2$ by R, the values of the loads necessary to produce zero resultant deflections at their points of application are, from Equations [11] and [13]

$$P = 0.022450\ qa^2; \quad Q = 0.121098\ qa^2; \quad R = 0.243396\ qa^2$$

The maximum deflection occurs on a line bisecting the quadrant, and from Equations [11] and [13] the deflection at a point on this bisector and at radius r is

$$w = \frac{q}{64D}(a^2 - r^2)^2 - \frac{P}{16\pi D}\left[(a^2 - r^2) - r^2 \log \frac{a^2}{r^2}\right]$$

$$- \frac{Q}{128\pi D}\left[30(a^2 - r^2) - (a^2 + 16r^2 - 4\sqrt{2}\,ar) \log \frac{16a^2 + r^2 - 4\sqrt{2}\,ar}{a^2 + 16r^2 - 4\sqrt{2}\,ar}\right.$$

$$\left. - (a^2 + 16r^2 + 4\sqrt{2}\,ar) \log \frac{16a^2 + r^2 + 4\sqrt{2}\,ar}{a^2 + 16r^2 + 4\sqrt{2}\,ar}\right]$$

$$- \frac{R}{32\pi D}\left[6(a^2 - r^2)\right.$$

$$- (a^2 + 4r^2 - 2\sqrt{2}\,ar) \log \frac{4a^2 + r^2 - 2\sqrt{2}\,ar}{a^2 + 4r^2 - 2\sqrt{2}\,ar}$$

$$\left. - (a^2 + 4r^2 + 2\sqrt{2}\,ar) \log \frac{4a^2 + r^2 + 2\sqrt{2}\,ar}{a^2 + 4r^2 + 2\sqrt{2}\,ar}\right] \quad \ldots [15]$$

From Equation [15] and by interpolation, the maximum deflection was found to be $0.00071655\ qa^4/D$ at a radius $r = 0.594a$.

BIBLIOGRAPHY

1 "Strength of a Semicircular Plate," by R. Kuno, *Journal of the Society of Mechanical Engineers of Japan*, vol. 37, 1934, p. 101.

2 "The Bending of the Clamped Sectorial Plate," by G. F. Carrier, JOURNAL OF APPLIED MECHANICS, Trans. ASME, vol. 66, 1944, p. A-134.

3 "The Bending of a Uniformly Loaded Clamped Plate in the Form of a Circular Sector," by H. R. Hassé, *Quarterly Journal of Mechanics and Applied Mathematics*, vol. 3, 1950, p. 271.

4 "Étude des spectres des équations aux dérivées partielles de la théorie des plaques élastiques," by A. Weinstein, *Memorial des Science Mathematique*, vol. 88, 1937, p. 1.

5 "On the Bending of a Clamped Plate," by A. Weinstein and D. H. Rock, *Quarterly of Applied Mathematics*, vol. 2, 1944, p. 262.

6 "Bending of the Clamped Plates," by W. B. Stiles, JOURNAL OF APPLIED MECHANICS, Trans. ASME, vol. 69, 1947, p. A-55.

7 "Some Problems in the Bending of Thin Plates," by G. F. Carrier and F. S. Shaw, Proceedings, Symposium on Applied Mathematics, vol. 3, 1950, p. 125.

8 "The Flexure of Circular Plates," by J. H. Michell, Proceedings of the London Mathematical Society, vol. 34, 1902, p. 223.

Bending of a Cylindrically Aeolotropic Circular Plate With Eccentric Load

By A. M. SEN GUPTA,[1] SIBPUR, HOWRAH, WEST BENGAL, INDIA

The problem of small-deflection theory applicable to plates of cylindrically aeolotropic material has been developed, and expressions for moments and deflections produced have been found by Carrier[2] in some symmetrical cases under uniform lateral loadings and with different boundary conditions. The author has also found the moments and deflection in the case of an unsymmetrical bending of a plate loaded by a distribution of pressure of the form $p = p_0 r \cos\theta$, with clamped edge. The object of the present paper is to investigate the problem of the bending of a cylindrically aeolotropic circular plate of uniform thickness under a concentrated load P applied at a point A at a distance b from the center, the edge being clamped.

Nomenclature

The following nomenclature is used in the paper:

r, θ, z = cylindrical co-ordinates
e_r, e_θ, $\nu_{r\theta}$ = radial, tangential, and shear strains
σ_r, σ_θ, $\tau_{r\theta}$ = radial, tangential, and shear stresses
a_{ij} $(i, j = 1, 2, \ldots 6)$ = elastic constants
u, v, w = radial, tangential, and longitudinal displacements
M_r, M_θ, $M_{r\theta}$, $M_{\theta r}$ = bending and twisting moments acting on per unit length of element dr, $rd\theta$
Q_r, Q_θ = shear forces per unit length of element
$k = a_{11}/(a_{11}a_{22} - a_{12}^2)$
$\beta = a_{12}/a_{11}$
$\alpha = a_{22}/a_{11}$
h = thickness of plate
p = applied lateral load per unit area of element
$D' = h^3k/12$, $\sigma' = \dfrac{2}{ka_{66}} - \beta$
$c = 1/\alpha$, $\sigma = \sigma'/\alpha$
ν = Poisson's ratio
E = Young's modulus of elasticity
$D = h^3E/12(1 - \nu^2)$
$G = E/2(1 + \nu)$
ω, ω_1 = deflection of outer and inner portion of plate
$\delta = \sqrt{\alpha}$
$\pm(p_m + q_m)$, $\pm(p_m - q_m)$ = roots of equation[3]

$$c\lambda^4 - (c + 1 + 2\sigma m^2)\lambda^2 + (m^2 - 1)^2 = 0$$

$\pm k_1$ = roots of foregoing equation when $m = 1$

Mathematical Treatment

Let the origin of co-ordinates be at the center of the middle plane which coincides with the $r\theta$-plane and the axis of Z normal to this plane considered positive downward. We assume, as in the case of isotropy, that linear elements perpendicular to the middle plane of the plate before bending remain straight and normal to the deflection surface of the plate after bending. Further, it is assumed that the thickness of the plate is constant and small in comparison with the radius of the plate, so that the effects of the normal and shearing forces σ_z, τ_{rz}, $\tau_{\theta z}$ on the deflection are negligible.

Under these assumptions we have for a case of plane stress in the $r\theta$-plane

$$\left.\begin{aligned} e_r &= a_{12}\sigma_\theta + a_{22}\sigma_r \\ e_\theta &= a_{11}\sigma_\theta + a_{12}\sigma_r \\ \nu_{r\theta} &= a_{66}\tau_{r\theta} \end{aligned}\right\} \quad \ldots\ldots\ldots\ldots [1]$$

The relations between strain and displacements are

$$\left.\begin{aligned} e_r &= \partial u/\partial r \\ e_\theta &= u/r + (1/r)(\partial v/\partial\theta) \\ \nu_{r\theta} &= \partial v/\partial r - v/r + 1/r(\partial u/\partial\theta) \end{aligned}\right\} \quad \ldots\ldots\ldots [2]$$

Assuming that the neutral surface $(z = 0)$ remains undisplaced horizontally, we can take the values of u and v at any point z as given by

$$\left.\begin{aligned} u &= -z(\partial\omega/\partial r) \\ v &= -z/r(\partial\omega/\partial\theta) \end{aligned}\right\} \quad \ldots\ldots\ldots\ldots [3]$$

The equations of equilibrium of the element $dr\ rd\theta$ are

$$\left.\begin{aligned} &\frac{d}{dr}M_r - \frac{1}{r}\frac{d}{d\theta}M_{r\theta} + \frac{1}{r}(M_r - M_\theta) - Q_r = 0 \\ &\frac{1}{r}\frac{d}{d\theta}M_\theta - \frac{d}{dr}M_{r\theta} - \frac{2}{r}M_{r\theta} - Q_\theta = 0 \\ &\frac{d}{dr}(rQ_r) + \frac{d}{d\theta}Q_\theta + rp = 0 \end{aligned}\right\} \quad \ldots [4]$$

where

$$\left.\begin{aligned} M_r &= -D'\left[\frac{d^2\omega}{dr^2} - \beta\left(\frac{1}{r}\frac{d\omega}{dr} + \frac{1}{r^2}\frac{d^2\omega}{d\theta^2}\right)\right] \\ M_\theta &= -D'\left[\alpha\left(\frac{1}{r}\frac{d\omega}{dr} + \frac{1}{r^2}\frac{d^2\omega}{d\theta^2}\right) - \beta\frac{d^2\omega}{dr^2}\right] \\ M_{r\theta} &= -M_{\theta r} = D'(\sigma' + \beta)\frac{d}{dr}\left(\frac{1}{r}\frac{d\omega}{d\theta}\right) \end{aligned}\right\} \quad \ldots [5]$$

From Equations [4] and [5] we obtain the following differential equation

---

[1] Department of Mathematics, Bengal Engineering College.

[2] "The Bending of the Cylindrically Aeolotropic Plate," by G. F. Carrier, Trans. ASME, vol. 66, 1944, p. 129.

[3] For $\sigma \geq \sqrt{c}$ both the values of λ^2 are real and positive for all values of m.

Contributed by the Applied Mechanics Division and presented at the Annual Meeting, Atlantic City, N. J., November 25–30, 1951, of The American Society of Mechanical Engineers.

Discussion of this paper should be addressed to the Secretary, ASME, 29 West 39th Street, New York, N. Y., and will be accepted until April 10, 1952, for publication at a later date. Discussion received after the closing date will be returned.

Note: Statements and opinions advanced in papers are to be understood as individual expressions of their authors and not those of the Society. Manuscript received by ASME Applied Mechanics Division, August 18, 1950. Paper No. 51—A-17.

$$\left[\frac{1}{r^4}\frac{d}{d\theta^4}+\frac{2\sigma}{r^2}\frac{d^4}{dr^2d\theta^2}-\frac{2\sigma}{r^3}\frac{d^2}{drd\theta^2}+\frac{2(1+\sigma)}{r^4}\frac{d^2}{d\theta^2}+c\frac{d^4}{dr^4}+\frac{2c}{r}\frac{d^3}{d}-\frac{d^2}{r^2\,dr^2}+\frac{1}{r^3}\frac{d}{dr}\right]\omega=\frac{pc}{D'}\quad\ldots[6]$$

Equation [6] is the same as equation 7 of Carrier.[2]

Using Equations [5] we obtain from the first two Equations of [4]

$$\left.\begin{aligned}Q_r &= -D'\left[\frac{d^3}{dr^3}+\frac{1}{r}\frac{d^2}{dr^2}-\frac{\alpha}{r^2}\frac{d}{dr}+\frac{\sigma'}{r^2}\frac{d^3}{drd\theta^2}-\frac{\alpha+\sigma'}{r^3}\frac{d^2}{d\theta^2}\right]\omega\\ &= -D'x(\omega)\ \text{(say)}\end{aligned}\right\}\quad\ldots[7]$$

and

$$Q_\theta=-D'\frac{1}{r}\frac{d}{d\theta}\left[\sigma'\frac{d^2}{dr^2}+\frac{\alpha}{r}\frac{d}{dr}+\frac{\alpha}{r^2}\frac{d^2}{d\theta^2}\right]\omega$$

In the particular case of isotropy, we have

$$\alpha=1,\qquad \beta=-\nu$$

$$k=\frac{E}{1-\nu^2},\qquad \sigma=\sigma'=c=1$$

$$\frac{1}{a_{66}}=G,\quad\text{and}\quad D'=D$$

On substitution of these values, Equations [5], [6], and [7] reduce, respectively, to equations 160, 162, and 161 of Timoshenko.[4]

Limitations of the Theory

As regards the limitations in the values of the elastic constants under which this theory is applicable to cylindrically aeolotropic plates, Carrier[2] observes that we must restrict the values of both $-a_{12}/a_{22}$ and $-a_{12}/a_{11}$ between 0 and 1, i.e., to say

$$\left.\begin{aligned}-\beta&=-\frac{a_{12}}{a_{11}}<1\\ -\frac{\beta}{\alpha}&=-\frac{a_{12}}{a_{22}}<1\end{aligned}\right\}\quad\ldots[8]$$

The arguments put forward to arrive at the restrictions regarding the values of $-a_{12}/a_{11}$ and $-a_{12}/a_{22}$ are based upon the probability that certain properties observed in isotropic materials will be retained by the aeolotropic material, and hence those arguments are hypothetical in nature.

Now, consistent with the assumptions made regarding their values in previous papers,[5,6] it is found that the Conditions [8] are fulfilled if we assume $\alpha=4$ and $\beta=-1/2$.

On the strength of this hypothesis, the following values have been used in this problem

$$\beta=-\frac{1}{2},\quad\alpha=4,\quad\sigma=\frac{3}{4}\quad\text{or}\quad\frac{a_{66}}{a_{11}}=3\quad\ldots[9]$$

It is to be noted here that for a particular case of isotropy taking $\nu=1/3$, the value of a_{66}/a_{11} is $8/3$.

Bending of a Cylindrically Aeolotropic Circular Plate Under a Concentrated Load P

We assume that the load P is applied at a point A at a distance b from the center 0 of the plate. Now, considering the plate as divided into two parts by the cylindrical section of radius b, we can find the deflection for each of these portions of the plate from the solution of the equation

$$\left[\frac{1}{r^4}\frac{d}{d\theta^4}+\frac{2\sigma}{r^2}\frac{d^4}{dr^2d\theta^2}-\frac{2\sigma}{r^3}\frac{d^3}{drd\theta^2}+\frac{2(\sigma+1)}{r^4}\frac{d^2}{d\theta^2}+c\frac{d^4}{dr^4}+\frac{2c}{r}\frac{d^3}{dr^3}-\frac{1}{r^2}\frac{d^2}{dr^2}+\frac{1}{r^3}\frac{d}{dr}\right]\omega=0\quad\ldots[10]$$

For the solution of this equation[5] we assume

$$\omega=R_0+\sum_{m=1}^{\alpha}R_m\cos m\theta+\sum_{m=1}^{\alpha}X_m\sin m\theta\quad\ldots[11]$$

where $R_0, R_1, R_2 \ldots x_1, x_2 \ldots$ are functions of the radial distance r only. Now, if the angle θ is measured from the radius OA, we should retain only terms containing $\cos m\theta$ of the Solution [11].

Hence, for the outer portion of the plate we get

$$\omega=R_0+\sum_{m=1}^{\alpha}R_m\cos m\theta\quad\ldots[12]$$

where

$$R_0=A_0r^{1+\delta}+B_0+C_0r^2+D_0r^{1-\delta}$$

$$R_1=A_1r^{1+k_1}+B_1r+C_1r^{1-k_1}+D_1r\log_e r\quad\ldots[13]$$

and for $m\geq 2$

$$R_m=A_mr^{1+p_m+q_m}+B_mr^{1+p_m-q_m}+C_mr^{1-p_m+k_m}+D_mr^{1-p_m-q_m}$$

We also get similar expressions for the functions $R_0', R_1', \ldots, R_m'$, corresponding to the inner portion of the plate. Using for the inner portion of the plate the constants A_m', B_m', C_m', D_m' instead of the constants A_m, B_m, C_m, D_m, and noting that from the conditions that moments, deflection, and shear forces must be finite at the center of the plate, we have

$$C_0'=D_0'=0$$
$$C_1'=D_1'=0$$
$$\ldots\ldots\ldots$$
$$\ldots\ldots\ldots$$
$$C_m'=D_m'=0$$

Hence we obtain

$$\left.\begin{aligned}R_0'&=A_0'r^{1+\delta}+B_0'\\ R_1'&=A_1'r^{1+k_1}+B_1'r\end{aligned}\right\}\quad\ldots[14]$$

for $m\geq 2$

$$R_m'=A_m'r^{1+p_m+q_m}+B_m'r^{1+p_m-q_m}$$

Thus, for each term of the Series [12], we have to determine six constants, namely, four for the outer portion of the plate and two for the inner portion.

The six equations necessary for the determination of these six constants may be obtained from the boundary conditions and the conditions of continuity along the circle of radius b.

Thus, since the outer edge of the plate is clamped, we have the boundary conditions

[4] "Theory of Plates and Shells," by S. Timoshenko, McGraw-Hill Book Company, Inc., New York, N. Y., and London, England, 1940.

[5] "Stress Distribution in Cylindrically Aeolotropic Plates," by G. F. Carrier, Trans. ASME, vol. 65, 1943, p. 117.

[6] "Stresses in Some Aeolotropic and Isotropic Circular Disks of Varying Thickness Rotating About the Central Axis," by A. M. Sen Gupta, Bulletin of the Calcutta Mathematical Society, vol. 41, September, 1949.

$$\left.\begin{aligned}(\omega)_{r=a} &= 0\\ \left(\frac{d\omega}{dr}\right)_{r=a} &= 0\end{aligned}\right\} \quad \ldots\ldots\ldots\ldots\ldots\ldots [15]$$

As there are no external moments applied along the circle of radius b, we obtain from the conditions of continuity along the circle

$$\omega = \omega_1, \quad \frac{d\omega}{dr} = \frac{d\omega_1}{dr}, \quad \frac{d^2\omega}{dr^2} = \frac{d^2\omega_1}{dr^2} \text{ for } r = b \quad \ldots\ldots [16]$$

Finally, since Q_r is continuous at all points of the circle $r = b$ except at the point A, where it has a discontinuity, we get the last equation necessary.

Thus representing the load P in a series of the form

$$\frac{P}{\pi b}\left\{\frac{1}{2} + \sum_{m=1}^{\alpha} \cos m\theta\right\}$$

and using for Q_r the symbolical expression in Equations [7], we get

$$D'[X(\omega)]_{r=b} - D'[X(\omega_1)]_{r=b} = \frac{P}{\pi b}\left(\frac{1}{2} + \sum_{m=1}^{\alpha} \cos m\theta\right) \quad [17]$$

From the six equations obtained from Equations [15], [16], and [17] the six constants are calculated and functions R_m, R_m' are found to be as follows

$$R_0 = \frac{Pa^2}{4\pi(\alpha-1)D'}\left\{\frac{1}{1+\delta}\left[2 - \frac{\delta-1}{\delta}\left(\frac{b}{a}\right)^{1+\delta}\right]\left(\frac{r}{a}\right)^{1+\delta} + \frac{\delta-1}{\delta+1} + \frac{2}{\delta+1}\left(\frac{b}{a}\right)^{1+\delta} - \left(\frac{r}{a}\right)^2 - \frac{1}{\delta}\left(\frac{b}{a}\right)^2\left(\frac{b}{r}\right)^{\delta-1}\right\}$$

$$R_0' = \frac{Pa^2}{4\pi(\alpha-1)D'}\left\{\frac{1}{1+\delta}\left[2 - \frac{\delta-1}{\delta}\left(\frac{b}{a}\right)^{1+\delta}\right]\left(\frac{r}{a}\right)^{1+\delta} + \frac{\delta-1}{\delta+1} + \frac{2}{\delta+1}\left(\frac{b}{a}\right)^{1+\delta} - \left(\frac{r}{a}\right)^2 - \frac{1}{\delta}\left(\frac{b}{a}\right)^2\left(\frac{r}{b}\right)^{1+\delta}\right\}$$

$$R_1 = -\frac{Pb^{k_1+1}}{2\pi k_1^2 D'}\left[\frac{1}{r^{k_1}-1} - \frac{2a^{k_1}-b^{k_1}}{a^{2k_1}b^{k_1}}r^{1+k_1} + \frac{2(a^{k_1}-b^{k_1})}{a^{k_1}b^{k_1}}r - \frac{2k_1 r}{b^{k_1}}\log_e a/r\right]$$

$$R_1' = -\frac{Pb^{k_1+1}}{2\pi k_1^2 D'}\left[\frac{(a^{k_1}-b^{k_1})^2}{a^{2k_1}b^{2k_1}}r^{1+k_1} + \frac{2(a^{k_1}-b^{k_1})}{a^{k_1}b^{k_1}}r - \frac{2k_1 r}{b^{k_1}}\log_e a/b\right]$$

$$R_m = \frac{Pb^2}{8\pi p_m q_m(p_m-q_m)D'}\left\{\frac{p_m-q_m}{q_m}\left(\frac{r}{a}\right)^{p_m+q_m+1}\left[\left(\frac{b}{a}\right)^{p_m-q_m-1} - \frac{p_m}{p_m+q_m}\left(\frac{b}{a}\right)^{p_m+q_m-1}\right] + \left(\frac{r}{a}\right)^{p_m-q_m+1}\left[\frac{p_m-q_m}{q_m}\left(\frac{b}{a}\right)^{p_m+q_m-1} - \frac{p_m}{q_m}\left(\frac{b}{a}\right)^{p_m-q_m-1}\right] - \frac{p_m-q_m}{p_m+q_m}\left(\frac{b}{r}\right)^{p_m+q_m-1} + \left(\frac{b}{r}\right)^{p_m-q_m-1}\right\}$$

$$R_m' = \frac{Pb^2}{8\pi p_m q_m(p_m-q_m)D'}\left\{\frac{p_m-q_m}{q_m}\left(\frac{r}{a}\right)^{p_m+q_m+1}\left[\left(\frac{b}{a}\right)^{p_m-q_m-1} - \frac{p_m}{p_m+q_m}\left(\frac{b}{a}\right)^{p_m+q_m-1}\right] + \left(\frac{r}{a}\right)^{p_m-q_m+1}\left[\frac{p_m-q_m}{q_m}\left(\frac{b}{a}\right)^{p_m+q_m-1} - \frac{p_m}{q_m}\left(\frac{b}{a}\right)^{p_m-q_m-1}\right] - \frac{p_m-q_m}{p_m+q_m}\left(\frac{b}{r}\right)^{p_m+q_m-1} + \left(\frac{b}{r}\right)^{p_m-q_m-1}\right\} \quad \ldots [18]$$

Since R_m diminishes rapidly as m increases, only a few terms of the Series [12] need be calculated to obtain the deflection at any point with sufficient accuracy.

The solution R_0 which is independent of the angle θ, represents symmetrical bending of circular plates. Putting $b = 0$ in the series for R_0, we obtain the deflection for a circular plate under central concentrated load with clamped edge as

$$\omega = -\frac{Pa^2}{4\pi(\delta^2-1)D'}\left[\left(\frac{r}{a}\right)^2 - \frac{2}{1+\delta}\left(\frac{r}{a}\right)^{1+\delta} - \frac{\delta-1}{\delta+1}\right] \quad \ldots\ldots [19]$$

which is the same as the result given by Carrier[7] (Case 2). It is to be noted that δ in this paper is the same as α in Carrier's paper.

Again, for the particular case of isotropy $\alpha = \delta = 1$, $k_1 = 2$, $p_m = m$, $q_m = 1$, $D' = D$.

Putting these values in the Relations [18], except in those of R_0 and R_0', for in the case of isotropy the corresponding characteristic equation has two double roots and R_0 is a function of the form $A_0 + B_0r^2 + C_0\log_e r + D_0r^2\log_e r$, we obtain

$$R_1 = -\frac{Pb^2}{16\pi D}\left[\frac{1}{r} - \frac{2a^2-b^2}{a^4b^2}r^3 + \frac{2(a^2-b^2)}{a^2b^2}r - \frac{4r}{b^2}\log_e(a/r)\right]$$

$$R_1' = -\frac{Pb^2}{16\pi D}\left[\frac{(a^2-b^2)^2}{a^4b^4}r^3 + \frac{2(a^2-b^2)}{a^2b^2}r - \frac{4r}{b^2}\log_e(a/b)\right]$$

$$R_m = \frac{Pb^m}{8\pi m(m-1)D}\left\{\frac{r^m}{a^{2m}}\left[(m-1)r^2 - \frac{m(m-1)}{m+1}\frac{b^2r^2}{a^2} + (m-1)b^2 - ma^2\right] + \frac{1}{r^m}\left(r^2 - \frac{m-1}{m+1}b^2\right)\right\} \quad \ldots [20]$$

$$R_m' = \frac{Pb^m}{8\pi m(m-1)D}\left\{\frac{r^m}{a^{2m}}\left[(m-1)b^2 - ma^2 + \frac{a^{2m}}{b^{2m-2}}\right] + (m-1)\frac{r^{m+2}}{a^{2m}}\left[1 - \frac{m}{m+1}\frac{b^2}{a^2} - \frac{1}{m+1}\left(\frac{a}{b}\right)^{2m}\right]\right\}$$

These values of R_1, R_1', R_m, R_m' are the same as that given by Timoshenko.[7]

Using the functions in Equations [18] we obtain from Equation [12] the deflection under the load as

[7] Reference 4, p. 268: Timoshenko gives in the series for R_1 $(4r/b^2)\log_e(a/r)$, instead of $(4r/b^2)\log_e(a/b)$. This is evidently a typographical error, as otherwise, moments and shear forces will be infinite at the center of the plate.

$$(\omega)_{r=b,\theta=0} = \left[R_0 + \sum_{m=1}^{\infty} R_m\right]_{r=b} \quad \ldots\ldots\ldots [21]$$

For a particular case taking $\beta = -1/2$, $\alpha = 4$, $\sigma = 3/4$, and $b/a = 1/2$, we get the deflection under the load

$$(\omega)_{r=b,\theta=0} = \frac{Pa^2}{16\pi D'} (0.2044) \text{ approx.} \quad \ldots\ldots [22]$$

ACKNOWLEDGMENT

The author thanks Dr. B. Sen for his kind help in the preparation of this paper.

Linear Bending Theory of Isotropic Sandwich Plates by an Order-of-Magnitude Analysis

By GEORGE GERARD,[1] NEW YORK, N. Y.

By use of an order-of-magnitude analysis, the equilibrium and stress-strain relations for the faces and core of a sandwich plate are examined in terms of the thickness of the plate. The analysis results in a set of simplified stress-strain relations for the sandwich plate, in addition to which the basic assumptions of previous sandwich-plate bending theories are obtained as the end result.

Nomenclature

The following nomenclature is used in the paper:

E = modulus of elasticity
G = shear modulus, $G = E/2(1 + \nu)$
h = core thickness
$\bar{h}$ = centroidal distance between faces, $\bar{h} = h + t$
L = length
u, v, w = displacements
x, y, z = co-ordinate axes
$\alpha = \bar{E}/E$
σ = normal stress
τ = shear stress
ν = Poisson's ratio
ϵ = thickness parameter defined by Equation [5]

Note: Barred symbols are used to denote core parameters.

Introduction

The development of a linear bending theory for sandwich plates which has been given by various investigators[2,3,4] is based upon several fundamental assumptions concerning the behavior of the faces and the core. These assumptions are as follows:

(*a*) Although the normal to the middle surface of the plate does not remain normal after bending, plane sections do remain plane.

(*b*) The deformability of the core to transverse loads is negligible.

(*c*) The face-parallel stresses in the core are negligible.

With these assumptions a system of equations has been derived to describe the behavior of the sandwich plate under bending loads.

In this paper the complete equilibrium and stress-strain relations for the faces and the core of an isotropic sandwich plate are considered by examining the orders of magnitude of the stresses and displacements in terms of the thickness of the sandwich. This procedure is similar to that used by Goodier[5] in the development of homogeneous thin-plate theory. By use of this approach, the three assumptions which form the basis of previous sandwich-plate theories are obtained as the results of the order-of-magnitude analysis. In addition, a set of simplified stress-strain relations is obtained for the sandwich plate which are equivalent to results obtained previously.

Order-of-Magnitude Analysis

The distinguishing feature of a structural element which categorizes it as a plate is the fact that its thickness is small relative to the other dimensions, that is

$$\frac{h}{L_x}, \frac{h}{L_y} \ll 1 \qquad [1]$$

To exploit this fact in the order-of-magnitude analysis, the equilibrium equations are written as follows

$$\frac{\partial \sigma_x}{\partial(x/h)} + \frac{\partial \tau_{xy}}{\partial(y/h)} + \frac{\partial \tau_{xz}}{\partial(z/h)} = 0 \qquad [2]$$

$$\frac{\partial \tau_{yz}}{\partial(x/h)} + \frac{\partial \sigma_y}{\partial(y/h)} + \frac{\partial \tau_{yz}}{\partial(z/h)} = 0 \qquad [3]$$

$$\frac{\partial \tau_{zx}}{\partial(x/h)} + \frac{\partial \tau_{zy}}{\partial(y/h)} + \frac{\partial \sigma_z}{\partial(z/h)} = 0 \qquad [4]$$

The thickness parameter to be used in the order-of-magnitude analysis follows from Equation [1]

$$h/x, h/y \sim 0(\epsilon) \qquad [5]$$

where ϵ is a small number. It is also noted that

$$h/z \sim 0(1) \qquad [6]$$

As a starting point, the stress σ_z is chosen to have the value

$$\sigma_z \sim 0(\epsilon^4) \qquad [7]$$

This relationship is written for convenience and does not involve any loss of generality in what follows.

To perform the order-of-magnitude analysis, it is necessary to assume that for the faces, each term in a particular equilibrium equation is of the same order of magnitude. This assumption is based on the considerations that the order of magnitude of all the face stresses is insensitive to the orientation of the axes in the plane of the plate (x and y-axes) and that the behavior of the faces is little influenced by the presence of the core which is a weak elastic medium. From Equations [2], [3], [4], the orders of magnitude of the face stresses follow directly as given in Table 1.

---

[1] Assistant Professor of Aeronautical Engineering, College of Engineering, New York University. Jun. ASME.

[2] "On Bending of Elastic Plates," by E. Reissner, *Quarterly Applied Mathematics*, vol. 5, 1947, pp. 55–68.

[3] "A General Small-Deflection Theory for Flat Sandwich Plates," by C. Libove and S. B. Batdorf, NACA TN 1526, April, 1948.

[4] "Finite Deflections of Sandwich Plates," by E. Reissner, *Journal of the Aeronautical Sciences*, vol. 15, 1948, pp. 435–440.

Contributed by the Applied Mechanics Division and presented at the Annual Meeting, Atlantic City, N. J., November 25–30, 1951, of The American Society of Mechanical Engineers.

Discussion of this paper should be addressed to the Secretary, ASME, 29 West 39th Street, New York, N. Y., and will be accepted until April 10, 1952, for publication at a later date. Discussion received after the closing date will be returned.

Note: Statements and opinions advanced in papers are to be understood as individual expressions of their authors and not those of the Society. Manuscript received by ASME Applied Mechanics Division, April 9, 1951. Paper No. 51—A-31

[5] "On the Problems of the Beam and the Plate in the Theory of Elasticity," by J. N. Goodier, Transactions of the Royal Society of Canada, vol. 32, Section 3, 1938, pp. 65–88.

TABLE 1 ORDER OF MAGNITUDE OF FACE STRESSES

$0(\epsilon^0)$	$0(\epsilon^2)$	$0(\epsilon^2)$
σ_z (7)	τ_{xz} (4)	σ_x (2)
	τ_{yz} (4)	τ_{xy} (2,3)
		σ_y (3)

The number in parentheses indicates the equation from which the magnitude was deduced.

To determine the magnitude of the core stresses, it is necessary to observe the following continuity requirements at the interface, $z = \pm h/2$:

(*a*) Displacements u and v must be continuous.
(*b*) x and y derivatives of u and v must be continuous.
(*c*) z-direction stress components must be continuous.

Furthermore, a set of twelve stress-strain relations are necessary to describe completely the behavior of the sandwich element. The equations for face and core can be written jointly if the coefficient α is permitted to assume the following values:

(*a*) For the faces $\alpha = 1$ and $\nu_\alpha = \nu$.
(*b*) For the core which has an elastic modulus, $\bar{E}$, $\alpha = \bar{E}/E$, $\nu_\alpha = \bar{\nu}$, and barred quantities are used to denote core stresses

$$\alpha E \frac{\partial(u/h)}{\partial(x/h)} = \sigma_x - \nu_\alpha(\sigma_y + \sigma_z) \quad [8]$$

$$\alpha E \frac{\partial(v/h)}{\partial(y/h)} = \sigma_y - \nu_\alpha(\sigma_z + \sigma_x) \quad [9]$$

$$\alpha E \frac{\partial(w/h)}{\partial(z/h)} = \sigma_z - \nu_\alpha(\sigma_x + \sigma_y) \quad [10]$$

$$\frac{1}{2}\alpha E\left[\frac{\partial(u/h)}{\partial(y/h)} + \frac{\partial(v/h)}{\partial(x/h)}\right] = (1 + \nu_\alpha)\tau_{xy} \quad [11]$$

$$\frac{1}{2}\alpha E\left[\frac{\partial(u/h)}{\partial(z/h)} + \frac{\partial(w/h)}{\partial(x/h)}\right] = (1 + \nu_\alpha)\tau_{xz} \quad [12]$$

$$\frac{1}{2}\alpha E\left[\frac{\partial(v/h)}{\partial(z/h)} + \frac{\partial(w/h)}{\partial(y/h)}\right] = (1 + \nu_\alpha)\tau_{yz} \quad [13]$$

From continuity condition (*b*) and Equations [8], [9], and [11], it can be concluded that

$$\delta_z \sim 0(\alpha\,\sigma_z) \quad [14]$$

$$\delta_y \sim 0(\alpha\,\sigma_y) \quad [15]$$

$$\bar{\tau}_{xy} \sim 0(\alpha\,\tau_{xy}) \quad [16]$$

provided that the maximum values of the face-parallel core stresses do not exceed appreciably the values at the interface. Strictly, Equations [14] and [15] are valid only for $\bar{\nu} = 0$. It appears, however, that for many core materials this is a reasonable approximation.

It is necessary to assign an order of magnitude to the coefficient α to determine the core stresses. The value of α can be quite conveniently taken as $\alpha \sim 0(\epsilon^n)$. Since the value of ϵ is small but indefinite, the choice of a suitable value for the exponent n to describe a particular sandwich construction, i.e., the ratio of elastic moduli of the core and face, is not given by the preceding considerations. It was found that by letting $n = 2$, then in all cases terms such as ϵ^{n+2} appear in the analysis which are clearly negligible compared to terms of magnitude ϵ^n. If $n = 1$, then terms of only one higher order in ϵ appear and the analysis is not as direct. Consequently, the relation

$$\alpha \sim 0(\epsilon^2) \quad [17]$$

is used in the subsequent analysis.

Inserting Equation [17] and the magnitude of σ_z, σ_y and τ_{xy}, given in Table 1, into Equations [14], [15], and [16], the order of magnitude of the core stresses δ_z, δ_y and $\bar{\tau}_{xy}$ can be obtained as given in Table 2. From continuity requirement (*c*) the magnitude of the other core stresses follow directly from Equation [4].

TABLE 2 ORDER OF MAGNITUDE OF CORE STRESSES FOR $\alpha \sim 0(\epsilon^2)$

$0(\epsilon^2)$	$0(\epsilon^3)$
δ_x (14)	$\bar{\tau}_{xz}$ (4)
δ_y (15)	$\bar{\tau}_{yz}$ (4)
$\bar{\tau}_{yz}$ (16)	
δ_z (4)	

The order of magnitude of the face-parallel core stresses was determined directly from continuity considerations and not from equilibrium conditions. Consequently, if Equations [2] and [3] are used in conjunction with the orders of magnitude of the core stresses given in Table 2, and the higher-order terms in ϵ are neglected

$$\frac{\partial \bar{\tau}_{xz}}{\partial z} = 0; \quad \bar{\tau}_{xz} = \bar{\tau}_{xz}(x, y) \quad [18]$$

$$\frac{\partial \bar{\tau}_{yz}}{\partial z} = 0; \quad \bar{\tau}_{yz} = \bar{\tau}_{yz}(x, y) \quad [19]$$

The magnitude of the displacements u and v is obtained from Equations [8] and [9], or [11] using Tables 1 and 2 for the face or core stresses. In either case, it is found that

$$E\,u/h \sim 0(\epsilon) \quad [20]$$

$$E\,v/h \sim 0(\epsilon) \quad [21]$$

To evaluate the order of magnitude of the displacement w, it is necessary to proceed to Equation [12] or [13]. If the order of magnitude of w is deduced from Equation [10] instead of Equation [12] or [13], it is found that $Ew/h \sim 0(\epsilon^4)$. Therefore, from Equations [12] and [13] both u and v are not functions of z which is a contradictory result for the bending problem. This slight procedural difficulty is due to the fact that the six stress components are functions of only three displacements. From Equation [12] or [13] it is deduced that

$$E\,w/h \sim 0(1) \quad [22]$$

Results of Analysis

Equation [10], which is the only remaining relationship not used in the analysis, can be employed to deduce the character of the displacement w in the sandwich plate. If the higher-order terms in ϵ are neglected, then for the faces it is evident that

$$\left(\frac{\partial w}{\partial z}\right)_{face} = 0; \quad w = w(x, y) \quad [23]$$

In the core, if $\alpha \sim 0\,(\epsilon^2)$ then also

$$\left(\frac{\partial \bar{w}}{\partial z}\right)_{core} = 0; \quad \bar{w} = \bar{w}(x, y) \quad [24]$$

Thus, for both the faces and core, it can be concluded that the z-component normal stress deformability is negligible. It appears that the deformability becomes important only when $\alpha \sim 0(\epsilon^4)$ a case in which the elastic properties of the core are extremely weak. The fact that the transverse deformability is unimportant in bending of plates has been observed by other investigators[3,4] from various calculations. From the order-of-

magnitude analysis, it becomes quite clear that this fact is true in such cases where $\alpha \sim 0(\epsilon^2)$.

Further results of the order-of-magnitude analysis are embodied in the following simplified stress-strain relations for the sandwich plate which are obtained by retaining terms up to the order of ϵ^2 for the faces and ϵ^3 for the core

$$E\frac{\partial u}{\partial x} = \sigma_x - \nu\,\sigma_y \quad \ldots\ldots [25]$$

$$E\frac{\partial v}{\partial y} = \sigma_y - \nu\,\sigma_x \quad \ldots\ldots [26]$$

$$G\left(\frac{\partial u}{\partial y} + \frac{\partial v}{\partial x}\right) = \tau_{xy} \quad \ldots\ldots [27]$$

$$G\left(\frac{\partial u}{\partial z} + \frac{\partial w}{\partial x}\right) = \bar{\tau}_{xz} \quad \ldots\ldots [28]$$

$$G\left(\frac{\partial v}{\partial z} + \frac{\partial w}{\partial y}\right) = \bar{\tau}_{yz} \quad \ldots\ldots [29]$$

In these equations the face-parallel core stresses are neglected since from Table 2, $\bar{\sigma}_x$, $\bar{\sigma}_y$ and $\bar{\tau}_{xy}$ are of order ϵ^4. Reissner[4] obtained a similar set of equations by assuming at the start that the face-parallel core stresses are negligible.

A statement concerning the normal to the middle surface can be deduced by considering any point x, y, z on the normal to the middle surface and its image ξ, η, ζ after bending. The direction cosines of the image point are obtained from Equations [28] and [29]

$$\left.\begin{aligned} \partial\xi/\partial z &= -\partial w/\partial x + \bar{\tau}_{xz}/G \\ \partial\eta/\partial z &= -\partial w/\partial y + \bar{\tau}_{yz}/G \\ \partial\zeta/\partial z &= 1 \end{aligned}\right\} \quad \ldots\ldots [30]$$

The image of the middle surface is the line whose normal has the direction cosines

$$-\frac{\partial w}{\partial x}, -\frac{\partial w}{\partial y}, 1 \quad \ldots\ldots [31]$$

Comparing Equation [30] and terms [31] which are the direction cosines for the normal to the middle surface and a point which was on the normal before bending, it can be seen that the point ξ, η, ζ does not lie on the normal after bending. This follows from the fact that the two image points have different direction cosines and, therefore, are not parallel. Since the z-component shearing stresses were found from Equations [18] and [19] to be independent of the z-co-ordinate, it can be concluded from Equation [30] that the direction cosines are the same for any image point of the normal. This is a sufficient condition for the statement that plane sections remain plane for the sandwich plate. For the homogeneous plate, however, $G \to \infty$, and it is found that the direction cosines of the image point and the normal are identical.

Approximate Approach for Torsion Problem of a Shaft With a Circumferential Notch

By H. ŌKUBO,[1] SENDAI, JAPAN

The torsion problem of a bar with varying circular section has been treated by several investigators over a long period. Usually, the solution covering all points in a shaft is found first and then the maximum stress is obtained. Accordingly, the analysis usually becomes complicated and so only few cases have been treated completely. It is essential from the technical point of view, however, to find the stresses around a notch rather than the stresses at every point in a shaft. The approach employed in this paper is somewhat different from others, and the approximate values for the stresses on the surface of a shaft are found directly without solving the problem completely.

WE shall take cylindrical polar co-ordinates, and shall take the axis of the shaft as the z-axis. Then the problem is mathematically equivalent to the finding of a function which satisfies the differential equation[2]

$$\frac{\partial^2\psi}{\partial r^2} - \frac{3}{r}\frac{\partial\psi}{\partial r} + \frac{\partial^2\psi}{\partial z^2} = 0 \quad \ldots\ldots [1]$$

at all points within the shaft and the condition

$$\psi = \text{const} \quad \ldots\ldots [2]$$

at the boundary.

Let us consider a shaft with a circumferential notch, twisted by couples T applied at the ends. Imagine a very thin shell cut out from the shaft, of which the outer and inner surfaces are given by the equations

$$\psi = \alpha_0 = \text{const} \qquad \psi = \alpha_1 = \text{const} \quad \ldots\ldots [3]$$

respectively, and the former coincides with the surface of the shaft. Since the ends of the shaft are submitted to a simple torsion, denoting the couples acting on the ends of the shell by T_0, we have

$$T_0 = \frac{4t_0}{r_0} T \quad \ldots\ldots [4]$$

where r_0 and t_0 represent the radius and the thickness of the shell at the ends, respectively.

Consider a section of the shell cut by a plane containing the z-axis, as shown in Fig. 1. The direction of the resultant S of the shearing stress taken over the thickness coincides with the tangential direction of the shell at the point, hence the r, z-components of S are

$$S_r = S\cos\theta, \qquad S_z = S\sin\theta \quad \ldots\ldots [5]$$

where θ is the angle between the tangent and the z-axis.

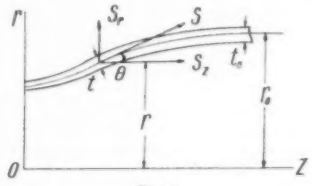

FIG. 1

The equilibrium condition for the couple gives the relation

$$2\pi r^2 S = T_0$$

and it follows

$$S = \frac{T_0}{2\pi r^2} = \frac{2t_0 T}{\pi r_0 r^2} \quad \ldots\ldots [6]$$

The shearing forces and the shearing stresses have the relations

$$S = t\tau, \quad \text{or} \quad S_z = t\tau_{\theta z}, \quad S_r = t\tau_{r\theta} \quad \ldots\ldots [7]$$

where t is the thickness of the shell at the point. Hence we have

$$\tau = \frac{2kT}{\pi r_0 r^2}, \quad \text{or} \quad \tau_{\theta z} = \frac{2kT}{\pi r_0 r^2}\cos\theta, \ \tau_{r\theta} = \frac{2kT}{\pi r_0 r^2}\sin\theta \quad [8]$$

where $k = t_0/t$.

Thus finding the value of k, from Equation [8] we readily can calculate the stresses on the surface of the shaft.

When the radius of the shell is very large compared with the dimensions of the notch, the curves given by Equation [3] can be replaced by the streamlines in a potential flow, the equation of which is given by

$$\phi(r, z) = \text{const} \quad \ldots\ldots [9]$$

Hence k can be expressed as

$$k = \left[\left(\frac{\partial\phi}{\partial r}\right)^2 + \left(\frac{\partial\phi}{\partial z}\right)^2\right]^{\frac{1}{2}} \Big/ \left[\left(\frac{\partial\phi}{\partial r}\right)_0^2 + \left(\frac{\partial\phi}{\partial z}\right)_0^2\right]^{\frac{1}{2}} \quad [10]$$

where $(\ )_0$ denotes the value at the ends of the shell.

Under the foregoing approximation, k coincides with the ratio of the velocity at the point to the velocity at infinite distances, in a two-dimensional flow. While the streamlines for various cases have been investigated extensively, these results can be immediately applicable to the present problem.

Examples. As a first example we will take the case of a shaft with a semicircular notch of radius a. The exact and the approximate solutions for the problem have been carried out by several

[1] Institute of High Speed Mechanics, Tōhoku University.

[2] "The Mathematical Theory of Elasticity," by A. E. H. Love, fourth edition, Dover Publications, New York, N. Y., 1927, p. 325.

Contributed by the Applied Mechanics Division and presented at the Annual Meeting, Atlantic City, N. J., November 25–30, 1951, of THE AMERICAN SOCIETY OF MECHANICAL ENGINEERS.

Discussion of this paper should be addressed to the Secretary, ASME, 29 West 39th Street, New York, N. Y., and will be accepted until April 10, 1952, for publication at a later date. Discussion received after the closing date will be returned.

NOTE: Statements and opinions advanced in papers are to be understood as individual expressions of their authors and not those of the Society. Manuscript received by ASME Applied Mechanics Division, March 21, 1951. Paper No. 51—A-16.

writers formerly.[3] However, the problem can be solved quite readily by the approximate method proposed in this paper.

Transferring the origin of the co-ordinates to the center of the circle ($z = 0, r = r_0$), the corresponding streamlines are given by a well-known formula, as[4]

$$\phi = r - \frac{ra^2}{r^2 + z^2} = \text{const} \quad \ldots\ldots [11]$$

hence at the bottom of the notch ($z = 0, r = -a$), it becomes

$$\frac{\partial \phi}{\partial r} = 2, \quad \left(\frac{\partial \phi}{\partial r}\right)_0 = 1, \quad \frac{\partial \phi}{\partial z} = \left(\frac{\partial \phi}{\partial z}\right)_0 = 0$$

and so $k = 2$. Then the stress at the bottom of the notch becomes

$$\tau_{max} = \frac{4T}{\pi r_0 (r_0 - a)^2} \quad \ldots\ldots [12]$$

The values of the maximum stress for various values of r_0/a, calculated from Equation [12], are given in Table 1. For the sake of comparison, the exact and the approximate values obtained, respectively, by Willers and Sonntag, are also given in the same table. As is seen in the table, the approximate values obtained in this paper more closely agree with the exact ones than those obtained by Sonntag, especially in cases of the moderate dimensions of the notch.

TABLE 1 MAXIMUM STRESS VALUES FOR VARIOUS VALUES OF r_0/a

(Unit $2T/\pi r_0^3$)

r_0/a	1	2.5	5	6.66..	8	10	11	13.33..	20	30	40	50	∞
Author	∞	5.56	3.13	2.77	2.61	2.47	2.42	2.34	2.22	2.14	2.10	2.08	2
Willers	∞	—	3.07	2.76	2.60	2.46	—	2.33	2.17	—	2.04	—	2
Sonntag	∞	6.6	3.25	2.84	2.64	2.49	2.44	2.36	2.22	2.15	2.10	2.09	2

As the second example let us consider a shaft with a semi-elliptic notch, the periphery of which is given by

$$\frac{z^2}{a^2} + \frac{r^2}{b^2} = 1 \quad \ldots\ldots [13]$$

If we transform the co-ordinates by the relation

$$z + ir = 2a' \cosh(\alpha + i\beta)$$

then $\alpha = \text{const}$ represents the periphery of an ellipse. The corresponding stream function can be expressed by

$$\phi = \left(a'e^{\alpha} - \frac{c'^2}{a'} e^{-\alpha}\right) \sin \beta \quad \ldots\ldots [14]$$

where $a = c' + a'^2/c'$, $b = c' - a'^2/c'$. At the bottom of the notch it becomes

$$\frac{\partial \phi}{\partial r} = 1 + \frac{b}{a}, \quad \left(\frac{\partial \phi}{\partial r}\right)_0 = 1, \quad \frac{\partial \phi}{\partial z} = \left(\frac{\partial \phi}{\partial z}\right)_0 = 0$$

hence we have

$$k = 1 + \frac{b}{a}$$

and it follows

$$\tau_{max} = \frac{2T\left(1 + \frac{b}{a}\right)}{\pi r_0 (r_0 - b)^2} = \frac{2T\left(1 + \sqrt{\frac{b}{\rho}}\right)}{\pi r_0 (r_0 - b)^2} \quad \ldots\ldots [15]$$

where ρ is the radius of curvature at the bottom of the notch.

Previously a similar formula for τ_{max} had been introduced by Neuber,[5] but his formula gives the value of τ_{max} in $r_0/(r_0 - b)$ multiple of the present one, e.g., for a semicircular notch of radius $0.15r_0$, the two formulas give

$$\tau_{max} \Big/ \frac{2T}{\pi r_0^3} = 2.77, \text{ and } 3.26, \text{ respectively}$$

and Equation [15] gives the result to a higher accuracy than the latter, since the exact value of the case is 2.76.

The values of the maximum stress for various dimensions of the notch have been calculated from Equation [15], and the relation between the maximum stress and the radius of curvature for several specified depths of the notch are shown by curves in Fig. 2.

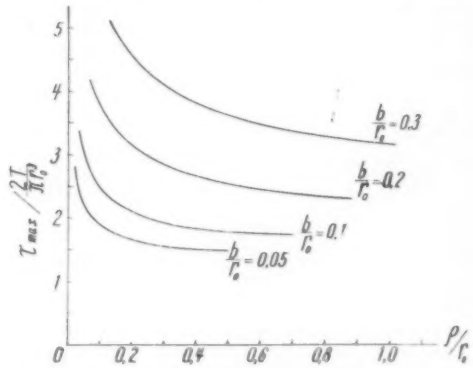

FIG. 2 RELATION BETWEEN MAXIMUM STRESS AND RADIUS OF CURVATURE

ACKNOWLEDGMENTS

A grant in aid of scientific research was given for this study by the Education Department of Japan. The author wishes to take this opportunity to thank Miss E. Itagaki, his assistant, for her earnest help in this study.

Appendix

Equation [15] has been given in a form covering all cases for the ratio of b/ρ. However, the validity of the formula is restricted to the cases of the moderate values of b/ρ since its accuracy is confirmed only in the particular case for $b = \rho$.

[3] "Die Torsion eines Rotationskorpers um seinne achsse," by F. A. Willers, *Zeitschrift fur Mathematik und Physik*, vol. 55, 1907, p. 251.

"Zur Torsion von runden Wellen mit verenderlichem Durchmesser," by R. Sonntag, *Zeitschrift für Angewandte Mathematik und Mechanik*, vol. 9, 1929, p. 3.

"Kerbspannungslehre," by H. Neuber, Julius Springer, Berlin, Germany, 1937, p. 127.

[4] "Hydrodynamics," by H. Lamb, The Macmillan Company, New York, N. Y., fourth edition, 1916, p. 75.

[5] Footnote 3, H. Neuber, 1937, p. 127.

Comparing the results shown in Fig. 2 with those of Sonntag,[6] we find that the latter becomes considerably larger than the former, as the decrease of ρ. As is shown in Table 1, his formula gives greater values compared with the exact ones for smaller values of r_0/a, which correspond to the cases where the streamlines are squeezed more intensely in hydrodynamic analogy. This may be considered as the main cause of the discrepancy in two formulas for smaller but moderate values of ρ.

[6] Footnote 3. R. Sonntag, vol. 9, 1929, p. 9; or C. B. Biezeno and R. Grammel, *Technische Dynamik*, 1939, p. 302.

On the Axisymmetric Problem of the Theory of Elasticity for an Infinite Region Containing Two Spherical Cavities[1]

By E. STERNBERG[2] and M. A. SADOWSKY,[3] CHICAGO, ILL.

This paper contains a solution in series form for the stress distribution in an infinite elastic medium which possesses two spherical cavities of the same size. The loading consists of tractions applied to the cavities, as well as of a uniform field of tractions at infinity, and both are assumed to be symmetric with respect to the common axis of symmetry of the cavities and with respect to the plane of geometric symmetry perpendicular to this axis. The loading is otherwise unrestricted. The solution is based upon the Boussinesq stress-function approach and apparently constitutes the first application of spherical dipolar co-ordinates in the theory of elasticity. Numerical evaluations are given for the case in which the surfaces of the cavities are free from tractions and the stress field at infinity is hydrostatic. The results illustrate the interference of two sources of stress concentration in a three-dimensional problem. The approach used here may be extended to cope with the general equilibrium problem for a region bounded by two nonconcentric spheres.

Introduction—Statement of Problem

THE equilibrium problem of the theory of elasticity for a region bounded by two nonconcentric spheres does not appear to have received any previous attention. This significant class of problems, the plane analogs of which are covered by available exact solutions (**1, 2**),[4] includes the case of the shell-shaped region bounded by two nonconcentric spheres, the infinite region containing two spherical cavities of arbitrary radii, as well as the limiting case of the semi-infinite region bounded by a plane and containing a spherical cavity.

In the present paper we confine ourselves to the particular instance in which the region is infinite and contains two cavities of the same radius. The loading is assumed to consist of tractions applied to the surfaces of the cavities and of a homogeneous field of tractions at infinity. Moreover, the loading is assumed to be symmetric both with respect to the common axis of symmetry of the two spheres and with respect to the plane of geometric symmetry perpendicular to this axis; it is otherwise unrestricted. The interest inherent in this problem is twofold: (*a*) The approach used may be generalized in dealing with the more complex problems referred to, even in the absence of symmetry restrictions. (*b*) The solution obtained illustrates the interference of two sources of stress concentration in a three-dimensional problem.

Axisymmetric Solutions in Spherical Dipolar Co-Ordinates—Spherical Dipolar Harmonics

Among the various available stress-function approaches to the rotationally symmetric, torsion-free problem of the theory of elasticity,[5] that based on the three-function approach[6] originated by Boussinesq (**4**) appears to be best suited for applications requiring the use of noncylindrical curvilinear co-ordinates. The Boussinesq approach has been employed extensively by H. Neuber (**5**) and by the present authors (**6, 7**). In case of torsion-free, rotational symmetry about the z-axis, and in the absence of body forces, the general solution of the displacement equations of equilibrium, following Boussinesq, is representable as the sum of the two displacement fields

$$2G[u, v, w] = \text{grad } \varphi \qquad [1]$$

$$2G[u, v, w] = \text{grad } (z\psi) - [0, 0, 4(1 - \nu)\psi] \qquad [2]$$

provided $\varphi(r, z)$ and $\psi(r, z)$ with

$$r = (x^2 + y^2 + z^2)^{1/2} \qquad [3]$$

are arbitrary harmonic functions, i.e.

$$\nabla^2\varphi = 0, \nabla^2\psi = 0 \qquad [4]$$

Here (x, y, z) are the Cartesian co-ordinates, $[u, v, w]$ the Cartesian components of displacement, G the shear modulus, and ν Poisson's ratio. The displacement fields, Equations [1] and [2], together with their associated fields of stress, which are obtained from the displacement-stress relations, henceforth will be referred to as the first and second Boussinesq solution, respectively. These solutions are readily transformed into general, orthogonal curvilinear co-ordinates. The corresponding transforms were given in a previous paper (**7**),[7] and need not be repeated at this place. We thus turn directly to spherical dipolar co-ordinates, the use of which is suggested by the geometry of the particular problem under consideration.

---

[1] The results contained in this paper were obtained in the course of an investigation conducted by the authors under contract N7onr-32906 with the Office of Naval Research, Department of the Navy, in Washington, D.C.

[2] Associate Professor of Mechanics, Illinois Institute of Technology. Jun. ASME.

[3] Associate Professor of Mathematics, Illinois Institute of Technology. Mem. ASME.

[4] Also treatises on the theory of elasticity. Numbers in parentheses refer to the Bibliography at the end of the paper.

Contributed by the Applied Mechanics Division and presented at the Annual Meeting, Atlantic City, N. J., November 25–30, 1951, of The American Society of Mechanical Engineers.

Discussion of this paper should be addressed to the Secretary, ASME, 29 West 39th Street, New York, N. Y., and will be accepted until April 10, 1952, for publication at a later date. Discussion received after the closing date will be returned.

Note: Statements and opinions advanced in papers are to be understood as individual expressions of their authors and not those of the Society. Manuscript received by ASME Applied Mechanics Division, April 17, 1951. Paper No. 51—A-10.

[5] See (**3**), chapter ix, for a comprehensive treatment of the rotationally symmetric problem.

[6] In the presence of rotational symmetry only two stress functions are involved.

[7] See Equations [14], [15] of the paper referred to.

Spherical dipolar co-ordinates[8] are introduced by means of the transformation

$$\left.\begin{aligned} x &= \frac{p}{q-p}\cos\gamma \\ y &= \frac{p}{q-p}\sin\gamma \\ z &= -\frac{\bar{q}}{q-p} \end{aligned}\right\} \quad \ldots\ldots [5]$$

where

$$\left.\begin{aligned} q &= \cosh\alpha, \quad \bar{q} = \sinh\alpha \\ p &= \cos\beta, \quad \bar{p} = \sin\beta \end{aligned}\right\} \quad \ldots\ldots [6]$$

The ranges of the curvilinear co-ordinates (α, β, γ) are

$$-\infty < \alpha < \infty, \quad 0 \leqslant \beta \leqslant \pi, \quad 0 \leqslant \gamma < 2\pi \quad \ldots\ldots [7]$$

so that

$$\left.\begin{aligned} 1 \leqslant q < \infty, \quad -\infty < \bar{q} < \infty \\ -1 \leqslant p \leqslant 1, \quad 0 \leqslant \bar{p} \leqslant 1 \end{aligned}\right\} \quad \ldots\ldots [8]$$

The co-ordinate surfaces form a triply orthogonal family. Indeed, Equations [5] imply

$$\left.\begin{aligned} \rho^2 + \left(z + \frac{q}{\bar{q}}\right)^2 &= \frac{1}{\bar{q}^2} \\ \left(\rho - \frac{p}{\bar{p}}\right)^2 + z^2 &= \frac{1}{\bar{p}^2} \\ y/z &= \tan\gamma \end{aligned}\right\} \quad \ldots\ldots [9]$$

[8] See (8), chapter X, for a brief discussion of this subject and for further references.

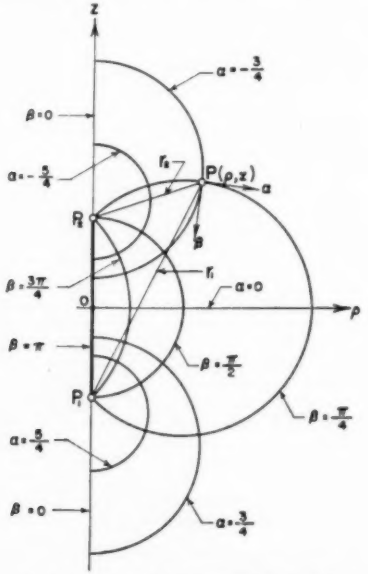

FIG. 1 SPHERICAL DIPOLAR CO-ORDINATES

(Traces of surfaces α = const and β = const on a meridional half-plane γ = const.)

where $\rho = (x^2 + y^2)^{1/2}$. The surfaces α = const are thus spheres of radius $1/\bar{q}$ centered on the z-axis at $z = -q/\bar{q}$. The surfaces β = const are surfaces of revolution the traces of which upon a meridional half-plane γ = const, $\rho \geqslant 0$ are circular arcs of radius $\frac{1}{\bar{p}}$ centered on the ρ-axis at $\rho = p/\bar{p}$; see Fig. 1. As $\alpha \to \pm\infty$, the spheres α = const contract toward the poles P_1 and P_2 which are located at $z = -1$ and $z = 1$, respectively. We also note that

$$r = (x^2 + y^2 + z^2)^{1/2} = \left(\frac{q+p}{q-p}\right)^{1/2} \quad \ldots\ldots [10]$$

and that the distances r_1 and r_2 of a point from the poles P_1 and P_2 are given by

$$\left.\begin{aligned} r_1 &= [x^2 + y^2 + (z+1)^2]^{1/2} = \frac{\sqrt{2}}{\mu}\, e^{-\alpha/2} \\ r_2 &= [x^2 + y^2 + (z-1)^2]^{1/2} = \frac{\sqrt{2}}{\mu}\, e^{\alpha/2} \end{aligned}\right\} \quad \ldots [11]$$

where

$$\mu = (q-p)^{1/2} \quad \ldots\ldots [12]$$

Computation of the metric coefficients associated with the mapping given in Equations [5], and subsequent substitution into Equations [14], [15] of reference (7), yield the displacement and stress fields of the Boussinesq solutions referred to spherical dipolar co-ordinates. In view of the rotational symmetry, the stress functions φ and ψ are at once assumed to depend upon α and β alone. We thus reach

$$\left.\begin{aligned} u_\alpha &= \frac{\mu^2}{2G}\,\varphi_\alpha \\ u_\beta &= -\frac{\mu^2 p}{2G}\,\varphi_p \end{aligned}\right\} \quad \ldots\ldots [13][9]$$

$$\left.\begin{aligned} \sigma_\alpha &= \mu^2(\mu^2\varphi_{\alpha\alpha} + \bar{q}\varphi_\alpha + p^2\varphi_p) \\ \sigma_\beta &= \mu^2[\mu^2 p^2\varphi_{pp} - (\mu^2 p + p^2)\varphi_p - \bar{q}\varphi_\alpha] \\ \sigma_\gamma &= -\mu^2[\bar{q}\varphi_\alpha - (1-qp)\varphi_p] \\ \tau_{\alpha\beta} &= -\mu^2 p[\mu^2\varphi_{\alpha p} - \varphi_\alpha + \bar{q}\varphi_p] \end{aligned}\right\} \quad \ldots [14]$$

$$\left.\begin{aligned} u_\alpha &= -\frac{1}{2G}\left[\bar{q}\psi_\alpha + (3-4\nu)\,\frac{qp-1}{\mu^2}\,\psi\right] \\ u_\beta &= \frac{\bar{q}p}{2G}\left[\psi_p - (3-4\nu)\,\frac{1}{\mu^2}\,\psi\right] \end{aligned}\right\} \quad \ldots [15]$$

$$\left.\begin{aligned} \sigma_\alpha &= -\mu^2\bar{q}\psi_{\alpha\alpha} - [\bar{q}^3 + 2(1-\nu)(qp-1)]\,\psi_\alpha \\ &\qquad - (1-2\nu)\,\bar{q}p^2\psi_p \\ \sigma_\beta &= -\mu^2\bar{q}p^2\psi_{pp} + [\mu^2\bar{q}p + (3-2\nu)\bar{q}p^2]\psi_p \\ &\qquad + [\bar{q}^2 - 2\nu(qp-1)]\,\psi_\alpha \\ \sigma_\gamma &= [\bar{q}^2 - 2\nu(qp-1)]\,\psi_\alpha + [qp - 1 + 2\nu p^2]\,\bar{q}\psi_p \\ \tau_{\alpha\beta} &= \mu^2\bar{q}p\psi_{\alpha p} - 2(1-\nu)\bar{q}p\psi_\alpha \\ &\qquad + [\bar{q}^2 + (1-2\nu)(qp-1)]\,p\psi_p \end{aligned}\right\} \quad \ldots [16]$$

In the foregoing equations u_α, u_β, and σ_α, σ_β, σ_γ, $\tau_{\alpha\beta}$ denote curvilinear components of displacement and stress, respectively. The displacement u_γ as well as the stresses $\tau_{\gamma\alpha}$ and $\tau_{\gamma\beta}$, which vanish identically by virtue of the assumed rotational symmetry, have been omitted altogether.

[9] Subscripts attached to functions which originally bear no subscript denote partial differentiation with respect to the argument indicated.

The stress functions $\varphi(\alpha, \beta)$ and $\psi(\alpha, \beta)$ must satisfy Laplace's equation, which here becomes

$$\phi_{\alpha\alpha} + \phi_{\beta\beta} - \frac{\bar{q}}{\mu^2}\phi_\alpha - \frac{1 - \bar{q}p}{p\mu^2}\phi_\beta = 0 \quad \ldots\ldots [17]$$

Equation [17] is not separable in the strict sense. However, it does possess solutions in the form

$$\phi(\alpha, \beta) = \mu A(\alpha)B(\beta) \quad \ldots\ldots [18]$$

Substitution of Equation [18] in [17], followed by separation of variables, leads to

$$\phi(\alpha, \beta) = \mu[C_n(\alpha) \text{ or } S_n(\alpha)][P_n(p) \text{ or } Q_n(p)] \quad \ldots\ldots [19]$$
$$(n = 0, 1, 2, \ldots\ldots)$$

where

$$\left.\begin{aligned} C_n(\alpha) &= \cosh (n + {}^1/_2)\alpha \\ S_n(\alpha) &= \sinh (n + {}^1/_2)\alpha \end{aligned}\right\} \quad \ldots\ldots [20]$$

and P_n, Q_n designate the Legendre polynomials and the Legendre functions of the second kind, respectively. Since the functions $Q_n(p)$ have a logarithmic singularity at $p = -1$ and $p = 1$, they give rise to harmonics which are singular along the z-axis.

The dipolar harmonics $\mu C_n(\alpha)P_n(p)$ and $\mu S_n(\alpha)P_n(p)$ are regular throughout the Cartesian space, including infinity, with the exception of the poles P_1, P_2, Fig. 1. These harmonics correspond to the exterior spherical harmonics

$$r^{-n-1}P_n(\omega) = \frac{(-1)^n}{\underline{n}}\frac{\partial^n}{\partial z^n}\left(\frac{1}{r}\right) \quad \ldots\ldots [21]$$
$$(n = 0, 1, 2, \ldots)$$

in which

$$\omega = \frac{z}{r} \quad \ldots\ldots [22]$$

It is essential for what follows to establish the connection between the exterior spherical harmonics and their dipolar counterparts; to this end we observe on the basis of Equation [21] that the functions

$$M_n(\alpha, \beta) = \frac{2^n}{\sqrt{2}\,\underline{n}}\frac{\partial^n}{\partial z^n}\left[(-1)^n\frac{1}{r_1} + \frac{1}{r_2}\right] \quad \ldots\ldots [23]$$
$$(n = 0, 1, 2, \ldots)$$

are likewise harmonic. According to Equations [11]

$$\left.\begin{aligned} \frac{1}{\sqrt{2}}\left(\frac{1}{r_1} - \frac{1}{r_2}\right) &= \mu S_0 P_0 \\ \frac{1}{\sqrt{2}}\left(\frac{1}{r_1} + \frac{1}{r_2}\right) &= \mu C_0 P_0 \end{aligned}\right\} \quad \ldots\ldots [24][10]$$

and the harmonics $M_n(\alpha, \beta)$ are thus identified as successive z-derivatives of the zero-order exterior dipolar harmonics. Moreover, it is shown by induction with the aid of the addition theorems for hyperbolic functions and of the recursion formulas

$$\left.\begin{aligned} (2n + 1)pP_n &= (n + 1)P_{n+1} + nP_{n-1} \\ p^2\frac{dP_n}{dp} &= nP_{n-1} - npP_n \end{aligned}\right\} \quad \ldots\ldots [25]$$

that

$$\frac{2^n}{\underline{n}}\frac{\partial^n}{\partial z^n}(\mu C_0 P_0) = \left\{\begin{array}{l} \mu\displaystyle\sum_{m=0}^{n}(-1)^{n+m}\binom{n}{m}C_m P_m \\ \text{if } n \ldots\ldots \text{even} \\ \mu\displaystyle\sum_{m=0}^{n}(-1)^{n+m}\binom{n}{m}S_m P_m \\ \text{if } n \ldots\ldots \text{odd} \end{array}\right\} \quad \ldots [26]$$

Equations [26] remain valid if C_m and S_m ($m = 0, 1, 2, \ldots$) are interchanged. In view of Equations [24] and [26], Equation [23] now yields

$$M_n(\alpha, \beta) = \mu\sum_{m=0}^{n}(-1)^m\binom{n}{m}C_m P_m \quad \ldots\ldots [27]$$

which in turn implies the reciprocal relation

$$\mu C_n P_n = \sum_{m=0}^{n}(-1)^m\binom{n}{m}M_m(\alpha, \beta) \quad \ldots\ldots [28]$$

Analogously, if we define the harmonics

$$N_n(\alpha, \beta) = -\frac{2^n}{\sqrt{2}\,\underline{n}}\frac{\partial^n}{\partial z^n}\left[(-1)^{n+1}\frac{1}{r_1} + \frac{1}{r_2}\right] \quad \ldots [29]$$
$$(n = 0, 1, 2, \ldots\ldots)$$

we find that

$$N_n(\alpha, \beta) = \mu\sum_{m=0}^{n}(-1)^m\binom{n}{m}S_m P_m \quad \ldots\ldots [30]$$

and consequently

$$\mu S_n P_n = \sum_{m=0}^{n}(-1)^m\binom{n}{m}N_m \quad \ldots\ldots [31]$$

The dipolar representation of interior harmonics of integral order, which are regular throughout the Cartesian space with the exception of infinity, appears not to have been considered in the literature; it is readily obtained by consideration of the interior spherical harmonics. Since $r^n P_n(\omega)$, $(n = 0, 1, 2, \ldots)$ is harmonic by virtue of Equation [21] the functions

$$R_n(\alpha, \beta) = \frac{1}{2\,\underline{n}}\left[(-1)^n r_1^{2n+1}\frac{\partial^n}{\partial z^n}\left(\frac{1}{r_1}\right) + r_2^{2n+1}\frac{\partial^n}{\partial z^n}\left(\frac{1}{r_2}\right)\right] \quad \ldots\ldots [32]$$
$$(n = 0, 1, 2, \ldots\ldots)$$

are also harmonic. Equations [11], [26] now yield

$$R_n(\alpha, \beta) = \mu^{-2n}\sum_{m=0}^{n}(-1)^m\binom{n}{m}\cosh (n - m)\alpha P_m(p) \quad \ldots [33]$$

Similarly, the corresponding interior harmonics which are odd in α, admit the representation

$$T_n(\alpha, \beta) = \mu^{-2n}\sum_{m=0}^{n}(-1)^m\binom{n}{m}\sinh (n - m)\alpha P_m(p) \quad \ldots\ldots [34][11]$$

[10] The arguments of C_n, S_n, and P_n will henceforth be assumed to be α, α, and p, respectively, unless otherwise specified.

[11] It is interesting to note that the functions R_n and T_n of even index are linearly dependent upon the corresponding functions of odd index.

In the particular problem to be considered, the required Boussinesq stress functions are found to be the interior dipolar harmonics

$$\varphi_n = \mu C_n(\alpha) P_n(p), \quad \psi_n = \mu S_n(\alpha) P_n(p) \ldots\ldots [35]$$
$$(n = 0, 1, 2, \ldots\ldots)$$

The solutions generated by φ_n and ψ_n of Equations [35], which will be designated as solutions $[D_n]$ and $[E_n]$, respectively, follow at once from Equations [13], [14], [15], and [16]. The computation yields, for solution $[D_n]$

$$\left.\begin{aligned} u_\alpha &= \frac{\mu}{4G}\,[\bar{q} P_n C_n + k\mu^2 P_n S_n] \\ u_\beta &= \frac{\mu\bar{p}}{4G}\,[P_n C_n - 2\mu^2 P_n' C_n] \end{aligned}\right\} \ldots\ldots [36]$$

$$\left.\begin{aligned} \sigma_\alpha &= \mu\left\{\left[\frac{(k^2+1)}{4}\mu^4 + \frac{\bar{q}^2}{2} - \frac{\bar{p}^2}{4}\right] C_n P_n \right. \\ &\qquad \left. + \bar{p}^2\mu^3 C_n P_n' + k\bar{q}\mu^2 S_n P_n \right\} \\ \sigma_\beta &= \mu\left\{\left[-\frac{k^2}{4}\mu^4 - \frac{\bar{q}^2}{4} + \frac{\bar{p}^2}{2}\right] C_n P_n \right. \\ &\qquad \left. + (p\mu^2 - 2p^2)\mu^2 C_n P_n' - \frac{k}{2}\bar{q}\mu^2 S_n P_n \right\} \\ \sigma_\gamma &= -\mu^2\left\{\frac{q}{2} C_n P_n + (qp-1) C_n P_n' \right. \\ &\qquad \left. + \frac{k}{2}\bar{q} S_n P_n \right\} \\ \tau_{\alpha\beta} &= \bar{p}\mu\left\{\frac{3}{4}\bar{q} C_n P_n - \frac{3}{2}\bar{q}\mu^2 C_n P_n' \right. \\ &\qquad \left. + \frac{3k}{4}\mu^2 S_n P_n - \frac{k}{2}\mu^4 S_n P_n' \right\} \\ &(n = 0, 1, 2, \ldots\ldots) \end{aligned}\right\} \ldots [37]$$

and for solution $[E_n]$

$$\left.\begin{aligned} u_\alpha &= \frac{-1}{4G\mu}\left\{[(7-8\nu)(qp-1) + q\mu^2] P_n S_n \right. \\ &\qquad \left. + k\bar{q}\mu^2 P_n C_n \right\} \\ u_\beta &= \frac{-\bar{q}\bar{p}}{4G\mu}\,[(7-8\nu) P_n S_n - 2\mu^2 P_n' S_n] \end{aligned}\right\} \ldots [38]$$

$$\left.\begin{aligned} \sigma_\alpha &= \frac{-1}{\mu}\left\{\left[\frac{k^2-4+8\nu}{4}\bar{q}\bar{p}\mu^2 - \frac{k^2+2-4\nu}{4}\bar{q}p\mu^2 \right.\right. \\ &\quad \left. + \frac{7-8\nu}{4}\bar{q}^2\right] S_n P_n + (1-2\nu)\bar{q}\bar{p}^2\mu^2 S_n P_n' \\ &\quad \left. + k[\bar{q}^2 + (1-\nu)(qp-1)]\mu^2 C_n P_n \right\} \\ \sigma_\beta &= \frac{1}{\mu}\left\{\left[\frac{k^2-6+8\nu}{4}\bar{q}\bar{p}\mu^2 - \frac{k^2+6-4\nu}{4}\bar{q}p\mu^2 \right.\right. \\ &\quad \left. + \frac{7-8\nu}{4}\bar{q}^2\right] S_n P_n + [(3-2\nu)\bar{p}^2 - qp \\ &\quad \left. + 1]\bar{q}\mu^2 S_n P_n' + \frac{k}{2}[\bar{q}^2 - 2\nu(qp-1)]\mu^2 C_n P_n \right\} \end{aligned}\right\} \ldots [39]$$

$$\left.\begin{aligned} \sigma_\gamma &= \mu\left\{(q-2\nu p)\frac{\bar{q}}{2} S_n P_n + (qp-1 \right. \\ &\quad \left. + 2\nu\bar{p}^2)\bar{q} S_n P_n' + \frac{k}{2}[\bar{q}^2 - 2\nu(qp-1)] C_n P_n \right\} \\ \tau_{\alpha\beta} &= \frac{p}{\mu}\left\{\left[\frac{1-2\nu}{2} q\mu^2 - \frac{7-8\nu}{4}\bar{q}^2\right] S_n P_n \right. \\ &\quad + \frac{1}{2}[3\bar{q}^2 + (2-4\nu)(qp-1)]\mu^2 S_n P_n' \\ &\quad \left. - \frac{k(5-4\nu)}{4}\bar{q}\mu^2 C_n P_n + \frac{k}{2}\bar{q}\mu^4 C_n P_n' \right\} \\ &(n = 0, 1, 2, \ldots\ldots) \end{aligned}\right\} \ldots [39] \text{ (con't)}$$

where

$$k = 2n + 1 \ldots\ldots [40]$$

We now examine certain physical aspects of the two aggregates of solutions $[D_n]$ and $[E_n]$, which are pertinent to our purposes. To this end we recall that the displacement field for a center of compression located at the origin is given by[12]

$$2G[u, v, w] = \text{grad}\ \frac{1}{r} \ldots\ldots [41]$$

whereas the solution for a concentrated load of magnitude[13] $8\pi(1-\nu)$, acting at the origin in an infinite medium, in the direction of the negative z-axis, is characterized by the displacement field

$$2G[u, v, w] = \text{grad}\ \frac{z}{r} - \left[0, 0, \frac{4(1-\nu)}{r}\right] \ldots\ldots [42]$$

It follows from Equations [1], [41], [23], [27] that the stress function $\varphi = M_n(\alpha, \beta) = \mu P_n C_n$, which belongs to solution $[D_n]$, gives rise to two centers of compression of the same strength, located at the poles P_1 and P_2 of the dipolar co-ordinate system. On the other hand, the foregoing considerations and Equations [2], [42], [29], [30] imply that $\psi = N_n(\alpha, \beta) = \mu P_n S_n$, which belongs to solution $[E_n]$, corresponds to centers of dilatation at P_1 and P_2 in addition to two equal and opposite forces, each of magnitude $8\pi(1-\nu)/\sqrt{2}$, applied at P_1 and P_2, respectively, the force at P_1 acting in the negative z-direction. The analogous basic singularities which are antisymmetric with respect to the plane $z = 0$ are generated by $\varphi = N_n(\alpha, \beta) = \mu P_n S_n$ and by $\psi = M_n(\alpha, \beta) = \mu P_n C_n$.

By aid of these considerations, and by virtue of Equations [1], [23], [24], and [29], we conclude that the stress functions $\varphi = M_n(\alpha, \beta)$ and $\varphi = N_n(\alpha, \beta)$ $(n = 1, 2, 3, \ldots)$ yield the sequence of higher singularities which is derived from the foregoing center of compression singularities through successive z-differentiations. In particular, $\varphi = M_1(\alpha, \beta)$ gives rise to a pair of compression doublets situated at the poles. Thus each member of the sequence of solutions generated by $\varphi = M_n(\alpha, \beta)$ and $\varphi = N_n(\alpha, \beta)$ $(n = 0, 1, 2, \ldots)$ has vanishing displacements and stresses at infinity, and is self-equilibrated in the sense that the tractions on any closed surface surrounding either one of the poles P_1 and P_2 but not the other, are statically equivalent to null. In view of Equations [28] and [35], each member of the aggregate of solutions $[D_n]$ $(n = 0, 1, 2, \ldots)$ also possesses these properties.

The connection between the sequence of solutions corresponding to $\psi = M_n(\alpha, \beta)$ and $\psi = N_n(\alpha, \beta)$ $(n = 1, 2, 3, \ldots)$ and

[12] See reference (9), chapter 8.

[13] This particular magnitude is chosen for convenience only.

the basic zero-order singularities just discussed is established by means of Equations [2], [29] and of the identity

$$\left.\begin{aligned}&\frac{\partial^n}{\partial z^n}\{\operatorname{grad}(z\psi) - [0,\ 0,\ 4(1-\nu)\psi]\}\\ &= n\ \operatorname{grad}\frac{\partial^{n-1}}{\partial z^{n-1}}(\psi) + \operatorname{grad}\left(z\frac{\partial\psi}{\partial z^n}\right) - \left[0,\ 0,\ 4(1-\nu)\frac{\partial^n\psi}{\partial z^n}\right]\\ &(n = 1, 2, 3, \ldots\ldots)\end{aligned}\right\} \quad [43]$$

In particular, we recognize the solution generated by $\varphi = N_0(\alpha, \beta) - \frac{1}{2}N_1(\alpha, \beta)$ together with $\psi = \frac{1}{2}M_1(\alpha, \beta)$, as appropriate to a pair of force doublets located at the poles P_1 and P_2. The results of the preceding discussion now permit the conclusion that both $\psi = M_n(\alpha, \beta)$ and $\psi = N_n(\alpha, \beta)$ $(n = 1, 2, 3, \ldots)$ give rise to aggregates of solutions, each member of which is self-equilibrated and vanishes at infinity. Equations [31], [35] reveal the significant fact that the individual members of the aggregate of solutions $[E_n]$ $(n = 0, 1, 2, \ldots)$, while vanishing at infinity, are not self-equilibrated. On the other hand, the difference between any two solutions within this aggregate is found to be self-equilibrated.

Solution of the Problem of Two Spherical Cavities

With reference to the spherical dipolar co-ordinates introduced by Equations [5] and [6], the problem stated in the Introduction now admits a convenient mathematical formulation. Let the two spherical cavities be bounded by the parametric surfaces $\alpha = \alpha_0 > 0$ and $\alpha = -\alpha_0$. According to Equations [9], the radius ϑ of each cavity is then given by

$$\vartheta = \frac{1}{\sqrt{q_0}} \quad [44]^{14}$$

and the ratio of the distance Δ between the two centers to the diameter 2ϑ becomes

$$s = \frac{\Delta}{2\vartheta} = \sqrt{q_0} \quad [45]$$

The boundary conditions to be considered are

$$\left.\begin{aligned}&\sigma_\alpha(\alpha_0, \beta) = \sigma_\alpha(-\alpha_0, \beta) = \frac{f(\beta)}{\mu_0}\\ &\tau_{\alpha\beta}(\alpha_0, \beta) = -\tau_{\alpha\beta}(-\alpha_0, \beta) = \frac{pg(\beta)}{\mu_0}\\ &0 \leqslant \beta \leqslant \pi\end{aligned}\right\} \quad [46]^{15}$$

where $f(\beta)$ and $g(\beta)$ are arbitrary, and μ is defined by Equation [12]. Furthermore, either

$$\sigma_r, \sigma_y, \tau_{xy}, \tau_{yz}, \tau_{zx} \to 0 \text{ and } \sigma_z \to \sigma \text{ as } r \to \infty, \text{ i.e., } \alpha, \beta \to 0 \quad [47]$$

or

$$\sigma_x, \sigma_y, \sigma_z \to \sigma \text{ and } \tau_{xy}, \tau_{yz}, \tau_{zx} \to 0 \text{ as } r \to \infty, \text{ i.e., } \alpha, \beta \to 0 \quad [48]$$

[14] The subscript zero attached to any function of α will henceforth designate its evaluation for $\alpha = \alpha_0$.

[15] The coefficients $1/\mu_0$ and $\bar{p}/\mu_0$ are introduced for later convenience.

We now assume the solution $[S]$ to the problem characterized by Equations [46] and [47] or [48] in the form

$$[S] = [U] + [R] \quad [49]$$

where $[U]$ is the uniform field [47] or [48], extended throughout the space, and $[R]$ represents the solution to a residual problem whose formulation is implicit in Equation [49]. In Equation [49], as in subsequent equations, the letters in brackets designate either a stress-tensor field or its associated displacement-vector field,[16] and addition as well as equality are to be interpreted accordingly. On transforming $[U]$ into spherical dipolar co-ordinates, we obtain, in case the state of stress at infinity is uniaxial, from Equation [47]

$$\left.\begin{aligned}&\sigma_\alpha = \frac{\sigma(qp-1)^2}{\mu^4},\quad \sigma_\beta = \frac{\sigma q^2 p^2}{\mu^4},\quad \sigma_\gamma = 0\\ &\tau_{\alpha\beta} = \frac{\sigma(qp-1)\sqrt{q}p}{\mu^4}\end{aligned}\right\} \quad [50]$$

and in case the state of stress at infinity is hydrostatic, from Equation [48]

$$\left.\begin{aligned}&\sigma_\alpha = \sigma_\beta = \sigma_\gamma = \sigma\\ &\tau_{\alpha\beta} = 0\end{aligned}\right\} \quad [51]$$

Therefore, the solution $[R]$ to the residual problem referred to in the foregoing is characterized by the boundary conditions

$$\left.\begin{aligned}&\sigma_\alpha(\alpha_0, \beta) = \sigma_\alpha(-\alpha_0, \beta) = \frac{1}{\mu_0}\left[f(\beta) - \frac{\sigma(q_0p-1)^2}{\mu_0^3}\right]\\ &\tau_{\alpha\beta}(\alpha_0, \beta) = -\tau_{\alpha\beta}(-\alpha_0, \beta) = \frac{\bar{p}}{\mu_0}\left[g(\beta) - \frac{\sigma(q_0p-1)\sqrt{q_0}}{\mu_0^2}\right]\end{aligned}\right\} \quad [52]$$

or

$$\left.\begin{aligned}&\sigma_\alpha(\alpha_0, \beta) = \sigma_\alpha(-\alpha_0, \beta) = \frac{1}{\mu_0}[f(\beta) - \sigma\mu_0]\\ &\tau_{\alpha\beta}(\alpha_0, \beta) = -\tau_{\alpha\beta}(-\alpha_0, \beta) = \frac{\bar{p}}{\mu_0}g(\beta)\end{aligned}\right\} \quad [53]$$

and, in either case

$$\sigma_\alpha, \sigma_\beta, \sigma_\gamma, \tau_{\alpha\beta} \to 0 \text{ as } \alpha, \beta \to 0 \quad [54]$$

Provided the functions $f(\beta)$ and $g(\beta)$ are sufficiently smooth, Equations [52], [53] admit the joint representation

$$\left.\begin{aligned}&\sigma_\alpha(\alpha_0, \beta) = \sigma_\alpha(-\alpha_0, \beta) = \frac{1}{\mu_0}\sum_{n=0}^{\infty}\xi_n P_n(p)\\ &\tau_{\alpha\beta}(\alpha_0, \beta) = -\tau_{\alpha\beta}(-\alpha_0, \beta) = \frac{\bar{p}}{\mu_0}\sum_{n=1}^{\infty}\eta_n P_n'(p)\end{aligned}\right\} \quad [55]$$

the Legendre series appearing here being assumed uniformly convergent for $-1 \leq p \leq 1$. We now obtain explicitly the Expansions [55] for the particular instance $f(\beta) = g(\beta) \equiv 0$, corresponding to traction-free surfaces of the cavities. For this purpose we recall the identity[17]

$$\frac{1}{\sqrt{1-2tp+t^2}} = \sum_{n=0}^{\infty}t^n P_n(p) \quad [56]$$

[16] Within an arbitrary additive rigid displacement.

[17] See reference [8], p. 335.

in which the infinite series converges uniformly for $0 < t < 1$ and $-1 \leq p \leq 1$. Making the substitution

$$t = e^{-\alpha_0} \quad (\alpha_0 > 0) \qquad [57]$$

we reach

$$\frac{1}{\mu_0} = \sqrt{2} \sum_{n=0}^{\infty} e^{-k\alpha_0/2} P_n(p) \qquad [58]$$

where k is given by Equation [40]. By means of partial differentiation of Equation [58] with respect to α_0 and p, and by use of Equations [25], we finally find from Equation [52], corresponding to the uniaxial state of stress $\sigma_z = \sigma$ at infinity

$$\left.\begin{aligned} \xi_n &= \sqrt{2}\,\sigma e^{-k\alpha_0/2}\left[\bar{q}_0{}^2(2q_0 - k\bar{q}_0) + \frac{q_0{}^2}{k^2-4}(k\bar{q}_0 + 2q_0)\right] \\ &\quad (n = 0, 1, 2, \ldots\ldots) \\ \eta_n &= 2\sqrt{2}\,\sigma\bar{q}_0 e^{-k\alpha_0/2}\left[\frac{(2q_0 + k\bar{q}_0)q_0}{k^2-4} - \bar{q}_0{}^2\right] \\ &\quad (n = 1, 2, 3, \ldots\ldots) \end{aligned}\right\} \qquad [59]$$

and from Equations [53], corresponding to the hydrostatic state of stress $\sigma_x = \sigma_y = \sigma_z = \sigma$ at infinity

$$\left.\begin{aligned} \xi_n &= \sqrt{2}\,\sigma e^{-k\alpha_0/2}\frac{2q_0 + k\bar{q}_0}{k^2-4} \\ &\quad (n = 0, 1, 2, \ldots\ldots) \\ \eta_n &= 0 \quad (n = 1, 2, 3, \ldots\ldots) \end{aligned}\right\} \qquad [60]$$

The system of tractions Equations [46] applied to each of the two cavities, is either self-equilibrated or else statically equivalent to a resultant force along the z-axis. In the latter case the two resultant forces so arising are equal and opposite. It follows from Equations [46] that

$$P = 2\pi \int_0^{\pi} \left[(q_0 p - 1) f(\beta) + \bar{q}_0 \beta^2 g(\beta)\right] \frac{p}{\mu_0{}^2}\, d\beta \qquad [61]$$

where $|P|$ is the magnitude of each resultant force and $P > 0$ if the force exerted on the surface $\alpha = \alpha_0 > 0$ is directed in the positive z-direction. Since the tractions of $[U]$ at either cavity are self-equilibrated Equation [61] at the same time yields the stress resultant at $\alpha = \pm\alpha_0$ of the solution $[R]$ to the residual problem.

It is advantageous to reduce the residual problem in any case to one involving vanishing stress resultants at $\alpha = \pm\alpha_0$. In accordance with the discussion at the end of the preceding section, this is accomplished by setting

$$[R] = -\frac{\sqrt{2}P}{8\pi(1-\nu)}[E_0] + [R^*] \qquad [62]$$

where P is given by Equation [61], $[E_0]$ by Equations [39] with $n = 0$, and $[R^*]$ designates the solution to a modified residual problem. The boundary conditions at $\alpha = \pm\alpha_0$ appropriate to $[R^*]$ are immediate from Equations [62], [39], and [52] or [53]; they again admit the general representation [55]. Moreover, all stresses of $[R^*]$ must vanish at infinity. It should be observed that in case the cavities are free from loading, $P = 0$, $[R^*] = [R]$, and the coefficients ξ_n, η_n are given by Equations [59] or [60].

We now approach the determination of $[R^*]$ via the Boussinesq solutions. Because of the requirements of symmetry and regularity, as well as by virtue of the boundary conditions at infinity, the only dipolar harmonics among those listed in the preceding section, which are admissible as generating stress functions, are given by Equations [35]. The displacements and stresses of the corresponding solutions $[D_n]$ and $[E_n]$ were recorded as Equations [36], [37] and [38], [39]. As was demonstrated previously, the aggregate of solutions $[D_n]$ $(n = 0, 1, 2, \ldots)$ is self-equilibrated, whereas the individual members of the aggregate $[E_n]$ $(n = 0, 1, 2, \ldots)$ do not possess this property. For this reason, solutions $[E_n]$ as such are not suitable for the construction of $[R^*]$, the surface tractions of which at $\alpha = \pm\alpha_0$ are to be self-equilibrated. On the other hand, the difference $[E_i] - [E_j]$ of any two solutions within this aggregate was found to be self-equilibrated.

Our current purpose is to arrive at a doubly infinite aggregate of solutions, based on linear combinations of members of the aggregates $[D_n]$ and $[E_n]$, which conforms to the requirement of self-equilibrance; at the same time, this aggregate should yield simple forms for the boundary stresses $\sigma_\alpha(\alpha_0, \beta)$, $\tau_{\alpha\beta}(\alpha_0, \beta)$ of its constituent members in terms of which the prescribed tractions, Equations [55], ultimately must be expanded. A systematic investigation, motivated by this objective, leads us to assume $[R^*]$ in the form

$$[R^*] = a_0[A_0] + \sum_{n=1}^{\infty} \{a_n[A_n] + b_n[B_n]\} \qquad [63]$$

where the new solutions $[A_n]$ and $[B_n]$ are defined by

$$\left.\begin{aligned} [A_n] &= \sum_{i=0}^{n} (n + 1 - i)\,[D_i] \\ &\quad (n = 0, 1, 2, \ldots\ldots) \\ [B_n] &= \frac{2}{k^2-1}\sum_{i=0}^{n-1}\{[E_n] - [E_i]\} \\ &\quad (n = 1, 2, 3, \ldots\ldots) \end{aligned}\right\} \qquad [64]^{18}$$

The displacements and stresses of $[A_n]$ and $[B_n]$ are immediately obtainable from Equations [64] in conjunction with Equations [36] to [39]. We limit our attention to the stress components σ_α, $\tau_{\alpha\beta}$ which enter into the determination of the unknown coefficients of superposition a_n and b_n of Equation [63]. Guided by the form of the boundary conditions, Equations [55],[19] which are to be met identically in β, we thus expand $\mu\sigma_\alpha$ and $\mu\tau_{\alpha\beta}/p$ of solutions $[A_n]$, $[B_n]$ as series of Legendre polynomials and their derivatives, respectively. After exceedingly cumbersome computations involving the repeated use of Equations [25] and of the addition theorems for hyperbolic functions, we reach the following representations:

For solution $[A_n]$

$$\sigma_\alpha = \frac{(k+1)(k+3)}{32\mu}\left[-\frac{k-1}{k}C_{n+2}P_{n-1} + \left(\frac{3k+4}{k+2}C_{n+1} + C_{n+3}\right)P_n\right] \qquad [65]$$

[18] The simplifications derived from these particular linear combinations will be discussed later.

[19] Equations [55] are now understood to represent the boundary conditions appropriate to $[R^*]$.

$$-\left(\frac{3k+11}{k+4}C_n+\frac{3k+1}{k}C_{n+2}\right)P_{n+1}$$
$$+\left(C_{n-1}+\frac{3k+8}{k+2}C_{n+1}\right)P_{n+2}-\frac{k+5}{k+4}C_nP_{n+3}\Big]$$

$$\tau_{\alpha\beta}=\frac{p}{16\mu}\Big\{\frac{(k+1)(k+3)}{k}S_{n+2}P'_{n-1}$$
$$-(k+3)[3S_{n+1}+S_{n+3}]P'_n$$
$$+3\left[\frac{k^2+6k+7}{k+4}S_n+\frac{k^2+2k-1}{k}S_{n+2}\right]P'_{n+1}$$
$$-(k+1)[S_{n-1}+3S_{n+1}]P'_{n+2}$$
$$+\frac{(k+1)(k+3)}{k+4}S_nP'_{n+3}\Big\}$$
$$(n=0,1,2,\ldots\ldots) \qquad \ldots[65]\ (con't)$$

For solution $[B_n]$

$$\sigma_\alpha=\frac{1}{32\mu}$$
$$\Big\{(k-3)\left[\frac{k+2}{k-2}C_{n-1}-\left(1-\frac{4\lambda}{k-2}\right)C_{n+1}\right]P_{n-2}$$
$$-2\left[\left(k-1-\frac{2\lambda}{k}\right)C_{n-2}+\left(\frac{9k-4}{k}+6\lambda\right)C_n\right.$$
$$\left.-\left(k-\frac{2\lambda(k-1)}{k}\right)C_{n+2}\right]P_{n-1}+\Big[(k-3)\,C_{n-1}$$
$$+\left(\frac{3k^2+9k-26}{k-2}+\frac{4\lambda(3k+5)}{k+2}\right)C_{n-1}$$
$$-\left(\frac{3k^2-9k-26}{k+2}-\frac{4\lambda(3k-5)}{k-2}\right)C_{n+1}$$
$$-(k+3)C_{n+3}\Big]P_n-2\left[\left(k+\frac{2\lambda(k+1)}{k}\right)C_{n-2}\right.$$
$$\left.+\left(\frac{9k+4}{k}+6\lambda\right)C_n-\left(k+1-\frac{2\lambda}{k}\right)C_{n+2}\right]P_{n+1}$$
$$+(k+3)\left[\left(1+\frac{4\lambda}{k+2}\right)C_{n-1}-\frac{k-2}{k+2}C_{n+1}\right]$$
$$P_{n+2}\Big\} \qquad [66]$$

$$\tau_{\alpha\beta}=\frac{p}{16\mu}\Big(-\Big\{S_{n-1}-\left[1-\frac{4\lambda}{k-2}\right]S_{n+1}\Big\}P_n'_{-2}$$
$$+2\Big\{\frac{1}{k-1}\left[k-2+\frac{2\lambda}{k}\right]S_{n-2}+\frac{2(1+3\lambda)}{k-1}S_n$$
$$-\left[\frac{k}{k-1}-\frac{2\lambda}{k}\right]S_{n+2}\Big\}P'_{n-1}$$
$$-\Big\{\frac{k-3}{k-1}S_{n-2}+\frac{1}{k^2-1}\left[3k^2+2k+3\right.$$
$$\left.+\frac{4\lambda(3k^2+10k+5)}{k+2}\right]S_{n-1}-\frac{1}{k^2-1}\left[3k^2-2k+3\right.$$
$$\left.-\frac{4\lambda(3k^2-10k+5)}{k-2}\right]S_{n+1}-\frac{k+3}{k+1}S_{n+2}\Big\}P_n'$$
$$+2\Big\{\left[\frac{k}{k+1}+\frac{2\lambda}{k}\right]S_{n-2}+\frac{2(1+3\lambda)}{k+1}S_n$$
$$-\frac{1}{k+1}\left[k+2+\frac{2\lambda}{k}\right]S_{n+2}\Big\}P'_{n+1}$$
$$-\Big\{\left[1+\frac{4\lambda}{k+2}\right]S_{n-1}-S_{n+1}\Big\}P'_{n+2}\Big)$$
$$(n=1,2,3,\ldots\ldots) \qquad \ldots[66]\ (con't)$$

where $k=2n+1$
and

$$\lambda=1-2\nu \qquad \ldots[67]$$

The foregoing Legendre series for $\mu\sigma_\alpha$ and $\mu\tau_{\alpha\beta}/p$ of $[A_n]$ and $[B_n]$ terminate because the functions so expanded are polynomials in p.[a] The stresses σ_α, $\tau_{\alpha\beta}/p$, without prior multiplication by μ, are irrational functions of p, and would thus give rise to infinite Legendre series. This accounts in retrospect for the artificial introduction of the factor $1/\mu_0$ in the boundary conditions, Equations [46]. We note, furthermore, that σ_α and $\tau_{\alpha\beta}$ of $[A_n]$ involve the Legendre polynomials of order $n-1$ to $n+3$ and their derivatives, respectively; the corresponding stresses of $[B_n]$ involve the polynomials of order $n-2$ to $n+2$, and their derivatives.[20] Unfortunately, linear combinations of the elements of the aggregates $[D_n]$, $[E_n]$, giving rise to stress components σ_α and $\tau_{\alpha\beta}$ which involve exclusively P_n and P_n', respectively, are not available. This precludes an explicit determination of the coefficients of superposition through solution of two simultaneous equations at a time. Therefore we are compelled to accept an infinite system of linear algebraic equations for the coefficients a_0 a_n, b_n $(n=1,2,\ldots)$ appearing in $[R^*]$, Equation [63]. This system is obtained by equating to ξ_n and η_n of Equations [55] the coefficients of P_n and P_n' in $\mu_0\sigma_\alpha(\alpha_0,\beta)$ and $\mu_0\,\tau_{\alpha\beta}(\alpha_0,\beta)/p$ of solution $[R^*]$. A trivial computation yields

$$a_{n+1}\left[-\frac{(k+1)(k+3)(k+5)}{32(k+2)}C_{n+2}\right]$$
$$+a_n\frac{(k+1)(k+3)}{32}\left[C_{n+2}+\frac{3k+4}{k+2}C_{n+1}\right]$$
$$+a_{n-1}\frac{(k-1)(k+1)}{32}\left[-\frac{3k-5}{k-2}C_{n+1}\right.$$
$$\left.-\frac{3k+5}{k+2}C_{n-1}\right]$$
$$+a_{n-2}\frac{(k-3)(k-1)}{32}\left[\frac{3k-4}{k-2}C_{n-1}+C_{n-3}\right]$$
$$+a_{n-3}\left[-\frac{(k-5)(k-3)(k-1)}{32(k-2)}C_{n-1}\right]$$
$$+b_{n+2}\frac{k+1}{32}\Big\{\left[-1+\frac{4\lambda}{k+2}\right]C_{n+2}$$
$$+\frac{k+6}{k+2}C_{n+1}\Big\}$$
$$+b_{n+1}\frac{1}{16}\Big\{\left[k+2-\frac{2\lambda(k+1)}{k+2}\right]C_{n+2}$$
$$+\left[-\frac{9k+14}{k+2}-6\lambda\right]C_{n+1}+\Big[-(k+1)$$
$$+\frac{2\lambda}{k+2}\Big]C_{n-1}\Big\} \qquad \ldots[68]$$

[a] The analogous expansions for σ_α, $\tau_{\alpha\beta}$ of $[D_n]$ and of $[E_{n+1}]-[E_n]$ are found to involve the polynomials (and their derivatives) of order $n-3$ to $n+3$ and $n-2$ to $n+3$, respectively. This reveals the specific simplifications arising from the linear combinations of Equations [64].

$$+ b_n \frac{1}{32}\Bigg\{-(k+3)C_{n+2} + \left[-\frac{3k^2-9k-26}{k+2} + \frac{4\lambda(3k-5)}{k-2}\right]C_{n+1} + \left[\frac{3k^2+9k-26}{k-2} + \frac{4\lambda(3k+5)}{k+2}\right]C_{n-1} + (k-3)C_{n-3}\Bigg\}$$

$$+ b_{n-1}\frac{1}{16}\Bigg\{\left[k-1-\frac{2\lambda}{k-2}\right]C_{n+1} + \left[-\frac{9k-14}{k-2} - 6\lambda\right]C_{n-1} + \left[-(k-2) - \frac{2\lambda(k-1)}{k-2}\right]C_{n-3}\Bigg\}$$

$$+ b_{n-2}\frac{k-1}{32}\Bigg\{-\frac{k-6}{k-2}C_{n-1} + \left[1+\frac{4\lambda}{k-2}\right]C_{n-3}\Bigg\} = \xi_n \qquad \text{[68] (con't)}$$

$$(n = 0, 1, 2, \ldots\ldots)$$

$$a_{n+1}\left[\frac{(k+3)(k+5)}{16(k+2)}S_{n+3}\right] + a_n\frac{k+3}{16}[-S_{n+3} - 3S_{n+1}]$$

$$+ a_{n-1}\frac{3}{16}\left[\frac{k^2-2k-1}{k-2}S_{n+1} + \frac{k^2+2k-1}{k+2}S_{n-1}\right]$$

$$+ a_{n-2}\frac{k-3}{16}[-3S_{n-1} - S_{n-3}]$$

$$+ a_{n-3}\left[\frac{(k-5)(k-3)}{16(k-2)}S_{n-3}\right]$$

$$+ b_{n+2}\frac{1}{16}\Bigg\{\left[1-\frac{4\lambda}{k+2}\right]S_{n+3} - S_{n+1}\Bigg\}$$

$$+ b_{n+1}\frac{1}{8(k+1)}\Bigg\{\left[-(k+2) + \frac{2\lambda(k+1)}{k+2}\right]S_{n+3} + (2+6\lambda)S_{n+1} + \left[k+\frac{2\lambda}{k+2}\right]S_{n-1}\Bigg\}$$

$$+ b_n\frac{1}{16(k+1)(k-1)}\Bigg\{(k-1)(k+3)S_{n+3} + \left[3k^2-2k+3-\frac{4\lambda(3k^2-10k+5)}{k-2}\right]S_{n+1} + \left[-(3k^2+2k+3) - \frac{4\lambda(3k^2+10k+5)}{k+2}\right]S_{n-1} - (k-3)(k+1)S_{n-3}\Bigg\} \qquad \text{[69]}$$

$$+ b_{n-1}\frac{1}{8(k-1)}\Bigg\{\left[-k-\frac{2\lambda}{k-2}\right]S_{n+1} + [2+6\lambda]S_{n-1} + \left[k-2+\frac{2\lambda(k-1)}{k-2}\right]S_{n-3}\Bigg\}$$

$$+ b_{n-2}\frac{1}{16}\Bigg\{S_{n-1} + \left[-1-\frac{4\lambda}{k-2}\right]S_{n-3}\Bigg\} = \eta_n$$

$$(n = 1, 2, 3, \ldots\ldots)$$

The hyperbolic functions $C_n(\alpha)$, $S_n(\alpha)$ appearing in Equations [68] and [69] are to be evaluated for $\alpha = \alpha_0$. The parameters k and λ are given by Equations [40] and [67]. Furthermore, Equations [68] and [69] require the supplementary definitions $b_0 = b_{-1} = b_{-2} = 0$.

The problem of two spherical cavities, stated in Equations [46] and [47] or [48], has been reduced to the solution of the infinite system of linear algebraic Equations [68] and [69]. The formal solution of the problem is given by

$$[S] = [U] - \frac{\sqrt{2}P}{8\pi(1-\nu)}[E_0] + a_0[A_0] + \sum_{n=1}^{\infty}\{a_n[A_n] + b_n[B_n]\} \qquad \text{[70]}$$

as is confirmed by recourse to Equations [49], [62], and [63].

Numerical Examples and Discussion

An application of convergence criteria to the infinite series in Equation [70] is prohibitive in view of the unwieldy character of Equations [68] and [69]. Therefore we are forced to rely upon such indications regarding the convergence of the solution, Equation [70], as are obtainable from its application to, and numerical evaluation for specific examples. In preparation for such applications, we observe that the system of Equations [68] and [69] conforms to the following matrix scheme, in which the asterisks denote nonvanishing coefficients:

$$\begin{bmatrix}
* & * & * & * & 0 & 0 & 0 & 0 & 0 & 0 & 0 & 0 & 0 & 0 & 0 & 0 & \cdots \\
* & * & * & * & * & * & 0 & 0 & 0 & 0 & 0 & 0 & 0 & 0 & 0 & 0 & \cdots \\
* & * & * & * & * & * & 0 & 0 & 0 & 0 & 0 & 0 & 0 & 0 & 0 & 0 & \cdots \\
* & * & * & * & * & * & * & * & 0 & 0 & 0 & 0 & 0 & 0 & 0 & 0 & \cdots \\
* & * & * & * & * & * & * & * & 0 & 0 & 0 & 0 & 0 & 0 & 0 & 0 & \cdots \\
* & * & * & * & * & * & * & * & * & * & 0 & 0 & 0 & 0 & 0 & 0 & \cdots \\
* & * & * & * & * & * & * & * & * & * & 0 & 0 & 0 & 0 & 0 & 0 & \cdots \\
0 & 0 & * & * & * & * & * & * & * & * & * & * & 0 & 0 & 0 & 0 & \cdots \\
0 & 0 & * & * & * & * & * & * & * & * & * & * & 0 & 0 & 0 & 0 & \cdots \\
0 & 0 & 0 & 0 & * & * & * & * & * & * & * & * & * & * & 0 & 0 & \cdots \\
0 & 0 & 0 & 0 & * & * & * & * & * & * & * & * & * & * & 0 & 0 & \cdots \\
\cdots & \cdots & \cdots & \cdots & \cdots & \cdots & \cdots & \cdots & \cdots & \cdots & \cdots & \cdots & \cdots & \cdots & \cdots & \cdots & \cdots
\end{bmatrix}
\begin{bmatrix} a_0 \\ b_1 \\ a_1 \\ b_2 \\ a_2 \\ b_3 \\ a_3 \\ b_4 \\ a_4 \\ b_5 \\ a_5 \\ \cdots \end{bmatrix}
=
\begin{bmatrix} \xi_0 \\ \eta_1 \\ \xi_1 \\ \eta_2 \\ \xi_2 \\ \eta_3 \\ \xi_3 \\ \eta_4 \\ \xi_4 \\ \eta_5 \\ \xi_5 \\ \cdots \end{bmatrix} \qquad \text{[71]}$$

The solution of Equations [71] necessitates a method of successive approximations. In the particular examples which follow, the solution was accomplished by means of the usual segmentation process in which the matrix of the system is truncated so as to yield n equations in n unknowns. The value of n is then increased successively until a sufficient number of unknowns are stabilized within the limits of accuracy necessary to assure the desired number of significant figures in the stress values sought. A partial check on the degree of accuracy attained at every stage of the process is provided by a comparison of the corresponding surface tractions at $\alpha = \pm\alpha_0$ with their prescribed values.

We now discuss the numerical results obtained for the simplest technically significant case of loading in which the cavities are free from tractions, and the state of stress at infinity is one of hydrostatic tension $\sigma_x = \sigma_y = \sigma_z = 1$. Here $f(\beta) = g(\beta) = 0$ in Equations [46], and the right-hand members ξ_n, η_n of Equations [68] and [69], and thus also of Equations [71], are given by Equations [60] with $\sigma = 1$. The coefficients of superposition a_n, b_n were determined for Poisson's ratio $\nu = 1/4$ and for two values of the distance ratio $s = \Delta/2\vartheta$. Table 1 shows the values of a_n and b_n for $s = 3.76220$ and $s = 2$, which correspond to $\alpha_0 = 2$ and $\alpha_0 = 1.31696$, respectively. Only coefficients which were used in the subsequent stress computations are included, and the values given are stabilized in the sense that the results of the last two successive approximations coincide within the number of digits shown. This degree of stabilization was found to insure the stabilization of the computed stresses to within at least three significant figures; it required the solution of a maximum of ten and sixteen simultaneous equations, respectively, for the larger

TABLE 1 NUMERICAL VALUES OF COEFFICIENTS OF SUPERPOSITION FOR $\sigma_x = \sigma_y = \sigma_z = 1$ AT INFINITY; $\nu = 1/4$

	$s = 3.762198$		$s = 2$	
n	a_n	b_n	a_n	b_n
0	-1.401568×10^{-1}		-1.086921×10^{-1}	
1	-2.7858×10^{-2}	-9.092×10^{-3}	-8.9324×10^{-3}	-5.3731×10^{-3}
2	-4.891×10^{-3}	8.25×10^{-7}	-6.1374×10^{-4}	8.73×10^{-4}
3	-8.66×10^{-4}	2.2×10^{-4}	-4.182×10^{-4}	1.6×10^{-4}
4	-1.4×10^{-4}	2×10^{-5}	-2.88×10^{-5}	1×10^{-5}
5			-2.02×10^{-7}	7×10^{-8}
6			-1.5×10^{-6}	
7			-1×10^{-6}	

and the smaller of the two distance ratios considered. As was to be anticipated, the convergence of the solution becomes slower as the distance ratio approaches unity. Indeed, the solution diverges for the limiting case $s = 1$, $a_0 = 0$ in which the two cavities touch each other, as is apparent from the restrictions underlying the Expansion [56]. This limiting case, therefore, calls for a separate treatment.

On the basis of the coefficients of superposition listed in Table 1, the principal stresses at the poles and equators of the two cavities were evaluated. These results are summarized in Fig 2 which shows the upper cavity only. The numbers given here again represent stabilized values. Moreover, it is seen that those normal stresses which should vanish by virtue of the boundary conditions, do not exceed 0.005, which indicates that the maximum error in the remaining stresses is apt to be less than 1 per cent of the tractions applied at infinity.

As the distance ratio s approaches infinity, the two sources of stress concentration cease to interfere with each other, and the stress concentration around each cavity must tend toward that produced by a single spherical cavity in a body under hydrostatic tension at infinity. According to the classical solution for this limiting case[21]

$$\sigma_t = \frac{3}{2} \qquad [72]$$

in which σ_t is the normal stress at the surface of the cavity, acting on any plane passing through its center.

The results shown in Fig. 2 reveal that for a distance ratio $s = 3.76$ the limiting condition of noninterference is practically attained. The second set of stress values shown in Fig. 2 applies to $s = 2$ and illustrates the stress-concentration interference The mutual effect of the two cavities consists in raising the tangential stresses at the interior poles of the cavities, and to a lesser extent, also those at the exterior poles, while relieving the concentration in σ_β at the equators. The stress σ_γ at the equator is seen to be unaffected by the presence of a second cavity. It is interesting to note that even when the distance between the interior poles is but one diameter, the interference is relatively slight. Thus none of the stresses computed for this case deviates from the limiting value of $^3/_2$ by as much as 5 per cent. In the analogous plane problem (2), the interference effect in the foregoing sense is approximately 20 per cent at the same distance ratio.

In conclusion, it should be pointed out that superposition upon the solution discussed of the uniform hydrostatic stress field $\sigma_\alpha = \sigma_\beta = \sigma_\gamma = -1$ yields the corresponding stress values for the case in which the cavities are under constant unit internal pressure, and the medium is free from loading at infinity.

[21] See, for example reference (10), p. 326.

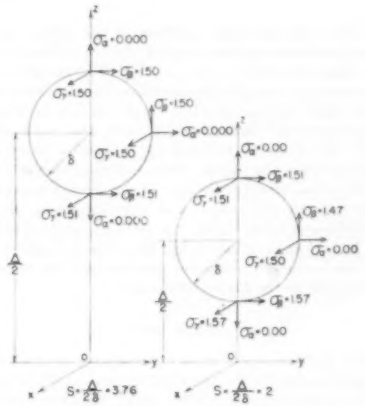

FIG. 2 PRINCIPAL STRESSES AT EQUATORS AND POLES FOR $\sigma_x = \sigma_y = \sigma_z = 1$ AT INFINITY; $\nu = 1/4$

ACKNOWLEDGMENT

The authors are greatly indebted to Mr. R. A. Eubanks, Graduate Assistant at Illinois Institute of Technology, for his invaluable aid both in the analytical and numerical work underlying this investigation.

BIBLIOGRAPHY

1 "Plane Strain Problems in Bipolar Co-Ordinates," by G. B. Jeffery, Philosophical Transactions of the Royal Society of London, series A, vol. 221, 1921, pp. 265–293.

2 "On the Stresses in a Plate Containing Two Circular Holes," by Chih-Bing Ling, *Journal of Applied Physics*, vol. 19, 1948, pp. 77–82.

3 "Tratado de Elasticidad," by E. Butty, Centro Estudiantes de Ingenieria, Buenos Aires, Argentine, 1946.

4 "Applications des Pontentiels," by J. Boussinesq, Gauthier-Villars, Paris, France, 1885.

5 "Kerbspannungslehre," by H. Neuber, J. W. Edwards, Ann Arbor, Mich., 1944.

6 "Stress Concentration Around an Ellipsoidal Cavity in an Infinite Body Under Arbitrary Plane Stress Perpendicular to the Axis of Revolution of the Cavity," by M. A. Sadowsky and E. Sternberg, Trans. ASME., vol. 69, 1947, pp. 191–201.

7 "Stress Concentration Around a Triaxial Ellipsoidal Cavity," by M. A. Sadowsky and E. Sternberg, JOURNAL OF APPLIED MECHANICS, Trans. ASME, vol. 71, 1949,pp. 149–157.

8 "The Theory of Spherical and Ellipsoidal Harmonics," by E. W. Hobson, University Press, Cambridge, England, 1931.

9 "A Treatise on the Mathematical Theory of Elasticity," by A. E. H. Love, fourth edition, Dover Publications, New York, N. Y., 1944.

10 "Theory of Elasticity," by S. Timoshenko, McGraw-Hill Book Company, Inc., New York, N. Y., 1934.

The Effect of a Rigid Circular Inclusion on the Bending of a Thick Elastic Plate[1]

By R. A. HIRSCH,[2] PROVIDENCE, R. I

The three-dimensional problem of the effect of a rigid circular inclusion on the bending of a thick elastic plate is solved approximately by the method of E. Reissner (1, 2).[3] Comparison is made for the limiting cases of vanishing inclusion size, (plane strain), and vanishing thickness (Poisson-Kirchoff plate theory), with the work of J. N. Goodier (3) and M. Goland (4). Graphs showing the transition from the plane-strain solution to the Poisson-Kirchoff solution are given. Stress concentrations are calculated and plotted versus the inclusion diameter-plate thickness ratio. The stress concentrations are found to be less than predicted by the classical plate theory when the inclusion diameter approaches the same order of magnitude as the plate thickness.

Introduction

THE problem of the effect of inclusions on the stresses in plates has been discussed for the cases of plane strain and transverse flexure according to the Poisson-Kirchoff theory of thin plates. These cases were discussed by Goodier (3) and Goland (4), respectively. It is the purpose of this paper to discuss the effect of a rigid inclusion on the bending of plates according to E. Reissner's theory of bending (1, 2). A. E. Green (5) has indicated a series method for the solution of the three-dimensional problem. The first terms of the series lead to results which correspond to the theory under consideration.

In brief review, the Reissner theory takes account of transverse shear deformation which is neglected in ordinary plate theory. The consequence of taking account of the transverse shear deformation is that a sixth-order system of equations is developed so that it is possible and in fact necessary to satisfy the three boundary conditions of the problem instead of only the two Kirchoff conditions. The solution of the new system of equations for the case where there is no distribution of transverse load is carried out in terms of the transverse deflection w and a stress function χ. All bending moments, shear-force resultants, and displacements are found by differentiating these quantities.

In discussing problems of stress concentration, due to circular holes or inclusions, it is convenient to use polar co-ordinates. The transformation to this system has been carried out by E. Reissner, and the equations as well as the general solutions are available elsewhere (1, 2).

Solution for Pure Bending

Consider an infinite plate of a homogeneous isotropic material with a circular inclusion of rigid material attached to the plate. The orientation of the co-ordinate systems and the loading is shown in Fig. 1. Employing Reissner's nomenclature

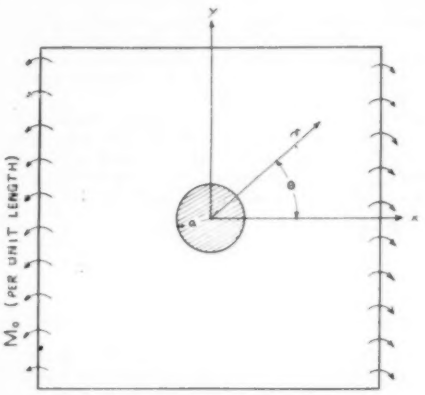

FIG. 1 ORIENTATION OF CO-ORDINATE AXES

(1, 2), the loading conditions at $r = \infty$ require that

$$\left.\begin{aligned} M_r &= \frac{M_0}{2}(1 + \cos 2\theta) \\ H_{r\theta} &= -\frac{M_0}{2}\sin 2\theta \\ V_r &= 0 \end{aligned}\right\} \quad \ldots\ldots\ldots\ldots [1]$$

At the edge of the inclusion ($r = a$) the condition of perfect rigidity is satisfied by allowing no deflection or rotation, so that

$$w = \beta_r = \beta_\theta = 0 \quad \ldots\ldots\ldots\ldots [2]$$

Appropriate expressions for the deflection and the stress function are given in reference (1). The resulting expressions for the bending and twisting moments and the transverse shear forces are

$$V_r = \frac{2}{r}\left[B_2 r^{-2} + D_2 K_2(\xi)\right]\cos 2\theta \quad \ldots\ldots\ldots [3]$$

$$V_\theta = \frac{2}{r}\left[B_2 r^{-2} + D_2\left\{K_2(\xi) + \frac{1}{2}\xi K_1(\xi)\right\}\right]\sin 2\theta \quad \ldots [4]$$

---

[1] This paper is from a thesis submitted in partial fulfillment of the requirements for the degree of MS in Applied Mathematics at Brown University.

[2] Graduate Student, Brown University.

[3] Numbers in parentheses refer to the Bibliography at the end of the paper.

Contributed by the Applied Mechanics Division and presented at the Annual Meeting, Atlantic City, N. J., November 25–30, 1951, of THE AMERICAN SOCIETY OF MECHANICAL ENGINEERS.

Discussion of this paper should be addressed to the Secretary, ASME, 29 West 39th Street, New York, N. Y., and will be accepted until April 10, 1952, for publication at a later date. Discussion received after the closing date will be returned.

NOTE: Statements and opinions advanced in papers are to be understood as individual expressions of their authors and not those of the Society. Manuscript received by ASME Applied Mechanics Division, November 16, 1950. Paper No. 51—A-12.

$$M_r = -(1+\nu)A_0 + (1-\nu)F_0 r^{-2} + [-2(1-\nu)E_2 - 6(1-\nu)F_2 r^{-4} - \nu B_2 r^{-2}]\cos 2\theta + \left\{ -\frac{12 B_2}{r^2\xi^2} - D_2\left[\frac{12K_2(\xi)}{\xi^2} + \frac{4K_1(\xi)}{\xi}\right]\right\}\cos 2\theta \quad \ldots [5]$$

$$M_\theta = -(1+\nu)A_0 - (1-\nu)F_0 r^{-2} + [2(1-\nu)E_2 - B_2 r^{-2} + 6(1-\nu)F_2 r^{-4}]\cos 2\theta + \left\{ \frac{12B_2}{r^2\xi^2} + D_2\left[\frac{12K_2(\xi)}{\xi^2} + \frac{4K_1(\xi)}{\xi}\right]\right\}\cos 2\theta \quad \ldots [6]$$

$$H_{r\theta} = 2(1-\nu)\left[E_2 + \frac{1}{4}B_2 r^{-2} - 3F_2 r^{-4}\right]\sin 2\theta - \left\{ \frac{12B_2}{r^2\xi^2} + D_2\left[\frac{12K_2(\xi)}{\xi^2} + \frac{4K_1(\xi)}{\xi} + K_0(\xi)\right]\right\}\sin 2\theta \quad \ldots [7]$$

$$\xi = \frac{\sqrt{10}\, r}{h}$$

where ν is Poisson's ratio. From the boundary conditions, Equations [1] and [2], the constants A_0, E_0, F_0, B_2, D_2, E_2, and F_2 may be determined

$$A_0 = -\frac{M_0}{2(1+\nu)}$$

$$E_0 = (1 - 2\ln a)\frac{M_0 a^2}{4(1+\nu)}$$

$$F_0 = \frac{M_0 a^2}{2(1+\nu)}$$

$$E_2 = -\frac{M_0}{4(1-\nu)} \quad \ldots [8]$$

$$D_2 = \frac{\dfrac{2M_0}{1-\nu}}{K_2(\mu) + \left[\dfrac{1}{2}\mu + \dfrac{4}{\mu(1-\nu)}\right]K_1(\mu)}$$

$$B_2 = \frac{-\dfrac{2M_0 a^2}{1-\nu}\left[K_2(\mu) + \dfrac{1}{2}\mu K_1(\mu)\right]}{K_2(\mu) + \left[\dfrac{1}{2}\mu + \dfrac{4}{\mu(1-\nu)}\right]K_1(\mu)}$$

$$F_2 = \frac{-\dfrac{M_0 a^4}{4(1-\nu)}\left\{K_2(\mu) + \left[\dfrac{1}{2}\mu - \dfrac{4}{\mu(1-\nu)}\right]K_1(\mu)\right\}}{K_2(\mu) + \left[\dfrac{1}{2}\mu + \dfrac{4}{\mu(1-\nu)}\right]K_1(\mu)} \quad \ldots [8]\ (Con't)$$

In the foregoing the K_n are the modified Bessel functions (6) and the notation $\mu = \sqrt{10}\, a/h$ has been adopted. Substituting the values of the constants from Equations [8] into Equations [3] to [7], the final expressions for the bending and twisting moments and shear-force resultants are obtained. To conserve space let

$$G(\mu) \equiv K_2(\mu) + \left[\frac{1}{2}\mu + \frac{4}{\mu(1-\nu)}\right]K_1(\mu) \quad \ldots [9]$$

then

$$V_\theta = \frac{4M_0 \sin 2\theta}{a(1-\nu)\,G(\mu)}\left\{\frac{a}{r}K_2(\xi) - \frac{a^2}{r^2}\left[K_2(\mu) + \frac{1}{2}\mu K_1(\mu)\right]\right\} \quad \ldots [10]$$

$$V_r = \frac{4M_0 \cos 2\theta}{a(1-\nu)G(\mu)}\left\{\frac{a}{r}\left[K_2(\xi) + \frac{1}{2}\xi K_1(\xi)\right] - \frac{a^2}{r^2}\left[K_2(\mu) + \frac{1}{2}\mu K_1(\mu)\right]\right\} \quad \ldots [11]$$

$$M_r = M_0\left\{\frac{1}{2} + \frac{1}{2}\frac{1-\nu}{1+\nu}\frac{a^2}{r^2} + \cos 2\theta\left[\frac{1}{2} + \frac{\left(\frac{3}{2}\frac{a^4}{r^4} + \frac{2\nu}{1-\nu}\frac{a^2}{r^2}\right)K_2(\mu) + \left(\frac{3}{4}\mu\frac{a^4}{r^4} + \frac{\nu\mu}{1-\nu}\frac{a^2}{r^2} - \frac{6}{\mu(1-\nu)}\frac{a^4}{r^4}\right)K_1(\mu)}{G(\mu)}\right] + \frac{4\cos 2\theta}{(1-\nu)\,G(\mu)}\left[\frac{6}{\xi^2}\left(\frac{a^2}{r^2}K_2(\mu) - K_2(\xi)\right) + \frac{1}{\xi}\left(3\frac{a^2}{r^2}K_1(\mu) - 2K_1(\xi)\right)\right]\right\} \quad \ldots [12]$$

$$M_\theta = M_0\left\{\frac{1}{2} - \frac{1}{2}\frac{1-\nu}{1+\nu}\frac{a^2}{r^2} + \cos 2\theta\left[-\frac{1}{2} + \frac{\left(\frac{2}{1-\nu}\frac{a^2}{r^2} - \frac{3}{2}\frac{a^4}{r^4}\right)K_2(\mu) + \left(\frac{\mu}{1-\nu}\frac{a^2}{r^2} - \frac{3}{4}\mu\frac{a^4}{r^4} + \frac{6}{\mu(1-\nu)}\frac{a^4}{r^4}\right)K_1(\mu)}{G(\mu)}\right] + \frac{4\cos 2\theta}{(1-\nu)G(\mu)}\left[\frac{6}{\xi^2}\left(K_2(\xi) - \frac{a^2}{r^2}K_2(\mu)\right) + \frac{1}{\xi}\left(2K_1(\xi) - 3\frac{a^2}{r^2}K_1(\mu)\right)\right]\right\} \quad \ldots [13]$$

$$H_{r\theta} = M_0 \sin 2\theta\left\{-\frac{1}{2} + \frac{\frac{a^2}{r^2}\left[K_2(\mu) + \frac{1}{2}\mu K_1(\mu)\right]\left(\frac{3}{2}\frac{a^2}{r^2} - 1\right) - \frac{6}{\mu(1-\nu)}K_1(\mu)}{G(\mu)} + \frac{2}{(1-\nu)G(\mu)}\left[\frac{12}{\xi^2}\left(\frac{a^2}{r^2}K_2(\mu) - K_2(\xi)\right) + \frac{2}{\xi}\left(3\frac{a^2}{r^2}K_1(\mu) - 2K_1(\xi)\right) - K_0(\xi)\right]\right\} \quad \ldots [14]$$

At the bond between plate and inclusion, Equations [10] to [14] become

$$V_\theta(a, \theta) = 0 \quad [15]$$

$$V_r(a, \theta) = -\frac{4M_0 \cos 2\theta}{a(1-\nu)}\left[\frac{\mu K_1(\mu)}{2G(\mu)}\right] \quad [16]$$

$$M_r(a, \theta) = M_0\left\{\frac{1}{1+\nu} + \frac{\cos 2\theta}{(1-\nu)G(\mu)}\,[2K_2(\mu) + \mu K_1(\mu)]\right\} \quad [17]$$

$$M_\theta(a, \theta) = \nu M_0\left\{\frac{1}{1+\nu} + \frac{\cos 2\theta}{(1-\nu)G(\mu)}\,[2K_2(\mu) + \mu K_1(\mu)]\right\} \quad [18]$$

$$H_{r\theta}(a, \theta) = -\frac{2M_0 \sin 2\theta}{(1-\nu)}\left[\frac{K_2(\mu)}{G(\mu)}\right] \quad [19]$$

Limiting Cases of the Solution

The limiting forms of the foregoing solution are obtained by (*a*) vanishing inclusion size, and (*b*) vanishing plate thickness. It is a requirement of a good solution that the limiting forms will agree reasonably well with the plane-strain solution for case (*a*) and with the Poisson-Kirchoff solution for case (*b*). This requirement has been stated previously by D. C. Drucker (7).

Case (*a*):

$$\lim_{a/h \to 0} V_r(a, \theta) = 0 \quad [20]$$

$$\lim_{a/h \to 0} M_r(a, \theta) = M_0\left[\frac{1}{1+\nu} + \frac{2}{3-\nu}\cos 2\theta\right] \quad [21]$$

$$\lim_{a/h \to 0} M_\theta(a, \theta) = \nu M_0\left[\frac{1}{1+\nu} + \frac{2}{3-\nu}\cos 2\theta\right] \quad [22]$$

$$\lim_{a/h \to 0} H_{r\theta}(a, \theta) = -M_0\left[\frac{2}{3-\nu}\right]\sin 2\theta \quad [23]$$

Fig. 2 shows the comparison of Equations [21] and [22], for $\theta = 0$ and $\pi/2$, respectively, with the results obtained by Goodier (3). The agreement is quite good for M_r at all values of Poisson's ratio. The maximum difference is less than 3 per cent.

Case (*b*):

$$\lim_{a/h \to \infty} V_r(a, \theta) = -\frac{4M_0 \cos 2\theta}{a(1-\nu)} \quad [24]$$

$$\lim_{a/h \to \infty} M_r(a, \theta) = M_0\left[\frac{1}{1+\nu} + \frac{2\cos 2\theta}{1-\nu}\right] \quad [25]$$

$$\lim_{a/h \to \infty} M_\theta(a, \theta) = \nu M_0\left[\frac{1}{1+\nu} + \frac{2\cos 2\theta}{1-\nu}\right] \quad [26]$$

$$\lim_{a/h \to \infty} H_{r\theta}(a, \theta) = 0 \quad [27]$$

These expressions agree exactly with the corresponding expressions of the classical theory obtained by Goland (4).

Referring to Equation [15], it is seen that in the present theory the shear force resultant V_θ vanishes at the boundary between the inclusion and the plate. The classical theory gives the value

$$V_\theta(r, \theta) = -\frac{4M_0 \sin 2\theta}{a(1-\nu)}\,\frac{a^3}{r^3} \quad [28]$$

Employing the procedure of reference (1) it can be shown that V_θ grows from the edge value zero to the value of Equation [28],

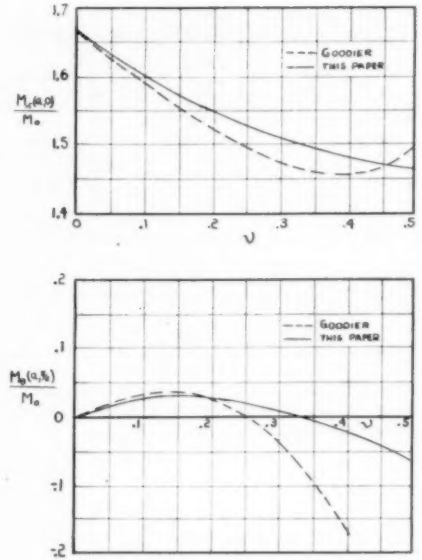

Fig. 2 Comparison of Limiting Case of Vanishing Inclusion Size With Plane-Strain Solution

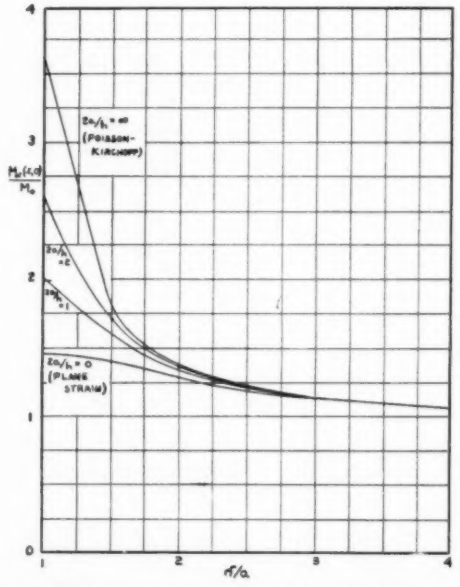

Fig. 3 Transition of Radial Bending Moment From Plane-Strain Solution to Poisson-Kirchoff Solution ($\nu = 0.3$)

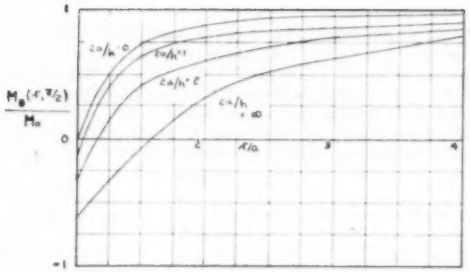

FIG. 4 TRANSITION OF ANGULAR BENDING MOMENT FROM PLANE-STRAIN SOLUTION TO POISSON-KIRCHOFF SOLUTION ($\nu = 0.3$)

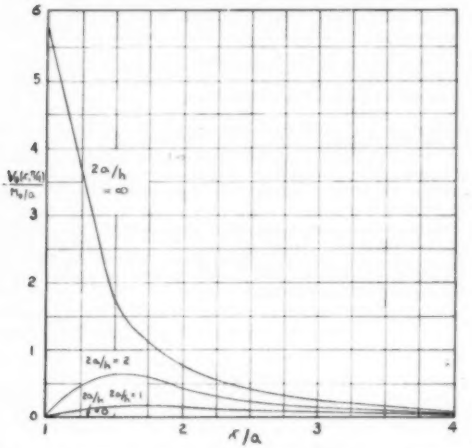

FIG. 5 TRANSITION OF RADIAL TRANSVERSE SHEAR FORCE RESULTANT FROM PLANE-STRAIN SOLUTION TO POISSON-KIRCHOFF SOLUTION ($\nu = 0.3$)

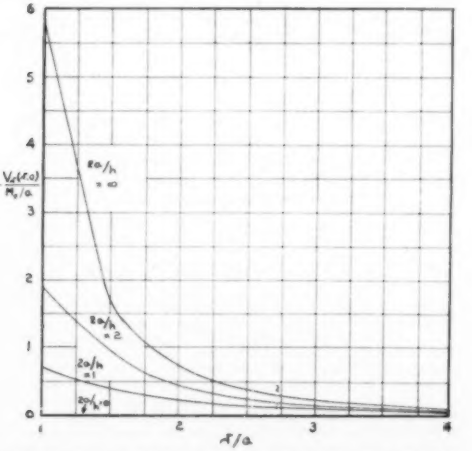

FIG. 6 TRANSITION OF ANGULAR TRANSVERSE SHEAR-FORCE RESULTANT FROM PLANE-STRAIN SOLUTION TO POISSON-KIRCHOFF SOLUTION ($\nu = 0.3$)

within a distance of the order of magnitude of the thickness from the boundary of the inclusion, for a very thin plate.

It is interesting to note the transition from the plane-strain solution to the classical thin-plate solution. The bending moments and shear-force resultants have been plotted, using Equations [10] to [13], as functions of r/a for values of $2a/h = 0, 1, 2, \infty$. The results are presented in Figs. 3 to 6.

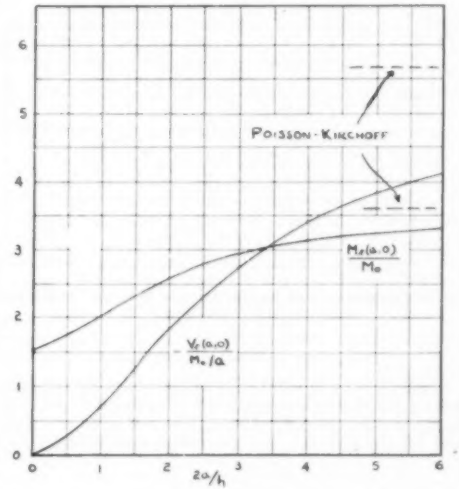

FIG. 7 STRESS CONCENTRATION AT $\theta = 0$ AND EDGE SHEAR-FORCE RESULTANT VERSUS DIAMETER-THICKNESS RATIO ($\nu = 0.3$)

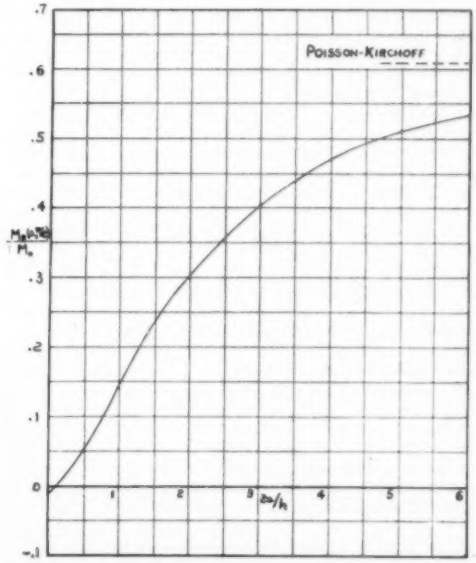

FIG. 8 STRESS CONCENTRATION AT $\theta = \pi/2$ VERSUS DIAMETER-THICKNESS RATIO ($\nu = 0.3$)

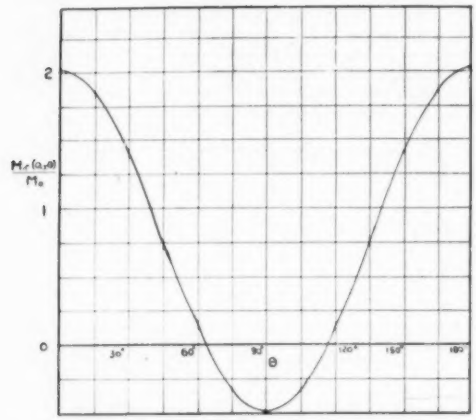

FIG. 9 DISTRIBUTION OF RADIAL BENDING MOMENT AROUND THE INCLUSION ($\nu = 0.3$, $2a/h = 1$)

DISCUSSION OF STRESS CONCENTRATIONS

In the plane-strain solution for simple tension the important stress concentrations are the stresses in the direction of the tension at $\theta = 0$ and $\pi/2$. The quantities $M_r(a, 0)$ and $M_\theta(a, \pi/2)$ are plotted versus the diameter-thickness ratio in Figs. 7[4] and 8, respectively, for Poisson's ratio of 0.3. The stress concentrations are less than predicted by the classical theory. For inclusions which have a radius of 3 times the thickness, the present calculations indicate an 8 per cent decrease for the $\theta = 0$ point. Fig. 7 also contains a plot of the edge shear-force resultant. Fig. 9 is a plot of the variation of the radial bending moment about the periphery of the inclusion for $\nu = 0.3$ and $2a/h = 1$.

BIBLIOGRAPHY

1 "The Effect of Transverse Shear Deformation on the Bending of Elastic Plates," by E. Reissner, JOURNAL OF APPLIED MECHANICS, Trans. ASME, vol. 67, 1945, pp. A-69–77.

2 "On Bending of Elastic Plates," by E. Reissner, *Quarterly of Applied Mathematics*, vol. 5, 1947, pp. 55–68.

3 "Concentration of Stress Around Spherical and Cylindrical Inclusions and Flaws," by J. N. Goodier, Trans. ASME, vol. 55, Paper APM—55-7, 1933.

4 "The Influence of the Shape and Rigidity of an Elastic Inclusion on the Transverse Flexure of Thin Plates," by M. Goland, JOURNAL OF APPLIED MECHANICS, Trans. ASME, vol. 65, 1943, pp. A-69–75.

5 "The Elastic Equilibrium of Isotropic Plates and Cylinders," by A. E. Green, Proceedings of the Royal Society of London, series A, vol. 195, February, 1949, pp. 522–533.

6 "A Treatise on Bessel Functions and Their Applications to Physics," by A. Gray, G. B. Mathews, and T. M. MacRobert, second edition, The Macmillan Company, London, England, 1931.

7 "The Photoelastic Analysis of Transverse Bending of Plates in the Standard Transmission Polariscope," by D. C. Drucker, JOURNAL OF APPLIED MECHANICS, Trans. ASME, vol. 64, 1942, pp. A-161–164.

[4] It has been brought to the author's attention that the results in Fig. 7 can be found in an MS thesis by C. C. Pai, entitled "Some Applications of a Theory of Plates Which Includes the Effect of Transverse Shear Deformation," submitted to the Massachusetts Institute of Technology in 1946.

Several Approximate Analyses of the Bending of a Rectangular Cantilever Plate by Uniform Normal Pressure

By W. A. NASH,[1] WASHINGTON, D. C.

Three methods of approximating the deflections and moments occurring in a rectangular cantilever plate subjected to uniform normal pressure over its entire surface are presented in this paper. The first is the application of the well-known finite-difference procedure. The second and third are collocation methods, one based upon polynomial solutions of the Lagrange equation, the other employing "mixed" hyperbolic-trigonometric terms satisfying this equation. In the last two methods the boundary conditions are satisfied exactly along the clamped edge and at a finite number of points along the free edges of the plate. The results obtained for the particular case of a cantilever plate with uniform normal load indicate that the use of a relatively small number of points in the collocation method yields values of deflections and moments that are in substantial agreement with those given by the finite-difference procedure. It cannot be concluded from these results that the collocation method using the assumed functions will give satisfactory results with fewer points than the finite-difference method for cantilever plates with loading different from the one investigated.

Nomenclature

The following nomenclature is used in the paper:

a = span of cantilever plate

D = flexural rigidity of plate $= \dfrac{E\,t^3}{12(1-\nu^2)}$

E = Young's modulus

M_x, M_y = bending moments per unit length of middle surface of plate

M_{xy}, M_{yx} = twisting moments per unit length of middle surface of plate

$M = \dfrac{M_x + M_y}{1+\nu}$

Q_x, Q_y = shearing forces, per unit length of middle surface of plate, parallel to z-axis

q = normal load per unit area acting on face of plate

R_x, R_y = reactions along an edge, per unit length of middle surface of plate, parallel with z-axis

t = thickness of plate

ν = Poisson's ratio = 0.3

$w = z$ — component of displacement of particle originally in middle plane of plate

x, y, z = rectangular co-ordinates

λ = lattice unit used in finite-difference analysis

Introduction

The problem of the bending of a rectangular cantilever plate under a loading normal to its surface has attracted the attention of investigators only in comparatively recent years. One of the first papers on this topic was by MacGregor (1)[2] who analyzed an infinitely long plate clamped along one edge and loaded by a concentrated force applied at the free edge. His solution was later generalized by Jaramillo (2) to include a concentrated force applied at an arbitrary point of the plate.

The problem of the bending of a cantilever plate of finite dimensions is extremely difficult to solve from the standpoint of a biharmonic analysis because of the unwieldy boundary conditions. Consequently, most investigators, to date, have confined themselves to various approximate methods. A finite-difference analysis of a cantilever plate with a span-to-chord ratio of 1:4 and loaded by a concentrated force at the middle of the longitudinal free edge was presented by Holl (3). Later, Sechler, Williams, and Fung (4, 5) carried out a detailed investigation of the deflections and moments occurring in both rectangular and skew cantilever plates subjected to uniform shear loading along the extreme free edge. Their approaches to this problem include the use of (*a*) the Rayleigh-Ritz method, using as "admissible" functions the normal modes of free vibration of clamped-free and free-free beams, respectively; and (*b*) relaxation of boundary conditions. The latter method proved to be more tedious and gave somewhat less accurate results than the former. Influence coefficients for a square cantilever plate were obtained by MacNeal (6) using an electrical analogy. His results are in close agreement with those obtained analytically by Barton (7), and experimentally by Dalley (8). The special case of an aerodynamic pressure distribution acting on a square cantilever plate has been discussed by Barton and Dalley (9). The frequencies and mode configurations of free vibration of cantilever plates having various span-to-chord ratios were obtained analytically by Young (10) and also by Barton (11).

More recently, Reissner and Stein (12) treated the problem of the combined torsion and bending of a cantilever plate of variable thickness by employing the minimum-potential-energy principle in conjunction with the assumption that the chordwise deflection shape may be represented by terms of a power series. The coefficients of these terms are taken to be arbitrary functions of the spanwise co-ordinate; minimization of the potential energy by means of the calculus of variations then leads to two ordinary linear differential equations for the bending deflections and the twist of the plate. These same differential equations were

---

[1] Physicist, Navy Department, David Taylor Model Basin. Jun. ASME.

Contributed by the Applied Mechanics Division and presented at the Annual Meeting, Atlantic City, N. J., November 25–30, 1951, of The American Society of Mechanical Engineers.

Discussion of this paper should be addressed to the Secretary, ASME, 29 West 39th Street, New York, N. Y., and will be accepted until April 10, 1952, for publication at a later date. Discussion received after the closing date will be returned.

Note: Statements and opinions advanced in papers are to be understood as individual expressions of their authors and not those of the Society. Manuscript received by ASME Applied Mechanics Division, August 3, 1950. Paper No. 51—A-28.

[2] Numbers in parentheses refer to the Bibliography at the end of the paper.

obtained by Schürch (13) using other methods in conjunction with a study of stresses and deflections in a sandwich plate.

All of the foregoing investigations, as well as that presented here, are predicated upon the ordinary thin-plate theory, which assumes that

1 The plate is composed of a material which is elastically homogeneous and isotropic.

2 The material follows Hooke's law.

3 The deflection of the plate is small compared to the thickness.

4 The thickness of the plate is small compared to its lateral dimensions.

Fundamental Equations. The well-known expressions in rectangular co-ordinates for bending and twisting moments, transverse shearing forces, and edge reactions per unit length of the middle surface of the plate, as well as the value of the corner reaction, may be found in reference (14). The Lagrange differential equation of the middle surface of the plate is (14)

$$\frac{\partial^4 w}{\partial x^4} + 2\,\frac{\partial^4 w}{\partial x^2 \partial y^2} + \frac{\partial^4 w}{\partial y^4} = \frac{q}{D} \qquad [1]$$

where w denotes deflection of plate at point (x, y); q is normal load per unit area acting on face of plate; and D represents flexural rigidity of plate.

The solution of the problem of the bending of a plate when a resultant normal load q per unit area acts on the faces of the plate thus reduces to the integration of Equation [1] subject to the boundary conditions.

Finite-Difference Method

By means of finite-difference equations it is possible to obtain approximate solutions to many plate problems which cannot be treated by exact methods. Since finite elements are used in the formation of difference-equation networks, rather than the corresponding infinitesimal elements associated with differential equations, only approximate results are obtained. The approximations usually become better as the elements become smaller.

The procedure for the finite-difference method has been examined in detail by Marcus (15) and by Holl (16). This method has been applied to plates having various contours and boundary conditions by Jensen (17), Ehasz (18), and Favre (19). Numerous references to earlier papers may be found in each of these publications.

An approximate solution to the problem of the bending of a rectangular cantilever plate having a span-to-chord ratio of 1:2 and loaded by uniform normal pressure over the entire upper surface of the plate is presented here. Use is made of the Marcus two-step membrane analog. The plate will be divided into lattice units of width $\lambda = a/2$, as indicated in Fig. 1. The notation used throughout this paper is shown therein. In applying this method it is convenient to introduce the notation

$$M = \frac{M_x + M_y}{1 + \nu} \qquad [2]$$

The procedure as outlined by Marcus (15) leads to the following linear equations

$$\left.\begin{aligned} -4\,M_5 + 2\,M_6 + M_4 + M_7 &= -q\lambda^2 \\ -4\,M_6 + M_1 + M_5 + M_2 + M_9 &= -q\lambda^2 \\ -4\,M_1 + M_6 + M_{11} + M_9 &= -q\lambda^2 \end{aligned}\right\} \qquad [3]$$

$$\left.\begin{aligned} -4\,w_5 + 2\,w_6 + w_4 &= -\frac{M_5\lambda^2}{D} \\ -4\,w_6 + w_1 + w_5 + w_9 &= -\frac{M_6\lambda^2}{D} \\ -4\,w_1 + w_6 + w_2 + w_{11} &= -\frac{M_1\lambda^2}{D} \end{aligned}\right\} \qquad [4]$$

$$\left.\begin{aligned} M_3 + M_{12} + M_1 + M_{14} &= -q\lambda^2 \\ -4\,M_2 + M_4 + M_6 + M_{13} &= -q\lambda^2 \\ -4\,M_4 + 2\,M_2 + M_5 + M_{16} &= -q\lambda^2 \end{aligned}\right\} \qquad [5]$$

$$\left.\begin{aligned} -4\,w_4 + 2\,w_3 + w_5 + w_{16} &= -\frac{M_4\lambda^2}{D} \\ -4\,w_3 + w_2 + w_4 + w_6 + w_{15} &= -\frac{M_3\lambda^2}{D} \end{aligned}\right\} \qquad [6]$$

The corner condition is

$$w_{13} + w_{11} - w_6 - w_{12} = 0 \qquad [7]$$

Along the clamped edge, since the slope is zero

$$\left.\begin{aligned} 2\,w_1\,D &= -M_9\lambda^2 \\ 2\,w_9\,D &= -M_8\lambda^2 \\ 2\,w_5\,D &= -M_7\lambda^2 \end{aligned}\right\} \qquad [8]$$

For the bending moments normal to the boundary to vanish along the free edges

$$\left.\begin{aligned} D(1-\nu)(2\,w_3 - w_4 - w_2) &= M_3\lambda^2 \\ D(1-\nu)(2\,w_4 - 2\,w_3) &= M_4\lambda^2 \\ D(1-\nu)(2\,w_1 - w_2) &= M_1\lambda^2 \\ D(1-\nu)(2\,w_2 - w_3 - w_{12}) &= 0 \\ D(1-\nu)(2\,w_3 - w_1 - w_{14}) &= 0 \end{aligned}\right\} \qquad [9]$$

For the reactions to vanish along the free edges

$$\left.\begin{aligned} &\lambda^2(M_{16} - M_5) - D(1-\nu) \times \\ &\qquad (-2\,w_{16} - 2\,w_6 + 2\,w_5 + 2\,w_{15}) = 0 \\ &\lambda^2(M_{15} - M_6) - D(1-\nu) \times \\ &\qquad (-2\,w_{15} - w_1 - w_5 + 2\,w_6 + w_{14} + w_{16}) = 0 \\ &\lambda^2(M_{14} - M_1) - D(1-\nu) \times \\ &\qquad (-2\,w_{14} - w_6 - w_{11} + 2\,w_1 + w_{15} + w_{13}) = 0 \\ &\lambda^2(M_{12} - M_3) - D(1-\nu) \times \\ &\qquad (-2\,w_{12} - w_6 - w_{15} + 2\,w_3 + w_{11} + w_{13}) = 0 \\ &\lambda^2(M_{11} - M_6) - D(1-\nu) \times \\ &\qquad (-2\,w_{11} - w_3 + 2\,w_6 + w_{12}) = 0 \end{aligned}\right\} \qquad [10]$$

Thus, using the lattice unit $\lambda = a/2$, the finite-difference procedure leads to a system of 25 linear equations containing 25 unknowns. This system of equations may be solved by Crout's method (20). The values of deflection and moment obtained by this analysis are tabulated in Table 1. Although six decimal places

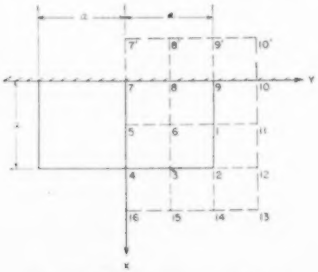

Fig. 1 Plate Co-Ordinate System

were carried throughout the computations, it does not seem justifiable to present the results to more than the four places indicated in the table.

TABLE 1. DEFLECTIONS, MOMENTS, AND SHEARS IN A RECTANGULAR CANTILEVER PLATE (SPAN-TO-CHORD RATIO 1:2) LOADED BY UNIFORM NORMAL PRESSURE

	Finite-difference method	Polynomial series (seven terms)	Polynomial series (nine terms)	Hyperbolic-trigonometric series (seven terms)
w_1	$0.1585qa^4/D$	$0.141qa^4/D$	$0.146qa^4/D$	$0.149qa^4/D$
w_2	$0.1579qa^4/D$	$0.139qa^4/D$	$0.145qa^4/D$	$0.148qa^4/D$
w_3	$0.1555qa^4/D$	$0.135qa^4/D$	$0.142qa^4/D$	$0.145qa^4/D$
w_4	$0.0635qa^4/D$	$0.057qa^4/D$	$0.059qa^4/D$	$0.060qa^4/D$
w_5	$0.0631qa^4/D$	$0.056qa^4/D$	$0.058qa^4/D$	$0.059qa^4/D$
w_6	$0.0603qa^4/D$	$0.053qa^4/D$	$0.054qa^4/D$	$0.055qa^4/D$
$(M_x)_1$	0	0	0	0
$(M_y)_1$	$0.0045qa^2$	$0.003qa^2$	$0.003qa^2$	$0.004qa^2$
$(M_x)_2$	0	0	0	0
$(M_y)_2$	$0.0065qa^2$	$0.004qa^2$	$0.005qa^2$	$0.005qa^2$
$(M_x)_3$	$-0.1248qa^2$	$-0.121qa^2$	$-0.123qa^2$	$-0.123qa^2$
$(M_y)_3$	$-0.0343qa^2$	$-0.027qa^2$	$-0.029qa^2$	$-0.030qa^2$
$(M_x)_4$	$-0.1241qa^2$	$-0.120qa^2$	$-0.121qa^2$	$-0.122qa^2$
$(M_y)_4$	$-0.0287qa^2$	$-0.021qa^2$	$-0.023qa^2$	$-0.023qa^2$
$(M_x)_5$	$-0.1271qa^2$	$-0.126qa^2$	$-0.126qa^2$	$-0.126qa^2$
$(M_y)_5$	0	0	0	0
$(M_x)_7$	$-0.5082qa^2$	$-0.501qa^2$	$-0.502qa^2$	$-0.503qa^2$
$(M_y)_7$	$-0.1525qa^2$	$-0.145qa^2$	$-0.148qa^2$	$-0.150qa^2$
$(M_x)_8$	$-0.5047qa^2$	$-0.500qa^2$	$-0.500qa^2$	$-0.501qa^2$
$(M_y)_8$	$-0.1514qa^2$	$-0.142qa^2$	$-0.144qa^2$	$-0.146qa^2$
$(M_x)_9$	$-0.4824qa^2$	$-0.489qa^2$	$-0.488qa^2$	$-0.487qa^2$
$(M_y)_9$	$-0.1447qa^2$	$-0.139qa^2$	$-0.140qa^2$	$-0.140qa^2$
$(Q_x)_4$	$0.5117qa$	$0.529qa$	$0.523qa$	$0.522qa$
$(Q_x)_6$	$0.5097qa$	$0.520qa$	$0.513qa$	$0.512qa$
$(Q_x)_7$	$0.4824qa$	$0.491qa$	$0.470qa$	$0.463qa$
$(R_x)_7$	$1.0314qa$	$1.072qa$	$1.062qa$	$1.059qa$
$(R_x)_8$	$1.0393qa$	$1.064qa$	$1.049qa$	$1.028qa$
$(R_x)_9$	$1.0563qa$	$1.032qa$	$1.032qa$	$1.060qa$

NOTE: The author realizes that the values of $(R_x)_7$, $(R_x)_8$, and $(R_x)_9$ are such as to be incompatible with over-all equilibrium. Since the elements considered in this analysis were of finite dimensions, and since the edge reactions involve several orders of differences, only approximate results may be expected.

COLLOCATION METHOD

It was stated previously that the solution of the problem of the bending of a thin plate by loads normal to its surface reduces to the integration of the Lagrange Equation [1] subject to the boundary conditions. Obviously, an approximate solution may be expected if a deflection function containing a finite number of arbitrary constants is chosen which will satisfy identically Lagrange's equation with the values of the constants being adjusted so that the boundary conditions are satisfied at a finite number of points. This procedure, in which the errors are made zero at a number of arbitrary selected points only, is called "collocation." Approximate solutions to plate problems by means of collocation methods have been presented by Cheng (21) and by Thorne (22). Two applications of this technique, as applied to the problem of the bending of the rectangular cantilever plate shown in Fig. 1, are presented here. The span-to-chord ratio is again 1:2 and the loading consists of uniform normal pressure over the entire upper surface of the plate. It is to be noted that collocation methods also may be applied to such a problem by using a series that satisfies the boundary conditions at all points but fails to satisfy the Lagrange equation. The constants may then be chosen so as to satisfy the differential equation at a finite number of points.

The solution of the Lagrange equation may be written in the form

$$w = w_1 + w_2$$

where w_1 will be taken to represent the deflection of a uniformly loaded cantilever beam, parallel to the x-axis and of span a. Thus w_1 satisfies Equation [1] and also the boundary conditions at $x = 0$ and $x = a$. However, it does not satisfy the boundary conditions along the free edges $y = \pm a$. The expression w_2 must satisfy the biharmonic equation

$$\nabla^4 w_2 = 0 \qquad [11]$$

Any solution of the biharmonic equation may be written in the form $xu_1 + u_2$, where u_1 and u_2 are harmonic functions of the rectangular co-ordinates x, y. Two types of biharmonic functions will now be considered, and linear combinations of each type will be formed to represent the function w_2.

Polynomial Series Approximation. It is well known that each of the real and also the imaginary parts of any analytic function of a complex variable satisfies Laplace's equation. If z denotes the complex variable defined by the relation $z = x + iy$, then the function z^n is analytic for all positive integral values of n. By choosing only the real part of such a function (since the deflection must be an even function with respect to y) and, in addition, by using only odd values of n, we may form the function w_2 in such a manner that the boundary conditions $w = \partial w/\partial x = 0$ are satisfied exactly along the clamped edge $x = 0$. Since the maximum moment probably occurs at or near the edge, it appears desirable to have the boundary conditions on this edge satisfied exactly.

Thus let us take the following series as approximately representing the deflection surface

$$w = \frac{qa^4}{D}\left[\left(\frac{1}{24}\frac{x^4}{a^4} - \frac{x^2}{6a^2} + \frac{x^2}{4a^2}\right) + \sum_{n=3,5,7\cdots}^{k} A_n \frac{x}{n^2a^{n+1}} R(x+iy)^n\right] \qquad [12]$$

where R denotes the real part of the complex variable. The constants A_n will be determined so as to satisfy the boundary conditions at a finite number of points. If the first seven terms in this series are used ($k = 15$), it is possible to have the bending moment normal to the edge and also the edge reaction both vanish at each of the points 1, 3, and 4, shown in Fig. 1, as well as equating the corner reaction at point 2 to zero. Thus

$$\left.\begin{aligned} M_x\left(\frac{a}{2}, a\right) &= R_y\left(\frac{a}{2}, a\right) = 0 \\ M_x(a, 0) &= R_x(a, 0) = 0 \\ M_x\left(a, \frac{a}{2}\right) &= R_x\left(a, \frac{a}{2}\right) = 0 \\ R_c &= 0 \end{aligned}\right\} \qquad [13]$$

This leads to a system of seven linear equations, each containing seven unknowns. Such a system may be solved by Crout's method. After the values of A_n have been determined, they may be substituted in Equation [12] to give the approximate representation of the deflection surface. The deflections and moments found by this approximation are indicated in Table 1.

If the first nine terms ($k = 19$) in Equation [12] are considered, it is possible to satisfy the previously mentioned boundary conditions, Equation [13], as well as two others. These were chosen so as to make

$$M_y\left(\frac{3a}{4}, a\right) = R_y\left(\frac{3a}{4}, a\right) = 0 \qquad [14]$$

In this case a system of nine linear equations, each containing nine unknowns, is obtained. The deflections and moments found by this approximation are tabulated in Table 1. Because of the small number of points used it does not appear justifiable to present the data to more than the three decimal places indicated.

Hyperbolic-Trigonometric Series Approximation. Harmonic functions may be found from Laplace's equation by the method of separation of variables. This procedure leads to four types of functions, one of which is

$$\sinh \frac{nx}{10a} \cos \frac{ny}{10a}$$

(The factor of 10 is used in the denominator so as to place the numerical values of the argument within the range that is commonly tabulated in tables of hyperbolic and circular functions.) Consequently, the deflection surface of the rectangular cantilever plate shown in Fig. 1 and loaded by uniform normal pressure may be represented approximately by the series

$$w = \frac{qa^4}{D}\left[\left(\frac{1}{24}\frac{x^4}{a^4} - \frac{x^3}{6a^3} + \frac{x^2}{4a^2}\right) + \sum_{n=1}^{k} B_n \frac{x}{na} \sinh \frac{nx}{10a} \cos \frac{ny}{10a}\right] \quad \ldots\ldots [15]$$

where the constants B_n are determined so as to satisfy the boundary conditions at a finite number of points. Again, the boundary conditions are satisfied exactly along the clamped edge.

By choosing the first seven constants B_n so as to satisfy Equations [13], a set of seven linear equations each containing seven unknowns is obtained. Again, these equations may be solved by Crout's method. However, the value of the determinant of the coefficients of the unknowns is very nearly zero and, consequently, it is necessary to carry out the calculations in Crout's method using 15 decimal places. After the values of B_n have been determined, they may be substituted in Equation [15] to give the approximate representation of the deflection surface. The deflections and moments at the various points in the plate as obtained by this method are tabulated in Table 1.

Conclusions

For the particular case of a rectangular cantilever plate with a span-to-chord ratio of 1:2 and loaded by uniform normal pressure over its entire upper surface the use of the collocation method employing a series of hyperbolic-trigonometric terms gives results that are in substantial agreement with those obtained by the classical finite-difference procedure. The calculation time involved in the use of the collocation method is considerably less than that required for a finite-difference analysis. A collocation method employing polynomial series yields results that agree almost as well with those of the finite-difference analysis as do the values obtained from the hyperbolic-trigonometric-series approximation. The application of the polynomial series is somewhat less tedious than that of the hyperbolic-trigonometric series.

BIBLIOGRAPHY

1 "Deflection of a Long Helical Gear Tooth," by C. W. MacGregor, *Mechanical Engineering*, vol. 57, 1935, p. 225.

2 "Deflections and Moments Due to a Concentrated Load on a Cantilever Plate of Infinite Length," by T. J. Jaramillo, Journal of Applied Mechanics, Trans. ASME, vol. 72, 1950, pp. 67–72.

3 "Cantilever Plate With Concentrated Edge Load," by D. L. Holl, Trans. ASME, vol. 59, 1937, p. 8.

4 "Theoretical and Experimental Effect of Sweep Upon the Stress and Deflection Distribution in Aircraft Wings of High Solidity," by Y. C. Fung, AFTR 5761, 1948 (four parts).

5 "An Initial Approach to the Over-All Structural Problems of Swept Wings Under Static Loads," by E. E. Sechler, M. L. Williams, and Y. C. Fung, IAS Preprint No. 257, December, 1949.

6 "The Solution of Elastic Plate Problems by Electrical Analogies," by R. H. MacNeal, Journal of Applied Mechanics, Trans. ASME, vol. 73, 1951, pp. 59–67.

7 "Finite Difference Equations for the Analysis of Thin Rectangular Plates With Combinations of Fixed and Free Edges," by M. V. Barton, Defense Research Laboratory Report No. 175, University of Texas, Austin, Tex., August 6, 1948.

8 "Experimental Values of Deflection, Stresses and Influence Coefficients for a Thin Square Plate Fixed Along One Edge," by J. W. Dalley, Defense Research Laboratory Report No. 189, University of Texas, Austin, Tex., November 5, 1948.

9 "Influence Coefficients for a Uniform Square Cantilever Plate With Application to the Determination of Deflections and Stresses for a Square Fin With a Pressure Distribution Corresponding to Mach Number 1.75," by M. V. Barton and J. W. Dalley, Defense Research Laboratory Report No. 195, University of Texas, Austin, Tex., January 28, 1949.

10 "Application of Ritz's Energy Method to Problems in the Vibration, Buckling and Bending of Rectangular Plates," by Dana Young, Defense Research Laboratory Report No. 209, University of Texas, Austin, Tex., April 30, 1949.

11 "Free Vibration Characteristics of Rectangular Cantilever Plates," by M. V. Barton, Defense Research Laboratory Report No. 212, University of Texas, Austin, Tex., May 24, 1949.

12 "Torsion and Transverse Bending of Cantilever Plates," by E. Reissner and M. Stein, NACA Technical Note 2369, June, 1951.

13 "Zur Statik von dünnen Flugzeug-Tragflächen," Mitteilungen No. 2, Institut fuer Flugzeugstatik und Flugzeugbau an der ETH, Zurich, Switzerland, 1950.

14 "Theory of Plates and Shells," by S. Timoshenko, McGraw-Hill Book Company, Inc., New York, N. Y., 1940, pp. 88–90.

15 "Die Theorie elastischer Gewebe und ihre Anwendung auf die Berechnung biegsamer Platten," by H. Marcus, second edition, Julius Springer, Berlin, Germany, 1932, p. 18.

16 "Analysis of Plate Examples by Difference Methods and the Superposition Principle," by D. L. Holl, Trans. ASME, vol. 58, 1936, p. A-81.

17 "Analyses of Skew Slabs," by V. P. Jensen, University of Illinois, Engineering Experiment Station, Bull. No. 332, September, 1941.

18 "Structural Skew Plates," by F. L. Ehasz, Proceedings of the ASCE, vol. 71, 1945, p. 805.

19 "Le calcul des plaques obliques par la methode des equations aux differences," by H. Favre, *Memoires*, Association Internationale de Ponts et Charpentes, Zurich, Switzerland, vol. 7, 1943–1944.

20 "A Short Method for Evaluating Determinants and Solving Systems of Linear Equations With Real or Complex Coefficients," by P. D. Crout, Trans. AIEE, vol. 60, 1941, pp. 1235–1241.

21 "The Analysis of Rectangular Plates Under Various Loading and Boundary Conditions," by P. T. Cheng, unpublished research work at University of Minnesota, Minneapolis, Minn., 1940.

22 "Square Plates Fixed at Points," by C. J. Thorne, Journal of Applied Mechanics, Trans. ASME, vol. 70, 1948, pp. 73–79.

Stresses and Deformations of Toroidal Shells of Elliptical Cross Section

With Applications to the Problems of Bending of Curved Tubes and of the Bourdon Gage[1]

By R. A. CLARK,[2] T. I. GILROY,[3] AND E. REISSNER[4]

This paper is concerned with the application of the theory of thin shells to several problems for toroidal shells with elliptical cross section. These problems are as follows: (*a*) Closed shell subjected to uniform normal wall pressure. (*b*) Open shell subjected to end bending moments. (*c*) Combination of the results for the first and second problems in such a way as to obtain results for the stresses and deformations in Bourdon tubes. In all three problems the distribution of stresses is axially symmetric but only in the first problem are the displacements axially symmetric.

The magnitude of stresses and deformations for given loads depends in all three problems on the magnitude of the two parameters bc/ah and b/c where b and c are the semiaxes of the elliptical section, a is the distance of the center of the section from the axis of revolution, and h is the thickness of the wall of the shell. For sufficiently small values of bc/ah trigonometric series solutions are obtained. For sufficiently large values of bc/ah asymptotic solutions are obtained. Numerical results are given for various quantities of practical interest as a function of bc/ah for the values 2, 1, $1/2$, $1/4$ of the semiaxes ratio b/c. It is suggested that the analysis be extended to still smaller values of b/c and to cross sections other than elliptical.

Introduction

FOR a closed shell, subjected to wall pressure, it is possible to obtain results for stresses under the assumption of no bending stresses in the walls. This is the so-called membrane solution which is well known (1, 2).[5] It is reasonable to expect that the membrane state of stress in the toroidal shell with elliptical cross section is a good approximation to the true state of stress if the shell is sufficiently thin. On the other hand, it cannot be universally applicable since the cylindrical shell with elliptical cross section can be considered as a special case of a toroidal shell and, in this special case, wall bending alone resists the wall pressure. The problem then is to obtain a solution which contains as limiting cases both the membrane solution for the sufficiently thin shell and the bending solution for the cylindrical shell, and which applies when neither of the two limiting cases is a good approximation to the true state. This is done in the first part of the present paper. It is found that the theory contains a parameter μ, defined as $\sqrt{12(1-\nu^2)}bc/ah$, where b and c are the semiaxes of the elliptical section, a is the distance of the center of the section from the axis of revolution, h is the thickness of the wall, and ν is Poisson's ratio. When μ is small compared with unity, the toroidal shell behaves like a cylindrical shell of the same cross section. When μ is large compared with unity, the membrane solution is applicable. In the in-between range, both bending and membrane action have to be considered.

The second part of the paper, which deals with the problem of tube bending, gives results for the tube with elliptical cross section which are extensions of known results for the tube with circular cross section. It was recently shown (3, 4) that the differential equations for curved-tube bending are similar in form to those for the complete shell of revolution. Consequently, most of the calculations for the shell subject to wall pressure can be utilized for the problem of the tube bending. It may be recalled that for this problem the effect of flattening of the cross sections is responsible for a reduction of the stiffness of the tube compared with the stiffness of the tube with straight axis. The magnitude of this effect also depends upon the parameter μ.

The third part of the present paper which deals with the theory of the Bourdon tube makes use of the results of the first two parts in the following manner:

Except for localized end effects, which fall within the scope of Saint Venant's principle, one may take the solution for the complete tube under the influence of uniform wall pressure and calculate the internal section bending moment due to the pressure. In the Bourdon tube this bending moment cannot be taken and, therefore, must be eliminated by a superposition of a suitable solution of the problem of bending due to moments applied at the ends of the tube. It is the effect of these superimposed end moments which causes the change of curvature of the fibers of the tube which is measured, in order to determine the unknown magnitude of the wall pressure. While the nature of this effect has been understood for some time (5, 6, 7), the present analysis is believed to go beyond what has been known so far.

The methods of solution employed are as follows: For small and moderate values of the parameter μ, trigonometric series expansions are used. The differential equations of the problem then lead to an infinite system of linear equations for the co-

[1] The work reported here was carried out with the support of the Office of Naval Research under Contract N5 ori-07834 with Massachusetts Institute of Technology.

[2] Department of Mathematics, Case Institute of Technology, Cleveland, Ohio; formerly Department of Mathematics, Massachusetts Institute of Technology, Cambridge, Mass.

[3] Department of Mathematics, Creighton University, Omaha, Neb.; formerly, Department of Mathematics, Massachusetts Institute of Technology.

[4] Department of Mathematics, Massachusetts Institute of Technology. Jun. ASME.

[5] Numbers in parentheses refer to the Bibliography at the end of the paper.

Contributed by the Applied Mechanics Division and presented at the Annual Meeting, Atlantic City, N. J., November 25–30, 1951, of THE AMERICAN SOCIETY OF MECHANICAL ENGINEERS.

Discussion of this paper should be addressed to the Secretary, ASME, 29 West 39th Street, New York, N. Y., and will be accepted until April 10, 1952, for publication at a later date. Discussion received after the closing date will be returned.

NOTE: Statements and opinions advanced in papers are to be understood as individual expressions of their authors and not those of the Society. Manuscript received by ASME Applied Mechanics Division in January, 1951. Paper No. 51—A-11.

efficients of the series. The infinite system is solved approximately by solving up to ten simultaneous equations.

For sufficiently large values of μ the differential equations of the problem are solved by asymptotic integration. In this manner simple explicit expressions are obtained for all quantities of interest. The practical range of validity of the asymptotic results and of the series results overlap so that the entire range of values of μ are covered in the present paper.

Small Deflection Theory of Thin Shells of Revolution Subjected to Rotationally Symmetric Loads

The following is a summary of the general theory upon which the present work is based. Details and a discussion of the historical development of the subject may be found in reference (8).

Using cylindrical co-ordinates r, θ, z, let the middle surface of a shell of revolution be represented by parametric equations of the form

$$r = r(\xi), \quad z = z(\xi) \ldots\ldots [1]$$

The differential of arc length along a meridian curve is then given by $ds = \alpha d\xi$ where

$$\alpha^2 = (r')^2 + (z')^2 \ldots\ldots [2]$$

and primes indicate differentiation with respect to the parameter ξ.

Let the components of displacement of points of the middle surface in the directions of r, θ, and z be denoted by u, v, and w, respectively, and let the angle β denote the rotation, due to deformation, of a tangent to a meridian curve, see Fig. 1(*a*). If the loading is rotationally symmetric, the displacements will also be symmetric as well as univalued, which implies that the component v vanishes.

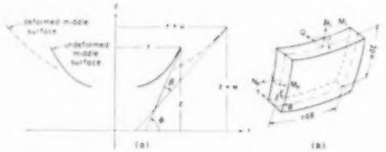

Fig. 1 Element of Shell of Revolution, Showing Deformation Variables and Stress Resultants and Couples

If it is assumed that deformation causes only small displacements and that normals to the middle surface are preserved during deformation, it can be shown that the strains in the middle surface of the deformed shell are related to the components of displacement by the equations

$$\epsilon_{\xi M} = \frac{u' - z'\beta}{r'} = \frac{w' + r'\beta}{z'_0}, \quad \epsilon_{\theta M} = \frac{u}{r} \ldots\ldots [3a, b]$$

and that the changes in the principal curvatures of the middle surface are given by

$$\kappa_\xi = \frac{\beta'}{\alpha}, \quad \kappa_\theta = \frac{r'\beta}{r\alpha} \ldots\ldots [4a, b]$$

Equations [3] imply the compatibility relation

$$(r\epsilon_{\theta M})' - r'\epsilon_{\xi M} = z'\beta \ldots\ldots [5]$$

If stress resultants N_ξ, N_θ, and Q, and stress couples M_ξ and M_θ, acting on an element of the shell, are defined in accordance with Fig. 1(*b*), and if components of load intensity in the r- and z-directions are called p_H and p_V, respectively, the equilibrium equations become

$$(rV)' + r\alpha p_V = 0 \ldots\ldots [6a]$$

$$(rH)' - \alpha N_\theta + r\alpha p_H = 0 \ldots\ldots [6b]$$

$$(rM_\xi)' - r'M_\theta + z'(rH) - r'(rV) = 0 \ldots\ldots [6c]$$

where H and V are horizontal and vertical stress resultants defined by the equations

$$\alpha N_\xi = r'H + z'V, \quad \alpha Q = -z'H + r'V \ldots\ldots [7a, b]$$

The stress-strain relations are

$$C\epsilon_{\xi M} = N_\xi - \nu N_\theta, \quad C\epsilon_{\theta M} = N_\theta - \nu N_\xi \ldots\ldots [8a]$$

$$M_\xi = D(\kappa_\xi + \nu\kappa_\theta), \quad M_\theta = D(\kappa_\theta + \nu\kappa_\xi) \ldots\ldots [8b]$$

where

$$C = Eh, \; D = Eh^3/12(1 - \nu^2) \ldots\ldots [9]$$

and E is the modulus of elasticity, ν is Poisson's ratio, and h is the thickness of the shell.

The foregoing basic equations of the theory can be reduced to two simultaneous second-order differential equations for the quantities β and (rH). Combining Equations [4], [6c], and [8b] for the first, and Equations [5], [6b], [7], and [8a] for the second, one obtains

$$\beta'' + \frac{(rD/\alpha)'}{(rD/\alpha)}\beta' - \left[\left(\frac{r'}{r}\right)^2 - \nu\frac{(r'D/\alpha)'}{(rD/\alpha)}\right]\beta + \frac{z'}{(rD/\alpha)}(rH) = \frac{r'}{(rD/\alpha)}(rV) \ldots\ldots [10a]$$

$$(rH)'' + \frac{(r/C\alpha)'}{(r/C\alpha)}(rH)' - \left[\left(\frac{r'}{r}\right)^2 + \nu\frac{(r'/C\alpha)'}{(r/C\alpha)}\right](rH) - \frac{z'}{(r/C\alpha)}\beta = \left[\frac{z'r'}{r^2} + \nu\frac{(z'/C\alpha)'}{(r/C\alpha)}\right](rV) + \nu\frac{z'}{r}(rV)' - \left[\frac{(r/C\alpha)'}{(r/C\alpha)} + \nu\frac{r'}{r}\right](r\alpha p_H) - (r\alpha p_H)' \ldots [10b]$$

Once Equations [10] have been solved for a given loading and given boundary conditions, all other quantities may be determined by means of Equations [3] to [8].

We now define, in the usual manner, "direct" stresses $\sigma_{\xi D}$, $\sigma_{\theta D}$ and "bending" stresses in the outermost fibers $\sigma_{\xi B}$, $\sigma_{\theta B}$ by the equations

$$\sigma_{\xi D} = N_\xi/h, \quad \sigma_{\theta D} = N_\theta/h \ldots\ldots [11a]$$

$$\sigma_{\xi B} = 6M_\xi/h^2, \quad \sigma_{\theta B} = 6M_\theta/h^2 \ldots\ldots [11b]$$

The stresses σ_ξ, σ_θ are then given by

$$\sigma_\xi = \sigma_{\xi D} + (2\zeta/h)\sigma_{\xi B} \ldots\ldots [12a]$$

$$\sigma_\theta = \sigma_{\theta D} + (2\zeta/h)\sigma_{\theta B} \ldots\ldots [12b]$$

where ζ is the distance, along a normal, from the middle surface, see Fig. 1(*b*).

Toroidal Shells of Elliptical Cross Section Subjected to Uniform Normal Pressure

For a toroidal shell of elliptical cross section, Equations [1] may be taken in the form

$$r = a + b\sin\xi, \quad z = -c\cos\xi \ldots\ldots [13]$$

where b and c are the semiaxes of the cross section, and a is the radius of the center line, see Fig. 2. According to Equation [2], we then have

$$\alpha = \sqrt{b^2 \cos^2 \xi + c^2 \sin^2 \xi} = c\sqrt{1 - e^2 \cos^2 \xi} \ldots [14]$$

where

$$e^2 = 1 - (b/c)^2 \ldots [15]$$

It is also convenient to define the parameters

$$\lambda = b/a, \ \mu = \gamma(bc/ah), \ \gamma = \sqrt{12(1 - \nu^2)} \ldots [16]$$

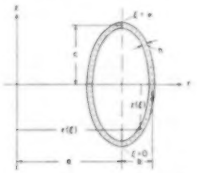

FIG. 2 CROSS SECTION OF TOROIDAL TUBE, SHOWING DIMENSIONS a, b, c, and h

Next, let p denote a uniform internal pressure intensity. Radial and axial components of load intensity are then given by

$$ap_R = z'p, \quad ap_V = -r'p \ldots [17]$$

If we now introduce the dimensionless stress function

$$\Psi = (\gamma/Eh^2)(rH) \ldots [18]$$

and assume that the thickness h of the shell is constant, we find, using Equations [13] to [17], that the two simultaneous differential Equations [10] assume the form

$$\beta'' + \left(\frac{\lambda \cos \xi}{1 + \lambda \sin \xi} - \frac{e^2 \sin \xi \cos \xi}{1 - e^2 \cos^2 \xi}\right)\beta' - \left[\left(\frac{\lambda \cos \xi}{1 + \lambda \sin \xi}\right)^2 + \frac{\nu\lambda \sin \xi}{(1 + \lambda \sin \xi)(1 - e^2 \cos^2 \xi)}\right]\beta + \frac{\mu \sin \xi}{1 + \lambda \sin \xi}\sqrt{\frac{1 - e^2 \cos^2 \xi}{1 - e^2}}\,\Psi = \frac{\mu \cos \xi}{1 + \lambda \sin \xi}\sqrt{1 - e^2 \cos^2 \xi}\,\frac{\gamma(rV)}{Eh^2} \ldots [19a]$$

$$\Psi'' + \left(\frac{\lambda \cos \xi}{1 + \lambda \sin \xi} - \frac{e^2 \sin \xi \cos \xi}{1 - e^2 \cos^2 \xi}\right)\Psi' - \left[\left(\frac{\lambda \cos \xi}{1 + \lambda \sin \xi}\right)^2 - \frac{\nu\lambda \sin \xi}{(1 + \lambda \sin \xi)(1 - e^2 \cos^2 \xi)}\right]\Psi - \frac{\mu \sin \xi}{1 + \lambda \sin \xi}\sqrt{\frac{1 - e^2 \cos^2 \xi}{1 - e^2}}\,\beta = \left[\frac{c}{b}\frac{\lambda^2 \sin \xi \cos \xi}{(1 + \lambda \sin \xi)^2} + \frac{\nu\lambda \cos \xi}{(1 + \lambda \sin \xi)(1 - e^2 \cos^2 \xi)}\right]\frac{\gamma(rV)}{Eh^2} - \left[\frac{(1 - e^2)\cos \xi}{1 - e^2 \cos^2 \xi}(1 + \lambda \sin \xi) + 2\lambda \sin \xi \cos \xi\right]\frac{\gamma acp}{Eh^2} \ldots [19b]$$

Membrane Solution. According to the so-called "membrane" theory of shells, a first approximation to the solution of the present problem may be obtained by neglecting the effect of bending of the shell walls. To neglect bending means that we take M_ξ and M_θ equal to zero by assuming that the bending stiffness factor $D = 0$. From Equation [6c], we then have

$$rH = (b/c)(rV)\cot \xi \ldots [20]$$

The quantity rV may be obtained directly from Equation [6a]. Using Equations [13] and [17], we find

$$rV = -\int^{\xi} ra\, p_V d\xi = abp \sin \xi \left(1 + \frac{\lambda}{2}\sin \xi\right) \ldots [21]$$

By means of Equations [20], [21], [6b], and [7a] we may finally determine the membrane stresses (denoted by the subscript M), namely

$$\sigma_{\xi M} = \frac{N_{\xi M}}{h} = \frac{b}{h}p\,\frac{1 + (\lambda/2)\sin \xi}{1 + \lambda \sin \xi}\sqrt{1 - e^2 \cos^2 \xi} \ldots [22]$$

$$\sigma_{\theta M} = \frac{N_{\theta M}}{h} = \frac{a}{h}p\,\frac{e^2 \sin \xi(1 + \lambda \sin \xi) + (\lambda/2)(b/c)^2}{\sqrt{1 - e^2 \cos^2 \xi}} \ldots [23]$$

The earliest reference known to the authors, which gives these membrane stresses for a toroidal shell with elliptical cross section is a paper by H. Lorenz (2). The same results are also given in reference (1).

Corrections to Membrane Solution. It is clear that the range of validity of the membrane solution must be limited, for the following reason: A straight cylindrical tube of elliptical cross section may be considered as a toroidal shell with infinite radius a. For this limiting case it is the bending stiffness of the walls which resists the pressure p. The question is then to determine the conditions under which (a) the membrane theory gives a good approximation to the actual stress distribution; (b) the toroidal shell behaves essentially as a straight cylindrical tube; and (c) neither of the two limiting situations applies. The answer to this question requires the solution of the differential Equations [19], with rV given by Equation [21].

In order to obtain this solution it is convenient to write

$$\Psi = \Psi_M + \eta \ldots [24]$$

where Ψ_M is the value of Ψ, according to the membrane theory and η is the correction to the membrane solution. Combining Equations [18], [20], and [21], we have explicitly

$$\Psi_M = \frac{\gamma}{Eh^2}\frac{b}{c}abp \cos \xi \left(1 + \frac{\lambda}{2}\sin \xi\right) \ldots [25]$$

We now substitute Ψ from Equation [24] into Equations [19]. In doing so we shall assume that the ratio $\lambda = b/a$ is small compared to unity. On the basis of this assumption we may neglect all terms in our equations which involve λ. A detailed discussion of this simplification may be found in reference (9). The basic differential equations of the problem assume now the following simpler form

$$\beta'' - \frac{e^2 \sin \xi \cos \xi}{1 - e^2 \cos^2 \xi}\beta' + \frac{c}{b}\mu \sin \xi \sqrt{1 - e^2 \cos^2 \xi}\,\eta = 0 \ldots [26a]$$

$$\eta'' - \frac{e^2 \sin \xi \cos \xi}{1 - e^2 \cos^2 \xi}\eta' - \frac{c}{b}\mu \sin \xi \sqrt{1 - e^2 \cos^2 \xi}\,\beta = -e^2 \frac{b}{c}\frac{\gamma abp}{Eh^2}\frac{\cos \xi}{1 - e^2 \cos^2 \xi} \ldots [26b]$$

Having solved Equations [26] for β and η, the various direct and bending stresses defined by Equations [11] are given by the following formulas

$$\sigma_{\xi D} = \sigma_{\xi M} + (Ehb/\gamma\alpha a)\,\eta\cos\xi \quad [27a]$$

$$\sigma_{\theta D} = \sigma_{\theta M} + (Eh/\gamma\alpha)\,\eta' \quad [27b]$$

$$\sigma_{\xi B} = (6Eh/\gamma^2\alpha)\,\beta',\ \sigma_{\theta B} = \nu\sigma_{\xi B} \quad [27c, d]$$

Formulas for the displacements u and w are obtained from Equation [3a]

$$u = \int (c\beta\sin\xi + b\,\epsilon_{\xi M}\cos\xi)d\xi \quad [28a]$$

$$w = -\int (b\beta\cos\xi - c\,\epsilon_{\xi M}\sin\xi)\,d\xi \quad [28b]$$

When bending is significant the strain $\epsilon_{\xi M}$ is small compared to the change of slope and may be neglected in Equations [28a] and [28b]. The following simpler formulas may then be used

$$u = c\int\beta\sin\xi\,d\xi, \quad w = -b\int\beta\cos\xi\,d\xi \quad [29a, b]$$

Fourier Series Solution of Differential Equations. For a closed shell all quantities must be of period 2π in the variable ξ, and the solutions of Equations [26] may be taken as Fourier series in ξ. Neglecting λ makes the solution of the problem symmetrical about the vertical axis of the elliptical cross section. This symmetry, together with symmetry about the horizontal axis, implies that Fourier expansions for β and η must be of the form

$$\beta = e^2\frac{b}{c}\frac{\gamma}{}\frac{abp}{Eh^2}\sum_{n=1}^{\infty} A_n\sin 2n\xi \quad [30a]$$

$$\eta = e^2\frac{b}{c}\frac{\gamma}{}\frac{abp}{Eh^2}\sum_{n=1}^{\infty} B_n\cos(2n-1)\xi \quad [30b]$$

If β and η are taken from Equations [30] and substituted in Equations [27] together with the membrane stresses from Equations [22] and [23] (again neglecting λ), one has the following expansions for direct and bending stresses

$$\sigma_{\xi D} = \frac{b}{h}p\left[\sqrt{1-e^2\cos^2\xi} + \frac{e^2}{2}\left(\frac{b}{c}\right)^2\frac{B_1 + \sum_{n=1}^{\infty}(B_n + B_{n+1})\cos 2n\xi}{\sqrt{1-e^2\cos^2\xi}}\right] \quad [31a]$$

$$\sigma_{\theta D} = e^2\frac{a}{h}p\,\frac{\sin\xi - (b/c)^2\sum_{n=1}^{\infty}(2n-1)B_n\sin(2n-1)\xi}{\sqrt{1-e^2\cos^2\xi}} \quad [31b]$$

$$\sigma_{\xi B} = \frac{6}{\gamma}e^2\frac{a}{h}\left(\frac{b}{c}\right)^2 p\,\frac{\sum_{n=1}^{\infty} 2nA_n\cos 2n\xi}{\sqrt{1-e^2\cos^2\xi}} \quad [31c]$$

Since it was assumed that $b/a = \lambda \ll 1$, the stress $\sigma_{\xi D}$ will, in general, be small compared with the stress $\sigma_{\theta D}$.

From Equations [29a, b] the following expressions are obtained for quantities δ_H and δ_V which indicate the amount of flattening and bulging of the tube

$$\delta_H = u\left(\frac{\pi}{2}\right) - u(0) = \frac{1}{2}be^2\frac{\gamma}{}\frac{abp}{Eh^2}\sum_{n=1}^{\infty}\frac{(-1)^{n+1}4n}{4n^2-1}A_n \quad [32a]$$

$$\delta_V = w\left(\frac{\pi}{2}\right) - w(0) = -\frac{1}{2}ce^2\frac{\gamma}{}\frac{abp}{Eh^2}\sum_{n=1}^{\infty}\frac{4n}{4n^2-1}A_n \quad [32b]$$

Recurrence relations for the coefficients A_n and B_n are determined by requiring the expansions, Equations [30], to satisfy Equations [26] identically. If we introduce the following auxiliary expansions

$$1/(1-e^2\cos^2\xi) = (a_0/2) + \sum_{m=1}^{\infty} a_m\cos 2m\xi \quad [33a]$$

$$\sqrt{1-e^2\cos^2\xi} = (b_0/2) + \sum_{m=1}^{\infty} b_m\cos 2m\xi \quad [33b]$$

and then substitute from Equations [30] into Equations [26], we obtain

$$\sum_{m=1}^{\infty}\Bigg[(2m)^2A_m + \sum_{k=1}^{\infty}\{(e^2/4)(a_{k-m} - a_{k+m})\,[(k-1)A_{k-1} - (k+1)A_{k+1}] - (\mu/4)(c/b)(b_{k-m} - b_{k+m})(B_k - B_{k+1})\}\Bigg]\sin 2m\xi = 0. \quad [34a]$$

$$\sum_{m=1}^{\infty}\Bigg[(2m-1)^2B_m + \sum_{k=1}^{\infty}\{(e^2/8)(a_{k-m} + a_{k+m-1})\,[(2k-3)B_{k-1} - (2k+1)B_{k+1}] - (\mu/4)(c/b)(b_{k-m} + b_{k+m-1})(A_{k-1} - A_k)\}\Bigg]\cos(2m-1)\xi = (1/2)\sum_{m=1}^{\infty}(a_{m-1} + a_m)\cos(2m-1)\xi \quad [34b]$$

where

$$A_0 = 0,\ B_0 = B_1,\quad a_{-k} = a_k,\ b_{-k} = b_k \quad [35]$$

Equations [34] lead to the following recurrence equations for A_n and B_n

$$\sum_{n=1}^{\infty}[(4n^2\delta_{mn} + nc_{mn})A_n - \mu\,d_{mn}B_n] = 0 \quad [36a]$$

$$\sum_{n=1}^{\infty}[\mu d_{mn}A_n + [(2n-1)^2\delta_{mn} + (2n-1)e_{mn}]B_n] = f_m \quad [36b]$$

$$m = 1, 2, 3, \ldots$$

where

$$\delta_{mn} = 1,\ n = m;\quad \delta_{mn} = 0,\ m \neq n$$

and

$$c_{mn} = (e^2/4)(a_{n-m+1} - a_{n-m-1} + a_{n+m-1} - a_{n+m+1}) \quad [37a]$$

$$d_{mn} = (c/4b)(b_{n-m} - b_{n-m-1} + b_{n+m-1} - b_{n+m}) \quad [37b]$$

$$e_{mn} = (e^2/8)(a_{n-m+1} - a_{n-m-1} + a_{n+m} - a_{n+m-2}) \quad [37c]$$

$$f_m = (1/2)(a_{m-1} + a_m) \quad [37d]$$

The coefficients a_m and b_m are given by

$$a_m = \frac{4}{\pi}\int_0^{\pi/2}\frac{\cos 2m\xi}{1-e^2\cos^2\xi}\,d\xi \quad [38a]$$

$$b_m = \frac{4}{\pi}\int_0^{\pi/2} \cos 2m\xi \sqrt{1 - e^2\cos^2\xi}\, d\xi \quad \ldots\ldots [38b]$$

Using contour integration, Equation [38a] becomes

$$a_m = 2\frac{c}{b}\left(\frac{1 - b/c}{1 + b/c}\right)^m \quad \ldots\ldots [39]$$

The evaluation of Equation [38b] involves elliptic integrals. For $b < c$ we find

$$b_0 = (4/\pi)\, E(e) \quad \ldots\ldots [40a]$$

$$b_1 = (8/3\pi\, e^2)\,[(1 - e^2)\, K(e) - \{1 - (e^2/2)\}\, E(e)] \quad \ldots\ldots [40b]$$

where K and E stand for complete elliptic integrals of the first and second kind, respectively. All other b_m may be obtained from the recurrence relation

$$b_m = \frac{4m - 4}{2m + 1}\frac{2 - e^2}{e^2} b_{m-1} - \frac{2m - 5}{2m + 1} b_{m-2},\ m \geq 2 \quad \ldots\ldots [41]$$

For $b > c$ one may use the formula

$$b_m(b/c) = (-1)^m (b/c)\, b_m(c/b) \quad \ldots\ldots [42]$$

Using Equation [39], one may also deduce that for $b < c$

$$c_{ms} = \begin{cases} -2\, q^{n-m}\,(1 - q^{2m}), & m < n \\ 2\, q^{2m}, & m = n \\ 2\, q^{m-n}\,(1 + q^{2n}), & m > n \end{cases} \quad \ldots\ldots [43]$$

$$e_{ms} = \begin{cases} -q^{n-m}(1 + q^{2m-1}), & m < n \\ -q^{2m-1}, & m = n \\ q^{m-n}(1 - q^{2n-1}), & m > n \end{cases} \quad \ldots\ldots [44]$$

where

$$q = \frac{1 - b/c}{1 + b/c} \quad \ldots\ldots [45]$$

For $b > c$

$$c_{ms}(b/c) = (-1)^{m+n}\, c_{ms}(c/b) \quad \ldots\ldots [46]$$

$$e_{ms}(b/c) = (-1)^{m+n+1} e_{ms}(c/b) \quad \ldots\ldots [47]$$

If the series, Equations [30], are each approximated by n-terms the recurrence relations, Equations [36], constitute $2n$ equations for the $2n$ unknowns A_k and B_k.

In view of similar work done concerning the bending of curved tubes of circular cross section (3), it is expected that the convergence of series, Equation [30], becomes slower as μ becomes larger. For the present work numerical calculations were made for the three cases $b/c = 1/4$, $b/c = 1/2$, and $b/c = 2$, using up to five terms in each of the series for β and η.

Limiting Case of Straight Tube of Elliptic Section. We obtain the limiting case $\mu = 0$ if we allow a to become infinitely large. Any portion of the toroidal shell then approaches a straight cylindrical shell of elliptical cross section. To obtain results for this limiting case it is necessary to modify the foregoing discussion somewhat since $\eta \to \infty$ as $a \to \infty$. If we replace η by

$$\eta = \eta_1/\mu \quad \ldots\ldots [48]$$

then η_1 remains finite as $\mu \to 0$. Substituting from Equation [48] and then letting $\mu \to 0$, Equations [26] take the form

$$\beta'' - \frac{e^2 \sin\xi\cos\xi}{1 - e^2\cos^2\xi}\beta' + \frac{c}{b}\sin\xi\sqrt{1 - e^2\cos^2\xi}\,\eta_1 = 0 \quad \ldots\ldots [49a]$$

$$\eta_1'' - \frac{e^2 \sin\xi\cos\xi}{1 - e^2\cos^2\xi}\eta_1' = -\gamma^2 c^2\left(\frac{b}{h}\right)^2 \frac{p}{E}\frac{\cos\xi}{1 - e^2\cos^2\xi} \quad \ldots\ldots [49b]$$

where in determining the coefficient of the term on the right of Equation [49b] we have used the definition of μ as given by Equations [16]. Equation [49b] may be integrated directly. Imposing the boundary conditions

$$\eta_1(\pi/2) = \eta_1(-\pi/2) = 0 \quad \ldots\ldots [50]$$

we find

$$\eta_1 = \gamma^2 c^2 (b/h)^2\,(p/E)\,(c/b)^2 \cos\xi \quad \ldots\ldots [51]$$

If we compare this solution with the series, Equation [30b], for η, we may readily deduce that, as $\mu \to 0$, the coefficients B_n in Equation [30b] have the limiting values

$$B_1 = (c/b)^2; \quad B_n = 0,\ n \neq 1 \quad \ldots\ldots [52]$$

Using the Expression [51] for η_1, Equation [49a] also may be integrated explicitly to obtain an expression for β involving elliptic integrals. Instead of doing this, however, it is found to be more desirable for the present purposes to have β expressed by a series analogous to Equation [30a]. This series is given immediately by writing $A_n = \mu A_n^*$ in Series [30a]. Using the definition of μ we have

$$\beta = \gamma^2 c^2 (b/h)^2\,(p/E)\sum_{n=1}^{\infty} A^*_n \sin 2n\xi \quad \ldots\ldots [53]$$

Recurrence equations for A_n^* are obtained if we also replace A_n by μA_n^* in Equations [36a] and take B_n from Equations [52]. The resulting relations are

$$\sum_{n=1}^{\infty}(4n^2\,\delta_{mn} + nc_{mn})A_n^* = (c/b)^2\, d_{m1};\ m = 1, 2, \ldots \quad [54]$$

where the various coefficients are again given by Equations [37], etc.

Using Equations [52] and $A_n = \mu A_n^*$, Equations [31] and [32] become

$$\sigma_{\xi DS} = \frac{b}{h}\frac{p}{\sqrt{1 - e^2\cos^2\xi}}, \quad \sigma_{\theta DS} = 0 \quad \ldots\ldots [55a, b]$$

$$\sigma_{\xi BS} = 6c^2\left(\frac{b}{h}\right)^2 \frac{b}{c}\, p\, \frac{\sum_{n=1}^{\infty} 2n\, A_n^* \cos 2n\xi}{\sqrt{1 - e^2\cos^2\xi}} \quad \ldots\ldots [55c]$$

$$\delta_{HS} = \frac{1}{2}\gamma^2 ce^2\left(\frac{b}{h}\right)^2 \frac{p}{E}\sum_{n=1}^{\infty}\frac{(-1)^{n+1}\,4n}{4n^2 - 1} A_n^* \quad \ldots\ldots [56a]$$

$$\delta_{VS} = -\frac{\pi}{2}\gamma^2 bc^2\left(\frac{b}{h}\right)^2 \frac{p}{E}\sum_{n=1}^{\infty}\frac{4n}{4n^2 - 1} A_n^* \quad \ldots\ldots [56b]$$

where μ is taken from Equation [16] and the subscript S is used to denote that these are the stresses and deflections of a straight tube. Strictly speaking, substituting from Equations [52] into [31b] for $\sigma_{\theta D}$ indicates only that $\sigma_{\theta D}$ takes the indeterminate form $0 \cdot \infty$. The limiting value [55b] is justified by showing that for small values of μ we have $B_1 = (c/b)^2 + O(\mu^2)$.

Solution by Asymptotic Integration. As μ becomes larger it is necessary to take more and more terms in the series, Equations [30] for β and η, in order to obtain satisfactory results. Obvi-

ously, such a procedure soon becomes impractical, making it desirable to have some other form of solution for large values of μ. Assuming that μ is large, we now determine approximate solutions of Equations [26] using a method of asymptotic integration first used in reference (3).

If μ is large the first derivative terms in Equations [26] will have a relatively unimportant effect on the solution except for very small values of b/c. Neglecting these terms and introducing the complex function

$$Z = \beta + i\eta \quad [57]$$

Equations [26] may be combined into the single equation

$$Z'' - i\mu \sin \xi \sqrt{\frac{1 - e^2 \cos^2 \xi}{1 - e^2}}\, Z = -\frac{iP \cos \xi}{1 - e^2 \cos^2 \xi} \quad [58]$$

where

$$P = e^2 (b/c) (\gamma abp/Eh^2) \quad [59]$$

If we assume that a particular solution of Equation [58] may be represented asymptotically by an expansion of the form

$$Z = \frac{1}{\mu}\left(Z_0 + \frac{1}{\mu} Z_1 + \frac{1}{\mu^2} Z_2 + \ldots\right) \quad [60]$$

we obtain, by substituting Equation [60] into Equation [58]

$$Z_0 = P \frac{\sqrt{1 - e^2} \cot \xi}{(1 - e^2 \cos^2 \xi)^{3/2}} \quad [61]$$

If ξ is limited to a range such that $\cot \xi = O(1)$ one expects Equation [61] to approximate a solution of Equation [58] within terms of order $1/\mu$. However, as ξ approaches 0 or π, $\cot \xi \to \infty$ so that Equation [61] is no longer valid. The basic idea now to be applied is to obtain a formula for an approximate solution of Equation [58] which satisfies Equation [58] approximately for small values of ξ and behaves like Equation [61], when ξ is not small. On the basis of symmetry considerations we may restrict our attention to the interval $-\pi/2 \leq \xi \leq \pi/2$, without loss of generality.

Let us now introduce

$$x = \mu^{1/3} \sin \xi \quad [62]$$

and consider the expression

$$Z_p = -\frac{iP}{\mu^{2/3}} \frac{\sqrt{1 - e^2} \cos \xi}{(1 - e^2 \cos^2 \xi)^{3/2}} T(x) \quad [63]$$

where the function $T(x)$ has yet to be determined. If ξ is not small then x is large since μ is large. If for large values of x, $T(x) \sim i/x$ then Equation [63] will behave like Equation [61], as is desired. For small values of ξ, Equation [63] may be approximated by

$$Z_p = -\frac{iP}{\mu^{2/3}} \frac{T(\mu^{1/3} \xi)}{1 - e^2} \quad [64]$$

and Equation [58] by

$$Z'' - i\mu\xi Z = -iP/(1 - e^2) \quad [65]$$

Substituting Z from Equation [64] into [65], we find that Equation [63] also satisfies Equation [58] approximately, provided $T(x)$ satisfies the equation

$$d^2T/dx^2 - ixT = 1 \quad [66]$$

Thus Equation [63] yields an approximate solution of Equation [58] which is valid for all values of ξ. It remains only to determine a solution of Equation [66] which satisfies appropriate boundary conditions for $x = 0$ and $x = \infty$.

From Equation [57] together with Equation [59] and $e^2 = 1 - (b/c)^2$ we find that Equation [63] implies

$$\beta = \frac{e^2}{\mu^{2/3}} \left(\frac{b}{c}\right)^2 \frac{\gamma abp}{Eh^2} \frac{\cos \xi}{(1 - e^2 \cos^2 \xi)^{3/2}} T_r(x) \quad [67a]$$

$$\eta = -\frac{e^2}{\mu^{2/3}} \left(\frac{b}{c}\right)^2 \frac{\gamma abp}{Eh^2} \frac{\cos \xi}{(1 - e^2 \cos^2 \xi)^{3/2}} T_i(x) \quad [67b]$$

$$\beta' = \frac{e^2}{\mu^{1/3}} \left(\frac{b}{c}\right)^2 \frac{\gamma abp}{Eh^2} \frac{\cos^2 \xi}{(1 - e^2 \cos^2 \xi)^{3/2}} \frac{dT_i}{dx} \quad [67c]$$

$$\eta' = -\frac{e^2}{\mu^{1/3}} \left(\frac{b}{c}\right)^2 \frac{\gamma abp}{Eh^2} \frac{\cos^2 \xi}{(1 - e^2 \cos^2 \xi)^{3/2}} \frac{dT_r}{dx} \quad [67d]$$

where subscripts r and i denote real and imaginary parts of $T(x)$, and where we have neglected the derivative of the factor $\cos \xi/(1 - e^2 \cos^2 \xi)^{3/2}$ in comparison with the derivatives of $T_r(x)$ and $T_i(x)$ with respect to ξ.

The boundary conditions at $\xi = 0$ which may be deduced from symmetry considerations and which are implied by series Equations [30] are $\beta(0) = 0$, $\eta'(0) = 0$. From Equations [67] it follows that we must require

$$(dT_r/dx)_{x=0} = 0, \quad T_i(0) = 0 \quad [68]$$

Conditions for $x = \infty$ may be written in the form

$$\lim_{x \to \infty} xT_r(x) = 0, \quad \lim_{x \to \infty} xT_i(x) = 1 \quad [69]$$

These four conditions serve to determine the required solution of Equation [66] uniquely. This solution is given in terms of power series and tabulated functions in reference (3). The real and imaginary parts $T_r(x)$, $T_i(x)$ and their derivatives have also been tabulated using numerical integration and the additional initial conditions which the definition of these functions implies, namely

$$T_r(0) = -1.288, \quad (dT_i/dx)_{x=0} = 0.939 \quad [70]$$

Curves for $T_r(x)$, $T_i(x)$ and their derivatives are plotted in Fig. 3.

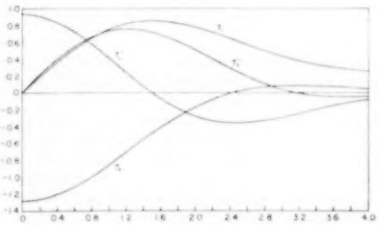

FIG. 3 VALUES OF FUNCTIONS T_r AND T_i AND THEIR DERIVATIVES T_r' AND T_i'

Taking β and η from Equations [67] and using Equations [27], [23], and [22], we now find that for large μ

$$\sigma_{\xi D} = \frac{b}{h} p \sqrt{1 - e^2 \cos^2 \xi} \left[1 - \frac{e^2}{\mu^{2/3}} \frac{(1 - e^2)^{3/2} \cos^2 \xi}{(1 - e^2 \cos^2 \xi)^{5/2}} T_r(x)\right] \quad [71a]$$

$$\sigma_{\theta D} = \frac{e^2 (a/h) p}{\sqrt{1 - e^2 \cos^2 \xi}} \left[\sin \xi - \frac{1}{\mu^{1/3}} \frac{(1 - e^2)^{3/2} \cos^2 \xi}{(1 - e^2 \cos^2 \xi)^{3/2}} \frac{dT_r}{dx}\right] \quad [71b]$$

$$\sigma_{\xi B} = \frac{6}{\gamma}\frac{e^2}{\mu^{1/2}}\frac{a}{h}p\frac{(1-e^2)^{1/2}\cos^2\xi}{(1-e^2\cos^2\xi)^2}\frac{dT_1}{dx} \quad \ldots\ldots [71c]$$

These formulas show that, as μ becomes larger, $\sigma_{\xi B}$ becomes negligibly small, while $\sigma_{\xi D}$ and $\sigma_{\theta D}$ approach the membrane stresses $\sigma_{\xi M}$ and $\sigma_{\theta M}$. Thus for sufficiently large values of μ the solution of the problem of the toroidal shell with elliptical cross section subjected to uniform normal wall pressure is indeed given by the membrane theory.

If we take u from Equation [29a], the quantity $\delta_H = u(\pi/2) - u(0)$ becomes after some transformations

$$\delta_H = ae^3(a/h)(p/E) \quad \ldots\ldots [72]$$

For δ_V we have, using Equations [29b] and [67a], the expression

$$\delta_V = -ae^2(a/h)(p/E)\int_0^{\mu^{1/2}}\frac{(1-e^2)^{1/2}\cos\xi}{(1-e^2\cos^2\xi)^{1/2}}T_4(x)dx \quad \ldots\ldots [73]$$

Discussion of Numerical Results. As we have noted, the dominant direct stress is $\sigma_{\theta D}$, provided μ is sufficiently large. This stress is obviously largest at $\xi = \pm\pi/2$. At $\xi = \pi/2$ the ratio of $\sigma_{\theta D}$, as given by Equation [31b], to the membrane stress $\sigma_{\theta M}$, given by Equation [23] (neglecting λ), is

$$\sigma_{\theta D,\max}/\sigma_{\theta M,\max} = 1 - (b/c)^2\sum_{n=1}^{\infty}(-1)^{n+1}(2n-1)B_n \quad \ldots [74]$$

Using the results of numerical calculations for the series coefficients A_n and B_n, this ratio has been plotted in Fig. 4 as a function of μ for the three cases $b/c = 1/4, 1/2, 2$. For large μ the asymptotic form, Equation [71b], simply gives $\sigma_{\theta D}(\pi/2) = \sigma_{\theta M}(\pi/2)$, which is indicated by a broken line in Fig. 4. We see that unless μ is sufficiently large the membrane solution may be considerably in error.

The dominant bending stress $\sigma_{\xi B}$ is largest at the points of maximum curvature of the shell, that is, at $\xi = 0$ or π for $b < c$ and at $\xi = \pm\pi/2$ for $b > c$. If we compare the maximum value of $\sigma_{\xi B}$ to the maximum value of the corresponding stress in a straight tube of the same cross section we have, from Equations [31c] and [55c]

$$\frac{\sigma_{\xi B,\max}}{\sigma_{\xi BS,\max}} = \frac{\sigma_{\xi B}(0)}{\sigma_{\xi BS}(0)} = \frac{\sum_{n=1}^{\infty} nA_n}{\mu\sum_{n=1}^{\infty} nA_n^*}, \quad b < c \quad \ldots\ldots [75]$$

or

$$\frac{\sigma_{\xi B,\max}}{\sigma_{\xi BS,\max}} = \frac{\sigma_{\xi B}(\pi/2)}{\sigma_{\xi BS}(\pi/2)} = \frac{\sum_{n=1}^{\infty}(-1)^{n+1}nA_n}{\mu\sum_{n=1}^{\infty}(-1)^{n+1}nA_n^*}, \quad b > c \quad \ldots [76]$$

The quantities given by Equations [75] and [76] are plotted as functions of μ in Fig. 5. The broken curves represent the values obtained for $\sigma_{\xi B}(0)/\sigma_{\xi BS}(0)$ with $b/c = 1/4$ and $b/c = 1/2$, using the asymptotic Equation [71c], and the exact value of $\sigma_{\xi BS}$. The corresponding formula is

$$\frac{\sigma_{\xi B,\max}}{\sigma_{\xi BS,\max}} = \frac{3.76b_0}{b_0 - b_1}\frac{1}{\mu^{1/2}} \quad \ldots\ldots [75a]$$

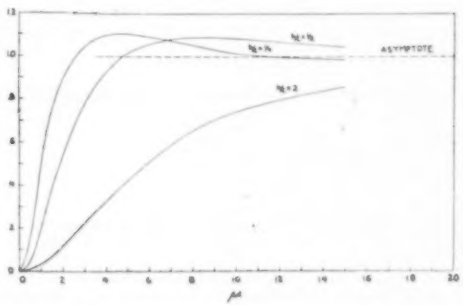

FIG. 4 RATIO OF DOMINANT DIRECT STRESS $\sigma_{\theta D}(\pi/2)$ IN TOROIDAL SHELL SUBJECTED TO UNIFORM WALL PRESSURE TO CORRESPONDING DIRECT STRESS OF MEMBRANE THEORY $\sigma_{\theta M}(\pi/2)$ AS FUNCTION OF $\mu = \sqrt{12(1-\nu^2)}\,(bc/ah)$ AND b/c

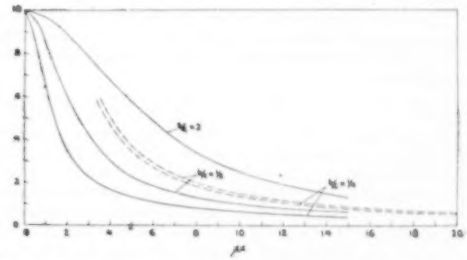

FIG. 5 RATIO OF MAXIMUM BENDING STRESS $\sigma_{\xi B}$ IN TOROIDAL TUBE SUBJECTED TO UNIFORM WALL PRESSURE TO CORRESPONDING STRESS $\sigma_{\xi BS}$ OF A STRAIGHT TUBE WITH SAME CROSS SECTION

The corresponding asymptote for $\sigma_{\xi B}(\pi/2)/\sigma_{\xi BS}(\pi/2)$ with $b/c = 2$ is the line $\sigma_{\xi B}(\pi/2) = 0$ to within the order of the approximation represented by Equation [71c].

Since $\sigma_{\theta D,\max} \to 0$ as $\mu \to 0$, it follows that for sufficiently small μ the maximum stress in the shell is due to the bending stress $\sigma_{\xi B}$. However, for sufficiently large μ the situation is reversed, since $\sigma_{\xi B}$ then becomes negligible compared to $\sigma_{\theta D}$. For $b/c = 1/2$, $\sigma_{\xi B}(0)$ and $\sigma_{\theta D}(\pi/2)$ are approximately equal for $\mu = 8$. For $b/c = 2$, $\sigma_{\xi B}(\pi/2)$ and $\sigma_{\theta D}(\pi/2)$ are approximately equal for $\mu = 4$.

In Fig. 6 we have plotted the ratios of the displacements δ_H and δ_V to the corresponding quantities for a straight tube. From Equations [32] and [56], these ratios are given by

$$\frac{\delta_H}{\delta_{HS}} = \frac{1}{\mu}\frac{\sum_{n=1}^{\infty}\frac{(-1)^{n+1}4n}{4n^2-1}A_n}{\sum_{n=1}^{\infty}\frac{(-1)^{n+1}4n}{4n^2-1}A_n^*} \quad \ldots\ldots [77]$$

$$\frac{\delta_V}{\delta_{VS}} = \frac{1}{\mu}\frac{\sum_{n=1}^{\infty}\frac{4n}{4n^2-1}A_n}{\sum_{n=1}^{\infty}\frac{4n}{4n^2-1}A_n^*} \quad \ldots\ldots [78]$$

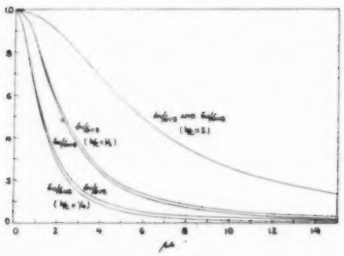

FIG. 6 RATIO OF MAXIMUM HORIZONTAL AND VERTICAL DISPLACEMENTS IN TOROIDAL TUBE SUBJECTED TO UNIFORM WALL PRESSURE TO CORRESPONDING DISPLACEMENTS FOR A STRAIGHT TUBE OF SAME CROSS SECTION

For the case $b/c = 2$ the values for the ratios δ_H/δ_{HS} and δ_V/δ_{VS} are not identical but differ by too small an amount to show in the graph.

In design considerations values for the deflections δ_H and δ_V are frequently estimated by neglecting the curvature of the center line of the toroidal shell. The present results indicate the conservativeness of such estimates.

BENDING OF CURVED TUBES OF ELLIPTICAL CROSS SECTION

In a previous paper (3) two of the present authors considered the problem of the bending of curved tubes from the point of view of shell theory. Results were obtained for tubes of circular cross section for the full range of values of μ. Corresponding results also were obtained for tubes of elliptical cross section for large values of μ. Since the problem of the bending of curved tubes is closely related mathematically to the problem of the tube subjected to wall pressure, we may extend the previous work on tubes of elliptical cross section to the range of smaller values of μ for which the asymptotic methods used before are no longer valid.

If we consider the center line of a curved tube to form an arc of a circle, then the tube forms part of a shell of revolution, and the theory outlined in the section, Small Deflection Theory of Thin Shells of Revolution, may be applied with a slight modification (4). The modification arises from the fact that for a curved tube the displacements u, w, and v no longer may be assumed to be axially symmetric and univalued. Instead we must assume that v is multivalued and of the form

$$v = k\,r\,\theta \qquad [79]$$

where k is a constant. If κ is the curvature of the center line of the tube (i.e., $\kappa = 1/a$) and $\Delta\kappa$ the change in curvature due to bending, then the constant k may be interpreted as the relative change in the curvature or

$$k = \Delta\kappa/\kappa \qquad [80]$$

On the basis of Equation [79], it is found that Equation [3b] is changed to

$$\epsilon_{\theta M} = (u/r) + k \qquad [81]$$

This modification of $\epsilon_{\theta m}$ adds the term $r'k$ to the right side of the compatibility Equation [5] which produces a corresponding modification of the right side of Equation [10b]. Aside from these changes the theory and equations of the section just mentioned remain the same.

Using the notation of the section, Toroidal Shells of Elliptical Cross Section, for a tube of elliptical cross section the foregoing modification of the theory introduces a term on the right of Equation [19b] which is of the form

$$\frac{\mu k \cos\xi}{1 + \lambda \sin\xi}\sqrt{1 - e^2\cos^2\xi} \qquad [82]$$

If terms in λ are again neglected and if we assume now that there is no pressure acting on the tube walls, the equations corresponding to Equations [19] for the bending of a curved tube subjected to an applied moment become

$$\beta'' - \frac{e^2\sin\xi\cos\xi}{1 - e^2\cos^2\xi}\beta' + \frac{c}{b}\mu\sin\xi\sqrt{1 - e^2\cos^2\xi}\,\Psi = 0 \qquad [83a]$$

$$\Psi'' - \frac{e^2\sin\xi\cos\xi}{1 - e^2\cos^2\xi}\Psi' - \frac{c}{b}\mu\sin\xi\sqrt{1 - e^2\cos^2\xi}\,\beta = \mu k\cos\xi\sqrt{1 - e^2\cos^2\xi} \qquad [83b]$$

Except for the form of the term on the right of Equation [83b] these equations are mathematically the same as Equations [26]. Consequently, the solutions of Equations [83] may likewise be expressed as Fourier series of the form

$$\beta = -\mu k\sum_{n=1}^{\infty} A_n'\sin 2n\xi \qquad [84a]$$

$$\Psi = -\mu k\sum_{n=1}^{\infty} B_n'\cos(2n-1)\xi \qquad [84b]$$

By analogy the recurrence equations for A_n' and B_n' are the same as Equations [36] for the coefficients A_n and B_n except that the right side of the second equation involves the coefficients in Expansion [33b] instead of those in Expansion [33a]. Explicitly, the term f_m on the right of Equation [36b] is now replaced by

$$f_m' = (1/2)(b_{m-1} + b_m) \qquad [85]$$

while the other quantities c_{mn}, d_{mn}, and e_{mn} are the same as before.

Having solved the recurrence equations and obtained the coefficients A_n' and B_n' a relation between the applied moment m, which produces the bending of a tube, and the constant k or the change of curvature $\Delta\kappa$, may be obtained from the following equation defining m

$$m = \int_0^{2\pi}(r - a)\alpha N_\theta d\xi \qquad [86]$$

Substituting from Equation [6b] for αN_θ, integrating by parts, and writing rH in terms of Ψ (using Equation [18]), Equation [86] becomes

$$m = -(Eh^3b/\gamma)\int_0^{2\pi}\Psi\cos\xi\,d\xi \qquad [87]$$

Introducing Ψ from Equation [84b] into Equation [87] we have

$$m = E(\pi hb^3c)B_1'\Delta\kappa \qquad [88]$$

where we have used the definition of μ given by Equations [16] and have set $k/a = \Delta\kappa$ according to Equation [80].

For a straight tube, elementary bending theory gives

$$m = EI\Delta\kappa \qquad [89]$$

where I is the moment of inertia of the cross section of the tube and EI is known as the stiffness factor for the tube. If we now define a "rigidity factor" ρ for a curved tube such that

$$m = \rho EI\ \Delta\kappa \quad [90]$$

then ρEI is the "effective" stiffness factor of the tube. Equating Formulas [88] and [90], we have

$$\rho = (\pi hb^2c/I)B_1' \quad [91]$$

The moment of inertia of the elliptical cross section is given by

$$I = \int_0^{2\pi} (r - a)^2 h a d\xi = \frac{1}{2}\pi(b_0 - b_1)hcb^2 \quad [92]$$

where b_0 and b_1 are given in terms of complete elliptic integrals by Equations [40]. Using Equation [92], Equation [91] becomes finally

$$\rho = 2B_1'/(b_0 - b_1) \quad [93]$$

For large values of μ it was found in reference (3) using asymptotic methods of integration, that

$$\rho = \frac{4}{b_0 - b_1}\frac{b}{c}\frac{1}{\mu} \quad [94]$$

A tabulation of the quantity $b_0 - b_1$ as a function of b/c shows that it may be approximated with an error of less than 1 per cent by the formula

$$b_0 - b_1 = \frac{2}{\pi}\left[\frac{8}{3} + \left(\pi - \frac{8}{3}\right)\left(\frac{b}{c}\right)^2\right] \quad [95]$$

Using this approximation and taking μ from Equations [16] the asymptotic representation, Equation [94] may also be written as

$$\rho = \frac{0.680}{\sqrt{1 - \nu^2}}\frac{ah/c^2}{1 + 0.178(b/c)^2} \quad [94a]$$

The rigidity factor ρ is plotted in Fig. 7 as a function of μ for the four cases $b/c = 1/4, 1/2, 1, 2$. The broken lines are

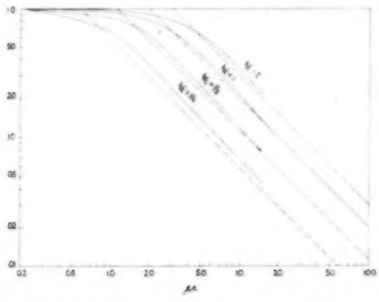

FIG. 7 RIGIDITY FACTOR ρ FOR STIFFNESS IN PURE BENDING OF CURVED TUBE WITH ELLIPTICAL CROSS SECTION FOR VARIOUS VALUES OF b/c AND $\mu = \sqrt{12(1 - \nu^2)}\ (bc/ah)$

the results of using the asymptotic Equation [94]. The curve for $b/c = 1$ is taken from reference (3). It is evident that as b/c becomes smaller, larger values of μ are required before the asymptotic solution agrees with the series solution.

We now turn to the consideration of the stress $\sigma_{\theta D}$. Combining Equations [6b], [11a], and [18], we have

$$\sigma_{\theta D} = (Eh/\gamma\alpha)\Psi' \quad [96]$$

If we compare this with the maximum fiber stress in a straight tube, namely

$$\sigma_{SM} = mb/I = \rho E(k/a)b \quad [97]$$

we have, taking Ψ from Equation [84b] and ρ from Equation [93]

$$\frac{\sigma_{\theta D}}{\sigma_{SM}} = \frac{b_0 - b_1}{2\sqrt{1 - e^2\cos^2\xi}}\sum_{n=1}^{\infty}\frac{B_n'}{B_1'}\sin(2n - 1)\xi \quad [98]$$

From work done concerning tubes of circular cross section, it is expected that for sufficiently small values of μ this stress is numerically largest at $\xi = \pm\pi/2$ but that as μ becomes larger the points of maximum fiber stress move closer and closer to the neutral surface.

It was also found in our previous work that for sufficiently large μ, say, $\mu \geq 5$ or so, the maximum stress occurring in a tube is the wall bending stress $\sigma_{\xi B}$ rather than the stress $\sigma_{\theta D}$. From Equation [27c], with β from Equation [84a] and σ_{SM} from Equation [97], we find

$$\frac{\sigma_{\xi B}}{\sigma_{SM}} = -\sqrt{\frac{3}{1 - \nu^2}}\frac{b_0 - b_1}{\sqrt{1 - e^2\cos^2\xi}}\sum_{n=1}^{\infty}\frac{nA_n'}{B_1'}\cos 2n\xi \quad [99]$$

For $b \leq c$, to which cases we will restrict attention here, the maximum of $\sigma_{\xi B}$ is at $\xi = 0$ or π, or

$$\frac{\sigma_{\xi B,\max}}{\sigma_{SM}} = -\sqrt{\frac{3}{1 - \nu^2}}\frac{b_0 - b_1}{b/c}\sum_{n=1}^{\infty}\frac{nA_n'}{B_1'} \quad [99a]$$

The corresponding asymptotic formula is, according to reference (3)

$$\frac{\sigma_{\xi B,\max}}{\sigma_{SM}} = \frac{0.415}{\sqrt{1 - \nu^2}}\frac{b_0 - b_1}{b/c}\mu^{1/2} \quad [99b]$$

In Fig. 8, the ratio $-\sqrt{1 - \nu^2}\,\sigma_{\xi B}(0)/\sigma_{SM}$ has been plotted for $b/c = 1/4, 1/2$, and 1. The notation is the same as for other curves. The curve for $b/c = 1$ and the asymptotes are taken from reference (3).

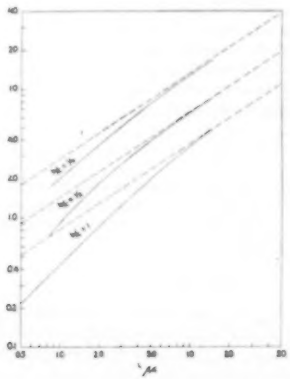

FIG. 8 RATIO OF MAXIMUM WALL BENDING STRESS FOR CURVED TUBE IN PURE BENDING TO MAXIMUM FIBER STRESS FOR STRAIGHT TUBE WITH SAME CROSS SECTION

Analysis of Bourdon Tubes With Elliptical Cross Section

The basic principle of a Bourdon tube is that if pressure is introduced into a curved tube, closed at the ends, the tube will uncurl by an amount proportional to the pressure, provided it is not otherwise restrained. This action may be explained as follows: Consider first the complete toroidal shell subjected to internal pressure. When $b < c$ this pressure produces circumferential compression in the portion of the wall nearest to the axis of the shell, and circumferential tension in the portion of the wall furthest away from the axis. Consequently, the internal pressure is associated with a resultant internal moment of the circumferential stresses $\sigma_{\phi D}$. Now take only a portion of the complete torus, with the same internal pressure and with the ends closed but not otherwise restrained. The shell can now no longer take the moment of the stresses $\sigma_{\phi D}$. It follows that, except for edge effects, the state of stress and deformation in the incomplete toroidal shell may be considered as a superposition of two states, namely, that of the complete torus under internal pressure and that of the incomplete torus without wall pressure but acted upon by end bending moments. Both these states have been considered in the foregoing discussion.

The moment over a cross section produced by a pressure p may be computed from Equation [86]. With $N_\phi = h\sigma_{\phi D}$ and $\sigma_{\phi D}$ taken from Equation [27b], Equation [86] becomes

$$m_p = m_{pM} - (Eh^3b/\gamma)\int_0^{2\pi} \eta \cos \xi \, d\xi \quad [100]$$

where the term in η is obtained by integrating by parts and where m_{pM} is the value of the moment m_p according to membrane theory or

$$m_{pM} = \pi c^2 abcp \quad [101]$$

This moment m_{pM} is given by Lorenz (2, 5) and Schubert (10), but as far as is known, the correction to it due to wall bending has never been determined explicitly. If we introduce η from Equation [30b], Equation [100] reduces to

$$m_p = m_{pM}[1 - (b/c)^2 B_1] \quad [102]$$

For large μ, if we take η from Equation [67b] and introduce $x = \mu^{1/4} \sin \xi$ as variable of integration, we have

$$m_p = m_{pM}\left[1 + \frac{4}{\pi}\frac{1}{\mu}\int_0^{\mu^{1/2}} \frac{(1 - e^2)^{1/2} \cos \xi}{(1 - e^2 \cos^2 \xi)^{3/2}} T_r(x)dx\right] \quad [103]$$

In view of the behavior of $T_r(x)$, as shown in Fig. 3, the major contribution of the integrand to the integral in Equation [103] occurs for small values of ξ, in which range we may approximate the fraction in the integrand by unity. As an approximation for the entire integral we then take

$$\int_0^\infty T_r(x)\, dx = -\pi/2 \quad [104]$$

where the value $-\pi/2$ has been determined by numerical integration. Substituting this value in Equation [103] we have finally for large μ the following simple expression for the moment produced by the pressure p

$$m_p = m_{pM}[1 - (2/\mu)] \quad [105]$$

The ratio, m_p/m_{pM}, is plotted in Fig. 9, using Equation [102], and the numerical results of the trigonometric series solutions. It is noted that unless μ is fairly large the membrane moment m_{pM} is considerably in error.

For the Bourdon tube the moment m_p must be balanced by a moment m_b which is applied over the end sections of the tube, so that

$$m_b + m_p = 0 \quad [106]$$

The moment m_b is the same as the moment m given by Equations [87] and [88]. Consequently, we have

$$E\pi hb^2 cB_1'\Delta\kappa + m_{pM}[1 - (b/c)^2 B_1] = 0 \quad [107]$$

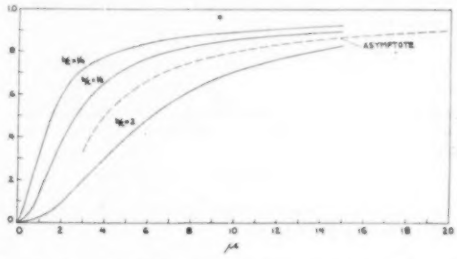

Fig. 9 Ratio of Moment m_p of Stresses $\sigma_{\phi D}$ for Complete Torus Subjected to Uniform Normal Wall Pressure p to Corresponding Moment m_{pM} According to Membrane Theory

From this relation there follows for the change of curvature $\Delta\kappa$ of the Bourdon tube the expression

$$\Delta\kappa = -\frac{m_{pM}}{E\pi hb^2 c}\frac{1 - (b/c)^2 B_1}{B_1'} \quad [107a]$$

In view of Equation [92] this may be written in the form

$$\Delta\kappa = -\frac{m_{pM}}{EI}\frac{1 - (b/c)^2 B_1}{2B_1'/(b_0 - b_1)} \quad [107b]$$

For large values of μ we introduce into Equation [106] the quantity m_p as given by Equation [105] and the quantity m_b as given by Equations [90] and [94]. This gives the following simple result

$$\Delta\kappa = -\frac{m_{pM}}{EI}\frac{b_0 - b_1}{4}\frac{c}{b}(\mu - 2) \quad [108]$$

Equations [107b] and [108] may be compared with the formula $\Delta\kappa = -m_{pM}/EI$ which was obtained by Lorenz, reference (2) and again used in reference (7). Lorenz's formula was once more suggested by Schubert (10). We note that this earlier formula presupposed that the rigidity factor ρ is replaced by 1 at the same time the moment m_p is replaced by m_{pM}. Now the approximation $\rho = 1$ is good only for very small values of μ and the approximation $m_p = m_{pM}$ is good only for very large values of μ; so using them simultaneously cannot very well be undertaken. This fact is borne out by our numerical calculations, the results of which are given in Fig. 10. In Fig. 10 the formula $\Delta\kappa = -m_{pM}/EI$ would appear as a straight line with unit distance from the μ-axis.

Concerning the present calculations, it should be noted that when $b/c = 1/4$ and $\mu = 15$, the series solutions do not converge very rapidly. This is indicated by plotting separately the results obtained with 6, 8, and 10 simultaneous equations, respectively. The true result will be nearer the asymptotic result than that obtained by solving 10 simultaneous equations.

Our results indicate that as long as $c/b < 4$ the asymptotic Equation [108] is sufficiently accurate for practical purposes as soon as μ is larger than about 6 or bc/ah is larger than about 2. The following alternate form of Equation [108] also may be listed.

Write $\kappa = 1/a$, $\Delta\kappa = -\Delta a/a^2$. Then with m_{pM} from Equation [101] and I from Equation [92] we have

$$\frac{\Delta a}{a} = \frac{p}{E}\frac{a}{b}\frac{c^2 - b^2}{h^2}\left[\sqrt{3(1-\nu^2)} - \frac{ah}{cb}\right] \quad \ldots [108b]$$

This simple formula for the sensitivity of the tube is applicable as long as $c/b < 4$ as soon as cb/ah is larger than about 2. For sufficiently large values of cb/ah the second term inside the bracket may be omitted with the result of an even simpler formula.

Maximum Stresses in Bourdon Tube. Experience indicates that the critical stresses in a Bourdon tube are the bending stresses $\sigma_{\xi B}$ at those points where the curvature of the cross section is greatest, i.e., at the points $\xi = 0$ and $\xi = \pi$. As the stresses are obtained by combining those due to the internal pressure and those due to the superimposed bending moments at the ends of the tube, we have

$$\sigma_{\xi B.\max} = \sigma_{\xi B.p}(0) + \sigma_{\xi B.b}(0) \quad \ldots [109]$$

In Equation [109] we take $\sigma_{\xi B.p}$ from Equation [31a] and $\sigma_{\xi B.b}$ from Equation [99]. In Equation [99] we eliminate σ_{xM} by means of Equations [97], [106], [102], and [92] in this order. The end result is as follows

$$\frac{\sigma_{\xi B.\max}}{p} = \sqrt{\frac{12}{1-\nu^2}}\left(1 - \frac{b^2}{c^2}\right)\frac{ac}{bh}\sum_{n=1}^{\infty} n\left[A_n\frac{b^2}{c^2} + \frac{1 - \dfrac{b^2}{c^2}B_1}{B_1'}A_n'\right] \quad \ldots [110]$$

It was found to be convenient to express this stress in terms of the corresponding bending stress in a straight tube as given by Equation [55c]. This gives

$$\frac{\sigma_{\xi B.\max}}{\sigma_{\xi BS}(0)} = \frac{\displaystyle\sum_{n=1}^{\infty} n\left[A_n + \frac{(c/b)^2 - B_1}{B_1'}A_n'\right]}{\mu\displaystyle\sum_{n=1}^{\infty} n\,A_n^*} \quad \ldots [111]$$

In Equation [111] it should be observed that, by definition we have $A_n^* = \lim_{\mu\to 0} A_n/\mu$, and since according to Equation [52] $\lim_{\mu\to 0} B_1 = (c/b)^2$ it follows that Equation [111] implies the following limit relation

$$\lim_{\mu\to 0}\frac{\sigma_{\xi B.\max}}{\sigma_{\xi BS}(0)} = 1 \quad \ldots [111a]$$

Numerical calculations for the cases $b/c = 1/4$ and $1/2$ show that the values of $\sigma_{\xi B.\max}/\sigma_{\xi BS}(0)$ gradually decrease from their maximum 1, Fig. 11. Thus we have found the noteworthy result that the maximum bending stress in the Bourdon tube is always below, but often not very much below, the corresponding bending stress in a cylindrical tube of the same cross section subjected to the same wall pressure p.

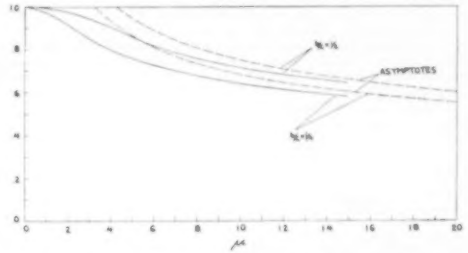

FIG. 11 RATIO OF MAXIMUM BENDING STRESS IN BOURDON TUBE TO CORRESPONDING STRESS IN CYLINDRICAL TUBE AS FUNCTION OF b/c AND μ

For sufficiently large values of μ we obtain in a similar fashion, from Equation [71c] and from the asymptotic formula for $\sigma_{\xi B.b}(0)$ in reference (3), the following asymptotic formula for $\sigma_{\xi B.\max}$

$$\frac{\sigma_{\xi B.\max}}{p} = \frac{0.814}{\sqrt{1-\nu^2}}\frac{ac}{bh}\left(1 - \frac{b^2}{c^2}\right)\mu^{3/4} \quad \ldots [112]$$

Equation [112] should be compared with Equation [110]. In Equation [112] we may again introduce the corresponding bending stress for the straight tube which is given by

$$\sigma_{\xi BS}(0) = \frac{3}{2}\left(1 - \frac{b^2}{c^2}\right)\left(\frac{c}{h}\right)^2 p\left(1 - \frac{b_1}{b_0}\right) \quad \ldots [113]$$

Consequently

$$\frac{\sigma_{\xi B.\max}}{\sigma_{\xi BS}(0)} = \frac{1.87 b_0}{b_0 - b_1}\frac{1}{\mu^{1/4}} \quad \ldots [113a]$$

where b_0 and b_1 are given as functions of b/c by means of Equation [40]. Equation [113a] is also plotted in Fig. 11 and it is seen that the exact curve and the asymptotic curve begin to approach each other when μ is greater than about 5.

Our comparisons of the asymptotic solution and of the series solution have been carried out for cross-section ratios of $1/4$ and $1/2$ and for these values of b/c agreement was found to be satisfactory. In practice one would generally use smaller values of b/c than these. It remains to be determined to what extent the asymptotic solution must be modified in order to apply for these smaller values of b/c. In particular, it seems desirable to investigate the behavior of the solution when the ratio b/c tends to zero.

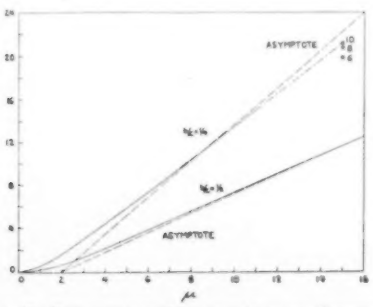

FIG. 10 DIMENSIONLESS CURVATURE CHANGE FUNCTION $\Delta\kappa(m_{pM}/EI)$ OF BOURDON TUBE AS FUNCTION OF b/c AND $\mu = \sqrt{12(1-\nu^2)}\,cb/ah$

ACKNOWLEDGMENT

The authors are indebted to Miss Katherine E. Kavanagh of the Massachusetts Institute of Technology Computation Laboratory for effective assistance.

BIBLIOGRAPHY

1 "Drang und Zwang," by A. Föppl and L. Föppl, R. Oldenbourg, Munich, Germany, 1944.

2 "Theorie der Röhrenfedermanometer," by H. Lorenz, *Zeitschrift des Vereines deutscher Ingenieure*, vol. 54, 1910, p. 1865.

3 "Bending of Curved Tubes," by R. A. Clark and E. Reissner, *Advances in Applied Mechanics*, Academic Press, New York, N. Y., vol. 2, 1951, pp. 93–122.

4 "On Bending of Curved Thin-Walled Tubes," by E. Reissner, Proceedings of the National Academy of Sciences, vol. 35, 1949, pp. 204–208.

5 "Theorie der Röhrenfedermanometer," by H. Lorenz, *Physikalische Zeitschrift*, vol. 18, 1917, p. 117.

6 "Mathematical Theories of Bourdon Pressure Tubes and Bending of Curved Pipes," by M. Tueda, Memoirs, College of Engineering, Kyoto Imperial University, vol. 8, 1934, pp. 102–115; vol. 9, 1936, pp. 132–152.

7 "An Elementary Theory of the Bourdon Gage," by A. Wolf Trans. ASME, vol. 68, 1946, pp. 207–210.

8 "On the Theory of Thin Elastic Shells," by E. Reissner, Reissner Anniversary Volume: *Contributions to Applied Mechanics*, p. 231, Edwards, Ann Arbor, Mich., 1949.

9 "On the Theory of Toroidal Tubes of Elliptical Cross Section Subjected to Uniform Wall Pressure," by T. I. Gilroy, SM thesis, Massachusetts Institute of Technology, January, 1950.

10 "Über Effekte zweiter Ordnung bei Biegung und Torsion dünnwandiger Rohre elliptischen Querschnitts," by G. Schubert, *Ingenieur-Archiv*, vol. 12, 1941, pp. 53–63.

11 "Stress and Strain in Thin Elliptical Cylinder Under Internal Pressure," by W. S. Brown, *The Engineer*, vol. 162, 1936, p. 201.

12 "The Bending of the Curved Tube of Elliptic Section," by M. T. Huber, Proceedings of the 7th Congress of Applied Mechanics, vol. 1, 1949, p. 322.

Torsion of Curved Beams of Rectangular Cross Section

By H. L. LANGHAAR,[1] URBANA, ILL.

Recently, W. Freiberger[2] obtained an exact solution of the problem of uniform torsion of a segment of a ring of circular cross section. This paper presents a solution of the problem for the rectangular cross section. O. Göhner[3] previously treated this case by an approximation method.

Introduction

UNIFORM torsion cannot be realized exactly if the axis of the beam has variable curvature. If the axis is a circular arc, uniform torsion can be obtained theoretically by fixing one end of the beam and applying a force P at the end of a radial lever that extends from the free end of the beam to the center of the arc, Fig. 1. The stress distribution that is obtained in this way is not pure torsion, in the usual sense, since a shearing force P exists on any cross section.

Formulation of the Problem

The axis of a curved beam is understood to be any specified curve that is normal to the cross sections of the beam. The arc length z, measured along the axis from a fixed point, serves as a co-ordinate for locating cross sections of the beam. Rectangular co-ordinates x, y, in the plane of a cross section are situated so that their origin is on the axis of the beam, and the y-axis coincides with the principal normal to the axis of the beam. The positive y-axis is directed away from the center of curvature of the axis of the beam, Fig. 1. The variables x, y, z, are curvilinear space co-ordinates. These co-ordinates are orthogonal if the axis of the beam is a plane curve.

The conventional stress notations are used. Göhner[3,4] has shown that when the radius of curvature R of the axis of the beam is constant, nontrivial solutions of the equations of elasticity exist that satisfy the conditions

$$\sigma_x = \sigma_y = \sigma_z = \tau_{xy} = 0, \quad \frac{\partial \tau_{zx}}{\partial z} = \frac{\partial \tau_{yz}}{\partial z} = 0$$

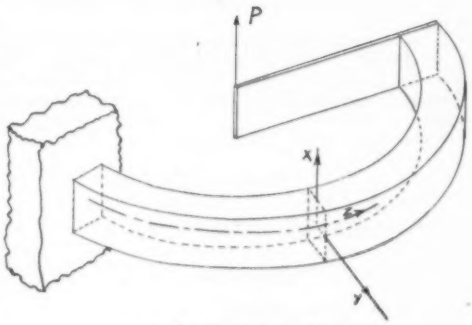

Fig. 1 General View of Beam

Then the equilibrium equations reduce to

$$\frac{\partial}{\partial x}\left[(R+y)^2\,\tau_{zx}\right] + \frac{\partial}{\partial y}\left[(R+y)^2\,\tau_{yz}\right] = 0 \qquad [1]$$

This equation may be derived by balancing the z-components of force on a differential volume element. Equation [1] shows that there is a function $\phi(x, y)$ such that

$$\tau_{zx} = \frac{R^2}{(R+y)^2}\frac{\partial \phi}{\partial y}, \quad \tau_{yz} = -\frac{R^2}{(R+y)^2}\frac{\partial \phi}{\partial x} \qquad [2]$$

Since a volume element of the beam is $(1 + y/R)\,dx\,dy\,dz$, the strain energy, per unit length of the axis, is

$$U = \frac{1}{2G}\int\int \frac{R+y}{R}\left(\tau_{zx}^2 + \tau_{yz}^2\right) dx\,dy \qquad [3]$$

The torque is

$$M_z = \int\int \left(x\tau_{yz} - y\tau_{zx}\right) dx\,dy \qquad [4]$$

By the principle of least work, the compatibility equation is obtained by minimizing U among stresses that satisfy Equations [2] and [4]. The auxiliary condition (Equation [4]) will be treated by the method of Lagrange multipliers. The modified strain-energy expression is

$$U = \int\int \left[\frac{R^2}{(R+y)^2}\left(\phi_x^2 + \phi_y^2\right) + \frac{2CP}{(R+y)^2}\left(x\phi_x + y\phi_y\right)\right] dx\,dy \qquad [5]$$

in which ϕ_x and ϕ_y are abbreviations for $\partial\phi/\partial x$ and $\partial\phi/\partial y$. The factor $2\,CP$ is a Lagrange multiplier. P denotes the shear load on the beam.

The Euler equation is

[1] Professor, Theoretical and Applied Mechanics Department, University of Illinois. Mem. ASME.

[2] "The Uniform Torsion of an Incomplete Tore," by W. Freiberger, *Australian Journal of Scientific Research*, series A, vol. 2, September, 1949, pp. 354–375.

[3] "Schubspannungsverteilung im Querschnitt eines Schraubenfeder," by O. Göhner, *Ingenieur-Archiv*, vol. 2, 1930, p. 619; also "Schubspannungsverteilung im Querschnitt eines Gedrillten Ringstabs mit Anwendung auf Schraubenfedern, by O. Göhner, *Ingenieur-Archiv*, vol. 2, 1931, p. 1.

[4] "Theory of Elasticity," by S. Timoshenko, art. 111, McGraw-Hill Book Company, Inc., New York, N. Y., 1934, p. 355.

Contributed by the Applied Mechanics Division and presented at the Annual Meeting, Atlantic City, N. J., November 25–30, 1951, of The American Society of Mechanical Engineers.

Discussion of this paper should be addressed to the Secretary, ASME, 29 West 39th Street, New York, N. Y., and will be accepted until April 10, 1952, for publication at a later date. Discussion received after the closing date will be returned.

Note: Statements and opinions advanced in papers are to be understood as individual expressions of their authors and not those of the Society. Manuscript received by ASME Applied Mechanics Division, February 28, 1951. Paper No. 51—A-14.

$$\frac{\partial}{\partial x}\frac{\partial F}{\partial \phi_x} + \frac{\partial}{\partial y}\frac{\partial F}{\partial \phi_y} = 0$$

in which F is the integrand of Equation [5]. Consequently, the compatibility equation is

$$\frac{\partial^2 \phi}{\partial x^2} + \frac{\partial^2 \phi}{\partial y^2} - \frac{3}{R+y}\frac{\partial \phi}{\partial y} + \frac{2CP}{R^2} = 0 \quad \ldots\ldots [6]$$

This equation was derived by Göhner by geometrical considerations.

As in the classical torsion problem, the boundary condition is $\phi = \text{const}$, since the normal component of the vector (τ_{xz}, τ_{yz}) is zero at the boundary. It is permissible to let the boundary value be zero, since solutions of Equation [6] contain an arbitrary additive constant.

The substitution

$$\phi = \psi - \frac{CPx^2}{R^2} \quad \ldots\ldots [7]$$

reduces Equation [6] to

$$\frac{\partial^2 \psi}{\partial x^2} + \frac{\partial^2 \psi}{\partial y^2} - \frac{3}{R+y}\frac{\partial \psi}{\partial y} = 0 \quad \ldots\ldots [8]$$

The boundary value for ψ is

$$\psi = \frac{CPx^2}{R^2} \quad \ldots\ldots [9]$$

The translation of co-ordinates

$$X = x, \quad Y = R + y \quad \ldots\ldots [10]$$

displaces the origin to the center of curvature of the axis. Equation [8] then becomes

$$\frac{\partial^2 \psi}{\partial x^2} + \frac{\partial^2 \psi}{\partial Y^2} - \frac{3}{Y}\frac{\partial \psi}{\partial Y} = 0 \quad \ldots\ldots [11]$$

Thus, for any given cross-sectional shape, the problem resolves itself into the determination of a function $\psi(x, Y)$ that satisfies Equation [11] and the boundary condition. If the cross section is symmetrical about the Y-axis, ϕ and ψ are even functions of x, since τ_{xz} and τ_{yz} are even and odd functions of x, respectively.

Deflection Theory

The displacement vector of a point Q in the beam is defined by its components u, v, w, on straight lines that are tangent to the co-ordinate lines at the point Q. If the approximations of the small-deflection theory of elasticity are used, the strains of line elements in the x, y, and z directions are

$$\left.\begin{aligned} \epsilon_x &= \frac{\partial u}{\partial x}, \quad \epsilon_y = \frac{\partial v}{\partial y} \\ \epsilon_z &= \frac{R}{R+y}\frac{\partial w}{\partial z} + \frac{v}{R+y} \end{aligned}\right\} \quad \ldots\ldots [12]$$

The shearing strains between pairs of line elements that lie along the co-ordinate lines are

$$\left.\begin{aligned} \gamma_{xz} &= (R+y)\frac{\partial}{\partial x}\left(\frac{w}{R+y}\right) + \frac{R}{R+y}\frac{\partial u}{\partial z} \\ \gamma_{yz} &= (R+y)\frac{\partial}{\partial y}\left(\frac{w}{R+y}\right) + \frac{R}{R+y}\frac{\partial v}{\partial z} \\ \gamma_{xy} &= \frac{\partial v}{\partial x} + \frac{\partial u}{\partial y} \end{aligned}\right\} \quad \ldots [13]$$

Equations [12] and [13] may be obtained by transforming the strain-displacement relations from rectangular co-ordinates to the co-ordinates x, y, z. This is a routine problem of tens or calculus.

The usual stress-strain relations exist. Consequently, since $\sigma_x = \sigma_y = \sigma_z = \tau_{xy} = 0$, it follows that $\epsilon_x = \epsilon_y = \epsilon_z = \gamma_{xy} = 0$. Also γ_{xz} and γ_{yz} are independent of z. Freiberger[2] has shown that these conditions lead to the following equations for the displacement components

$$u = kz, \qquad v = 0, \qquad w = w(x, y) \quad \ldots\ldots [14]$$

These equations show that the cross sections do not undergo any rotations nor deformations in their planes; they are merely translated in the x-direction.

The constant k may be calculated by Castigliano's theorem. In view of Equations [2] and [3], the strain energy per unit length of the axis is

$$U = \frac{R^2}{2G}\int\int \frac{\phi_x^2 + \phi_y^2}{(R+y)^3}\,dx\,dy \quad \ldots\ldots [15]$$

This equation may be transformed by the divergence theorem

$$\int\int\left(\frac{\partial A}{\partial x} + \frac{\partial B}{\partial y}\right)dx\,dy = \oint A\,dy - B\,dx$$

Set

$$A = \frac{\phi\phi_x}{(R+y)^3}, \quad B = \frac{\phi\phi_y}{(R+y)^3}$$

Then, in view of Equation [6] and the boundary condition, $\phi = 0$

$$U = \frac{CPR}{G}\int\int \frac{\phi}{(R+y)^3}\,dx\,dy \quad \ldots\ldots [16]$$

The shear force on a section is

$$P = \int\int \tau_{xz}\,dx\,dy = \int\int \frac{R^2\phi_y}{(R+y)^2}\,dx\,dy \quad \ldots [17]$$

The formula for integration by parts

$$\int\int A\frac{\partial B}{\partial y}\,dx\,dy = -\int\int B\frac{\partial A}{\partial y}\,dx dy - \oint AB\,dx$$

yields, with Equation [17]

$$P = 2R^2\int\int \frac{\phi}{(R+y)^3}\,dx\,dy \quad \ldots\ldots [18]$$

Equations [16] and [18] yield

$$U = \frac{CP^2}{2GR} \quad \ldots\ldots [19]$$

This is the strain energy per unit length. The strain energy in a length z is, accordingly

$$V = \frac{CP^2 z}{2GR} \quad \ldots\ldots [20]$$

Castigliano's theorem asserts $u = \partial V/\partial P$. Consequently

$$u = \frac{CPz}{GR} \quad \ldots\ldots [21]$$

Equations [19] and [21] reveal the physical significance of the constant C.

Solution for the Rectangular Section

The general principle of similarity for elastic structures determines the effect of the size of the beam. Consequently, there is no loss of generality if the width of the cross section is set equal to π, Fig. 2.

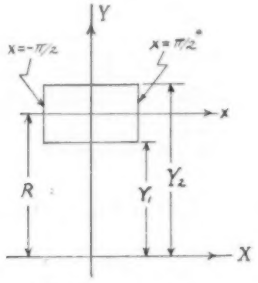

Fig. 2 Cross Section of Beam

A solution of the following form will be sought

$$\psi = \frac{\pi^2 CP}{4R^2} + \sum_{1,3,5,\cdots} a_n \cos nx \quad \ldots\ldots [22]$$

The coefficients a_n are functions of Y. Since the series vanishes for $x = \pm\pi/2$, Equation [22] automatically satisfies the boundary condition (Equation [9]) on the edges $x = \pm\pi/2$.

Equation [11] yields the following differential equation for the coefficients

$$\frac{d^2 a_n}{dY^2} - \frac{3}{Y}\frac{da_n}{dY} - n^2 a_n = 0 \quad \ldots\ldots [23]$$

The substitution $a_n = W Y^2$ reduces this to the modified Bessel equation of order 2. The general solution is

$$a_n = CP\frac{Y^2}{R^2}[A_n I_2(nY) + B_n K_2(nY)] \quad \ldots\ldots [24]$$

in which I_2 and K_2 are modified Bessel functions.[5]

For the boundaries $Y = Y_1$ and $Y = Y_2$ (Fig. 2), Equations [9] and [22] yield

$$\sum_{1,3,5,\cdots} a_n \cos nx = \frac{CP}{R^2}\left(x^2 - \frac{\pi^2}{4}\right) \quad \ldots\ldots [25]$$

This equation is valid in the range $0 \leqq x \leqq \pi/2$. The range may be extended to $(-\pi, \pi)$ by the introduction of the following function

$$f(x) = \frac{CP}{R^2}\left(x^2 - \frac{\pi^2}{4}\right), \quad 0 \leqq x \leqq \frac{\pi}{2}$$

$$f(x) = f(-x), \quad f(x) = -f(\pi - x), \; x > \frac{\pi}{2}$$

The cosine series for this function has only odd coefficients. Consequently the coefficients a_n in Equation [25] are obtained by a Fourier expansion of the function $f(x)$ in the range $(-\pi, \pi)$. The result is

$$a_n = -\frac{8CP}{\pi R^2 n^2}(-1)^{\frac{n-1}{2}}, \quad n = 1, 3, 5, \ldots\ldots [26]$$

Thus the values of the coefficients are determined on the boundaries.

Equations [24] and [26] yield

$$\left.\begin{aligned} A_n &= \frac{8(-1)^{\frac{n-1}{2}}[Y_2^2 K_2(nY_2) - Y_1^2 K_2(nY_1)]}{\pi n^3 (Y_1 Y_2)^2 [I_2(nY_2)K_2(nY_1) - I_2(nY_1)K_2(nY_2)]} \\ B_n &= \frac{-8(-1)^{\frac{n-1}{2}}[Y_2^2 I_2(nY_2) - Y_1^2 I_2(nY_1)]}{\pi n^3 (Y_1 Y_2)^2 [I_2(nY_2)K_2(nY_1) - I_2(nY_1)K_2(nY_2)]} \end{aligned}\right\} \quad \ldots [27]$$

The constants A_n and B_n may be computed by Equations [27] when Y_1 and Y_2 are given.

Equations [7], [22], and [24] yield

$$\phi = -\frac{CPx^2}{R^2} + \frac{CPY^2}{R^2}\sum_{1,3,5,\cdots}[A_n I_2(nY) + B_n K_2(nY)]\cos nx \quad \ldots [28]$$

An irrelevant additive constant has been discarded from Equation [28].

If z is a large positive number, the functions $I_\nu(z)$ and $K_\nu(z)$ have the following asymptotic approximations

$$I_\nu(z) \approx \frac{e^z}{\sqrt{2\pi z}}, \quad K_\nu(z) \approx e^{-z}\sqrt{\frac{\pi}{2z}}$$

By virtue of these formulas, Equation [28] reduces to the formula for the torsion function of a straight bar of rectangular cross section, if R becomes infinite and $\lim CP/R^2 = \text{const.}$

Equations [2] and [28] yield

$$\tau_{zs} = CP\sum_{1,3,5,\cdots} n[A_n I_1(nY) - B_n K_1(nY)]\cos nx \quad \ldots [29]$$

$$\tau_{yz} = \frac{2CPx}{Y^2} + CP\sum_{1,3,5,\cdots} n[A_n I_2(nY) + B_n K_2(nY)]\sin nx \quad \ldots [30]$$

The shearing force P on a cross section is

$$P = \int\int \tau_{zs}\, dx\, dY$$

Consequently, by Equation [29]

$$1 = 2C\sum_{1,3,5,\cdots}\frac{(-1)^{\frac{n-1}{2}}}{n}\{A_n[I_0(nY_2) - I_0(nY_1)] + B_n[K_0(nY_2) - K_0(nY_1)]\} \quad \ldots [31]$$

This equation determines the constant C.

For the evaluation of the functions I_2 and K_2, the following recursion formulas are useful

$$I_2(z) = I_0(z) - \frac{2}{z}I_1(z)$$

$$K_2(z) = K_0(z) + \frac{2}{z}K_1(z)$$

Watson[6] has tabulated the functions I_0, I_1, K_0, K_1 for real arguments up to 16. For larger values of the arguments, the asymptotic series may be used

[5] "Bessel Functions," by G. N. Watson, The Macmillan Company, New York, N. Y., 1944, p. 79.

$$I_\nu(z) = \frac{e^z}{\sqrt{2\pi z}}\left[1 - \frac{4\nu^2 - 1^2}{(8z)^1\,\underline{1}} + \frac{(4\nu^2 - 1^2)\,(4\nu^2 - 3^2)}{(8z)^2\,\underline{2}} - \dots\right]$$

$$K_\nu(z) = e^{-z}\sqrt{\frac{\pi}{2z}}\left[1 + \frac{4\nu^2 - 1}{(8z)\,\underline{1}} + \frac{(4\nu^2 - 1^2)\,(4\nu^2 - 3^2)}{(8z)^2\,\underline{2}} + \dots\right] \quad [32]$$

For $z > 16$, good approximations are obtained with the first two terms of the series.

Numerical Example

Let $Y_1 = 4$, $Y_2 = 6$, $R = 5$. Then Equations [27] become

$$A_n = \frac{(-1)^{\frac{n-1}{2}}\,[9K_2(6n) - 4K_2(4n)]}{18\pi\, n^3[I_2(6n)K_2(4n) - I_2(4n)\,K_2(6n)]}$$

$$B_n = \frac{-(-1)^{\frac{n-1}{2}}\,[9I_2(6n) - 4I_2(4n)]}{18\pi n^3[I_2(6n)K_2(4n) - I_2(4n)K_2(6n)]}$$

These equations yield

$A_1 = -1.197 \times 10^{-3}$, $A_3 = 4.704 \times 10^{-10}$, $A_5 = -7.747 \times 10^{-16}$

$A_7 = 2.015 \times 10^{-21}$, $B_1 = -8.704$, $B_3 = 2.280 \times 10^3$

$B_5 = -2.012 \times 10^6$, $B_7 = 2.653 \times 10^9$

Hence Equation [31] yields $C = 24.75$.

For $P = 1$, Equations [29] and [30] yield

$$Y = 4 \begin{cases} \tau_{xz} = 2.400 \cos x - 0.387 \cos 3x + 0.146 \cos 5x \\ \qquad -0.076 \cos 7x + \dots \\ \tau_{yz} = 0 \end{cases}$$

$$Y = 4.5 \begin{cases} \tau_{xz} = 1.069 \cos x - 0.078 \cos 3x + 0.011 \cos 5x \\ \qquad -0.002 \cos 7x + \dots \\ \tau_{yz} = 2.446\, x - 2.242 \sin x + 0.093 \sin 3x - 0.012 \\ \qquad \sin 5x + 0.002 \sin 7x - \dots \end{cases}$$

$$Y = 5.0 \begin{cases} \tau_{xz} = 0.150 \cos x - 0.006 \cos 3x + \dots \\ \tau_{yz} = 1.981\, x - 1.662 \sin x + 0.029 \sin 3x - 0.002 \\ \qquad \sin 5x + \dots \end{cases}$$

$$Y = 5.5 \begin{cases} \tau_{xz} = -0.642 \cos x + 0.046 \cos 3x - 0.006 \cos 5x \\ \qquad + 0.001 \cos 7x - \dots \\ \tau_{yz} = 1.637\, x - 1.492 \sin x + 0.049 \sin 3x \\ \qquad -0.006 \sin 5x + 0.001 \sin 7x - \dots \end{cases}$$

$$Y = 6.0 \begin{cases} \tau_{xz} = -1.528 \cos x + 0.210 \cos 3x - 0.074 \cos 5x \\ \qquad + 0.037 \cos 7x - \dots \\ \tau_{yz} = 0 \end{cases}$$

Stresses computed by these equations have been tabulated on a cross-sectional drawing of the beam, Fig. 3.

For a straight bar with the same torque (5 units), the maximum stress is 1.69.[6] This occurs at the point $x = 0$, $Y = 4$. In this example, the stress at this point is 2.10.

The deflection formula (Equation [21]) yields

$$u = \frac{4.95\, P\, z}{G}$$

The strain energy formula (Equation [19]) yields

$$U = \frac{2.475\, P^2}{G}$$

Comparison With Liesecke's Charts

Basing his calculations on the theory of Göhner, G. Lie-

[6] Reference 4, p. 249.

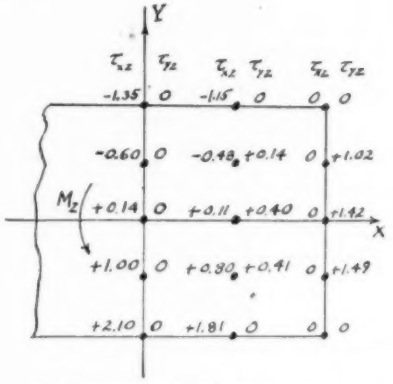

Fig. 3 Stress Distribution on a Cross Section: $Y_1 = 4$, $Y_2 = 6$, $P = 1$

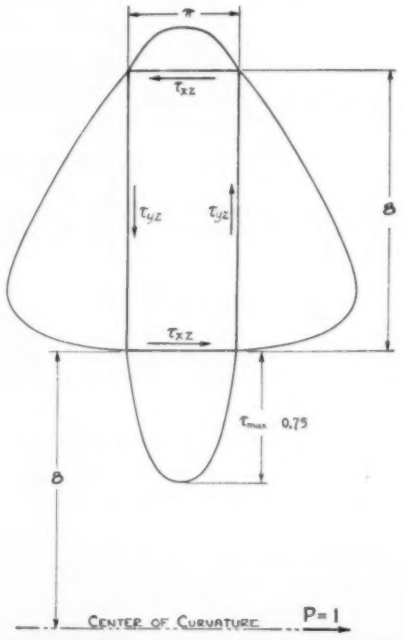

Fig. 4 Graph of Shearing Stress at the Boundary

secke[7] has constructed charts that give the maximum stress and the deflection of a curved beam of rectangular cross section, loaded as shown in Fig. 1. If the effect of pitch is neglected, these charts are applicable to helical rectangular-bar springs.

Using the Bessel-function equations in this paper, J. Krahula has checked several points of Liesecke's charts. In each case the width of the beam has been taken to be π units (Fig. 2), and the load P has been taken to be 1 unit. Also, in the deflection formula (Equation [21]), the ratio z/G has been set equal to unity. Table 1 gives Krahula's results and the corresponding values from Liesecke's charts. The results indicate close agreement between Göhner's solution and the Bessel-function solution.

Since, in some cases, the maximum shearing stress occurs on the flat sides of the beam, rather than on the concave side, Krahula has plotted the shearing stress on the entire periphery of his deepest cross section, Fig. 4. This cross section, which has the greatest aspect ratio that is included in Liesecke's charts, still has the maximum stress on the short edge. Evidently, the stress distribution shown in Fig. 4 is quite different from that which results by torsion of a straight bar of the same cross section. The difference is partly attributable to the fact that the curved beam carries a shear load P.

TABLE 1 COMPARISON OF RESULTS

Dimensions			Maximum shearing stress		Deflection	
			By equation derived in this paper	By Liesecke charts	By equations derived in this paper	By Liesecke charts
Y_1	Y_2	C				
8	16	25.2	0.754	0.735	2.10	2.06
4	8	9.84	0.960	0.925	1.04	1.58
4	6	24.75	2.10	2.12	4.95	4.97

Acknowledgment

Mr. J. Krahula has generously assisted the author by working out the numerical examples.

Postscript

The author learned belatedly that the formula for the stress function, Equation [28], was stated previously by J. H. Michell.[8] He showed that this equation satisfies the differential equation of the problem, and he determined the coefficients to satisfy the boundary conditions.

[7] "Berechnung zylindercher Schraubenfedern mit rechteckigen Drahtquerschnitt," by G. Liesecke, *Zeitschrift des Vereines deutscher Ingenieure*, vol. 77, 1933, pp. 425 and 892.

[8] "Uniform Torsion and Flexure of Incomplete Tores," J. H. Michell, Proceedings of the London Mathematical Society, vol. 31, 1899, pp. 140-141.

On the Direction of Fatigue Cracks in Polycrystalline Ingot Iron

By F. A. McCLINTOCK,[1] CAMBRIDGE, MASS.

A statistical analysis is developed to show how a microscopic shear failure can result in the apparent tensile failure of polycrystalline iron in rotary bending fatigue tests.

Introduction

FATIGUE cracks in single crystal specimens of iron, tested in rotary bending, progress on surfaces of high shear stress, that is, diagonally across the specimen (1).[2] On the other hand, the average surface of cracks in polycrystalline specimens is that of a plane of maximum tension, or one perpendicular to the axis of the specimen. Microscopic examination shows that the cracks in polycrystalline specimens are not straight, but tend to zigzag from one crystal to another (2, 3, 4, 5, 6). This seems to indicate that cracks in both the single-crystal specimens and in the individual crystals of the polycrystalline specimens progress on surfaces of high shear stress, and that the average direction of the cracks in the polycrystalline specimens is due to the random orientation, in the various crystals, of planes of maximum shear stress containing a <111> direction. This hypothesis will now be checked in detail.

To simplify the problem, assume that cracks progress only on planes of maximum shear stress. The intersections of these planes with the surface of the specimen will be lines making angles of 45 to 135 deg to the specimen axis. Assume that, after a crack has traversed one grain, it must progress on a surface of maximum shear stress in the next grain. Although there may be a tendency for cracks to continue on the same surface, the requirement that they progress on surfaces of high shear stress containing a <111> direction is likely to cause a change of surface. If the crystal orientations are random, the effect may be considered to be the same as a random choice of a plane of maximum shear stress in the neighboring crystal. The easiest way to check this hypothesis is to use it to predict the directions that the cracks take on the surface of the specimen and then to compare the predicted value with that found experimentally.

Analysis

In accordance with Fig. 1, let S_3 be the specimen axis and S_2 the normal to the specimen surface. Let ν be the normal to the plane of maximum shear stress, which makes an angle of 45 deg with S_3. Let ψ be the angle at which the plane of maximum shear stress intersects the surface; ψ may vary from +45 deg to −45 deg as ν moves around S_3 in a cone. The relation between ψ and θ is given by

$$\tan \psi = \cos \theta \quad [1]$$

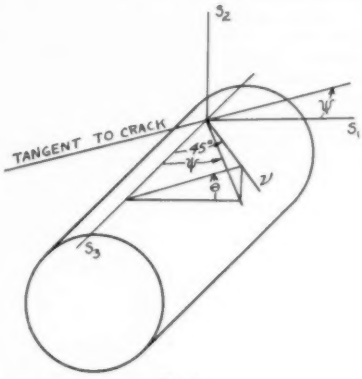

FIG. 1

If all values for θ are equally likely, then the probability that θ will lie between θ and $\theta + d\theta$ is given by

$$p(\theta)d\theta = d\theta/2\pi \quad \text{for} \quad 0 \leq \theta \leq 2\pi \quad [2]$$

Since

$$d\theta = d\psi/\cos^2 \psi \sqrt{1 - \tan^2 \psi} \quad [3]$$

and since the same values for ψ can arise from both positive and negative values of θ, the corresponding probability distribution of ψ is given by

$$p(\psi)d\psi = 2d\psi/2\pi \cos^2 \psi \sqrt{1 - \tan^2 \psi}$$
$$\text{for} \quad -\pi/4 < \psi < \pi/4 \quad [4]$$

For a crack of unit length the deviation in the S_3 direction is

$$w = \sin \psi \quad [5]$$

Therefore

$$d\psi = dw/\sqrt{1 - w^2} \quad [6]$$

and the distribution function of w is

$$p(w)dw = dw/\pi(1 - w^2)\sqrt{1 - 2w^2}$$
$$\text{for} \quad -1/\sqrt{2} < w < 1/\sqrt{2} \quad [7]$$

This distribution has zero mean and a variance

$$\sigma_w^2 = \int_{-1/\sqrt{2}}^{1/\sqrt{2}} \frac{w^2 dw}{\pi(1 - w^2)\sqrt{1 - 2w^2}} \quad [8]$$

[1] Assistant Professor of Mechanical Engineering, Massachusetts Institute of Technology. Jun. ASME.

[2] Numbers in parentheses refer to the Bibliography at the end of the paper.

Contributed by the Applied Mechanics Division and presented at the Annual Meeting, Atlantic City, N. J., November 25–30, 1951, of The American Society of Mechanical Engineers.

Discussion of this paper should be addressed to the Secretary, ASME, 29 West 39th Street, New York, N. Y., and will be accepted until April 10, 1952, for publication at a later date. Discussion received after the closing date will be returned.

Note: Statements and opinions advanced in papers are to be understood as individual expressions of their authors and not those of the Society. Manuscripts received by ASME Applied Mechanics Division, January 24, 1951. Paper No. 51—A-9.

In order to evaluate the integral, change the variable back to ψ

$$\sigma_w^2 = \int_{-\pi/4}^{\pi/4} \frac{\sin^2\psi d\psi}{\pi\cos\psi\sqrt{1-2\sin^2\psi}} \quad [9]$$

The presence of the trigonometric functions suggests the substitution $z = e^{i\psi}$, whence

$$\frac{\sin^2\psi\, d\psi}{\pi\cos\psi\sqrt{1-2\sin^2\psi}} = \frac{\sqrt{2}\left(z - \frac{z^2}{2} - \frac{1}{2z}\right)dz}{(z^2+1)\sqrt{z^4+1}} \quad [10]$$

The differential dz is taken as a segment of the unit circle in a counterclockwise direction for $d\psi > 0$. On the contour shown, Fig. 2, the arguments of these differentials decrease by $\pi/2$ at

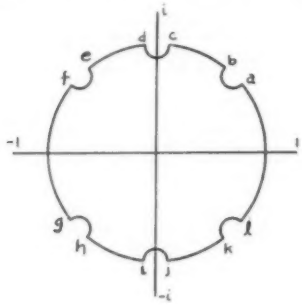

FIG. 2

$z = \pm 1/\sqrt{2} \pm i/\sqrt{2}$ and by π at $z = \pm i$. Therefore the integral from $\psi = -\pi/4$ to $\pi/4$ equals that from $\psi = 3\pi/4$ to $5\pi/4$, and the integral will be imaginary elsewhere on the unit circle. The integrals along the indentations at $z = \pm 1/\sqrt{2} \pm i/\sqrt{2}$ become vanishingly small as the radii of the indentations approach zero. The integrals along the indentations at $z = \pm i$ are given by

$$\lim \int_i^j = \lim \int_c^d = -\frac{1}{2}\left(2\pi i \operatorname*{Res}_{z=i} \frac{\sqrt{2}\left(z - \frac{z^2}{2} - \frac{1}{2z}\right)}{\pi i(z^2+1)\sqrt{z^4+1}}\right) \quad [11]$$

Their total contribution to the contour integral is -2. Now applying the residue theorem to the entire contour, and considering only the real parts

$$\mathrm{Rl}\oint = \lim 2\int_l^a - 2 = Rl\, 2\pi i \operatorname*{Res}_{z=0} \frac{\sqrt{2}\left(z - \frac{z^2}{2} - \frac{1}{2z}\right)}{\pi i(z^2+1)\sqrt{z^4+1}} \quad [12]$$

Finally

$$\sigma_w^2 = 1 - \frac{1}{\sqrt{2}} \quad [13]$$

If the crack traverses n grains on the surface, the total deviation in the S_3 direction will be the sum of the deviations across each grain. This total deviation will have a distribution with mean zero and variance equal to the sum of the individual variances

$$n\sigma_w^2 = n\left(1 - \frac{1}{\sqrt{2}}\right) \quad [14]$$

For a crack of unit length, the progress of the crack in the S_1 direction is given by

$$u = \cos\psi \quad [15]$$

Therefore

$$d\psi = \frac{-du}{\sqrt{1-u^2}} \quad [16]$$

and since the same value of u can arise from two values of ψ, the distribution function of u is

$$p(u)du = \frac{2\,du}{\pi u\sqrt{1-u^2}\sqrt{2u^2-1}} \quad \text{for} \quad \frac{1}{\sqrt{2}} < u < 1 \quad [17]$$

The mean of this distribution is

$$m_u = \int_{1/\sqrt{2}}^1 \frac{2\,du}{\pi\sqrt{1-u^2}\sqrt{2u^2-1}} \quad [18]$$

In order to evaluate Equation [18], change the variable to $\phi = 2\arccos u$

$$m_u = \int_0^{\pi/2} \frac{d\phi}{\pi\sqrt{\cos\phi}} \quad [19]$$

This integral is evaluated by Dwight (7)

$$m_u = \frac{\Gamma(1/4)}{2\sqrt{\pi}\,\Gamma(3/4)} \quad [20]$$

The variance of the distribution of u is

$$\sigma_u^2 = \int_{1/\sqrt{2}}^1 \frac{2u\,du}{\pi\sqrt{1-u^2}\sqrt{2u^2-1}} - m_u^2 \quad [21]$$

Let $\sqrt{1-u^2} = r$; then $-u\,du/\sqrt{1-u^2} = dr$ and

$$\sigma_u^2 = \int_0^{1/\sqrt{2}} \frac{2dr}{\pi\sqrt{1-2r^2}} - m_u^2 \quad [22]$$

$$= \frac{1}{\sqrt{2}} - \frac{1}{4\pi}\left[\frac{\Gamma(1/4)}{\Gamma(3/4)}\right]^2 = 0.0106 \quad [23]$$

Therefore the total length in the S_1-direction of a crack across n grains will be distributed with mean $0.8346\,n$, and standard deviation $0.103\sqrt{n}$. For large values of n, the deviation may be neglected in comparison to the mean value. Then the number of grains of linear dimension g traversed by a crack which progresses for a distance S_1 around the specimen is given by

$$n = S_1/0.8346\,g \quad [24]$$

COMPARISON WITH EXPERIMENT

For comparison with the theory derived in the foregoing, twelve Moore-type specimens of ingot iron were run at 27,000 psi and examined. The grain size, found by counting the grains intercepted per unit length of a straight line, was 250 to 300 grains per in. The deviation from the circumferential direction of the center 90 deg (0.236 in.) was measured for the major crack of each specimen. The number of grains traversed, from

Equation [24], was 71 to 85. The standard deviation of the deviations of these cracks in the axial direction was 0.0238 in., and the 98 per cent confidence interval for the standard deviation of the population from which this sample was drawn is 0.0166 in. to 0.0469 in.[2] The foregoing theory predicts that the standard deviation would be between 0.0167 in. and 0.0183 in. If anything, the cracks are farther from the circumferential direction than predicted. This might be due to a tendency for cracks to continue on the same surface at grain boundaries. The main point, however, is that the theory adequately explains how a shear failure can cause a crack which, from a macroscopic point of view, appears to be on a surface of high tensile stress.

Conclusion

In the past, fatigue failures in iron have often been thought of as tensile failures (8, 9). The shear failures obtained in torsion tests have been explained by a loss of the statistical isotropy of the polycrystalline material due to cold work (10). The results of this study suggest that fatigue failures are truly shear failures. The circumferential cracks obtained in polycrystalline iron in bending tests can be explained by a statistical theory such as that given herewith. The axial and circumferential cracks in torsion tests on polycrystalline iron can be explained by a shear failure on a microscopic scale, coupled with a tendency of cracks not to turn a right angle at grain boundaries. The helical cracks observed in torsion tests on steel under certain conditions (10) remain to be explained.

[2] That is, these limits were obtained using statistical methods that are correct 98 per cent of the time they are applied.

Acknowledgment

The foregoing work is part of a PhD thesis carried out at the California Institute of Technology. The author would like to thank his adviser, Prof. D. E. Hudson, and also Prof. G. W. Housner for their advice and encouragement in connection with this work.

Bibliography

1 "Fatigue Tests of Single Crystals of Ingot Iron," by Frank A. McClintock. Proceedings of the First National Congress of Applied Mechanics, 1951.

2 "The Fracture of Metals Under Repeated Alternations of Stress," by J. A. Ewing and J. C. W. Humphrey, Philosophical Transactions of the Royal Society of London, series A, vol. 200, 1903, p. 241.

3 "On the Resistance of Iron and Steel to Reversals of Direct Stress," by T. F. Stanton and L. Bairstow, Proceedings of The Institution of Civil Engineers, vol. 166, 1906, p. 78.

4 "Behavior of Metals Subjected to Repeated Stresses," by H. J. Gough and D. Hanson, Proceedings of the Royal Society of London, series A, vol. 104, 1923, p. 538.

5 "Observations on the Microstructure of the Path of Fatigue Failure in a Specimen of Armco Iron," by F. F. Lucas, Transactions of the American Society of Steel Treating, vol. 11, April, 1927, p. 531.

6 "A Study of Slip Lines, Strain Lines, and Cracks in Metals Under Repeated Stress," by H. F. Moore and T. Ver, University of Illinois Engineering Experiment Station Bulletin No. 208, 1930.

7 "Tables of Integrals and Other Mathematical Data," by H. B. Dwight, The Macmillan Company, New York, N. Y., 1947, 854.1.

8 "The Failure of Metals by Fatigue," Melbourne University, Australia, 1947, p. 8.

9 "The Prevention of the Failure of Metals Under Repeated Stress," Battelle Memorial Institute, Columbus, Ohio, 1941, p. 179.

10 "The Concentration of Stress in the Neighborhood of a Small Spherical Flaw," by R. V. Southwell and H. J. Gough, *Philosophical Magazine*, series 7, vol. 1, 1926, p. 71.

Supersonic Flow With Variable Specific Heat

By F. P. DURHAM,[1] BOULDER, COLO.

Formulas are developed for stagnation conditions and one-dimensional flow through shock waves, including Rankine-Hugoniot values, taking into account the variation of the specific heat of air with temperature by means of the concept of mean specific heats. These formulas are reduced to correction factors that may be applied to the widely used constant specific-heat formulas up to a Mach number of 7. The corrections involved are appreciable in the case of the density change through a shock wave and for the total pressure ratio across a shock wave, as well as for stagnation pressures and temperatures. The limitations imposed by the deviation of a gas at high pressure from the ideal equation of state, relaxation time, and dissociation are discussed.

Nomenclature

The following nomenclature is used in the paper:

$A\ (p_t/p)$, $A\ (T_t/T)$, $A\ (\mathbf{M}_n{}^2)$, $A\ (p_2/p_1)$, $A\ (T_2/T_1)$, $A\ (\rho_2/\rho_1)$, $A\ (p_{t1}/p_{t2})$, $A\ (p_{t2}/p_1)$ = Correction factors to be applied to quantity in parentheses to take into account variation of specific heat with temperature

a = speed of sound = $\sqrt{kgRT}$
g = acceleration due to gravity = 32.17 fps
h = enthalpy, Btu per lb
k = ratio of specific heat at constant pressure to specific heat at constant volume
c_p = instantaneous value of specific heat at constant pressure
c_{pm} = mean specific heat defined by Equation [7]
$c_{p\theta}$ = exponential mean specific heat defined by Equation [9]
c_v = instantaneous value of specific heat at constant volume
J = mechanical equivalent of heat, 778 ft-lb/Btu
$\mathbf{M}$ = Mach number = $V/\sqrt{kgRT}$
$\mathbf{M}_n$ = "normal component" of Mach number = $u/\sqrt{kgRT}$
p = pressure, psf
R = gas constant for air = 53.3 ft-lb/lb deg F
T = temperature, deg R
u = component of velocity normal to shock wave, fps
V = velocity, fps
v = component of velocity parallel to shock wave, fps; specific volume, cu ft per lb
θ = specific-heat ratio across shock wave, defined by Equation [8]
θ_e = exponential stagnation specific-heat ratio, defined by Equation [10]
θ_t = stagnation specific-heat ratio defined by Equation [12a]
Ω = specific-heat function defined by Equation [24]
ρ = density of air, slugs per cu ft

Subscripts:

t = stagnation conditions
1 = station before shock wave
2 = station after shock wave

Introduction

The most widely used one-dimensional compressible-flow and shock-wave formulas are based on the assumption of an ideal gas having constant specific heat. These relations are probably valid up to a Mach number of 2.5. It is well known, however, that the specific heat for air is not constant over as wide a temperature range as that for which the ideal-gas relation $pv = RT$ applies. For a higher Mach number range, say, from 3 to 7, it is believed that the use of the ideal-gas relation may still apply with reasonable accuracy if the variation of specific heat with temperature is considered.

Various investigators have obtained Rankine-Hugoniot values for flow through a shock wave based on a variable specific heat as given in references (1, 2).[2] The purpose of this paper is to develop equations for stagnation conditions, and flows through shock waves involving stagnation pressures, as well as the Rankine-Hugoniot values, based on the device of a mean specific heat. The advantages of such an approach are the relative simplicity of the solutions and the fact that the relations developed are algebraically similar to the widely used relations based on a constant specific heat. The limitations imposed by the effects of pressure, dissociation, and relaxation time will be discussed in a later section of this paper.

Basic Assumptions

The following assumptions will be made regarding the flows considered:

1 The equation of state for the gas may be expressed by

$$p = \rho g R T \quad [1]$$

2 The specific heat is a function of temperature alone, that is

$$c_p = f(T) \quad [2]$$

3 The relation between the specific heat at constant pressure and the specific heat at constant volume may be expressed by

$$c_p = c_v + R/J \quad [3]$$

4 The total energy in the flow is constant and the effects of the dissociation are negligible. As a result of this assumption and assumption 2, the total temperature in the flow is constant, that is

$$T_{t1} = T_{t2} \quad [4]$$

5 There is no change in momentum in a direction parallel to

[1] Assistant Professor of Aeronautical Engineering, University of Colorado.

Contributed by the Applied Mechanics Division and presented at the Annual Meeting, Atlantic City, N. J., November 25–30, 1951, of The American Society of Mechanical Engineers.

Discussion of this paper should be addressed to the Secretary, ASME, 29 West 39th Street, New York, N. Y., and will be accepted until April 10, 1952, for publication at a later date. Discussion received after the closing date will be returned.

Note: Statements and opinions advanced in papers are to be understood as individual expressions of their authors and not those of the Society. Manuscript received by ASME Applied Mechanics Division, March 21, 1951. Paper No. 51—A-13.

[2] Numbers in parentheses refer to the Bibliography at the end of the paper.

the shock wave in passing through a shock wave. This is equivalent to assuming the component of velocity parallel to the shock wave does not change in passing through a shock wave, that is

$$v_1 = v_2 \quad [5]$$

6 The stream-tube area in a plane parallel to the shock wave does not change in passing through a shock wave. From this assumption and the continuity equation

$$\rho_1 u_1 = \rho_2 u_2 \quad [6]$$

7 The flow is outside of any boundary layer.

With the exception of assumption 2 all of these assumptions, or their equivalents, are made in the derivation of the most widely used one-dimensional shock-wave formulas.

Mean-Specific-Heat Correction Factors

The method to be used to take into account the variation in specific heat with temperature is based on the concept of a mean specific heat.

From the first law of thermodynamics, assumptions 1 and 2 and the definition of enthalpy, it can be easily shown that

$$dh = c_p dT \quad [7a]$$

Thus for unit weight of gas undergoing a change from T_x to T_y

$$h_y - h_x = \int_{T_x}^{T_y} c_p dT \quad [7b]$$

It is frequently desirable to express a change in enthalpy as the product of a factor called the mean specific heat and the difference of two temperatures, such that

$$h_y - h_x = c_{pm}(T_y - T_x) \quad [7c]$$

Eliminating the enthalpy change from Equations [7b] and [7c] gives

$$c_{pm} = \frac{\int_{T_x}^{T_y} c_p dT}{T_y - T_x} \quad [7]$$

For the purposes of this paper, however, it is more convenient to define the following specific-heat ratio

$$\theta = c_{pm}/c_p \quad [8a]$$

such that

$$h_y - h_x = \theta c_p (T_y - T_x) \quad [8]$$

where c_p is the instantaneous value of specific heat at temperature T_x.

For isentropic processes, it is possible to define an exponential specific heat for a gas undergoing a change from condition x to condition y such that

$$\frac{p_y}{p_x} = \left(\frac{T_y}{T_x}\right)^{c_{pe}J/R} \quad [9a]$$

From Equation [9a]

$$c_{pe} = \frac{R}{J} \frac{\ln(p_y/p_x)}{\ln(T_y/T_x)} \quad [9b]$$

For an ideal gas and an isentropic process, however, it can be easily shown that

$$\frac{R}{J} \ln(p_y/p_x) = \int_{T_x}^{T_y} c_p \frac{dT}{T} \quad [9c]$$

From Equation [9c] Equation [9b] may be written

$$c_{pe} = \frac{\int_{T_x}^{T_y} c_p \frac{dT}{T}}{\ln(T_y/T_x)} \quad [9]$$

Defining as before a specific-heat ratio

$$\theta_e = c_{pe}/c_p \quad [10a]$$

Equation [9a] may be written

$$\frac{p_y}{p_x} = \left(\frac{T_y}{T_x}\right)^{\theta_e c_p J/R} \quad [10b]$$

where c_p is the instantaneous value of specific heat at temperature T_x. But from Equation [3]

$$c_p J/R = k/(k-1) \quad [10c]$$

so that Equation [10b] becomes

$$\frac{p_y}{p_x} = \left(\frac{T_y}{T_x}\right)^{\theta_e k/(k-1)} \quad \text{(isentropic)} \quad [10]$$

where k is the ratio of c_p to c_v at temperature T_x.

Equations [8] and [10] show that by the choice of proper correction factors it is possible to obtain changes in enthalpy, pressure, and temperature based upon values of specific heat at the initial temperature of the process. The evaluation of the mean specific heats must be determined from tables or charts expressing fluid properties as functions of temperature such as references (3) and (4).

Stagnation Conditions

The stagnation condition in a fluid in steady motion is defined as the condition that would exist in the fluid if it were brought to rest reversibly and adiabatically. The stagnation condition refers to a point in the fluid.

From the general energy equation of thermodynamics and the definition of the stagnation condition, at a point in a fluid

$$h_t - h = V^2/2gJ \quad \text{(isentropic)} \quad [11]$$

Making use of Equation [8] this becomes

$$\theta_t c_p (T_t - T) = V^2/2gJ \quad [12a]$$

where c_p is the value of specific heat at temperature T, and θ_t is evaluated for the temperature range $T_t - T$. Rearranging this equation and substituting for Jc_p from Equation [10c] results in

$$\frac{T_t}{T} = 1 + \frac{(k-1)V^2}{2\theta_t\, kgRT} \quad [12]$$

Based upon the assumptions previously made, the speed of sound in the gas is given by

$$a = \sqrt{kgRT} \quad [13]$$

where k is the ratio of c_p to c_v at temperature T. By definition, the Mach number is given by

$$\mathbf{M} = V/a = V/\sqrt{kgRT} \quad [14]$$

Substituting from Equation [14] in Equation [13] results in

$$\frac{T_t}{T} = 1 + \frac{k-1}{2\theta_t} \mathbf{M}^2 \quad [15]$$

where k is evaluated at T and θ_t is evaluated for a temperature range $T_t - T$.

The widely used equation for this temperature ratio is

$$\frac{T_t}{T} = 1 + \frac{k-1}{2}\mathbf{M}^2 \quad [16]$$

A correction factor to be applied to Equation [16] to correct for specific-heat variation may be defined as the ratio of Equations [15] and [16]

$$A(T_t/T) = \frac{1 + \dfrac{k-1}{2\theta_t}\mathbf{M}^2}{1 + \dfrac{k-1}{2}\mathbf{M}^2} \quad [17]$$

Equation [15] may be used to determine the ratio of the total or stagnation pressure to the static pressure at a point in a steady flow. Since Equation [15] represents an isentropic process, Equation [10] may be used to give

$$\frac{p_t}{p} = \left(1 + \frac{k-1}{2\theta_t}\mathbf{M}^2\right)^{\theta_e k/(k-1)} \quad [18]$$

where k is evaluated at T, and θ_t and θ_e are evaluated for the temperature range $T_t - T$.

The widely used relation for total pressure corresponding to Equation [18] is

$$\frac{p_t}{p} = \left(1 + \frac{k-1}{2}\mathbf{M}^2\right)^{k/(k-1)} \quad [19]$$

As before, a correction factor to be applied to Equation [19] may be defined from Equations [18] and [19] such that

$$A(p_t/p) = \frac{\left(1 + \dfrac{k-1}{2\theta_t}\mathbf{M}^2\right)^{\theta_e k/(k-1)}}{\left(1 + \dfrac{k-1}{2}\mathbf{M}^2\right)^{k/(k-1)}} \quad [20]$$

Shock-Wave Flow

The concept of a mean specific heat may be applied to the flow through a shock wave in the following manner:

From the assumptions previously made it can be easily shown for the flow through a plane shock wave, either normal or oblique

$$p_1 + \rho_1 u_1^2 = p_2 + \rho_2 u_2^2 \quad [21a]$$

From Equations [21a] and [6]

$$u_1^2 - u_2^2 = (p_2 - p_1)\left(\frac{1}{\rho_2} + \frac{1}{\rho_1}\right) \quad [22]$$

Since the total energy in the flow is assumed constant, the general energy equation for flow through a shock wave is

$$h_1 + V_1^2/2gJ = h_2 + V_2^2/2gJ \quad [23a]$$

By virtue of Equation [8] this relation becomes

$$\frac{V_1^2 - V_2^2}{2gJ} = \theta c_p(T_2 - T_1) \quad [23b]$$

where c_p is evaluated at T_1 and θ is determined for the temperature range $T_2 - T_1$. However, since $v_1 = v_2$

$$V_1^2 - V_2^2 = u_1^2 - u_2^2 \quad [23c]$$

Making use of Equations [23c], [10c], and [1], Equation [23b] may be written

$$u_1^2 - u_2^2 = \frac{2k\theta}{k-1}\left(\frac{p_2}{\rho_2} - \frac{p_1}{\rho_1}\right) \quad [23d]$$

Equating the right-hand members of Equations [22] and [23d], and solving for ρ_2/ρ_1, in terms of p_2/p_1 gives

$$\frac{\rho_2}{\rho_1} = \frac{1 + \left(\dfrac{2k\theta}{k-1} - 1\right)p_2/p_1}{\dfrac{2k\theta}{k-1} - 1 + p_2/p_1} \quad [23]$$

where k is evaluated at T_1 and θ is determined for the temperature range $T_2 - T_1$. Equation [23] corresponds to the familiar Rankine-Hugoniot relation for the density ratio across a shock wave. Before θ can be determined, however, it is necessary to develop an expression for the ratio T_2/T_1.

In order to simplify the algebra involved, it is convenient to define a new parameter that is also a function of temperature

$$\Omega = \frac{2k\theta}{k-1} - 1 \quad [24]$$

Substituting from Equation [24] into Equation [23] gives

$$\frac{\rho_2}{\rho_1} = \frac{1 + \Omega p_2/p_1}{\Omega + p_2/p_1} \quad [25]$$

It is often more convenient to express Equation [25] in terms of Mach number. Making use of Equation [6], u_2 may be eliminated from Equation [21a] to give

$$\frac{p_2}{p_1} - 1 = \frac{\rho_1 u_1^2}{p_1}(1 - \rho_1/\rho_2) \quad [26]$$

The so-called "normal component" of Mach number is defined by

$$\mathbf{M}_n = u/\sqrt{kgRT} \quad [27]$$

If ρ_2/ρ_1 in Equation [26] is replaced from Equation [1], the right-hand member is multiplied and divided by k, and Equation [27] made use of, Equation [26] becomes

$$\frac{p_2}{p_1} - 1 = k\mathbf{M}_{n_1}^2(1 - \rho_1/\rho_2) \quad [27a]$$

Substituting Equation [37] in Equation [40] and solving for p_2/p_1 gives

$$p_2/p_1 = [k\mathbf{M}_{n_1}^2(\Omega - 1) - 1]/\Omega \quad [28]$$

The widely used formula for the pressure ratio is

$$\frac{p_2}{p_1} = \frac{\dfrac{2k}{k-1}\mathbf{M}_{n_1}^2 - 1}{\dfrac{k+1}{k-1}} \quad [29]$$

A correction factor may now be obtained from the ratio of Equations [28] and [29]

$$A(p_2/p_1) = \frac{[k\mathbf{M}_{n_1}^2(\Omega - 1) - 1]\dfrac{k-1}{k+1}}{\Omega\left(\dfrac{2k}{k-1}\mathbf{M}_{n_1}^2 - 1\right)} \quad [30]$$

The temperature ratio may be determined from Equation [1] and Equation [25] to be

$$\frac{T_2}{T_1} = \frac{p_2}{p_1}\frac{\Omega + p_2/p_1}{1 + \Omega p_2/p_1} \quad [31a]$$

Substituting for the pressure ratio from Equation [28] into Equation [31a] gives

$$\frac{T_2}{T_1} = \frac{[k\mathbf{M}_{n1}^2(\Omega - 1) - 1]\,(k\mathbf{M}_{n1}^2 + \Omega + 1)}{\Omega^2 k\mathbf{M}_{n1}^2} \quad [31]$$

The widely used formula for the temperature ratio is

$$\frac{T_2}{T_1} = \frac{\left(\frac{2k}{k-1}\mathbf{M}_{n1}^2 - 1\right)\left(k\mathbf{M}_{n1}^2 + \frac{2k}{k-1}\right)}{\left(\frac{k+1}{k-1}\right)^2 k\mathbf{M}_{n1}^2} \quad [32]$$

In this case, the correction factor obtained from the ratio of Equations [31] and [32] is

$$A(T_2/T_1) = \frac{[k\mathbf{M}_{n1}^2(\Omega - 1) - 1]\,(k\mathbf{M}_{n1}^2 + \Omega + 1)\left(\frac{k+1}{k-1}\right)^2}{\left(\frac{2k}{k-1}\mathbf{M}_{n1}^2 - 1\right)\left(k\mathbf{M}_{n1}^2 + \frac{2k}{k-1}\right)\Omega^2} \quad [33]$$

The correction factor for the density ratio may now be obtained by taking the ratio of the factors of Equations [30] and [33]

$$A(\rho_2/\rho_1) = \frac{\Omega\left(k\mathbf{M}_{n1}^2 + \frac{2k}{k-1}\right)\left(\frac{k-1}{k+1}\right)}{k\mathbf{M}_{n1}^2 + \Omega + 1} \quad [34]$$

A formula for the normal component of Mach number after the shock wave will now be determined. By making use of Equation [27], Equation [21a] may be changed to

$$\frac{p_2}{p_1} = \frac{1 + k\mathbf{M}_{n1}^2}{1 + k_2\mathbf{M}_{n2}^2} \quad [35]$$

In Equation [35], k_2 refers to the value of the specific-heat ratio at temperature T_2, while k is the value at T_1 as before. Eliminating p_2/p_1 between Equations [35] and [28] and solving for $\mathbf{M}_{n2}^2$ gives

$$\mathbf{M}_{n2}^2 = \frac{k\mathbf{M}_{n1}^2 + \Omega + 1}{k_2[k\mathbf{M}_{n1}^2(\Omega - 1) - 1]} \quad [36]$$

The widely used formula for $\mathbf{M}_{n2}^2$ corresponding to Equation [36] is

$$\mathbf{M}_{n2}^2 = \frac{\mathbf{M}_{n1}^2 + \frac{2}{k-1}}{\frac{2k}{k-1}\mathbf{M}_{n1}^2 - 1} \quad [37]$$

The correction factor for the normal component of Mach number can be obtained from the ratio of Equations [36] and [37] and is

$$A(\mathbf{M}_{n2}^2) = \frac{(k\mathbf{M}_{n1}^2 + \Omega + 1)\left(\frac{2k}{k-1}\mathbf{M}_{n1}^2 - 1\right)}{k_2[k\mathbf{M}_{n1}^2(\Omega - 1) - 1]\left(\mathbf{M}_{n1}^2 + \frac{2}{k-1}\right)} \quad [38]$$

To determine the total pressure ratio across a shock wave a more complicated expression is necessary than those that have been presented. The total pressure before the shock wave may be given by Equation [27]

$$\frac{p_{t1}}{p_1} = \left(\frac{T_{t1}}{T_1}\right)^{\frac{k\theta_e}{k-1}} = \left(1 + \frac{k-1}{2\theta_i}\mathbf{M}_1^2\right)^{\frac{k\theta_e}{k-1}} \quad [39a]$$

where θ_i is determined from the temperature range $T_{t1} - T_1$.

The ratio of total to static pressure after the shock wave is

$$\frac{p_{t2}}{p_2} = \left(\frac{T_{t2}}{T_2}\right)^{\theta_{e2}k_2/(k_2-1)} \quad [39]$$

where k_2 is evaluated at T_2 and θ_{e2} is determined from the temperature range $T_{t2} - T_2$. As before, however, it is convenient to use the value of k based upon T_1. This may be done by defining a new function β such that

$$\beta = \left(\frac{k-1}{k_2-1}\right)\frac{k_2}{k}\theta_{e2} \quad [40]$$

By virtue of Equation [40], Equation [39] may be written as

$$\frac{p_{t2}}{p_2} = \left(\frac{T_{t2}}{T_2}\right)^{\beta k/(k-1)} \quad [41]$$

Since $T_{t2} = T_{t1}$, from Equation [31a]

$$\frac{T_{t2}}{T_2} = \frac{T_{t1}}{T_1}\left(\frac{p_1}{p_2}\frac{1 + \Omega p_2/p_1}{\Omega + p_2/p_1}\right) \quad [42]$$

From Equations [41] and [42]

$$\frac{p_{t2}}{p_2} = \left[\frac{T_{t1}}{T_1}\left(\frac{p_1}{p_2}\frac{1 + \Omega p_2/p_1}{\Omega + p_2/p_1}\right)\right]^{\beta k/(k-1)} \quad [43]$$

From Equation [39a] and Equation [42] the total pressure ratio across the shock wave is

$$\frac{p_{t1}}{p_{t2}} = \frac{p_1}{p_2}\left(\frac{p_2}{p_1}\frac{\Omega + p_2/p_1}{1 + \Omega p_2/p_1}\right)^{\frac{\beta k}{k-1}}\left(\frac{T_{t1}}{T_1}\right)^{\frac{k}{k-1}(\theta_e - \beta)} \quad [44]$$

In terms of Mach number this may be expressed from Equations [28] and [39a] as

$$\frac{p_{t1}}{p_{t2}} = \frac{\Omega\left(1 + \frac{k-1}{2\theta_i}\mathbf{M}_1^2\right)^{\frac{k}{k-1}(\theta_e - \beta)}}{k\mathbf{M}_{n1}^2(\Omega - 1) - 1} \times \left\{\frac{[k\mathbf{M}_{n1}^2(\Omega - 1) - 1](k\mathbf{M}_{n1}^2 + \Omega + 1)}{\Omega^2 k\mathbf{M}_{n1}^2}\right\}^{\frac{\beta k}{k-1}} \quad [45]$$

The widely used formula for this pressure ratio is

$$\frac{p_{t1}}{p_{t2}} = \frac{\frac{k+1}{k-1}}{\frac{2k}{k-1}\mathbf{M}_{n1}^2 - 1}\left[\frac{\left(\frac{2k}{k-1}\mathbf{M}_{n1}^2 - 1\right)\left(\mathbf{M}_{n1}^2 + \frac{2}{k-1}\right)}{\left(\frac{k+1}{k-1}\right)^2\mathbf{M}_{n1}^2}\right]^{\frac{k}{k-1}} \quad [46]$$

It should be noted that Equation [46] is a function of $\mathbf{M}_{n1}$ alone since k is a constant. Equation [45] on the other hand, is a function of $\mathbf{M}_1$, Ω, β, θ_e, and θ_i as well as $\mathbf{M}_{n1}$.

The correction factor in this case is the ratio of the right-hand members of Equations [45] and [46]

$$A(p_{t1}/p_{t2}) = \frac{\text{Eq. [45]}}{\text{Eq. [46]}} \quad [47]$$

The final quantity to be determined here is the ratio of the total pressure after a shock wave to the static pressure before the shock wave. It is evident that

$$\frac{p_{t2}}{p_1} = \frac{p_{t2}}{p_{t1}} \frac{p_{t1}}{p_1} \quad \ldots\ldots [48a]$$

Substituting in Equation [48a] from Equations [45] and [39a] gives

$$\frac{p_{t2}}{p_1} = \frac{k\mathbf{M}_{n1}^2(\Omega - 1) - 1}{\Omega} \times \left\{ \frac{\Omega^2 k\mathbf{M}_{n1}^2 \left(1 + \frac{k-1}{2\theta_t}\mathbf{M}_1^2\right)}{[k\mathbf{M}_{n1}^2(\Omega - 1) - 1]\,(k\mathbf{M}_{n1}^2 + \Omega + 1)} \right\}^{\frac{k\theta}{k-1}} \quad \ldots\ldots [49]$$

The widely used formula for this pressure ratio is

$$\frac{p_{t2}}{p_1} = \left(\frac{2k\mathbf{M}_{n1}^2 - 1}{k+1}\right)^{\frac{1}{1-k}} \left(\frac{\frac{k+1}{k-1}\mathbf{M}_{n1}^2 \left(1 + \frac{k-1}{2}\mathbf{M}_1^2\right)}{\mathbf{M}_{n1}^2 + \frac{2}{k-1}} \right)^{\frac{k}{k-1}} \quad \ldots\ldots [50]$$

The correction factor in this case is the ratio of the right-hand members of Equations [49] and [50]

$$A(p_{t2}/p_1) = \frac{\text{Eq. [49]}}{\text{Eq. [50]}} \quad \ldots\ldots [51]$$

Presentation of Results

A series of calculations were performed based upon an ambient air temperature of 500 R to determine the various parameters and correction factors over a Mach number range of 3 to 7.

The parameter θ_t was determined directly from Equations [12a] and Table 1 of reference (3) with c_p taken as 0.24. Fig. 1 shows θ_t plotted versus Mach number.

The parameter θ_s was determined directly from Equations [9] and [10a] and Table 1 of reference (3) for the temperatures used to determine θ_t. Fig. 1 shows θ_s plotted versus Mach number.

The parameter θ was determined by iteration from Equation [31] and Table 1 of reference (3), using the values of θ_t determined in the foregoing as a first approximation. Fig. 2 shows θ plotted versus the "normal component" of Mach number.

The parameter Ω was calculated from Equation [24] and the previously determined values of θ with k taken as 1.4. This parameter is also plotted in Fig. 2.

Correction factors $A(T_t/T)$ and $A(p_t/p)$ were determined from Equations [17] and [20] and are plotted versus Mach number in Fig. 3. As shown in Fig. 3, the total pressure calculated from the variable specific-heat formula is 1.52 times greater at a Mach number of 7 than that calculated from the constant-specific-heat formula.

Correction factors $A(p_2/p_1)$, $A(T_2/T_1)$, $A(\rho_2/\rho_1)$ and $A(\mathbf{M}_{n1}^2)$ were determined from Equations [30], [33], [34], and [38] and are plotted versus normal component of Mach number in Fig. 4. As shown in Fig. 4, for a normal component of Mach number of 7 the variable specific heat-density ratio is 1.18 times the value calculated from constant specific-heat equations. Fig. 4 also shows appreciable differences in the temperature ratio and downstream component of Mach number as calculated by the two methods.

Based upon the values of Figs. 1, 3, and 4, and Equations [39] and [40], the parameter β was calculated and is plotted in Fig. 1. Since both $\mathbf{M}_1$ and $\mathbf{M}_{n1}$ are involved in Equations [45] and [49], correction factors $A(p_{t1}/p_{t2})$ and $A(p_{t2}/p_1)$ were calculated for normal shock waves where $\mathbf{M}_1 = \mathbf{M}_{n1}$ and are plotted versus Mach number in Fig. 3. As shown in Fig. 3, the correction for the ratio p_{t1}/p_{t2} is only slightly less than that for the ratio p_t/p.

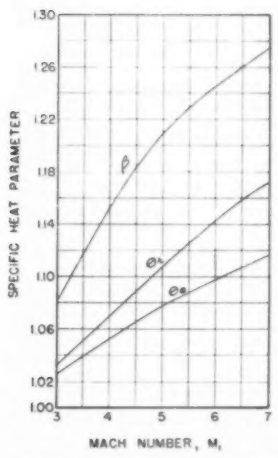

Fig. 1 Specific-Heat Parameters for Stagnation Conditions Versus Mach Number
(Free-stream temperature 500 R.)

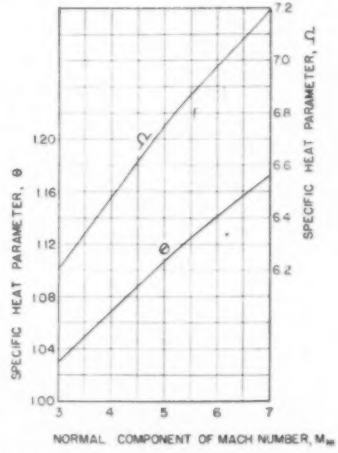

Fig. 2 Specific-Heat Parameters for Rankine-Hugoniot Values of Flow Through Plane Shock Waves Versus Normal Component of Mach Number
(Free-stream temperature 500 R.)

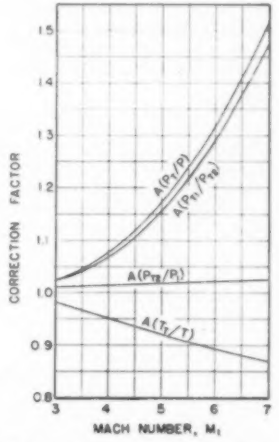

Fig. 3 Correction Factors for Stagnation Conditions and Flow Through Normal Shock Waves Versus Mach Number
(Free-stream temperature 500 R.)

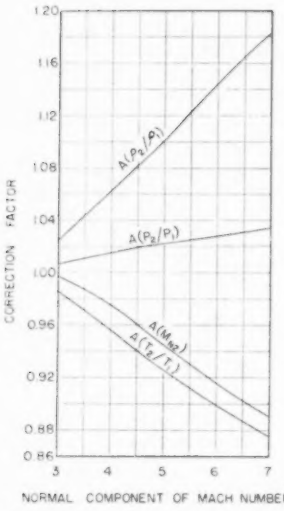

FIG. 4 CORRECTION FACTORS FOR RANKINE-HUGONIOT VALUES OF FLOW THROUGH PLANE SHOCK WAVES VERSUS NORMAL COMPONENT OF MACH NUMBER
(Free-stream temperature 500 R.)

DISCUSSION

The effect of pressure on specific heat has been neglected in the preceding developments. If the effect of pressure on specific heat is to be taken into account, the ideal gas relation $pv = RT$ can no longer be used. In this case it is necessary to use a more complicated equation of state such as the Beattie-Bridgeman or Berthelot equations. The use of a complex equation of state invalidates many of the terms used in the development of the equations, including the accepted relation for the speed of sound, $a = \sqrt{kgRT}$. As shown in reference (5), as long as the change in density is not large the specific heat is practically independent of pressure, and the deviation of behavior of air from $pv = RT$ is slight.

Fortunately, in flow through a shock wave up to normal components of Mach number of 7 the density change is not large. It is believed that no serious error should result in static conditions of pressure, temperature, and density from the use of the ideal-gas relation and the neglect of pressure effects on specific heat. This is borne out by a comparison of the results presented here with those of reference (1) in which the Rankine-Hugoniot relations were determined, based on Berthelot's equation of state. In the same Mach-number range, however, the total or stagnation pressure may be exceedingly large, and the use of the corrections presented, which involve total pressures, is more questionable than those involving static pressures. The best justification for the use of the relations involving total pressure is that they should be more accurate than similar equations based on constant specific heat.

Another phenomenon to be considered is the heat-capacity lag or relaxation time necessary for the specific heat of a gas to change with a change in temperature. The increase in specific heat of a gas with increasing temperature is attributed to the change of molecular motion from translation and rotation to translation, rotation, and vibration. The vibrational motion comes to equilibrium more slowly than translational or rotational motion so that a finite time is necessary for the specific heat of a gas to change. This time is undoubtedly much more than that required for a molecule to pass through a shock wave as discussed in reference (6), so that a certain time and distance are necessary after passing through a shock wave before the specific heat is in equilibrium. In the preceding developments, it has been assumed that the fluid downstream of a shock wave is at such a distance from the shock wave that the specific heat of the gas is not changing.

A third factor to be considered in a discussion of this type is that of chemical dissociation. Above a Mach number of 7 in normal air, stagnation temperatures and temperatures after a shock wave are so large that dissociation of the air takes place. The presence of dissociation invalidates the assumption of constant total temperature upon which the shock-wave equations are based. For this reason no attempt has been made in this paper to determine values for flow at a Mach number or normal component of Mach number greater than 7. Based on a free-stream temperature of 400 R instead of 500 R the Mach number range might be increased to 8 with reasonable accuracy.

BIBLIOGRAPHY

1 "One-Dimensional Flows of Imperfect Diatomic Gas," by A. J. Eggers, Jr., NACA-TN No. 1861, April, 1949.

2 "An Extension of the Theory of the One-Dimensional Shock-Wave Structure," by L. Meyerhoff, *Journal of the Aeronautical Sciences*, vol. 17, December, 1950, pp. 775–786.

3 "Gas Tables," by J. Keenan and J. Kaye, John Wiley & Sons, Inc., New York, N. Y., 1948.

4 "Mean Specific Heats for Working Media of Gas Turbine Power Plants," by N. A. Hall, SAE Quarterly Transactions, vol. 1, July, 1947, pp. 490–497.

5 "The Specific Heats of Certain Gases Over Wide Ranges of Pressures and Temperatures," by F. O. Ellenwood, N. Kulik, and N. R. Gay, Cornell University Engineering Experiment Station, Bulletin No. 30, 1942.

6 "Problems of Missiles at Extreme Speeds," by R. Smelt, Symposium on Ordnance Aero Ballistics, Naval Ordnance Laboratory, White Oak, Md., June, 1949.

A Contribution to the Theory of the Development and Stability of Detonation in Gases

By A. K. OPPENHEIM,[1] BERKELEY, CALIF.

The development of detonation of an explosive gas mixture contained in a constant-cross-section duct is analyzed on the basis of a unidimensional, gasdynamic treatment of a double-discontinuity combustion system. A steady and an unsteady system are considered, and it is shown that the latter yields an adequate explanation of the effect of coalition of the two discontinuities on the establishment and subsequent stability of the detonation wave. The locus of states behind the detonating combustion zone during the development of the process is determined and analyzed.

Nomenclature

The following nomenclature is used in the paper:

a = local velocity of sound
f = stream force function per unit area ($f = p + mV$)
k = adiabatic index
m = mass flow rate per unit area
$\mathbf{M}$ = Mach number of normal component of relative flow velocity with respect to discontinuity
p = pressure
q = enthalpy of formation, i.e., chemical energy to thermal-energy conversion per unit mass of reactants, or net thermal-energy addition to system
R = perfect-gas constant
s = entropy per unit mass
T = absolute temperature
u = internal energy per unit mass
V = normal component of relative flow velocity with respect to discontinuity
v = specific volume
W = relative flow velocity with respect to discontinuity
α = angle of inclination of Rayleigh line on the p-v diagram
δ = slope angle of an isotherm on p-v diagram
ϵ = nondimensional enthalpy of formation $\left(\epsilon = \frac{q}{RT_1}\right)$
θ = nondimensional temperature $\left(\theta = \frac{T}{T_1}\right)$
ν = nondimensional specific volume $\left(\nu = \frac{v}{v_1}\right)$
π = nondimensional pressure $\left(\pi = \frac{p}{p_1}\right)$
σ = nondimensional entropy increase $\left(\sigma = \frac{\Delta s}{R}\right)$
ϕ = slope angle of an isentrope on p-v diagram

Subscripts:

s = shock front
c = combustion front
K = fully developed deflagration
J = fully developed detonation
I = point of minimum entropy of Q-curve
1 = state of substance immediately in front of discontinuity or in front of combustion zone
2 = state of substance immediately behind single discontinuity or between shock front and combustion front within combustion zone
3 = state of substance immediately behind detonative combustion zone

Curves:

H = Hugoniot curve
$\mathbf{M}_1$ = locus of states of $\mathbf{M} = 1$ attained immediately behind single discontinuity
Q = locus of states immediately behind predetonation combustion zone (states of $\mathbf{M} = 1$ attained immediately behind double discontinuity system)
R = Rayleigh line

Introduction

The most successful application of gasdynamic analysis to combustion is that to detonation phenomena. This is due to the fact that a high-velocity combustion front is comparatively thin and, in the analysis, it can be treated as a discontinuity, that is, a zone in the flow field across which a finite change occurs without the variation of cross-sectional area and mass flow rate, and the effects of viscosity, diffusion, and thermal conductivity can be neglected. Therefore a great number of idealizations can be introduced into the analysis, and the results can be expected to check quite well with experimental data. The simplest way to obtain such data is from experiments on gaseous explosion in ducts of constant cross-sectional area, and the present paper will be concerned only with this case.

The classical theory based upon the Hugoniot curve representation of the locus of states behind a single discontinuity yields very satisfactory results concerned with the velocity of propagation of the so-called Chapman-Jouguet state (1, 2, 6, 7, 17),[2] but it fails to explain the development of detonation and the reason for its remarkable stability.

According to experimental evidence, which for the first time was presented by Bone, Fraser, and Wheeler (5) in 1935, and which is believed today (3, 16, 23) to be essentially correct, the development of gaseous detonation in a pipe can be described briefly as follows:

As the combustion accelerates in a pipe filled with an explosive

[1] Assistant Professor of Mechanical Engineering, University of California. Mem. ASME.

Contributed by the Applied Mechanics Division and presented at the Annual Meeting, Atlantic City, N. J., November 25–30, 1951, of The American Society of Mechanical Engineers.

Discussion of this paper should be addressed to the Secretary, ASME, 29 West 39th Street, New York, N. Y., and will be accepted until April 10, 1952, for publication at a later date. Discussion received after the closing date will be returned.

Note: Statements and opinions advanced in papers are to be understood as individual expressions of their authors and not those of the Society. Manuscript received by ASME Applied Mechanics Division, March 19, 1951. Paper No. 51—A-23.

[2] Numbers in parentheses refer to the Bibliography at the end of the paper.

mixture, the combustion front, during the predetonation period, is preceded by a shock front. In the final stages of the development of the process, the velocity of the combustion front is higher than that of the shock, and the detonation becomes established when the combustion coalesces with the shock front. Thereafter the detonation front is propagated at a velocity which is remarkably constant, which is only a function of the thermodynamic properties of the substance, and which is in excellent agreement with the value computed for the Chapman-Jouguet state.

It is obvious from the foregoing description that the analysis of such a process must be based upon the consideration of a system consisting of more than one discontinuity and hence that, during the development of the process, the states behind the combustion zone are not necessarily represented by the Hugoniot curve.

In the present paper the combustion zone is considered as a double-discontinuity system, but, otherwise, the analysis is restricted to the usual idealizations of an inviscid, thermally and molecularly nondiffusive substance in a unidimensional flow system. On this basis the following questions are considered:

1 What is the locus of states immediately behind the combustion zone with respect to a known given state of reactants in front of it during the development of the process?

2 What is the reason for the acceleration of the combustion zone?

3 Why is the propagation velocity of detonation so remarkably constant?

In contrast to the contemporary theories (8, 9, 20, 23), which consider some of these problems, but which are concerned more with the structure of the fully developed detonation wave than with the history of its development, the salient feature of the present method of attack is to seek, primarily, the solution to the first question, by an analysis of a simple, idealized system, and then to examine its contribution to the remaining questions. From this standpoint the theory of the Hugoniot curve is critically reviewed, and then the development of the detonation is analyzed on the basis (*a*) of a steady and (*b*) of an unsteady double-discontinuity system.

The Hugoniot-Curve Theory

The classical theory developed by Rankine, Hugoniot, Chapman, and Jouguet (1, 2, 6, 7, 17), as a check of experimental data obtained by Le Chatelier, Dixon, and others, is based upon the application of the principles of conservation of mass, momentum and energy to a single discontinuity system propagated through a substance considered as homogeneous on each side of the discontinuity, inviscid, thermally nonconductive and molecularly nondiffusive. The system is regarded as representing the idealized combustion zone in a constant-area duct where the frictional and heat-transfer wall effects are neglected.

The analysis is essentially the same as that concerned with the propagation of a plane shock (2, 13), the only difference being that, for an adiabatic shock front, the net thermal-energy addition to the system, $q = 0$, while, for an adiabatic combustion front, this energy is equal to that converted from chemical energy by combustion, i.e., $q > 0$.

Both phenomena can be analyzed as a single-discontinuity system represented in Fig. 1.

The system is restricted by the dynamic boundary conditions which imply that at the system's boundary cross sections the values of the stream-force function per unit area, $f = p + mV$, are, at each instant, equal to each other. A process at constant stream-force function per unit area is represented on any thermodynamic plane by a Rayleigh line, the properties of which are described in the Appendix. The Rayleigh line will be here referred to shortly as the *R*-line.

Although the process under consideration may not be strictly one of constant stream-force function per unit area throughout, the dynamic boundary conditions require that, at any instant, points representing state 1, immediately in front, and state 2, immediately behind the discontinuity, lie on an *R*-line, corresponding to the instantaneous velocity V_1 of the propagation of the discontinuity (see Fig. 1). The *R*-line can be regarded

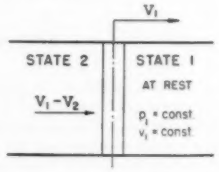

Fig. 1 Single-Discontinuity System

therefore as representing a reversible process which has the same effect as the irreversible one under consideration and hence the line integral along *R* of Tds from 1 to 2 is equal to the net thermal-energy addition to the system per unit mass of substance, or

$$q = \int_R^2 Tds \quad \ldots\ldots\ldots\ldots\ldots\ldots [1]$$

As is well known, the application of the energy equation to the system represented by Fig. 1 yields the Hugoniot equation

$$u_2 - u_1 - q = \frac{p_1 + p_2}{2}(v_1 - v_2) \quad \ldots\ldots\ldots [2]$$

The graphical representation of Equation [2] for q = const on any thermodynamic plane is known as the Hugoniot curve, which will be referred to shortly, as the *H*-curve. According to Equation [1], the *H*-curve is the locus of end points 2, of a family of *R*-lines passing through point 1, the line integral of Tds along each of the *R*-lines from 1 to 2 being constant and equal to q.

In Fig. 2, the pressure-specific volume diagram, are shown an H_s-curve, corresponding to the shock front ($q = 0$), and an H_c-

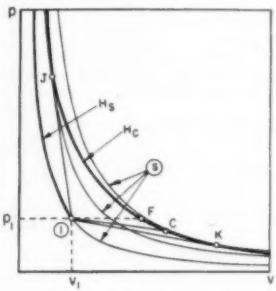

Fig. 2 Hugoniot Curves on Pressure - Specific Volume Diagram

curve, corresponding to the combustion front ($q > 0$). The H_c-curve is usually referred to as the Rankine-Hugoniot curve. Both curves are also shown on the nondimensional diagrams, Fig. 8, pressure-specific volume, and Fig. 9, temperature-entropy plane, plotted to scale for a highly idealized case of a perfect gas with $k_1 = k_2 = 1.400$, $R = 1.986$ cal/mol deg C and (only for the H_c-curve) $q = 20000$ cal/mol and $T_1 = 300$ deg K.

The equations of the H-curves plotted in Figs. 8 and 9 are derived from Equation [2] combined with the perfect-gas equation of state, $u = (RT)/(k-1) = (pv)/(k-1)$ and the definition of entropy, $\sigma = \log_e(v\,\theta^{1/k-1})$. Thus the equation of the H-curve in the nondimensional pressure - specific volume co-ordinates is

$$\frac{k+1}{k-1}\pi\nu - \pi + \nu - \left(2\epsilon + \frac{k+1}{k-1}\right) = 0 \quad \ldots\ldots [3]$$

where, for H_s, $\epsilon = 0$, and, for H_c, $\epsilon = q/(RT_1) = 33.5$, and in the nondimensional temperature-entropy co-ordinates

$$\sigma = \log_e\left[\theta\,\frac{1}{k-1}\,(x + \sqrt{x^2+\theta})\right] \quad \ldots\ldots [4]$$

where

$$x = \epsilon - \frac{k+1}{2(k-1)}\,(\theta - 1)$$

and for H_s, $x = -3(\theta - 1)$; for H_c, $x = 33.5 - 3(\theta - 1)$.

As is well known, the H_c-curve has a point of maximum entropy K, representing the state immediately behind the deflagration front, and a point of minimum entropy J, representing the Chapman-Jouguet state immediately behind a detonation front. The mathematical and thermodynamical properties of the H-curves were analyzed in detail by many authors, see, for example, (1, 2, 3, 6, 7, 16, 17, 20, 23); and the most important features are illustrated in Fig. 2. In particular it should be noted that the R-lines from 1 to K and from 1 to J are tangent to both the H_c-curve and to the isentropes passing through these points. It follows, therefore (see Appendix), that the detonation, as well as the deflagration front, is propagated with respect to the burned gases with a velocity equal to the local velocity of sound ($\mathbf{M}_2 = 1$). The question why the entropy at J is lower than that at K can be explained very simply on the basis of the geometrical characteristics of the R_J and R_K-lines shown in Fig. 9. Since, for a given H_c-curve

$$q = \int_R^2 Tds = \text{const}$$

the areas below each of these lines must be equal to each other, and hence $s_J < s_K$.

As it appears from the foregoing description, the classical Hugoniot-curve theory gives only an answer as to what possible changes may occur if the combustion front were treated as a single-discontinuity system, but it does not furnish any information as to how the process develops.

It should be noted that the H-curves are introduced not as process representations, but as loci of states satisfying the restriction, imposed by the requirement of constant net thermal-energy addition per unit mass of substance, in a single-discontinuity system represented in Fig. 1. By the application of the second law of thermodynamics to this system one may determine immediately in which direction the process may develop. In order to do it it is sufficient to consider any reversible process which would produce the same change as the process under consideration and, of course, the best suited for this purpose here is the process at constant stream-force function per unit area, represented by an R-line. From the characteristics of this line (see Appendix) and, since the system under consideration is, essentially, adiabatic, i.e., by second law $s_2 > s_1$, the following conclusions can be derived:

1 The change of state across a shock front may proceed only from lower to higher pressure and is associated with a decrease of specific volume (compression). A rarefaction front degenerates rapidly into a rarefaction fan, resulting in an isentropic change of state and, consequently, in Fig. 2, the lower branch of the H_s-curve has been substituted by an isentrope.

2 The change of state across a combustion front propagated initially at subsonic velocity may proceed only from higher to lower pressure and is associated with the increase of specific volume (rarefaction). A corresponding statement for a combustion front propagated initially at supersonic velocity is excluded from present consideration as not applicable to the analysis of the development of detonation in a gaseous medium which is initially at rest.

3 The maximum velocity of the combustion front with respect to burned gases immediately behind it (V_2) is equal to the local velocity of sound (maximum entropy of the R-line).

In view of the second conclusion, it appears that none of the states represented by the branch of the H_c-curve above the isobar through state 1 (above point F in Fig. 2), can be achieved by a single-discontinuity combustion system starting from rest as in the case under consideration. The state represented by point F would correspond to that immediately behind a combustion zone at rest with respect to burned gases (line 1-F being on the R-line with zero slope; see Appendix) which is practically impossible, but any other state between F and K (say, state C in Fig. 2), could be considered as plausible (weak deflagration) and, as the combustion front accelerates, fully developed deflagration, resulting in establishment of state K behind the front, could be finally achieved. However, an explanation of the reason for the acceleration of the combustion front remains unanswered[2] and, according to conclusion 3, the establishment of deflagration would limit the development of the process.

Furthermore, there is a fundamental difference, which is usually emphasized, for example (2, 7), in the direction of velocity of the burned gases with respect to the deflagration and that with respect to the detonation front. While, for deflagration, $p_2 < p_1$ and hence $V_2 > V_1$ (see Appendix), and the burned gases move in the opposite direction than the front, for detonation $p_2 > p_1$, $V_2 < V_1$, and the burned gases move, similarly as for a shock front, in the same direction as the discontinuity. If one would then admit, as quite a plausible assumption, that a deflagration front is formed as one of the intermediate stages in the development of detonation, there follows a question immediately how and when the relative velocity of the burned gas is reversed?

All these problems cannot be answered on the basis of a simple Hugoniot-curve theory, stipulating at all times the existence of a single discontinuity only, and it is clear, therefore, that this theory is insufficient for any analysis concerned with the development of the process.

Steady Double-Discontinuity Combustion System

The next step in the extension of the simple Hugoniot-curve theory is the consideration of a steady double-discontinuity combustion system. The assumption of a double-discontinuity system is borne out of experimental evidence (5), as described in the Introduction, is substantiated by the analysis of the dynamic character of the detonation wave, as pointed out by Jouguet (1), more rigorously justified by von Neumann (9), and described by Courant and Friedrichs (16). Furthermore, its origin can be traced down to the "physicochemical aspects" of the phenomenon, as shown by Ubbelohde (19), on the basis of the kinetic characteristic of the chemical reaction leading to detonation.

Although the majority of investigators were concerned only

[2] The acceleration may be attributed to the fact that the combustion front is not plain, and the velocity of propagation increases due to the increase of the area of the reaction surface, a consideration of this effect being outside the scope of the simple unidimensional theory.

with the structure of the fully developed detonation, there were some [for example (10, 11)] who considered the steady double-discontinuity system as representing also the predetonation stages of combustion.

According to this theory, the combustion zone is treated as consisting of a shock preceding a combustion front, both moving at the same instantaneous velocity, V_1, Fig. 3. The locus of states immediately behind the combustion zone is represented on the pressure-specific volume diagram, Fig. 4, as the $\mathbf{M}_1$-curve. It consists of the Chapman-Jouguet states of a family of H_ϵ-curves

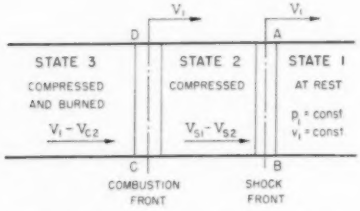

FIG. 3 STEADY DOUBLE-DISCONTINUITY SYSTEM

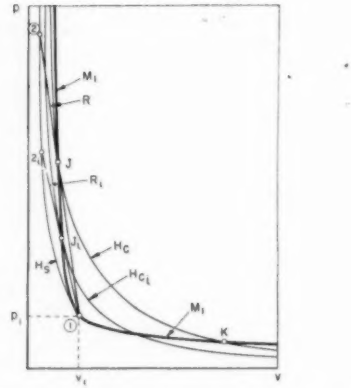

FIG. 4 DEVELOPMENT OF DETONATION AND DEFLAGRATION IN STEADY DOUBLE-DISCONTINUITY SYSTEM

corresponding to values of q from zero to that equal to the enthalpy of formation of the fully developed detonation. All these states have in common the characteristic property of the Chapman-Jouguet state, that is, the instantaneous velocity of the burned gases with respect to discontinuity is at all times sonic, and the locus of these states is therefore identical to that of $\mathbf{M} = 1$ attained across a single discontinuity ($\mathbf{M}_1$-curve). The $\mathbf{M}_1$-curves are shown plotted to scale for a highly idealized case of $k_1 = k_2 = 1.400$ on the nondimensional pressure-specific volume diagram, Fig. 8, and temperature-entropy diagram, Fig. 9.

The equations of these curves are derived in the Appendix and they are, respectively

$$\pi = \frac{\nu}{(k+1)\nu - k} \quad \ldots\ldots [5]$$

and

$$\sigma = \log_e \left\{ \theta^{k/k-1} \left[\left(\frac{k+1}{2} \right) \pm \sqrt{\left(\frac{k+1}{2} \right)^2 - \frac{k}{\theta}} \right] \right\} \quad \ldots [6]$$

At the same time, from the Hugoniot equation

$$\frac{k+1}{k-1}\pi\nu - \pi + \nu - \frac{k+1}{k-1} - 2\epsilon = 0 \quad \ldots\ldots [7]$$

where

$$\epsilon = \frac{q}{RT_1}$$

From Equations [5] and [7] any instantaneous state can be determined corresponding to a given value of q. For q, corresponding to complete combustion, these equations yield the parameters of states immediately behind the fully developed detonation and deflagration (points K and J).

The process at any instant during the development of detonation is represented by an R_i-line, see Fig. 4, and consists of the change from state 1 to 2_i across the shock front, and from 2_i to J_i across the combustion front. As the process develops, q is considered to increase monotonically, the slope of the R_i-line increases, and the combustion front accelerates to fully developed detonation. Thereafter the system cannot accelerate further without any change in its structure, since q achieved its maximum value, and this fact could be considered as an adequate explanation of the stability of detonation.

In the simple unidimensional treatment, the process of combustion in a constant-area duct may proceed from state 1 either to detonation, the states immediately behind the combustion zone lying on the upper branch of the $\mathbf{M}_1$-curve ($1 - J_i - J$ in Fig. 4), or to deflagration, in which case the system consists of a single discontinuity and the locus of states immediately behind the combustion zone is represented by the lower branch of the $\mathbf{M}_1$-curve ($1 - K$). In the first case $V_1 > V_{c2}$ and the burned gases move at all times in the same direction as the front, and in the latter $V_1 < V_{c2}$ and the burned gases move in the opposite direction. The deflagration and detonation are considered as representing completely different modes of combustion, and the former cannot form an intermediate stage during the development of the latter.

Although the acceleration and stability of detonation can be explained very simply according to the steady double-discontinuity theory, its main drawback lies in the fact that it does not reflect the experimentally observed effect of the coalition of the two fronts on the establishment of detonation.

UNSTEADY DOUBLE-DISCONTINUITY COMBUSTION SYSTEM

A more general definition of a double-discontinuity system than that in Fig. 3 is shown in Fig. 5. The two fronts move with different velocities and, consequently, the system within the boundary A-B-C-D is unsteady due to the change of mass and of stored energy between the two discontinuities. The velocity vectors in Fig. 7 represent absolute velocities expressed in terms of

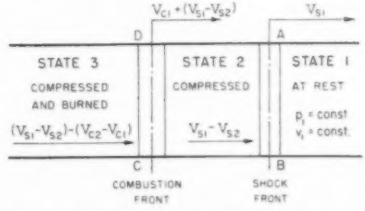

FIG. 5 UNSTEADY DOUBLE-DISCONTINUITY SYSTEM

the relative velocities immediately in front and immediately behind the discontinuities, V_{s1} and V_{s2} referring to the shock front, and V_{c1} and V_{c2} referring to the combustion front. It should be noted that the burned gases move in the same or in the opposite direction to that of the combustion system depending on whether $(V_{s2} - V_{c2})$ is bigger or smaller than $(V_{c2} - V_{c1})$.

The analysis of the predetonative combustion process treated as an unsteady double-discontinuity system was presented previously, by the same author, at the Seventh International Congress of Applied Mechanics, London, England, 1948 (18), and at the Institute for Heat Transfer and Fluid Mechanics, Los Angeles, Calif., 1950 (22), but only summaries of these presentations were published. The same idea was later described by Courant and Friedrichs (16), and earlier pointed out by others (8, 12), but the analytical implications of such a treatment, which are presented here, have not been published elsewhere.

In the analysis of the system in Fig. 5, instead of assuming, as was done previously, that the enthalpy of formation increases while the velocities of the two fronts are equal to each other, it is assumed that the enthalpy of formation is constant and that the velocity of the combustion front with respect to burned gases, V_{c2}, is sonic, the latter condition being retained from the steady double-discontinuity system theory. The reasoning underlying these assumptions can be outlined as follows:

Because of the rapidity with which the process of detonation develops, one may suspect that the combustion system is restricted only by the dynamic boundary conditions and that, very early in the development of the process, the enthalpy of formation achieves the value corresponding to complete combustion, and thereafter remains constant. Since the combustion is started at subsonic velocity then, as previously pointed out, by treating the combustion front as one associated with a monotonic thermal-energy increase, there follows from the characteristics of the R-line, expressing the restrictions imposed by the dynamic boundary conditions on the system, that the maximum velocity of propagation of the combustion front with respect to burned gases is equal to the local velocity of sound. This limiting velocity is assumed to be attained also soon after the initiation of the process.

The change of state across the double-discontinuity system is equal to the sum of the changes across each of the discontinuity, since the intermediate state (state 2 in Fig. 5), is homogeneous. Hence referring to Fig. 5, the locus of states 3, behind the combustion system, is determined by the following (see Fig. 6):

1 The change of state across the shock front, represented in Fig. 6 by the R_s-line from 1 to 2.

2 The change of state across the combustion front represented by the R_c-line from 2 to 3.

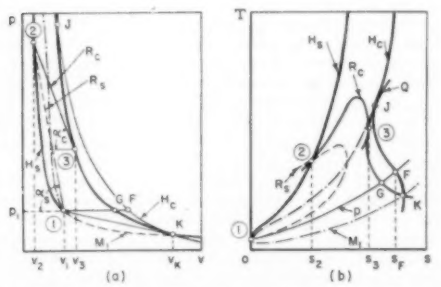

FIG. 6 INSTANTANEOUS PREDETONATION PROCESS IN UNSTEADY DOUBLE-DISCONTINUITY SYSTEM

3 The condition that Mach number at state 3 is unity, corresponding to the condition that R_s is tangent to the isentrope at state 3.

The change of state across R_s is given by the Rankine-Hugoniot equation

$$u_2 - u_1 = \frac{p_1 + p_2}{2}(v_1 - v_2) \quad \ldots\ldots\ldots\ldots [8]$$

the change of state across R_c by the Hugoniot equation

$$u_3 - u_2 - q = \frac{p_2 + p_3}{2}(v_2 - v_3) \quad \ldots\ldots\ldots\ldots [9]$$

and the condition of $\mathbf{M}_3 = 1$ (see Appendix) is

$$\frac{p_2 - p_3}{v_3 - v_2} = -\left(\frac{\partial p_2}{\partial v_2}\right)_s = k_2 \frac{p_2}{v_2} \quad \ldots\ldots\ldots\ldots [10]$$

the second equality sign above corresponding to the assumption of perfect-gas behavior of substance in the vicinity of state 3. Otherwise, these three equations refer to the characteristics of the system and hold true irrespective of the properties of the substance.

The equation of states 3 can be obtained by eliminating p_2 and v_2 from Equations [8], [9], and [10]. (The values of $u_1 = u(p_1, v_1)$, $u_2 = u(p_2, v_1)$ and $u_3 = u(p_3, v_3)$ are given by the equations of state for the substance under consideration.) The corresponding algebraic transformations are involved even for the highly idealized case of a perfect gas with constant specific-heat capacities. Hence, instead of attempting to derive the final form of $F(p_3, v_3) = 0$, it is best to consider Equations [8], [9], and [10] as parametric equations representing the locus of states behind the detonating combustion zone. Selecting, for instance, p_2 as a parameter, then, for a given p_1, v_1, and $u = u(p, v)$, v_2 can be determined from Equation [8] and, with these values of p_2 and v_2, Equations [9] and [10] can be solved for p_3 and v_3. The locus of states 3 will be referred to as the Q-curve.

The Q-curves corresponding to $k_1 = k_2 = k_3 = 1.400$, $R = 1.986$ cal/mol deg C, $q = 20{,}000$ cal/mol and $T_1 = 300$ deg K ($\epsilon = 33.5$) are shown, plotted to scale, on the nondimensional diagrams in Fig. 8 (in $\pi - \nu$ co-ordinates) and Fig. 9 (in θ—σ co-ordinates). The equation of the Q-curve in the $\pi - \nu$ co-ordinates is given by the following set of parametric equations corresponding to Equations [8], [9], and [10], respectively

$$\frac{k+1}{k-1}\pi_2\nu_2 - \pi_2 + \nu_2 - \frac{k+1}{k-1} = 0 \quad \ldots\ldots [11]$$

$$\frac{k+1}{k-1}\pi_3\nu_3 - \pi_2\nu_2 + \pi_2\nu_3 - \frac{k+1}{k-1}\pi_3\nu_3 - 2\epsilon = 0 \quad \ldots [12]$$

$$(k-1)\pi_3\nu_3 - k\pi_2\nu_2 - \pi_2\nu_2 = 0 \quad \ldots\ldots\ldots [13]$$

and the equation of the Q-curve in $\theta - \sigma$ co-ordinates is obtained from $F(\pi_3\nu_3) = 0$, determined by the foregoing equations and the expressions for σ and θ in terms of π and ν, i.e.

$$\sigma = \frac{1}{k-1}\log_e(\pi\nu^k), \quad \text{and} \quad \theta = \pi\nu$$

Geometrically the Q-curve is the locus of maximum entropy points of a family of Rayleigh lines started from all points of the Rankine-Hugoniot curve and satisfying the condition that the area below their subsonic branch on the temperature-entropy diagram is constant and equal to the enthalpy of formation, q (or ϵ on the nondimensional diagram).

Since the foregoing condition is satisfied by the R-lines passing through points K and J, the Q-curve passes through these points.

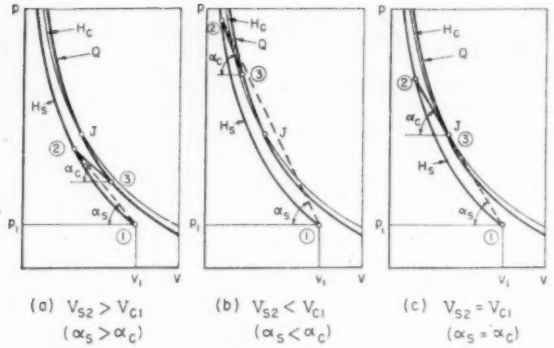

FIG. 7 DEVELOPMENT OF DETONATION IN UNSTEADY DOUBLE-DISCONTINUITY SYSTEM

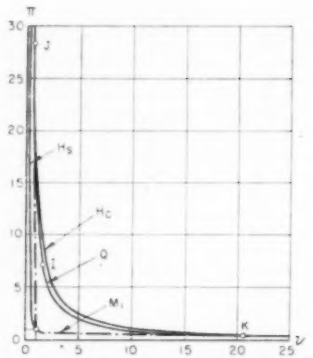

FIG. 8 NONDIMENSIONAL PRESSURE-SPECIFIC VOLUME DIAGRAM PLOTTED TO SCALE

As can be seen in Fig. 9, part of the Q-curve has lower entropy than that of any point of the corresponding H_c-curve. The point of minimum entropy of the Q-curve, denoted by I in Figs. 8 and 9, represents the state of burned gases immediately behind the double-discontinuity combustion system propagated into state 1 at rest, see Fig. 5, at the instant when they are also at rest. Considering the expression for the velocity of state 3, as shown in Fig. 5, it follows that the condition cited corresponds to

$$V_{c2} - V_{c1} = V_{s1} - V_{s2} \quad \ldots\ldots\ldots\ldots\ldots [14]$$

or, using the R-line equation (see Appendix, Equation [26]), to

$$(v_2 - v_2)(p_2 - p_2) = (v_1 - v_2)(p_2 - p_1) \quad \ldots\ldots [15]$$

which, together with Equations [8], [9], and [10] determines the co-ordinates of state I.

Thus when the gases immediately behind the combustion system in Fig. 5 are at states corresponding to lower pressure, temperature, and density than that of state 1, they move in the opposite direction to that of the system, and, when they are at states corresponding to higher pressure, temperature, and density, they move in the same direction as the combustion system.

The outlined theory is restricted only to the immediate vicinity of the combustion zone. If it were applied to a specific case of, say, a duct closed at one end, for which the products as well as the undisturbed reactants are at rest, then, for all the states, with the exception of state I, there must be considered one more change bringing the velocity of burned gases down to zero. This could be taken into account by an analysis of a three-discontinuity system, but, because of space limitation, this is considered to be outside the scope of the present paper.

The theory of the Q-curve will now be examined from the standpoint of its contribution to the development and stability of detonation.

The initial stages of the process cannot be analyzed on the basis of the idealized system under consideration because of the profound influence of irreversibilities, as a result of which the problem cannot be confined to a unidimensional treatment. The initial acceleration of the combustion system can be attributed to several causes such as the activation of molecules by the energy supplied from the ignition system, an increasing enthalpy of formation, or curvature of the combustion surface. If the analysis were confined to the unidimensional treatment, the combustion zone could be considered to be initially a single or a double-discontinuity system, and the corresponding states of products immediately behind the combustion zone would be represented, see Fig. 6, by the isobar passing through state 1 and the H_c-curve, or by the M_1-curve, or by any line within the region bounded by these lines.

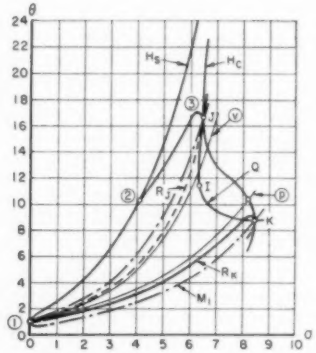

FIG. 9 NONDIMENSIONAL TEMPERATURE-ENTROPY DIAGRAM PLOTTED TO SCALE

In the analysis of the subsequent development of the process, at least a double-discontinuity system has to be considered, the corresponding states of products immediately behind the combustion zone tracing the Q-curve. At this mode of combustion the acceleration of the system can be explained by stipulating that, at any intermediate state, activated molecules give rise to compression waves, which reinforce the shock front. As the intensity of the shock front increases, so does the pressure at state 2 and the velocities of both the fronts, see Fig. 7. Soon the velocities of propagation achieve such high values that the unidimensional analysis can be considered to be sufficiently accurate.

In the final stages of the development of the process it is of interest to observe the relative velocities between the two fronts. With the help of the graphical representation of the process on the pressure - specific volume diagram in Fig. 7, this can be easily accomplished. It is sufficient to consider the relationship between relative velocities of the two fronts with respect to state 2.

The relative velocity of the shock front is (see Appendix, Equation [26])

$$V_{s2} = v_2 \sqrt{\tan \alpha_s} \quad [16]$$

and the relative velocity of the combustion front is

$$V_{c2} = v_2 \sqrt{\tan \alpha_c} \quad [17]$$

where angles α_s and α_c are those denoted in Fig. 7.

The relative velocity between the shock front with respect to the combustion front is, therefore

$$V_{s2} - V_{c2} = v_2 \left(\sqrt{\tan \alpha_s} - \sqrt{\tan \alpha_c} \right) \quad [18]$$

Hence the shock front has a higher or a lower velocity than the combustion front depending upon whether α_s is bigger or smaller than α_c.

At first, Fig. 7(*a*), $\alpha_s > \alpha_c$ and the shock moves at a higher velocity than the combustion front, but, as the intensity of the shock front increases, the relative velocity between the two fronts decreases until pressure of state 2 is so high that the velocity of the combustion front becomes higher than that of the shock front. The changes of state corresponding to such an instant are shown in Fig. 7(*b*), where, it can be noted, $\alpha_c > \alpha_s$. The combustion front can then "catch" the shock front, coalesce with it, and establish thus a fully developed detonation. The corresponding changes of state are represented in Fig. 7(*c*), where $\alpha_s = \alpha_c$, the products immediately behind the combustion zone being at the Chapman-Jouguet state. Thereupon the velocity of the system cannot increase any more because the shock front must precede the combustion front (8, 9, 12), and the only way in which the double-discontinuity system could accelerate further would be by the combustion overtaking the shock front.

Hence it can be concluded that, as a result of dynamic boundary restrictions, imposed on the detonating combustion system of constant cross-sectional area, combined with the condition that the high-velocity combustion front must be preceded by the shock front, once the two fronts coalesce, establishing thus a detonation front, the corresponding rate of combustion cannot be exceeded even if infinite rate of the combustion reaction was assumed to be possible.

The combustion rate at any instant is equal to the mass flow rate of compressed gases through the combustion front, and it can be determined from any of the following relationships (see Appendix, Equation [26], and Fig. 7)

$$m_c = \sqrt{\tan \alpha_c} = \sqrt{\frac{p_2 - p_1}{v_1 - v_2}} = \sqrt{k_2 \frac{p_2}{v_2}} \quad [19]$$

the last equality sign arising from the fact that $\mathbf{M}_2 = 1$.

The maximum combustion rate, corresponding to detonation is (see Appendix, Equations [26] and [27])

$$m_{cJ} = \sqrt{k_J \frac{p_J}{v_J}} = \mathbf{M}_1 \sqrt{k_1 \frac{p_1}{v_1}} = \mathbf{M}_1 \frac{a_1}{v_1} \quad [20]$$

where subscript J refers to the Chapman-Jouguet state.

Since the Mach number of the detonation front is expressed by the Mach number of the shock front, from Equation [20]

$$\mathbf{M}_D = \mathbf{M}_1 = \sqrt{\frac{k_J}{k_1} \frac{p_J/p_1}{v_J/v_1}} \quad [21]$$

or, in nondimensional co-ordinates, for $k_J = k_1$

$$\mathbf{M}_D = \sqrt{\frac{\pi_J}{\nu_J}} = \frac{\pi_J}{\sqrt{\theta_J}} = \frac{\sqrt{\theta_J}}{\nu_J} \quad [22]$$

For the numerical example illustrated in Figs. 8 and 9, $\mathbf{M}_D = 7$.

Conclusions

1 Assuming that a high-velocity combustion front can be treated as a discontinuity in the flow field, the analysis of the development and stability of detonation must be based on the consideration of, at least, a double-discontinuity system, consisting of a compression shock preceding the combustion front.

2 The locus of states behind a detonating combustion system, propagated into an explosive gas mixture, which is at a given, constant state, depends on whether the system is treated as steady or unsteady.

3 The most probable locus of states during the predetonation period is that behind an unsteady, double-discontinuity system for which the enthalpy of formation is assumed to be constant, and the velocity of the combustion front with respect to burned gases is sonic. On this basis, most of the experimentally observed facts associated with the development of detonation in a pipe can be explained adequately, even if the analysis is restricted to a unidimensional treatment.

4 The analysis helps the understanding of the flow dynamic phenomena associated with the development of detonation. It enables conclusions to be drawn which are concerned with the behavior of burned gases immediately behind the detonating combustion system, such as the variation of their velocity and pressure, which, so far, have not been checked experimentally. It is suggested, therefore, that experiments be performed which would include records of the variation of these parameters. The considerations described here will be of assistance in the planning of such experiments and in the analysis of their results.

BIBLIOGRAPHY[4]

1 "Méchanique des Explosifs," by E. Jouguet, O. Doin et Fils, Paris, France, 1917, 516 pp.

2 "Impact Waves and Detonation," by R. Becker, *Zeitschrift für Physik*, vol. 8, 1921, pp. 321–362; translation: NACA TM 505 and 506.

3 "Experimental Investigations Concerning the Limits of Detonation in Gaseous Mixtures," by R. Wendlandt, *Zeitschrift für Physicalische Chemie*, vol. 110, 1924, pp. 637ff; translation: NACA TM 553 and 554.

4 "Steam and Gas Turbines," by A. Stodola, translated by L. C. Loewenstein, McGraw-Hill Book Company, Inc., New York, N. Y., vol. 2, 1927, pp. 1022ff.

5 "Photographic Investigation of Flame Movements in Gaseous Explosions—Phenomenon of Spin in Detonation," by W. A. Bone, R. P. Fraser, and W. H. Wheeler, Philosophical Transactions of the Royal Society of London, series A, vol. 235, 1935, pp. 29–63.

6 "Combustion, Flames and Explosions in Gases," by B. Lewis and G. von Elbe, Cambridge University Press, London, England, 1938.

7 "Explosion and Combustion Process in Gases," by W. Jost, Julius Springer, Berlin, Germany, 1939; translated by H. O. Croft, McGraw-Hill Book Company, Inc., New York, N. Y., 1946, pp. 201ff.

8 "On the Theory of the Propagation of Detonation in Gaseous Systems," by Y. B. Zeldovich, *USSR Journal of Experimental and Theoretical Physics*, vol. 10, 1940, pp. 542–568; translation: NACA TM No. 1261, 1950.

9 "The Theory of Detonation Waves," by J. von Neumann, Progress Report, April 1, 1942, Office of Scientific Research and Development No. 549/PBL 31090(2-616).

10 "On the Detonation Process in Gases," by W. Döring, *Annalen der Physik*, vol. 43, 1943, pp. 421–436.

11 "Contributions to the Theory of Detonation," by W. Döring and G. Burkhardt, Forschungsbericht No. 1939, 1944; translation: Air Materiel Command, Wright-Patterson Air Force Base, Dayton, Ohio, Technical Report No. F-TS-1227-IA (GDAM A9-T-46), 1949.

12 "Theory of Combustion and Detonation of Gases," by Y. B. Zeldovich, Academy of Sciences of the USSR Institute of Chemical Physics, 1944; translation: Air Materiel Command, Wright-Patterson Air Force Base, Dayton, Ohio, as Technical Report No. F-TS-1226-IA (GDAM A9-T-45), 1949.

13 "The Mechanics and Thermodynamics of Steady One-Dimensional Gas Flow," by A. H. Shapiro and W. R. Hawthorne, JOURNAL OF APPLIED MECHANICS, Trans. ASME, vol. 69, 1947, pp. A-317–336.

[4] Arranged chronologically.

14 "Gas Dynamic Treatment of Exothermic and Endothermic Discontinuities," by D. G. Samaras, *Canadian Journal of Research*, vol. A26, 1948, pp. 1–21.

15 "On the Characterization of Fields of Diabatic Flow," by B. L. Hicks, *Quarterly of Applied Mathematics*, vol. 6, 1948, pp. 405–416.

16 "Supersonic Flow and Shock Waves," by R. Courant and K. O. Friedrichs, Interscience Publishers, Inc., New York, N. Y., 1948.

17 "Underwater Explosions," by R. H. Cole, Princeton University Press, Princeton, N. J., 1948.

18 "Dynamics of Combustion or Heat Addition to a Compressible Flow," by A. K. Oppenheim, VII International Congress of Applied Mechanics, II-29, 1948.

19 "Transition From Deflagration to Detonation: The Physico-Chemical Aspects of Stable Detonation," by A. R. Ubbelohde, Third Symposium on Combustion and Flame, and Explosion Phenomena, The Williams and Wilkins Company, Baltimore, Md., 1949.

20 "The Stability of Detonation," by H. Eyring, R. E. Powell, G. H. Duffey, and E. B. Parlin, *Chemical Reviews*, vol. 45, 1949, pp. 69–181.

21 "A Contribution to the Thermodynamics of Gas Flow," by R. I. Focke, *Forschung des Ingenieurwesen*, vol. 16, 1949, pp. 43–50.

22 "A Graphical Interpretation of Shock and Combustion Fronts and Its Application to the Theory of Detonation Phenomena," by A. K. Oppenheim, Institute for Heat Transfer and Fluid Mechanics, Los Angeles, Calif., 1950; abstracts of papers pp. 2–3.

23 "A Discussion on Detonation," by W. G. Penney, et al., Proceedings of the Royal Society, series A, vol. 204, 1950, pp. 1–33.

Appendix

Process at Constant Stream-Force Function Per Unit Area—the Rayleigh Line

The number of problems which can be treated as a single discontinuity is quite extensive and their analysis was presented by many authors (see e.g., references 13, 14, 15, 16, 21). The common feature of these analyses is the idealization that the change of state across the discontinuity takes place at constant stream-force function per unit area.[5] The corresponding process can be represented on a thermodynamic plane as a Rayleigh line,[6] which, on the pressure - specific volume diagram, is a straight line. Since the simplifications resulting from this fact are utilized in the analysis presented in this paper, they are here summarized. In the paper the Rayleigh line is referred to, shortly, as the *R*-line. The theory described here was presented, for the first time, by the same author, at the Seventh International Congress of Applied Mechanics (18).

The ensuing analysis is applicable to any plane discontinuity irrespective of its direction with respect to that of the flow, Fig. 10. For the system represented in Fig. 1 or Fig. 10 the continuity equation yields

$$\frac{V_1}{v_1} = \frac{V_2}{v_2} = m \quad \ldots\ldots [23]$$

and the momentum equation in the normal direction

$$p_1 + mV_1 = p_2 + mV_2 = f \quad \ldots\ldots [24]$$

[5] $f = p + mV$, referred to, in technical literature (13), as the "impulse function." The author of the present paper prefers to use the term "stream-force function" as less ambiguous than the "impulse function."

[6] As far as the author of the present paper has been able to verify, this term was introduced into the technical literature by Stodola (4) as the representation of the change of state across a shock front on the temperature-entropy diagram. The corresponding curve on the pressure-specific volume diagram should be called by the same name, as it is done here, instead of being assigned a new name, as it appears, for instance, in the Russian literature (8, 12) where it is referred to as "the constant velocity line of Todes." J. von Neumann (9) designates this line as line λ, Courant and Friedrichs (16) refer to it as to the line expressing the "mechanical shock conditions" without identifying it as the Rayleigh line.

Subscript 1 refers to conditions immediately in front and subscript 2 to conditions immediately behind the discontinuity V_1 and V_2 are normal components of relative velocities with respect to the discontinuity, and f the normal component of the stream-force function per unit cross-sectional area of the discontinuity.

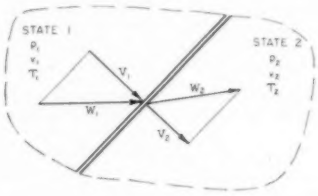

Fig. 10 General Case of a Plane Discontinuity System

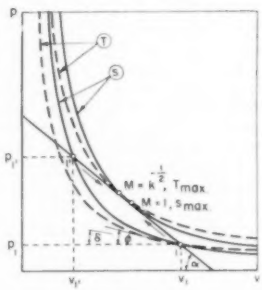

Fig. 11 Rayleigh Line on Pressure - Specific Volume Diagram

Equations [23] and [24] can be considered as representing the dynamic boundary conditions imposed on the system, consisting of a single discontinuity with no restriction as to its direction with respect to that of the flow stream.

Eliminating velocities from Equations [23] and [24], there obtains

$$\frac{p - p_1}{v_1 - v} = m^2 \quad \ldots\ldots [25]$$

which, for a discontinuity moving at constant velocity, corresponding to a constant mass flow rate, represents the equation of the *R*-line in the pressure - specific volume co-ordinates. Subscript 2 has been dropped since pressure and specific volume behind the discontinuity form the variables of the *R*-line.

The properties of the *R*-line on the *p-v* diagram are illustrated in Fig. 11. They are summarized as follows:[7]

1 The normal component of the flow velocity at any point of the *R*-line is given by

$$V = vm = v\sqrt{\frac{p - p_1}{v_1 - v}} = v\sqrt{\tan\alpha} \quad \ldots\ldots [26]$$

2 For the perfect-gas behavior of the substance in the neighborhood of state under question:

Slope of *R*-line is

$$\tan\alpha = k\frac{p}{v}\mathbf{M}^2 \quad \ldots\ldots [27]$$

[7] For meaning of symbols see Nomenclature and Fig. 11.

Ratio of slopes of R-line and isentrope at any point is

$$\frac{\tan \alpha}{\tan \phi} = \mathbf{M}^2 \quad \ldots [28]$$

Ratio of slopes of R-line and isotherm at any point

$$\frac{\tan \alpha}{\tan \delta} = k\mathbf{M}^2 \quad \ldots [29]$$

From the last two relationships there follow immediately the well-known characteristics of the R-line, namely, that, since at the point of maximum entropy the R-line is tangent to the isentrope, the corresponding Mach number, $\mathbf{M} = 1$, and, since at the point of maximum temperature the R-line is tangent to the isotherm, the corresponding Mach number, $\mathbf{M} = k^{-1/2}$.

The locus of states of $\mathbf{M} = 1$ attained immediately behind a single discontinuity is, from Equations [26] and [27], given by

$$\frac{p}{p_1} = \frac{v}{(1 + k)v - kv_1} \quad \ldots [30]$$

and the locus of states of $\mathbf{M} = k^{-1/2}$ is

$$\frac{p}{p_1} = \frac{v}{2v - v_1} \quad \ldots [31]$$

In order to indicate the parallelism between the properties of the R-line on the temperature-entropy diagram to that on the pressure - specific volume diagram, as just outlined, the diagram in Fig. 12 has been plotted. It represents only a special case of R-lines as a function of nondimensional co-ordinates; $\theta = T/T_1$ and $\sigma = (s - s_1)/R$ applied to a perfect gas with constant specific-heat capacities. The diagram corresponds to $k = 1.4$ = const and the R-lines, plotted there, to Mach numbers at state 1, $\mathbf{M}_1 = 2, 1, 0.5$, and $k^{-1/2} = 0.846$, respectively. In Fig. 11 there is also superimposed the curve of maximum temperature ($\mathbf{M} = k^{-1/2} =$ const), and that of maximum entropy ($\mathbf{M} = 1 =$ const) for the family of R-lines passing through the origin.

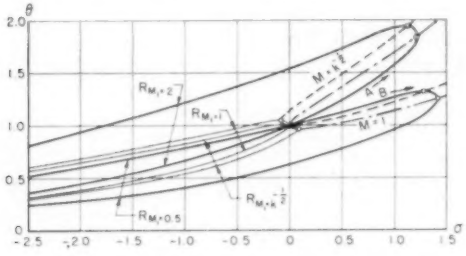

FIG. 12 RAYLEIGH LINES PLOTTED TO SCALE ON NONDIMENSIONAL TEMPERATURE-ENTROPY DIAGRAM

The equations of curves plotted in Fig. 12 are derived from the following:

(a) The equation of the R-line in the nondimensional pressure ($\pi = p/p_1$)—specific volume ($v = v/v_1$) co-ordinates

$$\frac{\pi - 1}{1 - v} = k\frac{\pi}{v}\mathbf{M}^2 = k_1\mathbf{M}_1^2 \quad \ldots [32]$$

where subscript 1 refers to state ($\pi = 1, v = 1$).

(b) The nondimensional equation of state

$$\theta = \pi v \quad \ldots [33]$$

(c) The definition of entropy which results in

$$\sigma = \frac{1}{k - 1}\log_e(\pi v^k) = \log_e(v\theta^{1/k-1}) \quad \ldots [34]$$

The equation of the R-line is then

$$\sigma = \log_e\left[\theta^{\frac{1}{k-1}}\frac{(1 + k_1\mathbf{M}_1^2) \pm \sqrt{(1 + k_1\mathbf{M}_1^2) - 4k_1\mathbf{M}_1^2\theta}}{2k_1\mathbf{M}_1^2}\right] \quad \ldots [35]$$

the equation of the $\mathbf{M} = 1$ curve

$$\pi = \frac{v}{(k + 1)v - k} \quad \ldots [5]$$

or

$$\sigma = \log_e\left\{\theta^{k/k-1}\left[\left(\frac{k + 1}{2}\right) \pm \sqrt{\left(\frac{k + 1}{2}\right)^2 - \frac{k}{\theta}}\right]\right\} \quad [6]$$

and the equation of the $\mathbf{M} = k^{-1/2}$ curve

$$\pi = \frac{v}{2v - 1} \quad \ldots [36]$$

or

$$\sigma = \log_e\left[\theta^{k/k-1}\left(1 \pm \sqrt{1 - \frac{1}{\theta}}\right)\right] \quad \ldots [37]$$

The parallelism between the two R-line representations can be easily noticed by comparing Fig. 11 to Fig. 12. The main difference between these two representations is that in Fig. 11 any point of the R-line can be considered to represent state 1 (an assumption of pressure and specific volume corresponding to the Mach number of this state would fix the scales for p and v), while in Fig. 11 state 1 is always represented by the point ($\sigma = 0, \theta = 1$), and the shape of the R-line depends upon the value of $\mathbf{M}_1$. Thus if point 1 or point 1′ in Fig. 11 were considered as representing state 1, they would both be represented by the point ($\sigma = 0, \theta = 1$) in Fig. 12. Moving in the direction of the arrow indicated near point 1 in Fig. 11 corresponds to following, in the direction of arrow A, a "supersonic" R-line in Fig. 12 (say, $R\mathbf{M}_1 = 2$); moving in the direction of arrow indicated near point 1′ in Fig. 11 corresponds to following, in the direction of arrow B, a subsonic R-line (say, $R\mathbf{M}_1 = 0.5$) in Fig. 12.

ACKNOWLEDGMENT

The theory upon which the present paper is based was conceived when the author was associated with the City and Guilds College of the Imperial College of Science and Technology, University of London. The author wishes to acknowledge his thanks to Prof. O. A. Saunders, Head of the Department of Mechanical Engineering at that College, for inspiring encouragement, and to Mr. R. Tyler, Lecturer at the same College, for his kind help in performing initial computations for the graphs presented in this paper.

The Time Required for Constant-Volume Combustion

By A. S. CAMPBELL,[1] ORONO, ME.

By combining the results of an elementary thermodynamic analysis of the temperature distribution in the burned gases of a constant-volume bomb with an examination of the velocity relations at the flame front, it is possible to relate the "normal burning velocity" to the time rate of production of burned gases. Integration of this equation leads to an estimate of the time required for the combustion process.

Introduction

In the elementary discussion of constant-volume combustion of gaseous mixtures it is assumed that the products of combustion reach a uniform temperature. A more detailed examination of the combustion process has shown that during the course of burning, and at the instant combustion is concluded, a temperature gradient exists in the burned portion of the gases. Consequently, the final uniform temperature is not reached until the temperature gradient has dissipated itself through heat conduction.

Since the flame front moves through the unburned gas at finite velocity, it is clear that the charge located between the ignition electrodes burns before the charge located at the walls of the bomb. If the unburned gas is subdivided into infinitesimal layers, and it is assumed that the burning process proceeds from layer to layer, it may be assumed that each layer burns at essentially constant pressure. Thus constant-volume combustion is found to be a series of constant-pressure combustions.

The existence of the temperature gradient was first demonstrated experimentally by Hopkinson[2] in 1906. The subject has been discussed theoretically by Flamm and Mache,[3] and by Lewis and von Elbe.[4] The results of both discussions lead to a relation between the mass fraction burned and the fractional pressure rise, as well as a formulation for the temperature distribution in the burned gas. The discussion in this paper is not essentially different from that of Lewis and von Elbe.

Since one is interested in temperature relationships in the gas, the analytical treatment requires that we assume ideal gases with constant heat capacities. Obviously, one also assumes no change in the composition of the burned gases. Recently Hottel, Williams, and Satterfield[5] have shown how the same problem can be treated with the use of charts for the equilibrium thermodynamic properties of the burned gas. Their method of solution gives a more realistic estimate of the magnitude of the temperature gradient.

The purpose of this paper is to employ the results of the analytical study of the progressive burning process to derive a relation between the so-called "normal burning velocity" and the time rate at which unburned gas is converted to burned gas. Such a relation can then be used to form an estimate of the total time required for the entire burning process.

Temperature Distribution in the Burned Gas

The problem is stated as follows: Given a mass M of combustible gas mixture at pressure P_i and temperature T_i, confined in a rigid, nonconducting bomb of volume V; compute the temperature distribution in the gases at any stage of the combustion process.

The analysis is made with the following assumptions:

1 Burned and unburned gases are ideal.

2 All heat capacities are constant.

3 No heat transfer takes place in the burned or unburned gas, or normal to the flame front.

4 The composition of the burned gas is fixed (no dissociation).

5 The pressure is uniform at all times.

The following equations may now be written:

Conservation of energy

$$Mc_u(T_i - \theta_u) = m_u c_u(T_u - \theta_u) + c_b \int^{m_b} (T_b - \theta_b)dm_b \quad [1]$$

Conservation of mass

$$M = m_u + m_b \quad [2]$$

Condition for constant volume

$$\frac{MR_uT_i}{P_i} = \frac{m_uR_uT_u}{P} + \frac{R_b}{P}\int_0^{m_b} T_b dm_b \quad [3]$$

Here the subscripts u and b refer to unburned and burned gases, respectively. Constant-volume heat capacities are denoted by c, the gas constant (mass basis) by R, absolute temperature by T, and pressure by P. Subscript i refers to conditions prior to combustion. The datum temperatures for internal energy are denoted by θ. According to the energy equation we have assumed that the unburned gas is uniformly compressed, and have anticipated a temperature gradient in the burned gas; accordingly, the internal energy of the burned mass m_b, is represented by the integral.

Since the magnitude of the total internal energy in the bomb

[1] Dean, College of Technology, University of Maine. Jun. ASME.

[2] "Explosions of Coal Gas and Air," by B. Hopkinson, Proceedings of the Royal Society of London, series A, vol. 77, 1906, p. 387.

[3] Flamm and Mache, Wien, Berlin, Germany, vol. 126, 1917, p. 9.

[4] "Determination of the Speed of Flames and the Temperature Distribution in a Spherical Bomb From Time-Pressure Records," by B. Lewis and G. von Elbe, *Journal of Chemical Physics*, vol. 2, 1934, p. 283.

[5] "Thermodynamic Charts for Combustion Processes," Part 1, by H. C. Hottel, and others, John Wiley & Sons, Inc., New York, N. Y., 1949.

Contributed by the Applied Mechanics Division and presented at the Annual Meeting, Atlantic City, N. J., November 25–30, 1950, of The American Society of Mechanical Engineers.

Discussion of this paper should be addressed to the Secretary, ASME, 29 West 39th Street, New York, N. Y., and will be accepted until April 10, 1952, for publication at a later date. Discussion received after the closing date will be returned.

Note: Statements and opinions advanced in papers are to be understood as individual expressions of their authors and not those of the Society. Manuscript received by ASME Applied Mechanics Division, December 13, 1950. Paper No. 51—A-15.

is quite arbitrary, either θ_u or θ_b may be assigned arbitrarily. It is clearly advantageous to make the selection

$$\theta_u = T_i$$

This fixes the value of θ_b, to be determined later. If we denote by n the mass fraction of gas in the burned state

$$n = \frac{m_b}{M}$$

then the progress of the combustion process may be designated by stating the value of $0 \leqq n \leqq 1$. Lastly, we denote by

$$\alpha = \frac{c_u}{c_b}$$

the ratio of the constant volume heat capacities. Hence dividing Equation [1] by Mc_b, and Equation [3] by M, and noting that θ_b is a constant, we have

$$\alpha(1 - n)(T_u - T_i) + \int_0^n T_\theta dn = n\theta_b \quad \ldots\ldots [4]$$

and

$$\frac{P}{P_i} T_i = (1 - n)T_u + \int_0^n T_\theta dn \quad \ldots\ldots [5]$$

Here we have neglected any difference in value between R_u and R_b, an assumption justified when air is used as the oxidizer and the mole change due to combustion is small.

Eliminating the integral between Equations [4] and [5]

$$\alpha(1 - n)(T_u - T_i) + \frac{P}{P_i} T_i - (1 - n)T_u = n\theta_b \quad \ldots [6]$$

Now when $n = 1$ the combustion is completed and $P = P_e$. Hence from Equation [6]

$$\theta_b = \pi T_i, \quad \pi = \frac{P_e}{P_i}$$

where π is the combustion pressure ratio. This value for θ_b is physically obvious, in view of the choice for θ_u; since from Equation [4] for $n = 1$

$$\theta_b = \int_0^1 T_\theta dn$$

Clearly θ_b is the uniform temperature which the burned gases would attain following the completion of combustion.

Since there is to be no heat transfer in the gases, we may assume that compressions are isentropic, hence

$$\frac{T_u}{T_i} = \left(\frac{P}{P_i}\right)^{\sigma_u}, \quad \sigma_u = \frac{\gamma_u - 1}{\gamma_u}, \quad \gamma = \frac{c_p}{c_v}$$

Inserting this expression for the temperature ratio, and the value for θ_b, Equation [6] reduces to a relation between the mass fraction burned and the instantaneous pressure P

$$n = \frac{\alpha - \frac{P}{P_i} + (1 - \alpha)\left(\frac{P}{P_i}\right)^{\sigma_u}}{\alpha - \frac{P_e}{P_i} + (1 - \alpha)\left(\frac{P}{P_i}\right)^{\sigma_u}} \quad \ldots\ldots [7]$$

In this equation n is not particularly sensitive to changes in the value of α, and the simpler equation

$$n = \frac{P - P_i}{P_e - P} \quad \ldots\ldots [8]$$

is correct to within 3 per cent for practical purposes. Thus the mass fraction burned is equal to the fractional rise in pressure.

It is interesting to compute the volume fraction occupied by the burned gas

$$q = \frac{V_b}{V}$$

$$= 1 - \frac{1 - n}{[n(\pi - 1) + 1]^{1 - \sigma_u}} \quad \ldots\ldots [9]$$

Fig. 1 shows a plot of q versus n for a moderate pressure ratio ($\pi = 5$) and a diatomic unburned gas ($\sigma_u = 0.29$). Note that when 50 per cent of the gas is burned it occupies 77 per cent of the total volume. Equation [9] has value for photographic studies of constant-volume combustion.

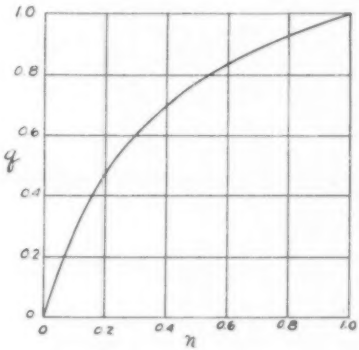

FIG. 1
(Equations [9] $\pi = 5$, $\sigma_u = 029$.)

To compute the temperature distribution at any point in the combustion process it is necessary to evaluate the temperature increase due to combustion. Referring to Fig. 2(*a*), assume the area to the left of the plane flame front is the burned gas. The flame front advances from left to right. In the next instant a small mass of gas, Δm_b, burns and attains the temperature T_b^*, as shown in Fig. 2(*b*). The pressure thus increases from P to $P + \Delta P$, and all temperatures are accordingly increased by the factor λ

$$\lambda_b = \left(\frac{P + \Delta P}{P}\right)^{\sigma_b}$$

$$\lambda_u = \left(\frac{P + \Delta P}{P}\right)^{\sigma_u}$$

Writing the energy equation between these two states

$$c_b \int_0^{m_b} (T_b - \theta_b)dm_b + m_u c_u (T_u - \theta_u)$$

$$= c_b \int_0^{m_b} (\lambda_i T_b - \theta_b)dm_b + \Delta m_b c_b (T_b^* - \theta_b) + (m_u - \Delta m_b)c_u(\lambda_u T_u - \theta_u$$

Using the values for θ_u and θ_b just found, and dividing by $Mc_b(1 - \lambda_u)$ we have

$$\frac{1-\lambda_b}{1-\lambda_u}\int_0^n T_b dn + \alpha(1-n)T_u =$$

$$\frac{\Delta n}{1-\lambda_u}\{T_b^* - \pi T_i - \alpha(\lambda_u T_u - T_i)\} \quad [10]$$

Approximately

$$\frac{1-\lambda_b}{1-\lambda_u} \approx \frac{\sigma_b}{\sigma_u} \approx \alpha$$

for small ΔP; and

$$\frac{\Delta n}{1-\lambda_u} \approx -\frac{\Delta n}{\sigma_u \dfrac{\Delta P}{P}}$$

But from Equation [8]

$$\frac{\Delta n}{\Delta P} = \frac{1}{P_i(\pi-1)}$$

so that

$$\frac{\Delta n}{1-\lambda_u} = -\frac{P/P_i}{\sigma_u(\pi-1)}$$

Substituting in Equation [10], dividing by α, and letting $\Delta m_b \to 0$

$$\int_0^n T_b dn + (1-n)T_u =$$

$$-\frac{P/P_i}{\alpha\sigma_u(\pi-1)}\{T_b^* - \pi T_i - \alpha(T_u - T_i)\}$$

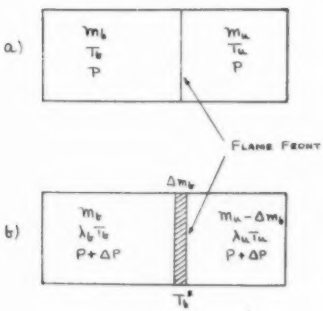

Fig. 2

Substituting for the left-hand side from Equation [5], and noting again that the compression is isentropic, we have as the expression for ΔT_c, the temperature rise due to combustion

$$\Delta T_c = T_b^* - T_u$$
$$= \{\varphi - (1-\alpha)[n(\pi-1)+1]^{\sigma_u}\}T_i \quad [11]$$

where

$$\varphi = \pi - \alpha - \alpha\sigma_u(\pi-1)$$

Consequently the temperature rise varies during the combustion process. The following table shows the trend, a decrease in ΔT_c as n increases:

Equation [11]

$\pi = 5$, $\sigma_u = 0.29$, $\alpha = 0.6$, $T_i = 1000$ R

n	ΔT_c deg R
0	3930
0.2	3860
0.4	3810
0.6	3770
0.8	3730
1.0	3700

The decrease of ΔT_c is to be expected, since, during the latter stages of the process, there is a preponderance of burned gas, which has the higher heat capacity and therefore requires more energy for its compression.

For the special circumstance of $\alpha = 1$, Equation [11] reduces to

$$\Delta T_c = \frac{\pi-1}{\gamma} T_i \quad [12]$$

as one would expect.

To compute the temperature gradient one must designate the particular piece of gas whose temperature is sought, as well as the progress of combustion. Imagine that before combustion begins the unburned gas is divided into infinitesimal layers containing equal masses, and so chosen that at any instant during combustion the flame front occupies one layer. In the case of a spherical bomb with central ignition, for example, we subdivide the unburned gas into infinitesimal spherical shells. Now label each layer with an x-value, so that $x = 0$ at the center of the bomb, and $x = 1$ at the wall. Thus the value of x denotes the particular piece of gas under examination, while the value of n denotes the stage of the combustion process. Thus the temperature of the burned gas is denoted by $T_b(x, n)$, for $x < n$. Clearly, for $x > n$ the gas particle is in the unburned state.

Initially the gas is at T_i. As combustion proceeds the temperature increases due to isentropic compression, and the flame front advances toward the gas particle under consideration. Clearly, the particle burns when $x = n$, at which point the pressure is P_x. From Equation [8]

$$P_x = [x(\pi-1)+1]P_i$$

Thus the temperature of each particle of unburned gas at the instant before combustion is

$$T_i\left(\frac{P_x}{P_i}\right)^{\sigma_u}$$

As the flame front passes through the particle, the temperature jumps by the amount ΔT_c, given by Equation [11] with $n = x$. The particle is now in the burned state, and its temperature continues to increase as combustion increases. If the pressure is P, then the burned gas has been compressed from P_x to P, hence its temperature is

$$\left[T_i\left(\frac{P_x}{P_i}\right)^{\sigma_u} + \Delta T_c\right]\left(\frac{P}{P_x}\right)^{\sigma_b}$$

but

$$\frac{P}{P_x} = \frac{P}{P_i}\frac{P_i}{P_x}$$

Substituting for the pressure ratios we have

$$T_b(x,n) = \{\varphi + \alpha[x(\pi-1)+1]^{\sigma_u}\}\left\{\frac{n(\pi-1)+1}{x(\pi-1)+1}\right\}^{\sigma_b} T_i \quad [13]$$

The temperature difference between the first piece to burn ($x = 0$) and the last piece to burn ($x = 1$), is a maximum when the burning is complete ($n = 1$) and amounts to

$$T_b(0, 1) - T_b(1, 1) = [\varphi(\pi^{\sigma_b} - 1) + \alpha(\pi^{\sigma_b} - \pi^{\sigma_u})]T_i$$

For example, if $\pi = 5$, $\sigma_u = 0.29$, $\sigma_b = 0.20$, $\alpha = 0.61$, then $\varphi = 4.32$ and

$$T_b(0, 1) - T_b(1, 1) = 2.40T_i$$

Consequently, if the initial temperature is 537 R, the temperature difference between the first and last pieces to burn is about 1300 F. In actual explosion this figure would be considerably reduced by heat conduction and mixing.

Time Required for Combustion

In deducing the foregoing results, we have neglected any kinetic effects, so that in effect we have supposed that the flame front moved with an infinitesimal velocity. For the purpose of estimating the time required for combustion we shall use some of the results obtained. Needless to say, the estimate so obtained is necessarily very crude, for we now suppose the flame moves with finite velocity, and in some actual explosions the velocity is quite large.

If A_x is the area of the flame surface at any time, and V_b is the volume of the burned gas, then S_x, the velocity of the flame surface (relative to the bomb wall) is

$$S_x = \frac{1}{A_x}\frac{dV_b}{dt}$$

From Equation [3]

$$V_b = \frac{Rm_uT_i}{P_i} - \frac{mR_uT_u}{P}$$

Thus

$$S_x = -\frac{MR_u}{A_x}\frac{d}{dt}\left[\frac{(1-n)T_u}{P}\right]$$

Using Equation [8], and noting that for isentropic compression

$$\left(\frac{\partial T_u}{\partial P}\right) = \frac{R_uT_u}{P(c_p)_u}$$

$$S_x = \frac{MR_uT_u}{PA_x}\left[\frac{1-n}{\gamma_u} + \frac{P}{P_i(\pi-1)}\right]\frac{d}{dt}(\ln P) \quad \ldots [14]$$

It is convenient to leave the result in this form, although it is clear that the result may be stated as a function of n or P alone.

Consider now the velocity of an arbitrary particle of burned gas, $S_b(x, n)$. This particle has a certain x-value attached to it. If we denote by A_x the area formed by a surface passing through all particles with the same x-value, then

$$S_b(x, n) = \frac{1}{A_x}\frac{d}{dt}V_b(x, n)$$

where $V_b(x, n)$ is the volume contained within A_x. Clearly

$$V_b(x, n) = \frac{R_b}{P}\int_0^{xM} T_b(x, n)dm_b$$

hence

$$S_b(x, n) = \frac{MR_b}{A_x}\frac{d}{dt}\left[\frac{1}{P}\int_0^x T_b dn\right]$$

Since x has a fixed value

$$S_b(x, n) = \frac{MR_b}{A_x}\left[\int_0^x \left(\frac{\partial T_b}{\partial P}\right)dn - \frac{1}{P}\int_0^x T_b dn\right]\frac{d}{dt}(\ln P)$$

which reduces to

$$S_b(x, n) = -\frac{MR_b}{PA_x\gamma_b}\frac{d}{dt}(\ln P)\int_0^x T_b dn$$

We are particularly interested in the velocity of the burned gas at the flame front, which we denote by S_b^*. This is obtained by setting $x = n$, giving

$$S_b^* = S_b(n, n) = -\frac{MR_b}{PA_x\gamma_b}\frac{d}{dt}(\ln P)\int_0^n T_b dn$$

Substituting for the integral from Equation [5]

$$S_b^* = -\frac{MR_bT_u}{PA_x\gamma_b}\left[\frac{P}{P_i}\left(\frac{T_i}{T_u}\right) - (1-n)\right]\frac{d}{dt}(\ln P) \quad [15]$$

where A_x is again the area of the flame surface.

Denoting the velocities at the flame front as shown in Fig. 3, we imagine the flame front moving from left to right with velocity S_x. Because of this movement the unburned gas is undergoing

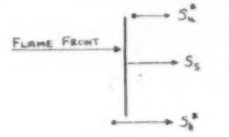

Fig. 3

compression, resulting in motion to the right, with an unburned gas velocity S_u^* at the flame front. Similarly, the burned gas has the velocity S_b^* at the flame front. If the density is denoted by ρ, and we write conservation of matter at the flame front, then

$$\rho_u(S_x - S_u^*) = \rho_b^*(S_x - S_b^*)$$

Solving for S_u^*

$$S_u^* = \left(1 - \frac{\rho_b^*}{\rho_u}\right)S_x + \frac{\rho_b^*}{\rho_u}S_b^*$$

If we make use of the simple expression for the temperature rise due to combustion, Equation [12], thus assuming $\alpha = 1$, so that $\gamma_u = \gamma_b = \gamma$, $R_u = R_b = R$, then since $\rho_b^*/\rho_u = T_u/T_b^*$

$$S_u^* = \left(\frac{MRT_u}{PA_x}\right)\left(\frac{1-n}{\gamma}\right)\frac{d}{dt}(\ln P) \quad \ldots [16]$$

Provided the time rate of change of pressure is finite at the instant combustion is completed, Equation [16] gives $S_u^* = 0$, for $n = 1$. Thus the assumptions we have made give a physically acceptable result.

The normal burning velocity S_i is defined as the rate at which the flame front advances relative to the unburned gas. For a given fuel and oxidizer mixture, S_i is a physical property of the mixture, and is a function of atomic composition, pressure, and temperature. Its variation with the latter has not been investigated extensively. From Equations [14] and [16] we obtain

$$S_i = S_x - S_u^* = \frac{MRT_u}{P_iA_x}\frac{1}{\pi - 1}\frac{d}{dt}(\ln P)$$

Upon making the right-hand side a function of n only we have

$$S_t = \frac{MRT_i}{P_i A_s}\,[n(\pi - 1) + 1]^{\sigma_u - 1}\,\frac{dn}{dt} \quad \ldots\ldots [17]$$

If one is willing to assume S_t is constant, or better, that we may assign a mean value to S_t, then Equation [17] may be integrated to give a relation between the time t, measured from the start of combustion, and n, the mass fraction burned. It is interesting to observe how the vessel shape and location of the ignition spark can affect the results. If the bomb is a long tube of length L, and constant cross-sectional area, then the flame surface is effectively a plane of constant area. From Equation [17]

$$\frac{S_t}{L} = [n(\pi - 1) + 1]^{\sigma_u - 1}\,\frac{dn}{dt}$$

or

$$\left(\frac{S_t}{L}\right) t = \frac{[n(\pi - 1) + 1]^{\sigma_u} - 1}{\sigma_u\,(\pi - 1)} \text{ (Long tubes)}$$

The time τ required for combustion is then

$$\tau = \frac{(\pi)^{\sigma_u} - 1}{\sigma_u(\pi - 1)}\left(\frac{L}{S_t}\right)$$

Clearly L/S_t is the time for the completion of combustion for a tube with one end open, with combustion started at that end, for under these conditions, combustion would have proceeded at constant pressure without compression of the unburned charge.

For a spherical bomb of radius R_0 and central ignition, the volume fraction occupied by the burned gas is

$$q = \left(\frac{r_s}{R_0}\right)^3$$

where r_s is the radius of the flame surface. Thus in Equation [17]

$$\frac{S_t}{R_0} = \frac{1}{3}\left[\frac{1}{(q)^{2/3}\,[n(\pi - 1) + 1]^{1 - \sigma_u}}\right]\frac{dn}{dt} \text{ (Sphere central ignition)}$$

where q being a function of n is given by Equation [9].

For a spherical bomb of radius R_0 and surface ignition (i.e., ignition simultaneously initiated at all points on the surface, perhaps by suddenly increasing the wall temperature)

$$q = 1 - \left(\frac{r_s}{R_0}\right)^3$$

and therefore

$$\frac{S_t}{R_0} = \frac{1}{3}\left[\frac{1}{(1 - q)^{2/3}\,[n(\pi - 1) + 1]^{1 - \sigma_u}}\right]\frac{dn}{dt}$$

(Sphere surface ignition)

Neither case for the sphere is integrable. By numerical integration, assuming S_t constant, one may compare the times required for combustion for surface and central ignition, τ_s and τ_c, respectively. For the particular condition $\pi = 8$, $\sigma_u = 0.29$ one finds

$$\frac{\tau_s}{\tau_c} = 1.98$$

In view of the form of the integrals one can expect that the ratio of the two times is not greatly affected by the value of π.

For the case of the sphere with central ignition, an approximate integrand may be written

$$\frac{S_t}{R_0} \approx \frac{1}{3(\pi)^{1 - \sigma_u}\,(n)^{2/3}}\,\frac{dn}{dt}$$

which integrates to give

$$\left(\frac{S_t}{R_0}\right) t \approx \frac{(n)^{1/3}}{(\pi)^{1 - \sigma_u}} \text{ (Sphere central ignition)}$$

so that the mass fraction burned is proportional to the cube of the elapsed time since the onset of combustion.

Measurement of Recovery Factors and Friction Coefficients for Supersonic Flow of Air in a Tube

1—Apparatus, Data, and Results Based on a Simple One-Dimensional Flow Model

By J. KAYE,[1] J. H. KEENAN,[2] K. K. KLINGENSMITH,[3] G. M. KETCHUM,[4] AND T. Y. TOONG[5]

For the past few years a program has been under way to obtain reliable data on the rate of heat transfer to air moving at supersonic speeds. The investigation was limited to air flowing at supersonic speeds in a round tube. The program was divided into two separate parts, the first for measurement of the adiabatic wall temperatures of a supersonic stream and the second for the heat-transfer rate. The first part of this program is described here. The details of three experimental test combinations used to measure the adiabatic wall temperature and local state of a supersonic stream of air are presented. The experimental data for forty runs, in the form of measured pressure and temperature distributions, are included. The range of diameter Reynolds number covered is from 0.15×10^6 to 5×10^6. The length Reynolds number extends to 120×10^6. The Mach number at the inlet to the round tube is about 2.6. The calculated quantities such as the local apparent friction coefficient, recovery factor, local Mach number, and so forth, are obtained from the simple one-dimensional flow model for which the properties of the stream are uniform at any cross section of the tube and boundary-layer effects are ignored. A subsequent paper deals with the calculation of these quantities when account is taken of the boundary-layer growth in the tube on the basis of a two-dimensional flow model.

Nomenclature

The following nomenclature is used in the paper:

A = cross-sectional area
c_p = specific heat at constant pressure
c_v = specific heat at constant volume
c_w = discharge coefficient of nozzle
D = inside diameter of pipe
f = local apparent coefficient of friction, $2g\tau/\rho V^2$
$\bar{f}$ = mean apparent coefficient of friction
G = flow per unit area, w/A
g = acceleration given to unit mass by unit force
k = ratio of specific heats, c_p/c_v
L = distance from end of curved contour of nozzle
L_{max} = maximum length of duct for steady adiabatic constant-area flow with friction
M = Mach number, $V/\sqrt{gkRT}$
Pr = Prandtl number, $c_\mu g/\lambda$
p = static pressure
R = perfect-gas constant
r = recovery factor, $(t_{aw} - t_m)/(t_{oi} - t_m)$
s = entropy per unit mass
Re_D = diameter Reynolds number, $DG/\mu g$
Re_L = length Reynolds number, $LG/\mu g$
T = temperature, deg F abs
t = temperature, deg F
V = velocity
w = mass rate of flow
ρ = density
λ = thermal conductivity
μ = viscosity
τ = shear stress at wall
ψ = $4fL_{max}/D$

Superscript * refers to throat of supersonic nozzle where $\mathsf{M} = 1$
Subscripts:

oi = upstream stagnation conditions
of = downstream stagnation conditions
aw = adiabatic wall conditions
m = mean stream conditions
j = station numbers
r = atmospheric conditions
s = isentropic conditions
v = vacuum in test combination B

Introduction

A research program, sponsored by the Office of Naval Research, has been under way for several years with the objective of obtaining reliable data on the rate of heat transfer to air moving at supersonic speeds in a round tube. This program consists of two separate parts. In the first part a well-insulated apparatus was used to measure the values of the local adiabatic wall temperature and local static pressure of a supersonic stream of air in a

[1] Associate Professor of Mechanical Engineering, Massachusetts Institute of Technology, Cambridge, Mass. Jun. ASME.
[2] Professor of Mechanical Engineering, Massachusetts Institute of Technology. Fellow ASME.
[3] United Aircraft Corporation, East Hartford, Conn. Jun. ASME.
[4] General Electric Company, Schenectady, N. Y. Jun. ASME.
[5] Research Assistant in Mechanical Engineering, Massachusetts Institute of Technology.

Contributed by the Applied Mechanics Division and presented at the Annual Meeting, Atlantic City, N. J., November 25-30, 1951, of The American Society of Mechanical Engineers.
Discussion of this paper should be addressed to the Secretary, ASME, 29 West 39th Street, New York, N. Y., and will be accepted until April 10, 1952, for publication at a later date. Discussion received after the closing date will be returned.
Note: Statements and opinions advanced in papers are to be understood as individual expressions of their authors and not those of the Society. Manuscript received by ASME Applied Mechanics Division, May 25, 1951. Paper No. 51—A-29(a).

round tube. In the second part an apparatus using steam condensing outside a round brass tube was employed to measure the local coefficients of heat transfer to a similar supersonic stream of air from the same nozzle.

It was recognized that the reliability of the preliminary results obtained in this program (1)[6] could be questioned because of the presence of possible systematic errors. Since work of a similar nature was not available for comparison, it was decided to try to eliminate any systematic errors by the construction, (*a*) of a new adiabatic apparatus of different design, and (*b*) of a new heat exchanger of different design. The design, construction, and testing of this new adiabatic apparatus have been completed.

A critical intercomparison was made of the measurements of local recovery factors and local apparent friction coefficients obtained from these different combinations of adiabatic apparatus (2). The results of this study disclosed no significant systematic errors. Hence it was concluded that the measurements made with the different combinations of adiabatic apparatus were reliable and worthy of publication.

Method of Testing

Objective. The work described here is limited to the adiabatic flow of air at supersonic speeds in a round tube. The objective is to measure accurately the local adiabatic wall temperatures and the local static pressures of this supersonic stream of air. From these measurements and some auxiliary data, the local recovery factors and local apparent coefficients of friction can be calculated on the basis of a particular type of flow model. The simple and useful one-dimensional flow model, selected for the calculations given in this report, is based on the assumption of uniform properties at each cross section of the tube. The analysis of these same measurements by means of other flow models, including a fairly simple two-dimensional flow model, will be given in a future publication.

General Description of Air Flow. Air leaving a compressor is cleaned and dried thoroughly. The air is brought to some desired stagnation temperature by means of heat exchangers and then flows through a stagnation tank into a supersonic nozzle and through the adiabatic test section. The air then passes through a second stagnation tank and finally into the discharge line. An ejector is used on the discharge line to maintain the necessary large pressure ratios across the supersonic nozzle and adiabatic test section.

Preparation of the Air Stream. Two independent sources of dry air have been used. The first source is based on the drying method shown schematically in Fig. 1. Air originally at 180 psia passes through an ice bath, or precooler, and a filter to remove the the major portion of the oil and water vapor in the air. The air is then cooled down to about —60 F in a dehumidifier or regenerator where the remaining condensable constituents are removed as a solid phase on the walls. This dehumidifier has been described previously (1). The specific humidity of the air entering the test section is about 1.5×10^{-6} lb of water vapor per lb of air.

The second source of dry air is available from an air-liquefaction apparatus operated under the direction of Prof. S. C. Collins. In this apparatus the incoming high-pressure air is cleaned and cooled in a regenerator to a temperature of about —280 F by means of liquid air. This dry air with a specific humidity of less than 10^{-13} lb of water vapor per lb of dry air, is by-passed around the liquefaction apparatus for use in the supersonic-flow experiments. In Fig. 1 this air, labeled as dry air at 150 psi, is led directly to the constant-temperature water bath.

The two independent sources of dry air serve as a means of eliminating possible systematic errors due to the condensation of water vapor in the supersonic stream of air. In several instances, measurements of friction coefficients and recovery factors made under identical conditions indicated no systematic deviations which could be attributed to the source of dry air.

Experimental Apparatus

Several combinations of apparatus have been used during the past few years for this investigation. The first adiabatic test section yielded much experience on which later designs were

[6] Numbers in parentheses refer to the Bibliography at the end of the paper.

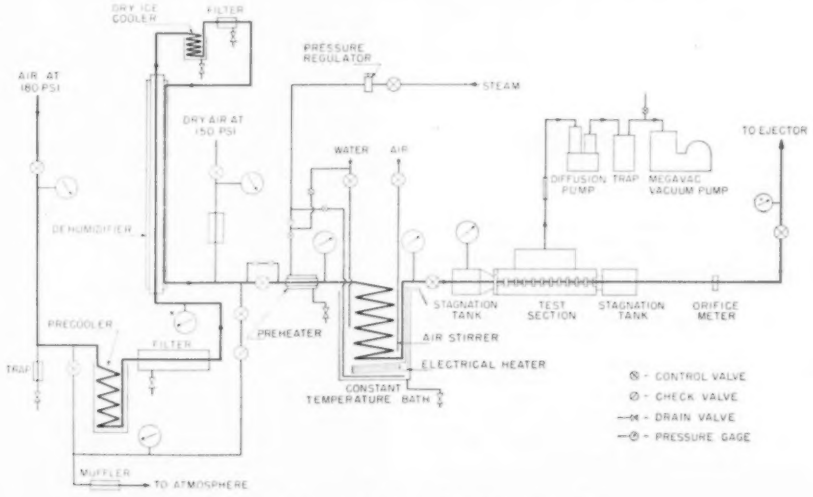

Fig. 1 Schematic Layout of Test Combination B

based. A detailed description of all the modifications, however, would require too much space. Hence the details will be given only of the latest adiabatic apparatus, and the previous modifications will be described briefly.

The three combinations of test apparatus used since the start of this program will be described by the following code:

TEST COMBINATIONS

Symbol	Nozzle	Test section	Insulation
A-1	Brass	Textolite	14-In. rock wool
A-2	Brass	Lucite	14-In. rock wool
B	Stainless steel	Lucite	High vacuum

The first test combination to be operated successfully as an adiabatic test section was A-1. In combination A-2, a lucite test section replaced the textolite section of A-1, with hardly any other changes. The latest test combination, B, represented major design changes in the use of a new type of supersonic nozzle and in a different means of insulating the lucite test section.

In all three test combinations the stream of dried air is brought to a desired stagnation temperature by passing through two heaters. The first air heater, shown in Fig. 1, is a shell-and-tube heat exchanger in which the air is heated to within 5 F of the desired temperature by means of a stream of hot water. The second air heater is a long copper coil placed in a large water bath which is maintained at a constant temperature within ±0.2 F by means of an electric heater and thermostatic control system.

The stagnation temperature and pressure of the air stream are measured in the upstream stagnation tank which is just downstream of the constant-temperature bath. This tank is constructed from a 3-in-diam pipe. The air is slowed down to a uniform low velocity by means of baffles and fine-mesh wire screening. Nine thermocouples, suspended on a cross of nylon thread fastened to the inner walls of the stagnation tank, are used to measure the temperature distribution and the mean temperature of the air stream. Although in all measurements the stagnation tank walls are carefully insulated, the nine thermocouples are shielded individually against net radiant-heat interchange with the tank walls. In tests made for systematic errors, this outer insulation was removed from the tank walls and a layer of dry ice was substituted. No effect on the readings of these shielded thermocouples could be detected.

In all the runs presented here the maximum variation in temperature over the cross section of the upstream stagnation tank was less than 1 F and the average deviation from the mean was about 0.3 F.

Test Section. The older adiabatic test section, represented by test combinations A-1 and A-2, consisted of an axially symmetrical brass nozzle followed by a straight section of a round tube made from a material of low thermal conductivity. The radial heat transfer to the round tube was reduced by covering it with a layer of rock wool 14 in. thick. The supersonic nozzle and test section are shown in reference (1). A critical examination of the results obtained with this older adiabatic apparatus indicated the following possible sources of systematic errors:

1 Radial heat flow over most of the test section.
2 Longitudinal heat flow at both ends of the test section.
3 Longitudinal heat flow along the tubes used to measure the pressure distribution.
4 A fairly thick boundary layer at the exit of the long brass nozzle used to produce the supersonic stream of air.
5 A velocity distribution peculiar to this nozzle.
6 The thermocouples, their calibration, and their location in the bosses cut in the tubes of textolite and lucite.

In order to eliminate effectively most of these possible sources of systematic errors, test combination B, a completely new adiabatic test section, was designed and constructed.

New Supersonic Nozzle. The profile of the convergent-divergent brass nozzle used in the older apparatus was designed by a method described by Shapiro (3). Although a nozzle with this profile had been used previously as a satisfactory means of obtaining shock-free expansion, it was recognized that the length of its divergent section could be reduced considerably by designs based on the method of characteristics in supersonic flow.

A new supersonic nozzle was designed with the objective of keeping the length of its divergent section to a minimum. Actually, two designs were carried out, one based on the analytical method described by Foelsch (4), and the other based on the semigraphical method of Sauer (5). In both methods a cone-shaped divergent section is connected to a short cylindrical section by a curved contour. The equation of this contour was obtained by Foelsch by linearization of the characteristic equations for supersonic axially symmetric flow, whereas the contour was obtained by Sauer by a graphical solution of the same equations. The final designs showed that the Foelsch nozzle was only about 0.12 in. longer than the Sauer nozzle. To be on the safe side with respect to producing a shock-free supersonic flow, the slightly longer Foelsch nozzle was chosen. The details of the new supersonic nozzle, including the x-y co-ordinates of the exit contour, are shown in Fig. 2. This stainless-steel nozzle is provided also with two small holes for insertion of thermocouples.

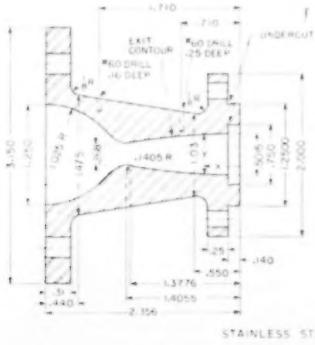

X-Y COORDINATES OF EXIT CONTOUR

x	y	x	y
.140	.5015	.800	.4390
.200	.4979	.860	.4289
.260	.4938	.920	.4180
.320	.4895	.980	.4056
.380	.4848	1.040	.3924
.440	.4799	1.100	.3766
.500	.4745	1.160	.3582
.560	.4686	1.220	.3370
.620	.4622	1.280	.3130
.680	.4554	1.340	.2886
.740	.4477	1.376	.2736

STAINLESS STEEL NOZZLE

Fig. 2

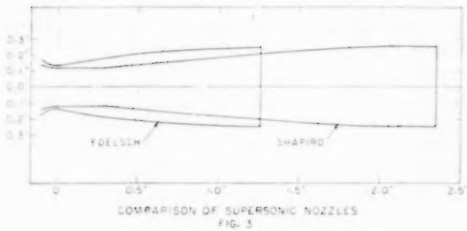

FIG. 3

The comparison of the brass nozzle based on the Shapiro design with the steel nozzle based on the Foelsch design, given in Fig. 3 in a scale drawing, shows the large reduction in the length of the divergent section achieved by the latter design.

The new steel nozzle with its short divergent contour, in comparison with the longer one of the previous brass nozzle, provides a different velocity profile as well as a different boundary-layer thickness at nozzle exit.

The longitudinal heat transfer from the nozzle to the lucite test section is considerably reduced by the new stainless-steel nozzle since the thermal conductivity of stainless steel is considerably less than that of brass.

New Test Section. A new lucite test section was designed and constructed to eliminate, in so far as possible, the remaining sources of systematic error. An assembly drawing of the new test section and the details of the lucite tube are given in Fig. 4. The reducer, end plate, and steel nozzle are shown in Fig. 5. The partially assembled test section is shown in Fig. 6.

On the extreme left in Figs. 4, 5, and 6, a well-rounded bell-mouth reducer, constructed from thick-walled textolite, directs the air from the upstream stagnation tank to the stainless-steel nozzle. The nozzle is connected to the lucite collar and then to the lucite test section. The pressure taps connected to the bosses on the lucite test section are arranged in angular sequence about the axis of the tube. The lucite test section is joined downstream to a lucite end plate which is opposite a similar plate upstream connected to the steel nozzle by a flange. A textolite casing is mounted between these two lucite end plates; it is arranged so that the entire annulus between this casing and the lucite test section can be highly evacuated during a test run. The tubes used to measure the pressure and the many thermocouple wires

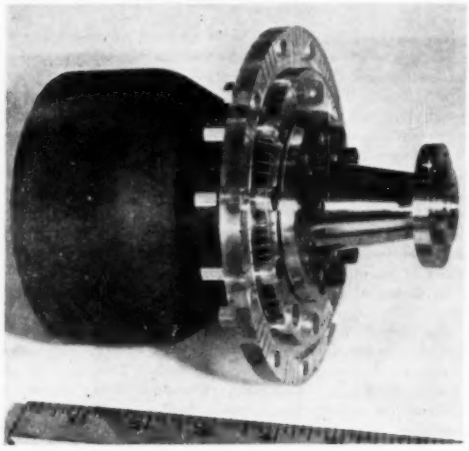

FIG. 5 REDUCER, END PLATE, AND STEEL NOZZLE

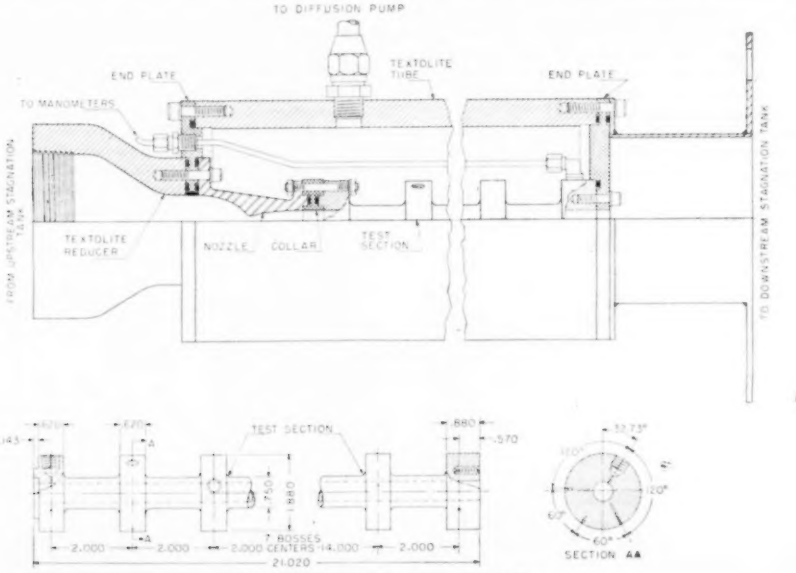

FIG. 4 DETAILS OF TEST COMBINATION B

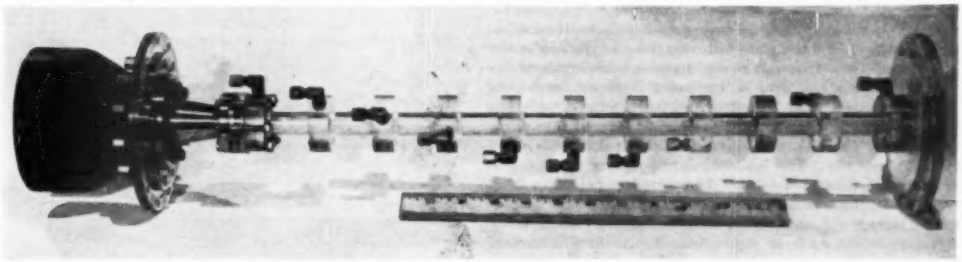

FIG. 6 STAINLESS-STEEL NOZZLE WITH LUCITE TEST SECTION

are led out of this evacuated space through the upstream end plate. The many fine slots machined in the upstream end plate shown in Fig. 5 are used to hold the individual thermocouple wires in place for making vacuum seals.

The temperature distribution in the bosses of the lucite tube is obtained by insertion of thermocouples in wells sunk in the bosses to different depths at different locations. The details of these thermocouple wells in the bosses are shown in Fig. 4. One of the wells is provided with a single-junction thermocouple for measurement of the temperature at a known distance from the inside wall of the lucite tube, whereas the two other wells are fitted with a differential thermocouple to measure the radial temperature difference in the bosses. In addition to using a new set of differential thermocouples in the bosses of the new lucite tube, a group of thermocouples is cemented to the outside wall of the lucite tube between the bosses. In the measurements which were made with test combination B, excellent agreement was obtained between the readings of the thermocouples in the bosses and the adjacent thermocouples on the outside of the test section. Thermocouples are also inserted in the wells of the steel nozzle to discover the magnitude of the temperature gradient in this nozzle.

After assembly of pressure lines and thermocouples, several layers of aluminum foil were wrapped around these lines and around the lucite test section to reduce radiation effects to a minimum. After assembly of the textolite casing it was painted to seal all minute holes, and the pressure in the evacuated space was reduced to the order of 2 to 15 microns of mercury. It was necessary to install vacuum pumps and other auxiliary equipment to maintain these low pressures.

The main reasons for using the evacuated space between the lucite tube and the textolite casing are to reduce radial heat transfer through the lucite tube to a minimum and to reduce the thermal capacity of the "insulating device" to a small value. In the previous test combinations A-1 and A-2, the large thermal capacity of the 14-in. thickness of rock wool used for insulation could have introduced transient effects in the measurements. Longitudinal heat flow is also reduced by use of the stainless-steel nozzle, which was placed in this evacuated space, and by use of a low-conductivity material—textolite—for the reducer just upstream of this nozzle.

After assembly of test combination B, many tests were made to check the new design features of this apparatus. The pressure in the evacuated space was varied considerably to check the heat flow to the lucite tube with and without air flow in the tube. The outside of the textolite casing was covered with dry ice and the transient effects on the thermocouples in the lucite tube were investigated. The insulation covering the upstream stagnation tank and the pipe leading to the textolite reducer was removed, the surfaces were covered with dry ice, and the transient effects were studied. These tests and others indicated that all undesirable heat flows—by conduction, radiation, and convection—were minimized by the new design with the possible exception of some longitudinal conduction to the first and last stations in the lucite tube.

TEST RESULTS

The adiabatic flow measurements obtained with test combinations A-1, A-2, and B are presented in Appendix A. In addition, the calculated results based on a simple one-dimensional flow model are given in Appendix A. The analysis, method of calculation, and a sample calculation are given in Appendix B.

The number of runs made with each test combination and the range of Reynolds numbers are given in the following summary:

SUMMARY OF TESTS

Test combination	No. of runs	Minimum $Re_D \times 10^{-6}$	Maximum $Re_D \times 10^{-6}$	Maximum $Re_L \times 10^{-3}$
A-1	12	0.76	4.7	107
A-2	10	0.50	4.6	117
B	18	0.15	4.8	105

The diameter Reynolds number is based on the tube diameter and on the mean stream properties at the first station, whereas the length Reynolds number is based on the distance from the end of the curved contour of each nozzle and on the mean stream properties at that distance.

The representation of all the data given in Appendix A on two or three charts is a difficult task. If, for example, all the recovery factors were plotted on a single chart, there would be considerable difficulty in interpretation of the results in terms of the phenomena occurring in the compressible flow of air in the tube. It has been found that a better grasp and analysis of these phenomena can be obtained by examining the test results for selected values of the diameter Reynolds number. This selection has been made to permit comparison of the test results based on the simple one-dimensional flow model with the well-known behavior of boundary-layer development on a flat plate with zero pressure gradient in the direction of flow.

Six values of the diameter Reynolds number have been selected to cover the range from laminar flow to turbulent flow in the boundary layer of the tube. For each of these six values of the Reynolds number a separate chart has been prepared showing the measured values of the modified pressure ratio and of the temperature ratio as well as the calculated values of the local recovery factor and local apparent coefficient of friction. On some of these charts it has been found to be impractical to give all the results pertaining to a given diameter Reynolds number at the first station; in these cases the values given represent, in general, the most widely divergent values so that the omitted data would lie between these divergent values.

The results shown in the six charts, Figs. 7, 8, 9, 10, 11, and 12, will be discussed in terms of the development of the incompressible boundary layer on a flat plate with zero pressure gradient in the direction of flow. It is well known that this boundary layer develops as a laminar layer of increasing thickness, undergoes transition over a finite length of flow to become a turbulent boundary layer, and continues to grow in thickness in the direction of flow. The transition starts at a critical value of the length Reynolds number. The laminar boundary layer has a nearly linear distribution of velocity. The turbulent boundary layer consists of a thin laminar sublayer and a much thicker outer portion in turbulent motion; most of the decrease in velocity in the turbulent boundary layer occurs, however, in the thin laminar sublayer.

Laminar Boundary Layer. Figs. 7, 8, and 9 present results for the different test combinations for the smallest values of the diameter Reynolds numbers at the first station. Fig. 7 shows two runs for test combination B at the smallest value of the diameter Reynolds number attained in all these measurements, namely, 0.15×10^6. Fig. 8 compares results from combinations A-2 and B at a Reynolds number of about 0.5×10^6. Fig. 9 compares measurements from all three combinations at a Reynolds number of about 0.8×10^6. The measured static pressures are given in terms of the dimensionless modified pressure ratio so that the values from the different test combinations could be placed on a comparable basis. The measured adiabatic wall temperatures are given in terms of the dimensionless ratio, T_{aw}/T_{o1}. The local apparent coefficient of friction is, in reality, an average value over the short distance between two adjacent stations.

Figs. 8 and 9 illustrate the excellent agreement of the temperature measurements from the different test combinations. A horizontal straight line could be used to represent the ratio of adiabatic wall temperature to stagnation temperature with an average deviation of less than 0.4 per cent for all values except those at the first and last stations. The measured values of the modified pressure ratio from the different test combinations are also in good agreement. It should be noted that this parameter is related simply to the Mach number calculated on the basis of the one-dimensional flow model (Appendix B) and is very sensitive to variations in the diameter Reynolds number, particularly at small values of the Reynolds number. The calculated recovery factors and local apparent friction coefficients are also in excellent agreement for the different test combinations. The agreement of the values of local apparent coefficients of friction for these test combinations is good compared with similar published data for subsonic velocities. Hence it appears from the measurements in Figs. 8 and 9 that gross systematic errors are absent.

The interpretation of the data on friction in Figs. 7, 8, and 9 is fairly simple on the basis of plate-type flow. Near the tube entrance a laminar boundary layer is formed which extends for a considerable distance downstream. The frictional effects of this laminar layer decrease with increasing length Reynolds number as for a flat plate. The presence of a sudden increase in the frictional effects at a length Reynolds number of about 10^6 in Fig. 8, and about 2×10^6 in Fig. 9, indicates a transition to a turbulent boundary layer. These values of the critical Reynolds number agree well with published values for transition on a flat plate with zero pressure gradient. On the other hand, if the diameter Reynolds number is sufficiently small, as in Fig. 7, the frictional effects continue to decrease throughout the entire length of flow in the tube. The absence of any indication of a transition in Fig. 7 is additional evidence supporting the basic hypothesis of the existence of a laminar boundary layer over the entire length of the test section.

The true local coefficient of friction for incompressible flow with zero pressure gradient over a flat plate is also shown in Figs. 7, 8, and 9 by the curve marked "flat plate-laminar." The effect of compressibility at Mach numbers near 2.5 is to reduce the true coefficient of friction by several per cent (6, 7). The friction data given in Figs. 7 and 8 for supersonic flow in a tube have a considerably different slope than the theoretical slope for a flat plate. In addition, the calculated values of the local apparent coefficient of friction lie considerably above the flat-plate values near the entrance of the tube. If these higher values near the tube entrance were due to the changing velocity profile of the stream, then they should be compared with the curve marked Langhaar. This curve represents the local apparent friction coefficients deduced from the results given by Langhaar (8), who took account of the effect of the changing velocity distribution near the entrance of a tube for an incompressible fluid.

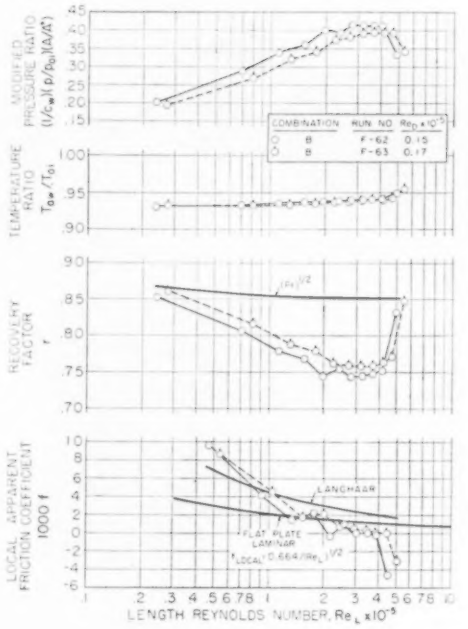

FIG. 7

The one-dimensional flow model, certainly the simplest device for calculation purposes, should yield accurate values only in the limiting cases where the thickness of the boundary layer is small compared with the radius of the tube, or where the flow is fully developed. That this flow model is inadequate for calculations of supersonic flow of air in a tube is shown here by the calculated negative values of the local apparent coefficient of friction in Figs. 7, 8, and 9. That this flow model is not fully adequate for the entrance region is probably the reason the apparent friction coefficient differs radically from the true coefficient since the laminar boundary layer increases rapidly in thickness. However, as the diameter Reynolds number increases, as in Figs. 7, 8, 9, and 10, the effect of thickness of this laminar boundary layer on the one-dimensional flow model calculations decreases, as might be expected. The differences between the values of the friction coefficient in a tube and those for a flat plate in Figs. 7 and 8 may be due, in part, to the effect of pressure gradient in the tube and to the effect of initial turbulence.

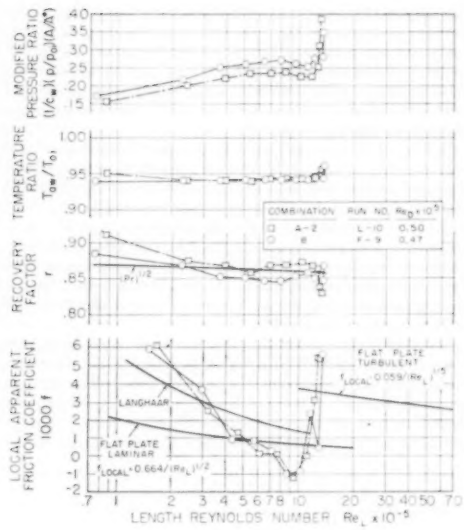

FIG. 8

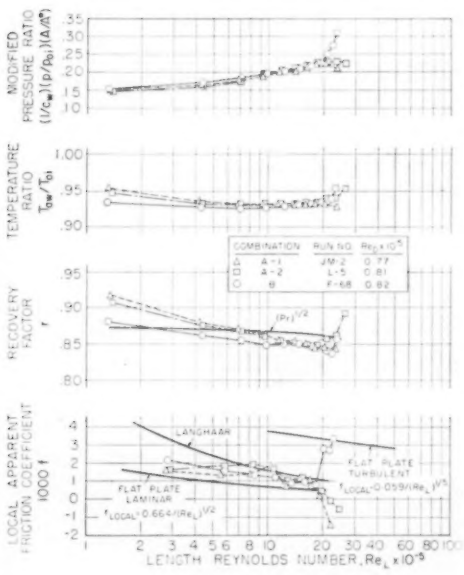

FIG. 9

The small values of the local apparent friction coefficient in Fig. 9 indicate the presence of a very small frictional effect over most of the length of supersonic flow in the tube. This effect has been verified by repetition of these tests. The additional data, given in Appendix A, are not plotted here in the interest of simplicity. The tests which are shown in Fig. 9 were selected to show the maximum deviations between the values obtained from the three test combinations.

The extraordinary agreement between the measurements of local apparent coefficient of friction in Fig. 9 and the curve shown for incompressible flow over a flat plate with zero pressure gradient may be coincidental. This agreement could indicate, however, that a plate-type flow existed for almost the entire length of the tube, and that the effect of the pressure gradient is small. This agreement is much better in Fig. 9 than in Figs. 7 and 8; the interpretation could be that the greater-diameter Reynolds number in Fig. 9 probably corresponds to a thinner boundary layer in the laminar region and hence to less departure from one-dimensional flow conditions than in Figs. 7 and 8. Finally, it should be noted that the local apparent friction coefficients are in better agreement with the Langhaar curve in Fig. 9 than in Figs. 7 and 8.

The curve labeled "flat plate—turbulent" in Figs. 8 and 9 corresponds to the local true coefficient of friction, given by von Kármán (9), for fully developed turbulent flow on a flat plate. It is evident that for diameter Reynolds numbers of 0.5 and 0.8 × 10^5 the flow in the tube never attains the condition corresponding to fully developed turbulent flow.

The measurements of Stalder, Rubesin, and Tendeland (10) for a laminar boundary layer on a flat plate with supersonic flow indicate a recovery factor of 0.88 over a range of length Reynolds number from about 0.2 × 10^5 to 2 × 10^5. The recovery factors calculated from the present measurements made near the tube entrance are in agreement with this value with a deviation of about 1 to 2 per cent except for those shown in Fig. 7. In addition, the recovery factors calculated from the present measurements made near the tube entrance, shown on Figs. 8, 9, 10, 11, and 12, and corresponding to the laminar boundary layer in the tube are in fair agreement with the theoretical prediction for a flat plate, namely, that the recovery factor will vary as the square root of the Prandtl number. This theoretical relation is shown in Figs. 7, 8, 9, 10, 11, and 12. The Prandtl number is evaluated at the mean stream temperature.

Compared with Figs. 8, 9, 10, 11, and 12, Fig. 7 shows the greatest difference between the calculated values of the recovery factor and the curve representing the square root of the Prandtl number. However, if the values of the measured temperature ratio in Fig. 7 are compared with those in Figs. 8, 9, 10, 11, and 12, the differences between these measured values are relatively small, of the order of 2 per cent. Hence it is likely that the large difference in Fig. 7, of the order of 20 per cent, is a result of the inadequacy of the one-dimensional flow model, since the boundary-layer thickness at entrance to the tube is large compared with the radius for the conditions corresponding to Fig. 7.

The temperature measurements from the three test combinations shown in Fig. 9 are in excellent agreement over the test section except at the first and last stations. Other data obtained on repetition of these measurements would fall between the limits shown in Fig. 9. The calculated recovery factors exhibit again greater deviations and fluctuations than those present in the temperature measurements.

Boundary Layer in Transition. The friction coefficients in Figs. 8 and 9 correspond to a laminar boundary layer over most of the tube length followed by a transition near the tube exit. As the diameter Reynolds number is increased, by increasing the stagnation pressure at constant stagnation temperature, the point of transition to a turbulent boundary layer moves upstream toward the tube entrance. This effect is shown clearly in Figs. 7, 8, 9, 10, and 11.

The local apparent friction coefficients in Fig. 10 at a diameter Reynolds number at the first station of 1.1 × 10^5, show that the

flow in the boundary layer remains laminar for only the first three or four stations (10 to 14 diameters from nozzle exit), and that transition to a turbulent boundary layer occurs over the rest of the tube length. In addition, the friction coefficients in Fig. 11, at a diameter Reynolds number of 2×10^5, show a strongly irregular fluctuation from tube entrance to tube exit. Similarly in Fig. 12, at a diameter Reynolds number of about 5×10^5, the friction data show an irregular fluctuation from the first station to exit and indicate also that any laminar boundary layer which might exist in the tube must be upstream of the first station which is about 1.5 diameters from the plane of the nozzle exit.

The effect of the transition from the laminar to the turbulent type of boundary layer on the measured values of the adiabatic wall temperature is also shown in Figs. 9, 10, 11, and 12. In contrast with large changes which occur in the values of the local apparent friction coefficients, the values of the adiabatic wall temperatures are but slightly affected by this transitional phenomenon.

Turbulent Boundary Layer. Figs. 10, 11, and 12 illustrate the accord between the adiabatic wall temperatures measured with the three test combinations. Additional data, not shown on these charts, lie between the limiting values. The presence of gross systematic errors in temperature measurements is not indicated by these data. In addition, the calculated local apparent friction coefficients shown in Figs. 11 and 12 exhibit the same characteristic fluctuations for the three test combinations. This qualitative agreement, although subject to change on further analysis, indicates that there is no significant deviation introduced by the peculiarities of the flow associated with each of the two different supersonic nozzles.

The interpretation of the data on friction in Figs. 10, 11, and 12 indicates the presence of a turbulent boundary layer in the downstream portion of the tube. Although evidence of this turbulent boundary layer is just beginning to appear in Fig. 10, evidence of its presence is readily seen in Figs. 11 and 12. For purposes of comparison, the curves corresponding to laminar and turbulent boundary layers on a flat plate with zero pressure gradient are given on each chart.

In Fig. 10 the values of the local apparent friction coefficient near the upstream end of the tube are in excellent agreement with those for laminar flow on a flat plate. After the transition has occurred the values fluctuate about those for the flat plate with a turbulent boundary layer. The friction data shown in Fig. 11 are again in good agreement with the values for a flat plate with a turbulent boundary layer. However, the friction data shown in Fig. 12 for the largest-diameter Reynolds number attained in these measurements fluctuate to a greater degree about the flat-plate values than those in Fig. 11.

The calculated values of the recovery factors shown in Figs. 10, 11, and 12 are difficult to interpret in terms of the theoretical values for a turbulent boundary layer on a flat plate with zero pressure gradient. Theory indicates that this recovery factor should vary as the cube root of the Prandtl number; hence it should be represented by a curve approximately parallel to that

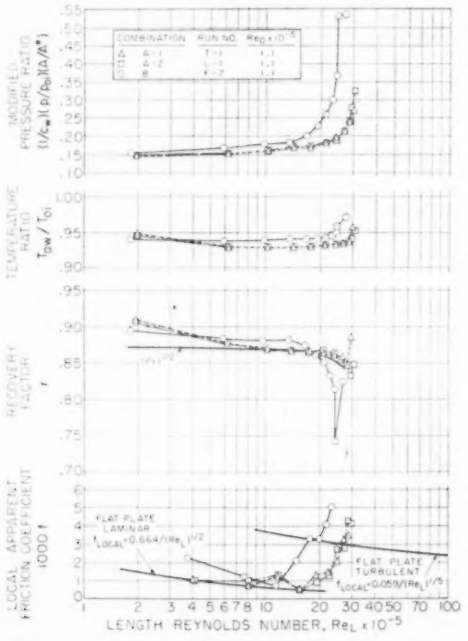

FIG. 10

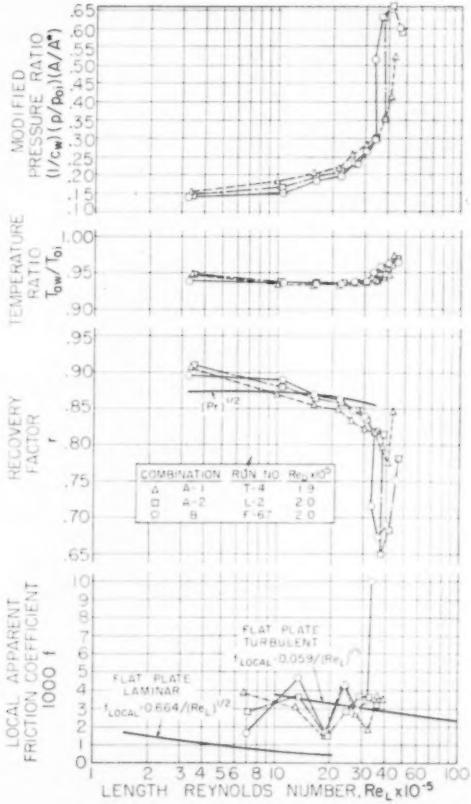

FIG. 11

shown for the square root of the Prandtl number but about 5 per cent higher. The values of the recovery factor shown in Figs. 10, 11, and 12 for the turbulent portion of the flow are not only considerably lower than this theoretical curve but also appear to fall rapidly toward the exit end of the tube. This apparent discrepancy between the measured and theoretical values for the recovery factors in a turbulent boundary layer may have been introduced into the calculations by the use of the simple one-dimensional flow model.

Evidence that this discrepancy may be only an apparent one is obtained from the measurements of Stalder, Rubesin, and Tendeland (10) for a turbulent boundary layer on a flat plate with supersonic flow of air. They found that the measured recovery factor increased by about 2 per cent after the transition from the laminar boundary layer. Examination of the curves for adiabatic wall temperature in Figs. 10, 11, and 12 shows that there is a rise of several per cent in the value of adiabatic wall temperature in the transition from the laminar to the turbulent boundary layer. Whether this rise of several per cent is significant is under investigation with the aid of a more detailed analysis of the supersonic flow of air in a round tube.

Comparison With Other Data

Due to space limitations, no detailed comparisons will be given here of the friction coefficients with those obtained from previously published data. It has been stated previously by Kaye, Keenan, and McAdams (1) that comparison with the supersonic friction coefficients of Keenan and Neumann (11) shows very good qualitative agreement and good quantitative agreement. In addition, comparison with the friction coefficients of Shapiro and Smith (12) for incompressible flow of air and water indicates likewise good qualitative agreement. It would appear desirable to analyze all these frictional data in a tube with the aid of an analysis more detailed than the simple one-dimensional flow model.

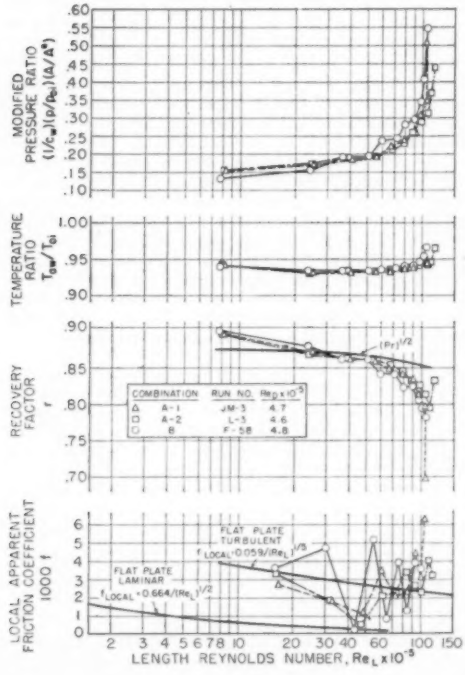

Fig. 12

Conclusions

Reliable data on the adiabatic flow of air at supersonic velocities in a round tube are presented. Intercomparison of the measurements of recovery factors and friction coefficients made with different test combinations and comparison with measurements available in the literature disclosed no significant systematic errors.

The calculated values of the local apparent friction coefficient conform to a simple hypothesis of the flow pattern in a round tube in terms of the boundary-layer development on a flat plate. For that portion of the tube where the flow in the boundary layer appears to be laminar, the calculated values of the local apparent friction coefficient are in good accord with both the experimental and theoretical values for an incompressible boundary layer over a flat plate, except for the data found at the smallest values of the diameter Reynolds number; this discrepancy can be explained, however, in terms of the inadequacy of the one-dimensional flow model for cases where the thickness of the laminar boundary layer is appreciable. For that portion of the tube where the flow in the boundary layer appears to be turbulent, the local apparent friction coefficients are in good agreement with the measured values for a turbulent boundary layer on a flat plate. Additional evidence of the conformity of these data to this simple hypothesis is found in the excellent agreement of the values of the transitional length Reynolds number found in the tube with those found in the literature for a flat plate.

The calculated values of the local recovery factor also support the hypothesis of the flow pattern in the tube in terms of the boundary-layer development on a flat plate. Where the flow in the tube boundary layer appears to be laminar and the pressure gradient in the direction of flow is small, the recovery factors are in excellent agreement with both the theoretical and experimental values for a laminar boundary layer on a flat plate. Where the flow in the tube boundary layer appears to be turbulent, however, the calculated values of the recovery factor are smaller by several per cent than those found for a turbulent boundary layer on a flat plate. This discrepancy may not be significant and is under study with the aid of a more detailed analysis of flow in the tube.

The discovery of a region of supersonic flow in a tube with very small frictional effects, given in the earlier work on this program (1), has been substantiated with an adiabatic apparatus of different design. This region corresponds to a diameter Reynolds number in the order of 1×10^4.

The one-dimensional flow model customarily used for the calculation of flow in a tube is satisfactory, perhaps, for use in design applications because of its simplicity. This model can be misleading, however, in the interpretation of the experimental results. For an adequate understanding of the phenomena which occur in the supersonic flow of a fluid in a passage, it is necessary to use a more detailed analysis based on a two-dimensional or axially symmetrical flow model. A treatment of some of these same data by this detailed type of analysis is presented in Part 2 of this series of papers.

Acknowledgments

The assistance of Robert H. Shoulberg, Robert E. Kendall, and George A. Brown in the final preparation of this report is gratefully acknowledged.

This investigation is sponsored as Contract Number N5-ori-07805 by the Office of Naval Research of the United States Navy.

BIBLIOGRAPHY

1 "Report of Progress on Measurements of Friction Coefficients, Recovery Factors, and Heat Transfer Coefficients for Supersonic Flow of Air in a Pipe," by J. Kaye, J. H. Keenan, and W. H. McAdams, Heat Transfer and Fluid Mechanics Institute, June, 1949, pp. 147–164.

2 "Measurement of Recovery Factors and Friction Coefficients for Supersonic Flow of Air in a Tube," by J. Kaye, J. H. Keenan, and R. H. Shoulberg, presented in the General Discussion on Heat Transfer, London, England, September, 1951.

3 "Nozzles for Supersonic Flow Without Shock Fronts," by A. H. Shapiro, JOURNAL OF APPLIED MECHANICS, Trans. ASME, vol. 66, 1944, p. A-93.

4 "The Analytical Design of an Axially Symmetric Laval Nozzle for a Parallel and Uniform Jet," by K. Foelsch, *Journal of the Aeronautical Sciences*, vol. 16, 1949, pp. 161–167.

5 "Method of Characteristics for Three-Dimensional Axially Symmetrical Supersonic Flows," by R. Sauer, NACA Technical Memorandum 1133, January, 1947.

6 "Temperature Effects in a Laminar Compressible-Fluid Boundary Layer Along a Flat Plate," by H. W. Emmons and J. G. Brainerd, JOURNAL OF APPLIED MECHANICS, Trans. ASME, vol. 63, 1941, p. A-105.

7 "Effect of Variable Viscosity on Boundary Layers, With a Discussion of Drag Measurements," by J. G. Brainerd and H. W. Emmons, JOURNAL OF APPLIED MECHANICS, Trans. ASME, vol. 64, 1942, p. A-1.

8 "Steady Flow in the Transition Length of a Straight Tube," by H. L. Langhaar, JOURNAL OF APPLIED MECHANICS, Trans. ASME, vol. 64, 1942, p. A-55.

9 "Turbulence and Skin Friction," by Th. von Kármán, *Journal of the Aeronautical Sciences*, vol. 1, 1934, pp. 1–20.

10 "A Determination of the Laminar-, Transitional-, and Turbulent-Boundary-Layer Temperature-Recovery Factors on a Flat Plate in Supersonic Flow," by J. R. Stalder, M. W. Rubesin, and T. Tendeland, NACA Technical Note 2077, June, 1950.

11 "Measurements of Friction in a Pipe for Subsonic and Supersonic Flow of Air," by J. H. Keenan and E. P. Neumann, JOURNAL OF APPLIED MECHANICS, Trans. ASME, vol. 68, 1946, p. A-91.

12 "Friction Coefficients in the Inlet Length of Smooth Round Tubes," by A. H. Shapiro and R. D. Smith, NACA Technical Note 1785, November, 1948.

13 "Viscosities of Several Common Gases Between 90° K and Room Temperature," by H. L. Johnston and K. E. McCloskey, *Journal of Physical Chemistry*, vol. 44, 1940, pp. 1038–1057.

14 "A Summary of Viscosity and Heat-Conduction Data for He, A, H_2, O_2, N_2, CO, CO_2, H_2O, and Air," by F. G. Keyes, Trans. ASME, vol. 73, July, 1951, pp. 589–596.

15 "Gas Tables," by J. H. Keenan and J. Kaye, John Wiley & Sons, New York, N. Y., 1948.

Appendix A

MEASUREMENTS AND CALCULATED RESULTS

This appendix contains the detailed dimensions of the three test combinations, the measured discharge coefficients of the two supersonic nozzles, the viscosity and Prandtl number for air, the original measurements for adiabatic flow, and the calculated results based on the one-dimensional flow model.

Details of Nozzles and Test Sections. The values of the nozzle throat diameter D^*, and the test section diameter D_t are given in Table 1 for the three test combinations.

TABLE 1 DIAMETERS OF NOZZLES AND TEST SECTIONS

Test combination	Nozzle	Test section	D^* (in.)	D_t (in.)
A-1	Brass	Textolite	0.2416	0.502
A-2	Brass	Lucite	0.2416	0.502
B	Stainless steel	Lucite	0.2685	0.5018

The length-diameter ratios of the three test sections are given in Table 2. The length is the distance from the end of the curved contour in the supersonic nozzle to the station in question.

TABLE 2 LENGTH-DIAMETER RATIOS OF STATIONS IN TEST SECTIONS

Station no.	Test combination		
	A-1	A-2	B
1	1.743	1.743	1.614
2	5.727	5.727	5.600
3	9.711	9.711	9.586
4	13.70	13.70	13.57
5	17.43	17.68	17.56
6	21.66	21.66	21.54
7	25.65	25.65	25.53
8	29.63	29.63	29.51
9	33.62	33.62	33.50
10	37.60	37.60	37.49
11	...	41.58	41.47

Discharge Coefficients of Supersonic Nozzles. Each of the supersonic nozzles was calibrated by means of a gasometer. In Fig. 13 the experimental values of the discharge coefficient are plotted against the Reynolds number, based on the throat diameter of the nozzle and isentropic flow from the initial state to critical pressure, $(\mathbf{Re}_{D^*})_s$.

The scatter of the experimental values in Fig. 13 is of the same order of magnitude for each nozzle, but is slightly less for the stainless-steel nozzle. At first a separate straight line was passed independently through each set of data but the two lines were found to be parallel and only slightly separated. Hence the single line shown in Fig. 13 has been used to represent the data for both nozzles with an estimated error of less than 0.2 per cent. The dashed portion of this line represents an extrapolation of the data. When all the experimental data were recalculated for the preparation of this report, Fig. 13 was used throughout.

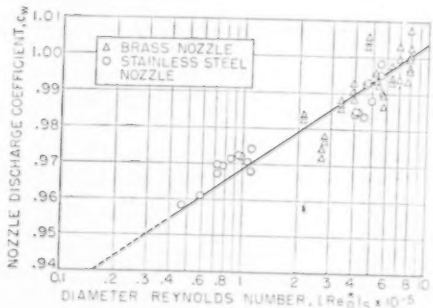

FIG. 13

Viscosity and Prandtl Number for Air. The viscosity and Prandtl number of air are given in Fig. 14, over a range of temperature from 200 to 520 F abs. The values of viscosity of air are from the work of Johnston and McCloskey (13). Their data agree well with the results of Keyes (14); between 160 and 500 F abs the maximum deviation is 0.2 per cent.

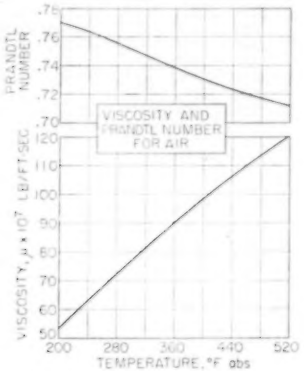

FIG. 14

The values for thermal conductivity for air are from Keyes' correlation (14). The values of specific heat at constant pressure for air are obtained from "Gas Tables" (15). The values for the Prandtl number for air were calculated with the aid of these specific heats and the viscosity and thermal conductivity from Keyes' equations.

Data and Calculated Results. The measured values of the local adiabatic wall temperature and the local static pressure are given in Table 3. In addition, the calculated results based on the simple one-dimensional flow model are given in Table 3.

Table 3 contains forty runs, of which 12 were made with combination A-1, 10 with A-2, and 18 with B. In addition to these forty runs, many more were made for special purposes, such as tests of thermal isolation of the test section, tests of effect of cooling various portions of the apparatus upstream of the test section, tests of effect of operation of combination B without a high-vacuum space, etc. These additional runs together with some preliminary runs made under less controlled conditions are not given here.

In order to keep the size of this paper within reasonable bounds, a critical examination was made after all the data were placed on a comparable basis. The final result was the selection of these forty runs as the most reliable, on the basis that these were the least affected by transient thermal effects. In addition, the runs omitted are all duplicates of those in Table 3. The deviation in measured pressures or temperatures between the duplicate runs and those given in Table 3 is less than 1 per cent, except for regions of transitional-type flow, where the maximum deviation is 3 per cent.

Appendix B

Analysis and Sample Calculation

Analysis. Consider the steady flow of air from a stagnation state through the supersonic nozzle and then through the round tube of constant cross-sectional area. The following assumptions are made:

1 The flow is one-dimensional, i.e., the fluid properties are uniform at any section.

2 The flow is adiabatic.

3 Air is a perfect gas with a constant specific heat; actually over the range in temperature under consideration here, the ratio of the specific heat at constant pressure to the specific heat at constant volume varies by only 1 part in 1400.

The equations used in the calculations are as follows

Continuity: $$w = \rho V A \quad [1]$$

Energy: $$c_p T_{oi} = c_p T + V^2/2g \quad [2]$$

Equation of state: $$p = \rho R T \quad [3]$$

Definition: $$\mathbf{M}^2 \equiv V^2/gkRT \quad [4]$$

Definition: $$c_w \equiv (w/A^*)/(w/A^*)_s \quad [5]$$

From these equations many useful relations can be derived. These are available in many texts.[7] The objective of the present analysis is to combine the foregoing equations to give a relation between measured quantities and a tabulated function of the Mach number.

For isentropic flow through the supersonic nozzle

$$G_s^* \equiv (w/A^*)_s = \sqrt{\frac{gk}{R}}\,\frac{k+1}{2}\,\frac{p^*}{\sqrt{T_{oi}}} \quad [6]$$

From the first four equations

$$G \equiv (w/A) = \sqrt{\frac{gk}{R}}\,pM\sqrt{1+\frac{k-1}{2}M^2}\Big/\sqrt{T_{oi}} \quad [7]$$

Combining Equations [4], [6], and [7]

$$\frac{1}{c_w}\,\frac{p}{p_{oi}}\,\frac{A}{A^*} = \left(\frac{2}{k+1}\right)^{2/(k-1)}\frac{1}{\mathbf{M}\sqrt{1+\frac{k-1}{2}\mathbf{M}^2}} \equiv f_1(\mathbf{M},k) \quad [8]$$

But the right-hand side of Equation [8] represents a unique function of the Mach number if k is constant. This function is tabulated in detail elsewhere.[8] Hence, from the measured values of c_w, p, p_{oi}, A, A^*, it becomes a very simple matter to determine the local Mach number in the constant-area tube.

The remaining equations and numerical constants used in the calculations are summarized as follows

$$G_s^* = 0.5318\ p_{oi}/\sqrt{T_{oi}} \quad [9]$$

Here, p_{oi} is expressed in psia, T_{oi} in deg F abs, G_s^* in lbm/in.^{2} sec.

$$T^* = 0.83333\ T_{oi} = 0.83333(t_{oi} + 459.69) \quad [10]$$

$$(\mathbf{Re}_D^*)_s \equiv G_s^* D^*/\mu^* \quad [11]$$

$$T_m/T_{oi} = 1/\left(1+\frac{k-1}{2}\mathbf{M}^2\right) \quad [12]$$

Note that (T_m/T_{oi}) is tabulated elsewhere.[8]

$$r \equiv \frac{T_{aw}-T_m}{T_{oi}-T_m} = \left(\frac{T_{aw}}{T_{oi}}-\frac{T_m}{T_{oi}}\right)\Big/\left(1-\frac{T_m}{T_{oi}}\right) \quad [13]$$

$$G = c_w G_s^* A^*/A \quad [14]$$

$$\mathbf{Re}_D \equiv GD/\mu_m \quad [15]$$

$$\mathbf{Re}_L \equiv GL/\mu_m = \mathbf{Re}_D(L/D) \quad [16]$$

[7] Some are summarized in Reference (15), p. 211.

[8] Reference (15), Table 30.

TABLE 3 ORIGINAL DATA AND CALCULATIONS BASED ON ONE-DIMENSIONAL FLOW MODEL

	Station No.	p psia	t_{aw} °F	$\frac{p A}{c_w p_{oi} A^*}$	$\frac{T_{aw}}{T_{oi}}$	M	$\frac{T_w}{T_{oi}}$	r	Re_D x10^{-5}	Re_L x10^{-5}	$\bar{F}$ x10^3	f x10^3
Run No. JM-1	oi	99.856	107.27									
August 19, 1947	1	3.531	73.91	0.1534	0.9412	2.51	0.4426	0.894	4.74	8.27		2.80
t_r = 83.0°F	2	4.003	68.73	.1739	.9320	2.31	.4832	.868	4.38	25.1	2.80	1.69
p_r = 14.754 psia	3	4.299	68.50	.1868	.9316	2.21	.5068	.861	4.20	40.7	2.25	1.18
c_w = 0.995	4	4.511	68.57	.1960	.9317	2.14	.5231	.857	4.08	55.9	1.89	3.44
G = 74.02 lb/ft^{2}sec	5	5.117	69.53	.2223	.9334	1.96	.5660	.847	3.81	66.4	2.26	2.16
	6	5.579	70.51	.2424	.9352	1.84	.5956	.840	3.64	78.9	2.24	2.37
	7	6.089	71.44	.2646	.9368	1.73	.6256	.831	3.49	89.6	2.26	4.44
	8	7.176	72.70	.3118	.9390	1.53	.6808	.809	3.25	96.3	2.57	2.98
	9	8.060	74.28	.3502	.9418	1.40	.7183	.793	3.11	104.5	2.62	6.21
	10	11.772	76.95	.5115	.9465	1.03	.8255	.693	2.79	104.8	3.02	
Run No. JM-2	oi	16.456	106.11									
August 19, 1947	1	0.5627	79.50	0.1525	0.9530	2.52	0.4407	0.916	0.766	1.33		1.59
t_r = 87.0°F	2	.6053	69.84	.1640	.9359	2.40	.4640	.880	.731	4.19	1.59	1.34
p_r = 14.735 psia	3	.6420	68.08	.1740	.9328	2.31	.4833	.870	.705	6.85	1.47	1.38
c_w = 0.968	4	.6807	67.47	.1845	.9317	2.22	.5027	.863	.680	9.31	1.44	1.86
G = 11.88 lb/ft^{2}sec	5	.7309	67.56	.1981	.9319	2.12	.5267	.856	.652	11.4	1.54	0.615
	6	.7503	67.55	.2033	.9319	2.08	.5355	.853	.642	13.9	1.34	1.09
	7	.7832	67.78	.2123	.9323	2.02	.5501	.849	.628	16.1	1.30	0.941
	8	.8122	67.79	.2201	.9323	1.97	.5625	.845	.615	18.2	1.25	0.0123
	9	.8160	67.80	.2212	.9323	1.97	.5642	.845	.614	20.6	1.11	-1.57
	10	.7677	65.91	.2081	.9290	2.05	.5433	.844	.634	23.9	0.811	
Run No. JM-3	oi	99.994	108.02									
August 21, 1947	1	3.531	75.14	0.1532	0.9421	2.51	0.4422	0.896	4.75	8.27		2.74
t_r = 75.5°F	2	3.993	69.67	.1733	.9324	2.32	.4819	.870	4.39	25.2	2.74	1.81
p_r = 14.891 psia	3	4.310	69.24	.1870	.9317	2.20	.5073	.861	4.19	40.7	2.28	1.18
c_w = 0.995	4	4.523	69.30	.1963	.9318	2.13	.5235	.857	4.08	55.8	1.91	3.43
G = 74.07 lb/ft^{2}sec	5	5.130	70.26	.2226	.9335	1.96	.5664	.847	3.80	66.3	2.27	2.11
	6	5.583	71.22	.2422	.9352	1.84	.5954	.840	3.64	78.9	2.24	2.28
	7	6.074	72.22	.2636	.9369	1.73	.6243	.832	3.50	89.7	2.24	4.41
	8	7.151	73.51	.3103	.9392	1.54	.6791	.811	3.26	96.5	2.55	3.07
	9	8.056	75.11	.3496	.9420	1.40	.7177	.795	3.11	104.5	2.62	6.26
	10	11.792	77.81	.5117	.9468	1.03	.8256	.695	2.78	104.4	3.02	
Run No. JM-4	oi	16.407	106.80									
August 25, 1947	1	0.5627	80.40	0.1531	0.9534	2.51	0.4420	0.916	0.759	1.32		1.60
t_r = 93.5°F	2	.6052	71.20	.1647	.9372	2.40	.4653	.882	.725	4.15	1.60	1.35
p_r = 14.657 psia	3	.6420	69.59	.1747	.9343	2.31	.4846	.873	.699	6.79	1.47	1.32
c_w = 0.967	4	.6787	68.99	.1847	.9333	2.22	.5031	.866	.675	9.25	1.42	1.30
G = 11.82 lb/ft^{2}sec	5	.7135	69.17	.1942	.9336	2.15	.5193	.862	.657	11.4	1.39	1.12
	6	.7483	69.10	.2036	.9335	2.08	.5360	.857	.638	13.8	1.33	1.09
	7	.7812	69.35	.2126	.9339	2.02	.5506	.853	.623	16.0	1.29	1.01
	8	.8122	69.39	.2210	.9340	1.97	.5639	.849	.611	18.1	1.25	0.495
	9	.8276	69.61	.2252	.9344	1.94	.5704	.847	.604	20.3	1.16	0.0609
	10	.8296	68.60	.2257	.9326	1.94	.5712	.843	.604	22.7	1.04	
Run No. JM-5	oi	24.009	106.26									
August 27, 1947	1	0.8093	79.06	0.1496	0.9519	2.55	0.4345	0.915	1.14	1.98		1.00
t_r = 74.9°F	2	.8481	69.41	.1567	.9349	2.48	.4494	.882	1.10	6.32	1.00	0.912
p_r = 14.804 psia	3	.8839	67.78	.1634	.9320	2.41	.4627	.873	1.07	10.4	0.958	0.859
c_w = 0.973	4	.9181	67.92	.1697	.9323	2.35	.4750	.871	1.05	14.4	0.925	0.821
G = 17.42 lb/ft^{2}sec	5	.9493	68.82	.1754	.9338	2.30	.4860	.871	1.03	17.9	0.900	0.940
	6	.9902	69.16	.1830	.9344	2.24	.5000	.869	1.00	21.7	0.909	1.97
	7	1.074	69.70	.1984	.9354	2.12	.5272	.863	0.955	24.5	1.09	3.24
	8	1.218	70.49	.2251	.9368	1.94	.5702	.853	.891	26.4	1.39	3.28
	9	1.377	71.36	.2546	.9383	1.78	.6124	.841	.838	28.2	1.63	6.77
	10	1.772	69.96	.3275	.9359	1.48	.6968	.788	.751	28.3	2.20	

TABLE 3 (continued) ORIGINAL DATA AND CALCULATIONS BASED ON ONE-DIMENSIONAL FLOW MODEL

	Station No.	p psia	t_{aw} °F	$\frac{pA}{c_w p_{oi} A^*}$	$\frac{T_{aw}}{T_{oi}}$	M	$\frac{T_m}{T_{oi}}$	r	Re_D x10^{-5}	Re_L x10^{-5}	$\bar{f}$ x10^3	f x10^3
Run No. JM-7	oi	59.970	106.90									
September 4, 1947	1	2.114	77.28	0.1542	0.9477	2.50	0.4441	0.906	2.82	4.92		3.07
t_r = 80.0°F	2	2.423	70.68	.1767	.9361	2.29	.4884	.875	2.59	14.8	3.07	1.75
p_r = 14.721 psia	3	2.607	69.83	.1901	.9346	2.18	.5128	.866	2.48	24.0	2.41	2.12
c_w = 0.987	4	2.839	69.92	.2071	.9347	2.06	.5416	.858	2.36	32.3	2.31	4.59
G = 44.11 lb/ft^{2}sec	5	3.345	71.06	.2440	.9367	1.83	.5979	.843	2.16	37.7	2.86	2.73
	6	3.724	72.19	.2717	.9387	1.70	.6345	.832	2.06	44.6	2.83	2.59
	7	4.098	73.36	.2989	.9408	1.58	.6667	.823	1.97	50.6	2.79	3.22
	8	4.633	75.06	.3379	.9438	1.44	.7069	.808	1.88	55.7	2.85	2.72
	9	5.188	77.51	.3784	.9491	1.32	.7423	.799	1.90	60.6	2.84	2.77
	10	5.981	91.97	.4362	.9736	1.17	.7838	.878	1.73	64.9	2.83	
Run No. JM-8	oi	39.861	107.11									
September 4, 1947	1	1.340	79.58	0.1480	0.9514	2.57	0.4312	0.915	1.91	3.34		3.84
t_r = 81.0°F	2	1.593	71.69	.1759	.9375	2.30	.4869	.878	1.71	9.82	3.84	2.49
p_r = 14.704 psia	3	1.767	70.72	.1951	.9358	2.14	.5215	.866	1.61	15.6	3.16	1.81
c_w = 0.981	4	1.899	70.57	.2096	.9355	2.04	.5459	.858	1.55	21.2	2.71	4.28
G = 29.13 lb/ft^{2}sec	5	2.212	71.75	.2442	.9376	1.83	.5982	.845	1.43	24.9	3.09	3.34
	6	2.522	72.88	.2784	.9396	1.67	.6429	.831	1.34	29.1	3.14	2.75
	7	2.792	74.24	.3083	.9420	1.54	.6770	.820	1.29	33.0	3.07	3.49
	8	3.198	76.25	.3531	.9456	1.39	.7209	.805	1.22	36.2	3.13	3.34
	9	3.720	79.19	.4108	.9507	1.23	.7667	.789	1.16	39.0	3.16	2.67
	10	4.629	92.98	.5111	.9751	1.03	.8253	.857	1.09	41.1	3.10	
Run No. JM-9	oi	23.949	105.40									
September 9, 1947	1	0.9048	76.99	0.1491	0.9497	2.56	0.4336	0.911	1.14	1.99		0.949
t_r = 79.8°F	2	.8414	67.53	.1559	.9330	2.48	.4476	.879	1.11	6.34	0.949	.914
p_r = 14.899 psia	3	.8771	65.92	.1625	.9301	2.42	.4610	.870	1.08	10.5	.932	.902
c_w = 0.973	4	.9129	66.13	.1691	.9305	2.36	.4740	.868	1.05	14.4	.922	.825
G = 17.39 lb/ft^{2}sec	5	.9440	67.14	.1749	.9323	2.30	.4850	.869	1.03	17.9	.899	.961
	6	.9858	67.58	.1826	.9331	2.24	.4993	.866	1.00	21.7	.912	2.12
	7	1.075	68.29	.1992	.9343	2.11	.5285	.861	0.953	24.4	1.11	3.30
	8	1.223	69.09	.2265	.9357	1.93	.5724	.850	.888	26.3	1.43	3.65
	9	1.401	70.26	.2596	.9378	1.75	.6191	.837	.830	27.9	1.70	3.41
	10	1.589	79.02	.2944	.9533	1.60	.6617	.862	.784	29.5	1.89	
Run No. T-1	oi	23.106	104.65									
October 24, 1947	1	0.7714	75.58	0.1481	0.9485	2.57	0.4315	0.909	1.11	1.93		1.04
t_r = 73.0°F	2	.8100	66.53	.1556	.9325	2.49	.4470	.878	1.07	6.13	1.04	0.769
p_r = 14.965 psia	3	.8390	65.08	.1611	.9299	2.43	.4582	.871	1.05	10.2	0.905	1.26
c_w = 0.973	4	.8874	65.14	.1704	.9300	2.34	.4764	.866	1.01	13.9	1.02	0.530
G = 16.79 lb/ft^{2}sec	5	.9067	66.12	.1741	.9317	2.31	.4835	.868	0.998	17.4	0.907	1.38
	6	.9647	66.63	.1853	.9326	2.22	.5041	.864	.960	20.8	1.01	1.43
	7	1.023	67.37	.1964	.9339	2.13	.5237	.861	.928	23.8	1.08	2.06
	8	1.110	68.13	.2131	.9353	2.02	.5516	.856	.887	26.3	1.22	3.23
	9	1.255	69.41	.2410	.9376	1.85	.5936	.846	.832	28.0	1.47	3.51
	10	1.429	81.17	.2744	.9584	1.68	.6379	.885	.782	29.4	1.70	
Run No. T-3	oi	64.613	107.00									
November 5, 1947	1	2.305	76.80	0.1559	0.9467	2.48	0.4476	0.904	3.02	5.26		3.10
t_r = 76.0°F	2	2.643	70.06	.1787	.9348	2.27	.4922	.872	2.77	15.9	3.10	1.70
p_r = 14.613 psia	3	2.836	69.18	.1918	.9333	2.17	.5158	.862	2.66	25.8	2.40	2.03
c_w = 0.988	4	3.076	69.29	.2080	.9335	2.05	.5433	.854	2.54	34.7	2.28	4.68
G = 47.57 lb/ft^{2}sec	5	3.635	70.35	.2458	.9353	1.82	.6004	.838	2.33	40.5	2.85	2.21
	6	3.964	71.50	.2681	.9374	1.71	.6300	.831	2.23	48.3	2.71	3.04
	7	4.436	72.63	.3000	.9394	1.58	.6679	.817	2.12	54.5	2.77	2.75
	8	4.925	74.35	.3331	.9424	1.46	.7022	.807	2.04	60.3	2.77	2.80
	9	5.524	76.74	.3736	.9466	1.33	.7384	.796	1.95	65.7	2.77	2.65
	10	6.294	91.65	.4256	.9729	1.20	.7769	.879	1.87	70.5	2.76	

TABLE 3 *(continued)* ORIGINAL DATA AND CALCULATIONS BASED ON ONE-DIMENSIONAL FLOW MODEL

	Station No.	p psia	t_{aw} °F	$\frac{p\,A}{c_w p_{oi} A^*}$	$\frac{T_{aw}}{T_{oi}}$	M	$\frac{T_m}{T_{oi}}$	r	Re_D x10^{-5}	Re_L x10^{-5}	$\bar{F}$ x10^3	f x10^3
Run No. T-4	oi	41.804	105.90									
November 10, 1947	1	1.486	76.55	0.1563	0.9481	2.48	0.4485	0.906	1.94	3.39		3.83
t_r = 76.0°F	2	1.757	69.34	.1848	.9354	2.22	.5032	.870	1.75	10.0	3.83	3.08
p_r = 14.829 psia	3	1.989	68.69	.2092	.9342	2.04	.5451	.855	1.63	15.9	3.45	1.46
c_w = 0.982	4	2.105	68.80	.2214	.9344	1.96	.5645	.849	1.58	21.7	2.79	4.36
G = 30.62 lb/ft^{2}sec	5	2.453	69.88	.2580	.9363	1.76	.6169	.834	1.46	25.5	3.16	2.68
	6	2.724	71.01	.2864	.9383	1.63	.6525	.822	1.40	30.3	3.06	1.85
	7	2.917	72.14	.3068	.9403	1.55	.6754	.816	1.36	34.8	2.86	3.73
	8	3.381	74.03	.3556	.9437	1.38	.7231	.797	1.28	38.0	2.98	3.50
	9	3.961	76.73	.4166	.9484	1.22	.7708	.775	1.22	40.9	3.05	-
	10	5.025	91.41	.5284	.9744	1.00	.8334	.946	1.14	43.0	-	-
Run No. T-5	oi	95.034	107.35									
November 17, 1947	1	3.431	74.56	0.1568	0.9422	2.47	0.4495	0.895	4.45	7.75		2.38
t_r = 80.0°F	2	3.814	68.39	.1743	.9313	2.31	.4839	.867	4.16	23.8	2.38	1.40
p_r = 14.733 psia	3	-	-	-	-	-	-	-	-	-	-	3.60
c_w = 0.994	4	4.286	67.98	.1959	.9306	2.14	.5228	.855	3.88	53.1	1.73	2.62
G = 70.37 lb/ft^{2}sec	5	4.891	68.90	.2235	.9322	1.95	.5678	.843	3.61	63.8	2.17	1.81
	6	5.430	69.95	.2482	.9340	1.81	.6037	.834	3.42	74.1	2.27	4.08
	7	5.806	70.90	.2653	.9357	1.73	.6265	.828	3.32	85.0	2.19	3.09
	8	6.751	72.52	.3085	.9386	1.54	.6773	.810	3.10	92.0	2.46	2.52
	9	7.608	74.89	.3477	.9428	1.41	.7160	.798	2.96	99.6	2.54	
	10	8.474	91.08	.3873	.9713	1.29	.7493	.886	2.85	107.3	2.54	
Run No. L-1	oi	22.935	102.97									
December 30, 1947	1	0.7617	72.48	0.1474	0.9458	2.57	0.4299	0.905	1.11	1.93		1.01
t_r = 72.0°F	2	.7988	63.96	.1545	.9307	2.50	.4449	.875	1.07	6.14	1.01	1.08
p_r = 14.722 psia	3	.8392	63.48	.1624	.9298	2.42	.4607	.870	1.04	10.1	1.04	1.36
c_w = 0.973	4	.8912	64.32	.1724	.9313	2.33	.4803	.868	1.00	13.7	1.15	0.540
G = 16.69 lb/ft^{2}sec	5	.9121	64.73	.1765	.9320	2.29	.4879	.867	0.986	17.4	0.998	0.988
	6	.9510	65.34	.1840	.9331	2.23	.5018	.866	.961	20.8	0.996	1.29
	7	1.003	66.08	.1940	.9344	2.15	.5196	.864	.932	23.9	1.05	2.71
	8	1.116	66.80	.2160	.9357	2.00	.5560	.855	.877	26.0	1.28	2.78
	9	1.241	68.12	.2400	.9381	1.86	.5923	.848	.831	27.9	1.47	4.28
	10	1.453	69.76	.2812	.9410	1.65	.6462	.833	.771	29.0	1.78	
	11	1.703	77.22	.3294	.9542	1.47	.6987	.848	.722	30.0	2.03	
Run No. L-2	oi	41.700	104.21									
January 6, 1948	1	1.419	75.54	0.1496	0.9492	2.55	0.4347	0.910	2.00	3.49		2.81
t_r = 72.0°F	2	1.613	68.64	.1700	.9369	2.35	.4757	.880	1.85	10.6	2.81	3.69
p_r = 14.711 psia	3	1.881	68.34	.1983	.9364	2.12	.5271	.865	1.68	16.3	3.25	1.51
c_w = 0.982	4	1.997	68.07	.2106	.9359	2.03	.5474	.858	1.63	22.3	2.67	2.87
G = 30.59 lb/ft^{2}sec	5	2.229	69.01	.2350	.9376	1.88	.5850	.850	1.54	27.2	2.72	3.69
	6	2.556	69.85	.2695	.9391	1.71	.6318	.834	1.44	31.1	2.92	3.61
	7	2.922	71.19	.3080	.9414	1.55	.6767	.819	1.36	34.8	3.03	3.20
	8	3.306	74.72	.3486	.9477	1.41	.7168	.815	1.29	38.3	3.05	-
	9	6.023	79.27	.6350	.9558	0.852	.8733	.651	1.10	37.1	-	-
	10	6.313	83.19	.6656	.9627	.817	.8823	.683	1.09	41.2	-	
	11	5.619	86.87	.5924	.9693	.905	.8591	.782	1.12	46.5	-	
Run No. L-3	oi	97.470	104.99									
January 9, 1948	1	3.461	72.00	0.1541	0.9416	2.50	0.4439	0.895	4.64	8.10		3.38
t_r = 75.0°F	2	4.020	67.12	.1790	.9329	2.27	.4926	.868	4.23	24.2	3.38	1.88
p_r = 14.417 psia	3	4.347	67.71	.1935	.9340	2.15	.5187	.863	4.03	39.2	2.63	0.546
c_w = 0.995	4	4.443	67.35	.1978	.9333	2.12	.5261	.859	3.98	54.6	1.94	2.11
G = 72.39 lb/ft^{2}sec	5	4.828	68.10	.2149	.9347	2.00	.5544	.853	3.80	67.3	1.98	2.30
	6	5.271	68.44	.2347	.9353	1.89	.5845	.844	3.63	78.7	2.04	3.41
	7	5.983	69.67	.2663	.9375	1.72	.6278	.832	3.42	87.6	2.27	2.66
	8	6.600	71.35	.2938	.9404	1.60	.6610	.824	3.27	96.9	2.33	2.24
	9	7.178	72.06	.3195	.9417	1.50	.6888	.813	3.16	106.2	2.32	4.03
	10	8.448	74.68	.3761	.9463	1.32	.7404	.793	2.97	111.8	2.51	3.23
	11	10.009	85.00	.4455	.9646	1.15	.7896	.832	2.82	117.4	2.58	

TABLE 3 (continued) ORIGINAL DATA AND CALCULATIONS BASED ON ONE-DIMENSIONAL FLOW MODEL

	Station No.	p psia	t_{aw} °F	$\frac{pA}{c_w p_{oi} A^*}$	$\frac{T_{aw}}{T_{oi}}$	M	$\frac{T_m}{T_{oi}}$	r	Re_D x10^{-5}	Re_L x10^{-5}	$\bar{f}$ x10^3	f x10^3
Run No. L-4	oi	74.916	104.58									
January 13, 1948	1	2.640	73.16	0.1535	0.9443	2.51	0.4428	0.900	3.57	6.22		3.79
t_r = 73.0°F	2	3.122	67.47	.1815	.9342	2.25	.4973	.869	3.21	18.4	3.79	1.45
p_r = 14.666 psia	3	3.315	67.59	.1928	.9345	2.16	.5174	.864	3.10	30.1	2.62	0.980
c_w = 0.991	4	3.449	67.43	.2005	.9342	2.10	.5308	.860	3.03	41.5	2.07	2.58
G = 55.44 lb/ft^{2}sec	5	3.814	68.28	.2218	.9357	1.96	.5651	.852	2.87	50.7	2.20	2.35
	6	4.168	68.84	.2424	.9367	1.84	.5956	.843	2.74	59.3	2.23	3.20
	7	4.690	70.00	.2727	.9387	1.69	.6359	.832	2.59	66.4	2.39	3.09
	8	5.259	71.85	.3058	.9420	1.55	.6743	.822	2.46	73.0	2.49	2.90
	9	5.877	72.86	.3418	.9438	1.43	.7105	.806	2.36	79.3	2.54	3.70
	10	6.904	76.29	.4015	.9499	1.26	.7600	.791	2.23	83.9	2.67	-
	11	9.207	85.68	.5354	.9665	0.989	.8365	.795	2.07	85.9		
Run No. L-5	oi	16.810	101.68									
January 16, 1948	1	0.5592	71.99	0.1484	0.9471	2.56	0.4321	0.907	0.806	1.40		1.62
t_r = 73.0°F	2	.6031	63.82	.1600	.9326	2.44	.4560	.876	.767	4.39	1.62	1.82
p_r = 14.903 psia	3	.6538	63.60	.1735	.9322	2.32	.4823	.869	.729	7.08	1.72	1.94
c_w = 0.968	4	.7095	63.61	.1882	.9322	2.19	.5094	.862	.694	9.50	1.80	1.66
G = 12.18 lb/ft^{2}sec	5	.7588	63.73	.2013	.9324	2.10	.5321	.856	.667	11.8	1.76	1.02
	6	.7899	64.02	.2096	.9329	2.04	.5458	.852	.652	14.1	1.61	1.14
	7	.8257	64.90	.2191	.9345	1.98	.5609	.851	.637	16.3	1.53	0.720
	8	.8487	65.04	.2252	.9347	1.94	.5703	.848	.628	18.6	1.42	0.417
	9	.8622	67.74	.2288	.9395	1.92	.5758	.857	.623	20.9	1.29	-0.160
	10	.8570	68.77	.2274	.9414	1.93	.5737	.862	.625	23.5	1.13	-0.624
	11	.8369	75.49	.2221	.9533	1.96	.5655	.893	.632	26.3	0.956	
Run No. L-6	oi	23.090	102.44									
January 20, 1948	1	0.7683	72.58	0.1476	0.9469	2.57	0.4305	0.907	1.11	1.94		0.985
t_r = 73.0°F	2	.8048	63.93	.1547	.9315	2.50	.4451	.877	1.08	6.19	0.985	1.11
p_r = 14.867	3	.8456	63.63	.1627	.9310	2.42	.4614	.872	1.05	10.2	1.05	1.34
c_w = 0.973	4	.8930	64.01	.1726	.9316	2.32	.4806	.868	1.01	13.8	1.14	0.515
G = 16.81 lb/ft^{2}sec	5	.9181	64.82	.1764	.9331	2.29	.4879	.869	0.995	17.6	0.987	1.02
	6	.9583	65.36	.1842	.9340	2.23	.5021	.868	.969	21.0	0.992	1.25
	7	1.009	66.17	.1939	.9355	2.15	.5194	.866	.939	24.1	1.04	2.97
	8	1.134	66.85	.2180	.9367	1.99	.5592	.856	.880	26.1	1.31	3.30
	9	1.285	68.05	.2469	.9388	1.82	.6019	.846	.826	27.8	1.56	4.61
	10	1.523	69.65	.2927	.9417	1.61	.6597	.829	.764	28.7	1.90	3.90
	11	1.766	77.08	.3394	.9549	1.43	.7083	.845	.719	29.9	2.10	
Run No. L-7	oi	18.641	101.92									
February 13, 1948	1	0.6165	70.91	0.1472	0.9448	2.58	0.4296	0.903	0.900	1.57		1.29
t_r = 75.0°F	2	.6551	63.18	.1564	.9310	2.48	.4488	.875	.864	4.95	1.29	0.593
p_r = 14.771 psia	3	.6731	63.34	.1607	.9313	2.44	.4574	.873	.849	8.25	0.943	1.93
c_w = 0.970	4	.7327	62.62	.1749	.9300	2.30	.4851	.864	.806	11.0	1.27	1.31
G = 13.53 lb/ft^{2}sec	5	.7744	63.26	.1849	.9312	2.22	.5035	.861	.779	13.8	1.28	1.77
	6	.8325	63.94	.1988	.9324	2.12	.5278	.857	.746	16.2	1.38	1.19
	7	.8727	65.38	.2084	.9349	2.05	.5438	.857	.727	18.6	1.35	0.213
	8	.8800	66.20	.2101	.9364	2.04	.5467	.860	.723	21.4	1.19	0.430
	9	.8949	67.26	.2137	.9383	2.01	.5524	.862	.717	24.1	1.09	0.642
	10	.9173	67.11	.2190	.9380	1.98	.5609	.859	.707	26.6	1.04	0.836
	11	.9471	67.67	.2261	.9390	1.94	.5718	.858	.696	28.9	1.02	
Run No. L-8	oi	20.535	102.94									
February 18, 1948	1	0.6412	74.96	0.1388	0.9503	2.67	0.4115	0.915	1.03	1.79		1.19
t_r = 78.0°F	2	.6799	66.48	.1472	.9352	2.58	.4296	.886	0.989	5.67	1.19	1.17
p_r = 14.683 psia	3	.7186	66.18	.1556	.9347	2.49	.4470	.882	.954	9.26	1.18	1.32
c_w = 0.971	4	.7630	65.33	.1652	.9332	2.39	.4663	.875	.918	12.6	1.23	0.873
G = 14.91 lb/ft^{2}sec	5	.7928	65.68	.1717	.9338	2.33	.4789	.873	.897	15.9	1.14	1.03
	6	.8286	66.20	.1794	.9347	2.27	.4934	.871	.873	18.9	1.12	1.09
	7	.8673	67.72	.1878	.9374	2.20	.5086	.873	.848	21.8	1.11	0.660
	8	.8910	68.37	.1929	.9386	2.16	.5177	.873	.835	24.7	1.05	0.410
	9	.9059	69.38	.1962	.9404	2.13	.5233	.875	.827	27.8	0.970	3.03
	10	1.020	69.72	.2209	.9410	1.97	.5638	.865	.775	29.1	1.20	-0.188
	11	1.013	70.70	.2194	.9427	1.98	.5613	.869	.778	32.3	1.06	

TABLE 3 (continued) ORIGINAL DATA AND CALCULATIONS BASED ON ONE-DIMENSIONAL-FLOW MODEL

	Station No.	p psia	t_{aw} °F	$\frac{p A}{c_w p_{oi} A^*}$	$\frac{T_{aw}}{T_{oi}}$	M	$\frac{T_s}{T_{oi}}$	r	Re_D x10^{-5}	Re_L x10^{-5}	$\bar{f}$ x10^3	f x10^3
Run No. L-9	oi	14.943	102.18									
February 25, 1948	1	0.5088	73.01	0.1522	0.9481	2.52	0.4400	0.907	0.702	1.22		3.55
t_r = 77.0°F	2	.5960	66.56	.1783	.9366	2.28	.4913	.875	.635	3.64	3.55	3.05
p_r = 14.672 psia	3	.6754	67.17	.2020	.9377	2.09	.5333	.866	.590	5.73	3.30	1.30
c_w = 0.966	4	.7110	66.63	.2127	.9367	2.02	.5508	.859	.573	7.85	2.64	0.270
G = 10.80 lb/ft^{2}sec	5	.7186	69.16	.2149	.9412	2.00	.5544	.868	.570	10.1	2.04	-0.0540
	6	.7170	69.21	.2145	.9413	2.01	.5536	.869	.571	12.4	1.62	-1.19
	7	.6843	68.71	.2047	.9404	2.07	.5377	.871	.586	15.0	1.15	-0.386
	8	.6739	68.52	.2016	.9401	2.10	.5325	.872	.591	17.5	0.935	4.32
	9	.7959	69.68	.2381	.9422	1.87	.5894	.859	.541	18.2	1.36	5.14
	10	.9624	69.77	.2878	.9423	1.63	.6541	.833	.494	18.6	1.78	4.42
	11	1.138	75.49	.3404	.9525	1.43	.7092	.837	.462	19.2	2.04	
Run No. L-10	oi	10.790	100.52									
February 27, 1948	1	0.3738	72.58	0.1556	0.9501	2.49	0.4471	0.910	0.499	0.870		6.06
t_r = 75.0°F	2	.4840	67.61	.2015	.9413	2.10	.5325	.874	.426	2.44	6.06	2.48
p_r = 14.736 psia	3	.5331	67.96	.2220	.9419	1.96	.5654	.866	.404	3.93	4.27	1.30
c_w = 0.961	4	.5600	70.16	.2332	.9405	1.89	.5823	.857	.394	5.40	3.28	0.137
G = 7.771 lb/ft^{2}sec	5	.5629	69.75	.2344	.9451	1.89	.5841	.868	.393	6.95	2.49	0.138
	6	.5658	69.99	.2356	.9455	1.88	.5858	.868	.392	8.49	2.02	-1.21
	7	.5405	69.54	.2250	.9447	1.94	.5701	.871	.401	10.3	1.48	0.00
	8	.5405	68.35	.2250	.9426	1.94	.5701	.866	.401	11.9	1.27	3.12
	9	.6076	70.92	.2530	.9472	1.79	.6103	.864	.378	12.7	1.50	5.45
	10	.7431	71.02	.3094	.9473	1.54	.6782	.836	.346	13.0	1.94	5.29
	11	.9202	76.02	.3832	.9563	1.30	.7461	.828	.319	13.3	2.28	
Run No. F-3	oi	48.550	110.33									
March 9, 1950	1	1.929	81.10	0.1409	0.9487	2.65	0.4160	0.912	2.97	4.79		3.25
t_r = 75.5°F	2	2.247	77.47	.1641	.9424	2.40	.4641	.892	2.68	15.0	3.25	4.87
p_r = 14.550 psia	3	2.757	76.40	.2014	.9405	2.10	.5322	.873	2.37	22.7	4.06	0.694
p_v = 3.0 microns	4	2.834	76.28	.2070	.9403	2.06	.5415	.870	2.34	31.7	2.94	4.65
c_w = 0.985	5	3.383	76.96	.2471	.9415	1.82	.6021	.853	2.13	37.4	3.36	3.34
G = 43.91 lb/ft^{2}sec	6	3.826	77.55	.2794	.9425	1.66	.6441	.838	2.01	43.3	3.36	1.52
	7	4.047	78.60	.2956	.9443	1.59	.6630	.835	1.96	50.1	3.05	2.81
	8	4.499	79.97	.3286	.9467	1.47	.6978	.824	1.88	55.5	3.02	7.52
	9	6.656	83.78	.4861	.9534	1.07	.8127	.751	1.66	55.6	3.58	-
	10	8.196	88.07	.5986	.9609	0.897	.8613	.718	1.59	59.5	-	-
	11	7.830	96.50	.5719	.9757	.934	.8515	.837	1.60	66.4	-	
	of	3.248	109.66									
Run No. F-4	oi	38.736	110.19									
March 9, 1950	1	1.516	81.40	0.1392	0.9495	2.67	0.4123	0.914	2.38	3.84		3.12
t_r = 74.9°F	2	1.757	78.27	.1613	.9440	2.43	.4588	.897	2.16	12.1	3.12	4.76
p_r = 14.561 psia	3	2.152	77.04	.1976	.9418	2.12	.5257	.877	1.91	18.3	3.94	1.53
p_v = 6.0 microns	4	2.286	76.66	.2099	.9412	2.04	.5463	.870	1.84	25.0	3.14	4.38
c_w = 0.982	5	2.700	77.35	.2479	.9424	1.81	.6033	.855	1.69	29.7	3.45	3.53
G = 34.93 lb/ft^{2}sec	6	3.076	77.81	.2824	.9432	1.65	.6477	.839	1.59	34.3	3.46	2.03
	7	3.316	79.06	.3045	.9454	1.56	.6729	.833	1.54	39.4	3.23	2.93
	8	3.711	80.94	.3408	.9487	1.43	.7096	.823	1.48	43.5	3.18	-
	9	6.532	86.28	.5998	.9580	0.896	.8617	.697	1.26	42.3	-	-
	10	6.975	89.55	.6404	.9638	.845	.8750	.710	1.25	46.8	-	-
	11	6.407	97.37	.5883	.9775	.911	.8576	.842	1.27	52.6	-	
	of	2.065	-									
Run No. F-7	oi	19.307	107.47									
March 14, 1950	1	0.8261	74.13	0.1538	0.9412	2.51	0.4433	0.894	1.11	1.78		2.29
t_r = 75.0°F	2	.9158	73.03	.1704	.9392	2.34	.4765	.884	1.04	5.80	2.29	1.23
p_r = 14.705 psia	3	.9653	73.45	.1797	.9400	2.26	.4939	.881	1.00	9.61	1.76	0.789
p_v = 5.1 microns	4	.9978	74.72	.1857	.9422	2.21	.5049	.883	0.982	13.3	1.43	2.16
c_w = 0.972	5	1.089	74.54	.2027	.9419	2.09	.5344	.875	.934	16.4	1.62	3.33
G = 17.28 lb/ft^{2}sec	6	1.239	74.39	.2306	.9417	1.91	.5785	.862	.871	18.8	1.96	3.28
	7	1.400	75.63	.2606	.9438	1.75	.6204	.852	.820	20.9	2.18	4.14
	8	1.631	76.59	.3036	.9455	1.56	.6719	.834	.767	22.6	2.46	5.05
	9	1.991	79.61	.3706	.9508	1.34	.7359	.814	.711	23.8	2.78	-
	10	2.883	83.70	.5365	.9581	0.987	.8370	.743	.641	24.0	-	-
	11	2.902	91.42	.5401	.9717	.981	.8385	.825	.640	26.5	-	
	of	0.7453	108.11									

TABLE 3 (*continued*) ORIGINAL DATA AND CALCULATIONS BASED ON ONE-DIMENSIONAL FLOW MODEL

	Station No.	p psia	t_{aw} °F	$\frac{pA}{c_w p_{oi} A^*}$	$\frac{T_{aw}}{T_{oi}}$	M	$\frac{T_w}{T_{oi}}$	r	Re_D x10^{-5}	Re_L x10^{-5}	$\bar{F}$ x10^3	f x10^3
Run No. F-9	oi	8.834	105.61									
March 14, 1950	1	0.4180	71.35	0.1721	0.9394	2.33	0.4798	0.883	0.467	0.754		5.81
t_r = 74.0°F	2	.5294	72.46	.2180	.9414	1.98	.5593	.867	.407	2.28	5.81	3.69
p_r = 14.707 psia	3	.6084	72.56	.2506	.9415	1.80	.6070	.851	.379	3.64	4.75	0.880
p_v = 1.8 microns	4	.6285	73.19	.2588	.9427	1.76	.6181	.850	.374	5.07	3.46	0.856
c_w = 0.960	5	.6486	73.29	.2671	.9428	1.72	.6288	.846	.368	6.46	2.81	0.258
G = 7.820 lb/ft^{2}sec	6	.6548	73.27	.2697	.9428	1.71	.6321	.845	.367	7.90	2.30	-1.00
	7	.6311	73.58	.2599	.9433	1.75	.6195	.851	.373	9.52	1.75	-0.841
	8	.6118	73.92	.2520	.9439	1.79	.6089	.857	.378	11.2	1.38	2.29
	9	.6656	74.73	.2741	.9454	1.69	.6376	.849	.364	12.2	1.49	0.442
	10	.6765	74.53	.2786	.9450	1.67	.6431	.846	.361	13.5	1.38	5.54
	11	.8344	83.83	.3436	.9615	1.42	.7122	.866	.331	13.7	1.79	
	of	.3615	105.61									
Run No. F-36	oi	24.911	109.89									
April 18, 1950	1	0.9920	72.42	0.1427	0.9342	2.63	0.4198	0.887	1.49	2.41		1.96
t_r = 81.0°F	2	1.089	72.42	.1566	.9342	2.48	.4491	.881	1.41	7.87	1.96	1.13
p_r = 14.655 psia	3	1.146	73.08	.1648	.9354	2.40	.4655	.879	1.36	13.0	1.54	3.31
p_v = 11 microns	4	1.320	72.84	.1898	.9350	2.18	.5122	.867	1.25	16.9	2.13	4.40
c_w = 0.975	5	1.570	74.00	.2258	.9370	1.94	.5712	.853	1.13	19.9	2.70	3.37
G = 22.31 lb/ft^{2}sec	6	1.781	75.19	.2561	.9391	1.77	.6145	.842	1.06	22.9	2.84	3.58
	7	2.032	77.07	.2922	.9424	1.61	.6592	.831	1.00	25.6	2.96	10.2
	8	3.225	81.46	.4638	.9501	1.12	.8005	.750	0.855	25.2	3.99	-
	9	4.360	85.77	.6270	.9577	0.861	.8708	.672	.800	26.8	-	-
	10	4.552	88.03	.6546	.9616	.829	.8792	.682	.795	29.8	-	-
	11	4.206	92.58	.6048	.9696	.889	.8635	.777	.806	33.4	-	
	of	1.031	106.62									
Run No. F-43	oi	24.280	105.33									
May 2, 1950	1	0.9926	68.55	0.1465	0.9349	2.59	0.4280	0.886	1.45	2.34		2.01
t_r = 73.5°F	2	1.090	66.57	.1608	.9314	2.43	.4577	.874	1.36	7.63	2.01	1.25
p_r = 14.690 psia	3	1.152	68.54	.1700	.9349	2.35	.4756	.876	1.32	12.6	1.63	2.99
p_v = 4.6 microns	4	1.307	68.49	.1928	.9348	2.16	.5175	.865	1.22	16.5	2.08	4.07
c_w = 0.975	5	1.533	69.63	.2262	.9368	1.93	.5719	.852	1.12	19.6	2.58	3.07
G = 21.93 lb/ft^{2}sec	6	1.720	71.00	.2538	.9392	1.78	.6113	.844	1.05	22.7	2.68	4.16
	7	2.005	72.95	.2959	.9427	1.59	.6633	.830	0.983	25.1	2.92	10.0
	8	3.193	77.68	.4711	.9511	1.10	.8046	.750	.838	24.7	3.94	-
	9	4.233	82.16	.6245	.9590	0.864	.8700	.685	.789	26.4	-	-
	10	4.445	84.57	.6558	.9633	.828	.8795	.695	.782	29.3	-	-
	11	4.117	89.50	.6075	.9720	.886	.8644	.793	.792	32.9	-	
	of	1.037	102.56									
Run No. F-56	oi	44.722	121.77									
July 21, 1950	1	1.726	87.74	0.1370	0.9415	2.70	0.4074	0.901	2.70	4.36		2.49
t_r = 76.0°F	2	1.947	83.38	.1545	.9340	2.50	.4449	.881	2.49	14.0	2.49	5.20
p_r = 14.722 psia	3	2.438	82.82	.1935	.9330	2.15	.5187	.861	2.17	20.8	3.84	0.963
p_v = 5.8 microns	4	2.534	82.87	.2012	.9331	2.10	.5318	.857	2.12	28.8	2.88	5.11
c_w = 0.984	5	3.083	83.94	.2447	.9349	1.83	.5989	.838	1.92	33.7	3.44	3.04
G = 40.01 lb/ft^{2}sec	6	3.449	85.18	.2737	.9371	1.69	.6371	.827	1.82	39.2	3.36	2.18
	7	3.738	86.20	.2967	.9388	1.59	.6642	.818	1.76	44.8	3.16	3.07
	8	4.200	88.80	.3333	.9433	1.46	.7025	.809	1.68	49.4	3.15	-
	9	7.598	95.07	.6030	.9541	0.891	.8629	.665	1.42	47.7	-	-
	10	8.079	97.97	.6413	.9591	.844	.8752	.672	1.41	52.8	-	-
	11	7.636	101.96	.6061	.9659	.888	.8639	.750	1.42	58.9	-	
	of	3.035	126.07									
Run No. F-57	oi	33.770	122.11									
July 25, 1950	1	1.331	85.47	0.1405	0.9370	2.65	0.4152	0.892	2.00	3.22		1.89
t_r = 81.5°F	2	1.458	84.05	.1538	.9346	2.51	.4435	.882	1.88	10.5	1.89	4.51
p_r = 14.659 psia	3	1.775	83.42	.1874	.9335	2.20	.5079	.865	1.66	15.9	3.20	1.69
p_v = 5.7 microns	4	1.901	83.80	.2007	.9341	2.10	.5310	.860	1.60	21.7	2.70	4.22
c_w = 0.980	5	2.238	84.73	.2362	.9360	1.88	.5867	.845	1.47	25.7	3.08	3.17
G = 30.08 lb/ft^{2}sec	6	2.517	86.02	.2656	.9380	1.73	.6269	.834	1.39	29.8	3.09	3.65
	7	2.883	87.54	.3042	.9406	1.56	.6724	.819	1.31	33.3	3.19	9.90
	8	4.903	92.65	.5175	.9494	1.02	.8284	.705	1.10	32.6	4.15	-
	9	6.057	97.05	.6393	.9569	0.847	.8746	.656	1.06	35.4	-	-
	10	6.279	99.35	.6627	.9609	.820	.8815	.670	1.05	39.4	-	-
	11	5.788	103.14	.6109	.9674	.881	.8656	.757	1.07	44.2	-	
	of	1.843	122.79									

TABLE 3 *(continued)* ORIGINAL DATA AND CALCULATIONS BASED ON ONE-DIMENSIONAL FLOW MODEL

	Station No.	p psia	t_{aw} °F	$\frac{p\,A}{c_w p_{oi} A^*}$	$\frac{T_{aw}}{T_{oi}}$	M	$\frac{T_a}{T_{oi}}$	r	Re_D x10^{-5}	Re_L x10^{-5}	$\bar{r}$ x10^3	f x10^3
Run No. F-58	oi	77.576	122.81									
July 29, 1950	1	2.937	88.01	0.1333	0.9403	2.74	0.3992	0.901	4.81	7.76		3.65
t_r = 84.0°F	2	3.505	84.22	.1591	.9338	2.45	.4541	.879	4.27	23.9	3.65	4.74
p_r = 14.576 psia	3	4.293	83.87	.1949	.9332	2.14	.5211	.860	3.77	36.2	4.20	0.276
p_v = 7.3 microns	4	4.342	83.98	.1971	.9333	2.13	.5249	.860	3.75	50.9	2.89	5.18
c_w = 0.992	5	5.303	85.01	.2407	.9351	1.85	.5932	.840	3.37	59.2	3.46	0.862
G = 69.91 lb/ft^{2}sec	6	5.477	85.91	.2486	.9365	1.81	.6042	.840	3.32	71.5	2.94	3.94
	7	6.333	86.98	.2874	.9385	1.63	.6536	.822	3.11	79.3	3.11	1.32
	8	6.650	88.71	.3018	.9415	1.57	.6700	.823	3.04	89.8	2.85	3.89
	9	7.727	90.77	.3507	.9450	1.40	.7187	.804	2.87	96.1	2.98	3.59
	10	9.093	94.75	.4127	.9518	1.23	.7680	.792	2.71	101.7	3.05	-
	11	12.171	102.79	.5524	.9656	0.962	.8437	.780	2.53	104.7	-	
	of	-	122.68									
Run No. F-59	oi	5.004	119.02									
July 29, 1950	1	0.2503	81.05	0.1837	0.9344	2.23	0.5012	0.868	0.244	0.393		5.12
t_r = 85.0°F	2	.3065	79.61	.2249	.9319	1.94	.5702	.842	.218	1.22	5.12	5.40
p_r = 14.564 psia	3	.3750	81.46	.2752	.9351	1.68	.6390	.820	.197	1.89	5.26	1.99
p_v = 7.7 microns	4	.4035	81.47	.2961	.9351	1.59	.6637	.807	.191	2.60	4.17	2.64
c_w = 0.951	5	.4458	83.22	.3272	.9382	1.48	.6965	.796	.184	3.22	3.79	1.37
G = 4.337 lb/ft^{2}sec	6	.4705	83.63	.3453	.9389	1.42	.7138	.796	.180	3.88	3.30	0.122
	7	.4728	82.65	.3470	.9372	1.41	.7154	.779	.180	4.58	2.77	0.396
	8	.4805	84.80	.3527	.9409	1.39	.7204	.788	.179	5.27	2.43	-0.0401
	9	.4797	85.29	.3521	.9417	1.39	.7199	.792	.179	5.98	2.12	0.273
	10	.4851	86.70	.3560	.9442	1.38	.7235	.798	.178	6.67	1.92	-4.06
	11	.4143	92.76	.3041	.9547	1.56	.6707	.862	.190	7.86	1.32	
	of	.253	115.13									
Run No. F-60	oi	14.665	119.21									
August 1, 1950	1	0.6276	80.30	0.1546	0.9328	2.50	0.4450	0.879	0.809	1.31		2.19
t_r = 82.8°F	2	.6924	76.36	.1705	.9260	2.34	.4767	.859	.760	4.26	2.19	1.61
p_r = 14.665 psia	3	.7417	76.04	.1827	.9254	2.24	.4994	.851	.728	6.98	1.90	0.787
p_v = 4.5 microns	4	.7664	76.76	.1888	.9267	2.19	.5104	.850	.714	9.70	1.53	1.71
c_w = 0.967	5	.8211	77.78	.2022	.9284	2.09	.5337	.847	.687	12.1	1.57	0.680
G = 12.92 lb/ft^{2}sec	6	.8435	78.89	.2078	.9304	2.05	.5428	.848	.677	14.6	1.39	1.06
	7	.8789	80.28	.2165	.9328	1.99	.5568	.848	.662	16.9	1.34	0.810
	8	.9067	81.14	.2233	.9342	1.95	.5675	.848	.651	19.2	1.26	2.46
	9	.9946	82.19	.2450	.9361	1.83	.5993	.840	.621	20.8	1.41	2.48
	10	1.090	84.49	.2685	.9400	1.71	.6306	.838	.595	22.3	1.53	2.91
	11	1.214	94.43	.2989	.9572	1.58	.6668	.872	.567	23.5	1.67	
	of	-	116.50									
Run No. F-62	oi	3.126	103.05									
August 3, 1950	1	0.1717	64.40	0.2033	0.9313	2.08	0.5353	0.852	0.148	0.239		9.64
t_r = 75.5°F	2	.2468	65.89	.2921	.9340	1.61	.6590	.806	.124	.694	9.64	4.18
p_r = 14.736 psia	3	.2893	67.08	.3424	.9361	1.43	.7111	.779	.116	1.11	6.91	1.52
p_v = 5.6 microns	4	.3079	67.93	.3644	.9376	1.36	.7307	.768	.114	1.54	5.11	2.20
c_w = 0.944	5	.3403	68.71	.4028	.9390	1.25	.7610	.745	.110	1.93	4.38	-0.325
G = 2.727 lb/ft^{2}sec	6	.3349	69.29	.3964	.9400	1.27	.7563	.754	.110	2.38	3.44	1.01
	7	.3527	70.03	.4175	.9413	1.22	.7713	.743	.108	2.77	3.04	0.00
	8	.3527	70.21	.4175	.9416	1.22	.7713	.745	.108	3.20	2.60	0.00
	9	.3527	70.45	.4175	.9421	1.22	.7713	.747	.108	3.63	2.28	-0.0797
	10	.3512	70.80	.4157	.9427	1.22	.7701	.751	.109	4.08	2.02	-4.59
	11	.2862	75.38	.3387	.9508	1.44	.7077	.832	.117	4.84	1.35	
	of	.1898	-									
Run No. F-63	oi	3.521	107.16									
August 3, 1950	1	0.1856	69.16	0.1947	0.9330	2.15	0.5208	0.860	0.170	0.274		8.68
t_r = 75.0°F	2	.2584	68.98	.2709	.9326	1.70	.6337	.816	.143	.801	8.68	4.57
p_r = 14.689 psia	3	.3063	70.10	.3212	.9346	1.50	.6905	.789	.133	1.28	6.63	1.75
p_v = 4.7 microns	4	.3280	71.08	.3439	.9364	1.42	.7125	.779	.130	1.76	5.00	2.06
c_w = 0.946	5	.3574	71.93	.3748	.9379	1.33	.7393	.762	.126	2.21	4.27	0.662
G = 3.067 lb/ft^{2}sec	6	.3682	72.73	.3861	.9393	1.30	.7484	.759	.125	2.68	3.54	0.445
	7	.3759	73.51	.3943	.9406	1.28	.7546	.758	.124	3.16	3.03	0.253
	8	.3806	73.94	.3991	.9414	1.26	.7583	.758	.123	3.64	2.63	-0.167
	9	.3775	74.37	.3959	.9422	1.27	.7558	.763	.124	4.14	2.28	-0.0433
	10	.3767	75.41	.3950	.9440	1.27	.7552	.771	.124	4.63	2.02	-3.09
	11	.3295	82.48	.3456	.9565	1.42	.7140	.848	.129	5.37	1.51	
	of	.1510	101.93									

TABLE 3 (continued) ORIGINAL DATA AND CALCULATIONS BASED ON ONE-DIMENSIONAL FLOW MODEL

	Station No.	p psia	t_{aw} °F	$\frac{pA}{c_w p_{oi} A^*}$	$\frac{T_{aw}}{T_{oi}}$	M	$\frac{T_a}{T_{oi}}$	r	Re_D x10^{-5}	Re_L x10^{-5}	$\bar{F}$ x10^3	f x10^3
Run No. F-67	oi	34.150	118.81									
August 14, 1950	1	1.360	83.79	0.1420	0.9395	2.64	0.4184	0.896	2.02	3.26		1.68
t_r = 78.7°F	2	1.475	83.04	.1539	.9382	2.50	.4435	.889	1.92	10.7	1.68	4.71
p_r = 14.768 psia	3	1.811	81.66	.1890	.9358	2.19	.5108	.869	1.69	16.2	3.20	1.70
p_v = 5.6 microns	4	1.940	81.83	.2024	.9361	2.09	.5340	.863	1.62	22.0	2.70	4.27
c_w = 0.980	5	2.286	82.70	.2386	.9376	1.86	.5902	.848	1.49	26.1	3.09	2.91
G = 30.51 lb/ft^{2}sec	6	2.546	84.01	.2657	.9398	1.72	.6270	.839	1.41	30.4	3.05	3.45
	7	2.892	84.09	.3019	.9400	1.57	.6700	.818	1.33	34.1	3.12	10.09
	8	4.952	90.67	.5168	.9514	1.02	.8280	.717	1.12	33.2	4.12	-
	9	6.107	95.02	.6373	.9589	0.849	.8740	.674	1.08	36.1	-	-
	10	6.299	97.37	.6574	.9629	.826	.8800	.691	1.07	40.2	-	-
	11	5.799	99.29	.6052	.9663	.889	.8636	.753	1.09	45.1	-	
	of	1.815	118.84									
Run No. F-68	oi	14.768	114.92									
August 14, 1950	1	0.6354	76.97	0.1554	0.9340	2.49	0.4467	0.881	0.820	1.32		2.12
t_r = 77.1°F	2	.6988	73.49	.1709	.9279	2.34	.4774	.862	.772	4.33	2.12	1.55
p_r = 14.768 psia	3	.7467	73.14	.1826	.9273	2.24	.4993	.855	.741	7.11	1.84	1.32
p_v = 5.6 microns	4	.7885	73.13	.1928	.9273	2.16	.5176	.849	.718	9.74	1.66	1.19
c_w = 0.967	5	.8271	74.93	.2023	.9304	2.09	.5338	.851	.699	12.3	1.55	0.884
G = 13.06 lb/ft^{2}sec	6	.8565	75.99	.2095	.9323	2.04	.5456	.851	.685	14.8	1.41	0.956
	7	.8890	76.24	.2174	.9327	1.99	.5583	.848	.672	17.1	1.34	0.761
	8	.9152	78.08	.2238	.9359	1.95	.5683	.851	.661	19.5	1.25	2.73
	9	1.014	78.98	.2481	.9375	1.81	.6035	.842	.628	21.0	1.44	2.67
	10	1.119	81.08	.2738	.9411	1.69	.6372	.838	.600	22.5	1.58	3.29
	11	1.265	88.74	.3093	.9544	1.54	.6781	.858	.569	23.6	1.75	
	of	0.5803	-									
Run No. F-69	oi	54.728	119.05									
August 18, 1950	1	2.040	86.26	0.1319	0.9433	2.76	0.3961	0.906	3.43	5.53		3.71
t_r = 82.8°F	2	2.444	81.56	.1580	.9352	2.46	.4520	.882	3.04	17.0	3.71	5.03
p_r = 14.728 psia	3	3.031	81.05	.1960	.9343	2.14	.5230	.862	2.66	25.5	4.37	0.546
p_v = 14 microns	4	3.098	81.09	.2003	.9344	2.10	.5305	.860	2.63	35.7	3.09	4.98
c_w = 0.987	5	3.753	82.06	.2426	.9361	1.84	.5960	.842	2.38	41.7	3.57	1.83
G = 49.23 lb/ft^{2}sec	6	4.016	83.05	.2597	.9378	1.75	.6192	.837	2.30	49.6	3.22	3.64
	7	4.593	82.67	.2970	.9371	1.59	.6646	.813	2.17	55.3	3.29	2.12
	8	4.974	86.03	.3216	.9429	1.50	.6909	.815	2.10	61.9	3.12	3.64
	9	5.763	89.24	.3726	.9485	1.33	.7376	.804	1.99	66.6	3.19	-
	10	9.197	94.57	.5947	.9597	0.902	.8599	.698	1.76	66.0	-	-
	11	9.072	99.26	.5866	.9658	0.913	.8570	.761	1.77	73.2	-	
	of	4.201	121.13									
Run No. F-70	oi	64.734	119.30									
August 19, 1950	1	2.442	85.62	0.1331	0.9418	2.75	0.3987	0.903	4.04	6.52		3.71
t_r = 84.6°F	2	2.923	81.33	.1593	.9344	2.45	.4546	.880	3.58	20.1	3.71	5.11
p_r = 14.734 psia	3	3.635	81.10	.1981	.9340	2.12	.5266	.861	3.14	30.1	4.41	0.461
p_v = 17 microns	4	3.702	81.30	.2018	.9344	2.09	.5329	.859	3.11	42.2	3.10	4.87
c_w = 0.990	5	4.462	82.26	.2432	.9360	1.84	.5967	.841	2.82	49.4	3.54	1.14
G = 58.39	6	4.654	83.23	.2537	.9377	1.78	.6112	.840	2.76	59.4	3.06	3.91
	7	5.375	82.88	.2930	.9371	1.60	.6600	.815	2.59	66.0	3.20	1.63
	8	5.712	86.18	.3113	.9428	1.53	.6802	.821	2.52	74.4	2.98	4.01
	9	6.693	88.21	.3648	.9463	1.36	.7310	.800	2.37	79.6	3.10	-
	10	9.982	93.53	.5441	.9555	0.975	.8402	.721	2.13	79.7	-	-
	11	10.502	100.95	.5724	.9683	0.933	.8517	.786	2.10	87.2	-	
	of	7.136	118.09									
Run No. F-72	oi	5.167	106.43									
August 25, 1950	1	0.2563	68.58	0.1820	0.9331	2.24	0.4981	0.867	0.261	0.422		4.46
t_r = 79.6°F	2	.3065	67.48	.2176	.9312	1.99	.5586	.844	.236	1.32	4.46	5.09
p_r = 14.790 psia	3	.3709	69.27	.2633	.9344	1.74	.6240	.825	.215	2.06	4.77	2.90
p_v = 4.4 microns	4	.4126	70.51	.2930	.9365	1.60	.6601	.813	.205	2.78	4.15	1.88
c_w = 0.952	5	.4427	71.28	.3144	.9379	1.52	.6834	.804	.199	3.49	3.58	0.877
G = 4.533 lb/ft^{2}sec	6	.4578	71.80	.3251	.9388	1.48	.6944	.800	.196	4.22	3.04	0.980
	7	.4756	71.28	.3377	.9379	1.44	.7067	.788	.193	4.93	2.70	1.12
	8	.4976	73.03	.3533	.9410	1.39	.7210	.789	.190	5.61	2.47	-0.679
	9	.4840	73.44	.3437	.9417	1.42	.7123	.797	.192	6.43	2.08	-0.302
	10	.4783	74.81	.3396	.9441	1.43	.7085	.808	.193	7.22	1.81	-2.42
	11	.4358	82.32	.3094	.9574	1.54	.6782	.868	.200	8.29	1.39	
	of	.2211	104.04									

TABLE 4 SAMPLE CALCULATION

Station No.	$\frac{L}{D}$	p (psia)	t_{aw} (°F)	$\frac{T_{aw}}{T_{oi}}$	G^*_6 ($\frac{lbm}{ft^2 sec}$)	T^* (°Fabs)	$\mu^*_m \times 10^5$ ($\frac{lbm}{ft\ sec}$)	(Re^*_D) $\times 10^{-5}$	c_w	$\frac{pA}{c_w p_{oi} A^*}$	M
--	msd.	msd.	msd.	--	Eq.(9)	Eq.(10)	Fig.14	Eq.(11)	Fig.13	--	Eq.(8)
Run No. F-9 oi		8.834	105.61								
March 14, 1950 1	1.614	0.4180	71.35	0.9394	28.45	471.08	1.120	0.5684	0.960	0.1721	2.33
t_T = 74.0°F 2	5.600	.5294	72.46	.9414						.2180	1.98
p_T = 14.707 psia 3	9.586	.6084	72.56	.9415						.2506	1.80
p_V = 1.8 microns 4	13.57	.6285	73.19	.9427						.2588	1.76
A/A^* = 3.493 5	17.56	.6486	73.29	.9428						.2671	1.72
6	21.54	.6586	73.27	.9428						.2697	1.71
7	25.53	.6311	73.58	.9433						.2599	1.75
8	29.51	.6118	73.92	.9439						.2520	1.79
9	33.50	.6656	74.73	.9454						.2741	1.69
10	37.49	.6765	74.53	.9450						.2786	1.67
11	41.47	.8344	83.83	.9615						.3436	1.42
of		.3615	105.61								

	$\frac{T_m}{T_{oi}}$	T_m (°Fabs)	$\mu_m \times 10^5$ ($\frac{lbm}{ft\ sec}$)	r	G ($\frac{lbm}{ft^2 sec}$)	Re_D $\times 10^{-5}$	Re_L $\times 10^{-5}$	$\psi_{(M)}$	$\psi_1 - \psi_j$	$\bar{f}$ $\times 10^3$	$\psi_j - \psi_{j+1}$	f $\times 10^3$
	Eq.(12)	--	Fig.14	Eq.(13)	Eq.(14)	Eq.(15)	Eq.(16)	Eq.(19)	--	Eq.(20)	--	Eq.(20)
oi												
1	0.4798	271.21	0.700	0.883	7.820	0.467	0.754	0.3931	0.00			
2	.5593	316.17	.803	.867		.407	2.28	.3005	.0927	5.81	0.0927	5.81
3	.6070	343.11	.862	.851		.379	3.64	.2417	.151	4.75	.0588	3.69
4	.6181	349.41	.875	.851		.374	5.07	.2277	.165	3.46	.0140	0.880
5	.6288	355.48	.888	.846		.368	6.46	.2140	.179	2.81	.0137	0.856
6	.6321	357.32	.892	.845		.367	7.90	.2099	.183	2.30	.0041	0.258
7	.6195	350.20	.877	.851		.373	9.52	.2259	.167	1.75	-.0160	-1.00
8	.6089	344.19	.864	.857		.378	11.2	.2393	.154	1.38	-.0134	-0.841
9	.6376	360.45	.899	.849		.364	12.2	.2028	.190	1.49	.0365	2.29
10	.6431	363.56	.906	.846		.361	13.5	.1958	.197	1.38	.0070	0.442
11	.7122	402.63	.987	.866		.331	13.7	.1074	.286	1.79	.0884	5.54
of												

The determination of the friction coefficient is accomplished as follows:

For an infinitesimal length of supersonic flow in a tube of constant area, it can be shown from the momentum theorem that

$$\frac{4f}{D}\,dx = \frac{1 - \mathbf{M}^2}{k\mathbf{M}^4\left(1 + \frac{k-1}{2}\,\mathbf{M}^2\right)}\,d\mathbf{M}^2 \quad \ldots\ldots [17]$$

Integration from a section at which x is zero and the Mach number is $\mathbf{M}$ to the section at which the Mach number is unity and x is the maximum possible length gives

$$4\bar{f}L_{max}/D = \frac{1 - \mathbf{M}^2}{k\mathbf{M}^2} + \frac{k+1}{2k}\ln\left[\frac{(k+1)\mathbf{M}^2}{2\left(1 + \frac{k-1}{2}\,\mathbf{M}^2\right)}\right] \quad \ldots [18]$$

$$\equiv \psi(\mathbf{M}) \quad \ldots\ldots [19]$$

Note that the function $\psi(\mathbf{M})$ is tabulated elsewhere.[9]

The mean apparent friction coefficient between two stations with Mach numbers of $\mathbf{M}_1$ and $\mathbf{M}_2$ is found from

$$4\bar{f}\Delta L/D = (4\bar{f}L_{max}/D)_{M(1)} - (4\bar{f}L_{max}/D)_{M(2)} = \psi_{M(1)} - \psi_{M(2)} \quad \ldots\ldots [20]$$

where ΔL is the distance between the two stations. If the two stations are adjacent, the mean apparent friction coefficient has been termed in this paper the "local" apparent friction coefficient at a point midway between the two stations. If the two stations correspond to the first and any other station in the tube, the resulting value has been termed the "mean" apparent friction coefficient up to the latter station. If the first station is not at the entrance to the tube, as in these measurements, the values of this mean coefficient at the upstream end of the tube may be in error.

Occasionally the calculations based on the one-dimensional flow model indicate that the stream changes from supersonic to subsonic flow in the tube. Since the foregoing analysis for friction coefficient is invalid for changes from supersonic to subsonic flow, values of the local apparent friction coefficient were not calculated for those states where the flow appeared to become subsonic.

Sample Calculation. A sample calculation of Run F-9 is given in Table 4. The calculations and equation numbers given in the headings refer to the preceding analysis.

[Part 2 of this paper will be published in a later issue of the JOURNAL OF APPLIED MECHANICS.—EDITOR.]

[9] Reference (15), table 42.

The Theoretical Analysis of Metal-Forming Problems in Plane Strain[1]

By E. H. LEE,[2] PROVIDENCE, R. I.

The plastic flow in plane strain of an ideally plastic material subjected to large strains is considered. Elastic strains are negligible and a rigid-plastic type of analysis is adopted. The equations to be satisfied are detailed, and they include stress and velocity equations in the plastic regions, as well as consideration of the stress field in the rigid regions to check the validity of small strains there. Complete solutions satisfying these conditions require the determination of the rigid-plastic boundaries to delineate the regions in which the various conditions must be satisfied. The fallacy of static determinacy of such problems in terms of the stress equations only is emphasized. The study of complete solutions indicates errors in solutions commonly accepted in the literature which are based on the stress equations only. Examples are discussed. The general occurrence of velocities in the boundary conditions of forming problems is pointed out, and the difficulty of setting such problems in terms of boundary stresses only is illustrated by examples.

Introduction

THE analysis of metal-forming problems is concerned with the distribution of large strains due to plastic flow. Strains of the order unity occur, so that elastic strains which are of the order 0.1 per cent, are negligible in comparison. Therefore we shall adopt a rigid-plastic type of analysis, in which elastic material is considered rigid. It is found that in certain regions of a body where the yield limit is exceeded, plastic flow is constrained by surrounding elastic material to be limited to the order of magnitude of elastic strains, so that these regions also can be considered rigid. Thus rigid regions appearing in the analysis have not necessarily been subjected to elastic strain only. This rigid-plastic type of analysis is satisfactory for determining the stress and strain distributions in the regions of appreciable plastic strain. The complete analysis of the "rigid" regions would require the consideration of elastic strains, but, for the study of metal-forming, it is the regions of appreciable strain which are of interest, so that the type of analysis used here is adequate.

We shall consider an ideally plastic material which flows plastically at a constant yield limit. The corresponding stress-strain relationship in tension is shown by the line AB in Fig. 1, and the theory corresponds to a true stress, natural strain relation of this type, for we deal with natural strain increments in the analysis. The adoption of this idealized relationship must not be thought of as neglecting work-hardening, but rather as averaging its effect over the field of flow. For when a complete solution of the type to be described has been obtained, the final strain distribution is determined, and so an average strain magnitude can be used to determine the appropriate average yield stress for substitution in the equations based on the ideal material. For example, if the average strain is OE in Fig. 1, AB would be an approximate idealization of the actual curve CD, and is seen to provide a reasonable approximation for the over-all range of strain. Neglecting work-hardening would imply a horizontal line through C in Fig. 1, which would involve considerable error.

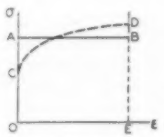

Fig. 1

The analysis of strain distributions on the basis of the foregoing idealizations has been found to give good agreement with experiments even in the case of lead, which exhibits a rounded stress-strain curve in the yield region with gradual development of plastic flow (1).[3]

The importance of determining strain distributions in the analysis of metal-forming is associated with the calculation of the work absorbed, and the efficiency of particular processes. If the object of a procedure is to reduce the section of a body, in most cases the resulting strain distribution involves internal deformation which absorbs work without contributing to the change of section. In assessing a particular process, such losses must be analyzed, and the way in which they are influenced by process variables must be determined. A complete solution of the type discussed in this paper would permit such an evaluation.

General Theory

We will now consider conditions in the regions of appreciable plastic flow. The ideal plastic material discussed in the previous section is one which deforms plastically when the yield limit, which is a function of the stress components, is maintained at a constant value. We shall use the Mises criterion (2) which has been found to be satisfactory for most metals. This gives, using Cartesian co-ordinates

$$(\sigma_y - \sigma_z)^2 + (\sigma_z - \sigma_x)^2 + (\sigma_x - \sigma_y)^2 + 6(\tau_{xy}^2 + \tau_{yz}^2 + \tau_{zx}^2) = 2Y^2 \quad [1]$$

where Y is the yield stress in tension.

[1] The conclusions presented in this paper were obtained in the course of research conducted under Contract N7onr-358 sponsored by the Office of Naval Research and the Bureau of Ships.

[2] Associate Professor of Applied Mathematics, Graduate Division of Applied Mathematics, Brown University. Mem. ASME.

Contributed by the Applied Mechanics and Metals Engineering Divisions and presented at the Annual Meeting, Atlantic City, N. J., November 25–30, 1951, of The American Society of Mechanical Engineers.

Discussion of this paper should be addressed to the Secretary, ASME, 29 West 39th Street, New York, N. Y., and will be accepted until April 10, 1952, for publication at a later date. Discussion received after the closing date will be returned.

Note: Statements and opinions advanced in papers are to be understood as individual expressions of their authors and not those of the Society. Manuscript received by ASME Applied Mechanics Division, November 20, 1950. Paper No. 51—A-8.

[3] Numbers in parentheses refer to the Bibliography at the end of the paper.

The resulting increments of plastic strain are given to a satisfactory degree of accuracy (3) by the Mises relation (2)

$$\frac{d\epsilon_x - d\epsilon_y}{\sigma_x - \sigma_y} = \frac{d\epsilon_y - d\epsilon_z}{\sigma_y - \sigma_z} = \frac{d\epsilon_z - d\epsilon_x}{\sigma_z - \sigma_x} = \frac{d\gamma_{xy}/2}{\tau_{xy}} = \frac{d\gamma_{yz}/2}{\tau_{yz}} = \frac{d\gamma_{zx}/2}{\tau_{zx}} = d\lambda' \geq 0 \quad [2]$$

combined with no volume change

$$d\epsilon_x + d\epsilon_y + d\epsilon_z = 0 \quad [3]$$

$d\lambda'$ is a parameter which represents the magnitude of the increment of plastic flow. It is determined by the constraint of the surrounding material, for each element is capable of unlimited flow at the yield limit, according to the concept of ideal plasticity. The term $d\lambda'$ must be positive to insure that the resulting strain corresponds with the stress applied; for example, to insure that under tensile stress, tensile and not compressive strain increments occur.

For flow in plane strain parallel to the xy-plane, the foregoing relations take simple forms. The flow condition becomes

$$(\sigma_x - \sigma_y)^2 + 4\tau_{xy}^2 = 4k^2 \quad [4]$$

where k is the yield stress in shear. For this case the Mises criterion coincides with the Tresca criterion of constant maximum shear stress. The strain-increment relations, Equations [3] and [2], can be expressed in terms of the distribution of particle velocity, which has components u_x, u_y parallel to the corresponding axes. They become

$$\frac{\partial u_x}{\partial x} + \frac{\partial u_y}{\partial y} = 0 \quad [5]$$

and

$$\frac{\frac{\partial u_x}{\partial x} - \frac{\partial u_y}{\partial y}}{\sigma_x - \sigma_y} = \frac{\frac{\partial u_x}{\partial y} + \frac{\partial u_y}{\partial x}}{2\tau_{xy}} = \lambda \geq 0 \quad [6]$$

where λ is a parameter which represents the rate of strain, and which is associated with the previous parameter λ'.

Many metal-forming problems are concerned with slow flow, such that inertia forces are negligible in comparison with the forces required to produce plastic deformation. We shall study this type of problem, so that the stress system must satisfy the equations of equilibrium

$$\frac{\partial \sigma_x}{\partial x} + \frac{\partial \tau_{xy}}{\partial y} = 0, \quad \frac{\partial \sigma_y}{\partial y} + \frac{\partial \tau_{xy}}{\partial x} = 0 \quad [7]$$

It might be mentioned that since time does not appear in the stress-strain relations, or in the equilibrium equations, the velocity components need not be referred to time, but to any other parameter, such as the displacement of a boundary, which is a measure of the progress of the deformation.

The conditions in the regions of plastic flow are specified by the three stress components σ_x, σ_y, and τ_{xy}, and the velocity components u_x and u_y. The stress components must obey the three Equations [4] and [7], and the velocity components must obey the Equations [5] and [6] which also include stresses.

Since Equation [4] implies constant maximum shear stress throughout the field of plastic flow, it is convenient, following Hencky (4), to consider the stress field in terms of the trajectories of maximum shear stress, or slip lines, shown in Fig. 2. These orthogonal trajectories are used to define curvilinear co-ordinates α, β. The stress system at each point is completely determined by the slip-line direction, defined by the angle φ in Fig. 2, and the average hydrostatic pressure p. In terms of these two variables, Equations [4] and [7] become[4]

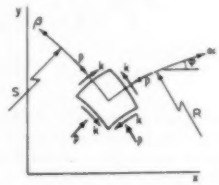

FIG. 2

$$\left.\begin{aligned} p + 2k\varphi &\text{ is constant along an } \alpha\text{-line} \\ p - 2k\varphi &\text{ is constant along a } \beta\text{-line} \end{aligned}\right\} \quad [8]$$

It is convenient also to work in terms of the radii of curvature of the slip lines, R and S shown in Fig. 2. Equations [4] and [7] are equivalent to the differential relations

$$\left.\begin{aligned} dS + Rd\varphi &= 0 \text{ along an } \alpha\text{-line} \\ dR - Sd\varphi &= 0 \text{ along a } \beta\text{-line} \end{aligned}\right\} \quad [9]$$

Referring the velocity equations to these co-ordinates, if u, v are the velocity components in the α, β directions, respectively, Equations [5] and [6] imply the differential relations

$$\left.\begin{aligned} du - vd\varphi &= 0 \text{ along an } \alpha\text{-line} \\ dv + ud\varphi &= 0 \text{ along a } \beta\text{-line} \end{aligned}\right\} \quad [10]$$

Let us now consider the rigid regions. They must be able to withstand the tractions to which their boundaries are subjected without appreciable deformation. These tractions may be due to stresses transmitted across plastic-rigid boundaries, or to surface loads. Moreover, the velocity distribution in plastic regions adjacent to plastic-rigid boundaries, must be compatible with the rigid-body motion of the rigid regions.

We wish to analyze the plastic deformation without determining the stress distribution in the rigid regions, which would involve an elastic-plastic analysis. We shall consider the influence of the rigid regions by requiring that it must be possible to extend the plastic stress distribution into the rigid regions to insure that all stress boundary conditions could be satisfied without exceeding the maximum shear stress k. In many cases where a rigid wedge extends into the plastic region, a narrowing of the wedge would produce lower external forces for deformation of the system. In such a case it is reasonable to expect that in this wedge the limiting stress distribution with constant maximum shear stress k will be developed in order to transmit the boundary stresses between the two parts of the plastic region. A less severe distribution involving shear stresses less than the maximum permissible would call for a wider wedge angle and so a greater external force. It is in such cases that the stress distribution in a rigid region is crucial in the development of the plastic solution. In other cases where the rigid material is not required to carry limiting stress, the plastic field should be extended to show that the plastic-rigid boundary tractions can be transmitted through a limiting stress region subjected to the maximum permissible shear stress, combined with additional supporting material. In this case, the limiting stress distribution would be expected to spread into the supporting material to give an elastic stress distribution with magnitudes of the maximum shear stress less than k.

[4] Details of this and the subsequent analysis of this section are given in reference (1).

The velocity condition adjacent to a rigid region requires the velocity field to be compatible with the rigid-body motion, which can be considered as at rest, by using velocities relative to that of the adjacent rigid body. This does not modify the velocity Equations [5] and [6]. Equations [5] and [6] constitute a pair of hyperbolic equations with the slip lines as characteristics. This implies that the boundary, which is a line of discontinuity of velocity or its derivatives, must be a slip line, but an independent proof of this requirement is given in the Appendix. This applies whether or not the boundary is moving relative to the rigid material.

In the next section we consider the application of the conditions and equations stated in this section to the analysis of metal-forming problems.

Complete Solutions

A complete solution is one which satisfies all the conditions discussed in the previous section. This term is used to distinguish such solutions from solutions of the stress equations only, Equations [4] and [7], which have been commonly accepted in the literature as satisfactory solutions of plastic-flow problems. The conditions to be satisfied are summarized as follows:

(*a*) The stress Equations [4] and [7] in the plastic region.

(*b*) The velocity Equations [5] and [6] in the plastic region, with a check of the sign of λ.

(*c*) Velocity compatibility of the plastic-rigid boundaries, that they are slip lines of the plastic fields.

(*d*) Satisfactory extension of the stress field into the rigid regions to check the validity of small strains there.

(*e*) Satisfaction of stress and velocity boundary conditions.

Since the theory considers large strains, the last condition may require considerations of the motion of the boundaries due to the flow occurring. However, a group of problems exists, called initial motion problems, in which the strains can be considered sufficiently large to adopt a rigid-plastic type of analysis, and yet sufficiently small to produce no appreciable deformation of the boundaries, so that the boundary conditions can be referred to the initial position of the boundaries. This combination is possible since elastic-strain magnitudes are so small.

Following Hencky (4), it has been commonly accepted (see, for example, references 5 and 6) that since the three stress components σ_x, σ_y, and τ_{xy} are given by the three stress Equations [4] and [7], plastic-flow problems in plane strain are statically determinate. However, as has been emphasized in recent papers (see, for example, references 7, 8, 9, 10), velocity magnitudes commonly occur in the boundary conditions and in the conditions which determine the extent of the plastic regions, so that a complete solution is necessary for the adequate analysis of a problem. Moreover, with any plastic-stress field, there is associated an infinite number of solutions of the velocity Equations [5] and [6], and so an infinity of plastic-flow problems. This state of affairs differs from the theory of elasticity in which a stress distribution uniquely determines a corresponding strain distribution, and so represents a complete solution. The lack of appreciation of this difference may have been partly responsible for the common acceptance of stress fields as adequate solutions to plastic-flow problems. In fact, as will be demonstrated in the next section, many stress solutions of physical problems which have appeared in the literature are at best only plausible, but may not even be approximations to the correct stress distributions. The check is whether a corresponding complete solution can be found, and in many cases the boundary conditions on velocities determine no corresponding velocity field, or only ones which do not represent the particular problem being considered.

Mises (11), and Geiringer (12) were the first to point out the need for complete solutions, and the fact that velocity magnitudes generally appear in the boundary conditions was emphasized by Geiringer and Prager (13). However, the influence of the rigid regions was not discussed in these papers, and this represents a severe complication in the problem. Initially, the regions in which the plastic equations are to be solved are not known, and the complete solution involves the free-boundary problem of the determination of the plastic-rigid boundaries.

The stress Equations [4] and [7], and the velocity Equations [5] and [6] are each equivalent to a pair of hyperbolic partial differential equations with the slip lines for characteristics. This suggests the possibility of the existence of discontinuities of the dependent variables or their derivations across these curves, and of building up solutions by joining particular solutions along characteristics. This is the way in which most solutions have been developed. It is found that discontinuities in stress derivatives, and in the tangential component of velocity can occur across slip lines. In the latter case, since velocity derivatives are not defined, the Mises flow relationship must be satisfied by a limiting process as discussed for the plastic-rigid boundary in the Appendix. Solutions with such velocity discontinuities satisfy equilibrium and the conditions of plasticity for the ideally plastic material under consideration. In this sense they are not to be thought of as approximations. However, at such discontinuities the idealization of the stress-strain relation will have its greatest effect, and in practice the influence of work-hardening will be to smooth out such discontinuities. Discontinuities in stress components can also occur in plane plastic flow as was pointed out by Prager (14), but these must be associated with elastic regions of infinitestimal width at the discontinuity surface (9), and conditions there do not satisfy the equations for plastic flow.

As an example of the influence of the rigid regions in determining a complete solution, let us consider the indentation of a perfectly rough obtuse-angled wedge into a plastic material. For simplicity we will consider the initial motion problem with the material boundaries as shown in Fig. 3. This is a special case of the indentation of a curved cylindrical indenter considered by Prandtl (15).

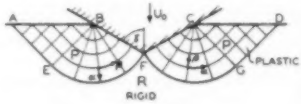

Fig. 3(*a*)

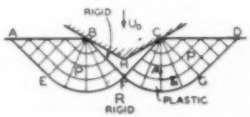

Fig. 3(*b*)

Consider first the plastic field shown in Fig. 3(*a*). It is built up from the well-known slip-line patterns used by Prandtl which are special solutions of Equations [9]. Along *AB* and *CD* the slip lines intersect the surface of the material at 45 deg to correspond with zero surface traction there. Since the wedge surfaces are perfectly rough, slip along them must occur in the plastic material and not at the material-wedge interface, so that *BF* and *CF* are slip lines.

The vertical velocity U_o of the punch and the fixed rigid region R, are combined with Equations [10] to determine a satisfactory velocity field. Term u is zero, and $v = U_o \sin \gamma$ throughout $ABFE$, where γ is the semiangle of the wedge. Since the plastic-rigid boundary $AEFGD$ is a slip line, we need now only check the stress distribution in the rigid region R. At the apex F the tangents to the boundaries of the rigid region form an acute-angled wedge, of angle 180 deg 2γ, with the maximum shear stress k on its surfaces as shown in Fig. 4(a).

We will consider the extension of the plastic stress field into such a wedge, and make the reasonable assumption that results based upon this will apply to the actual rigid region bounded by circular arcs, for the same conditions will apply at the apex in both cases. In addition to the shear traction shown in Fig. 4(a), there is a constant normal pressure on the wedge surface which does not influence plastic flow. The extension of the plastic fields shown in Fig. 4(a), leads to inconsistent shear-stress components on the central axis, which is emphasized by the direction of the shear-stress components shown on the material element toward the base of the wedge. The fact that these boundary tractions cannot be transmitted through such a wedge with a shear stress not greater than k can be checked alternatively from a study of the Mohr circle for the stress system at the apex, for the planes subjected to the shear stress k are not at right angles, so that the radius of the Mohr circle must be greater than k. Thus the solution shown in Fig. 3(a), cannot be considered a satisfactory complete solution since a stress field cannot be found for the rigid region compatible with small strains there.

Had the apex angle of the rigid region at F been 90 deg, Fig. 4(b) shows that the plastic fields could have been extended to produce a uniform stress distribution in the wedge with the maximum shear stress k throughout. With an apex angle greater than 90 deg, Fig. 4(c) shows that the plastic regions could be extended to a central supporting wedge subjected only to hydrostatic pressure with no shear stress. The hyperbolic nature of the equations of plastic flow, combined with the rigidity of the central region, subjected to hydrostatic pressure, implies no strain in the adjacent regions, so that the whole wedge remains rigid. Thus we have a stress system with shear stress not exceeding k, which maintains small strains in the wedge. We would in fact expect the regions to coalesce to give an elastic distribution with maximum shear stress less than k.

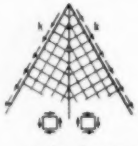

FIG. 4(a)

FIG. 4(b)

FIG. 4(c)

These considerations indicate that the only complete solution of the type considered is that shown in Fig. 3(b), in which the slip lines BF and CF are orthogonal. This insures satisfactory extension of the plastic fields in the rigid region below F, and in the rigid region $BHCF$. A uniform stress field in $BHCF$ gives acceptable tractions at the wedge surface since it is perfectly rough and can sustain any shear stress less than k. Thus, although satisfactory plastic solutions are given by a configuration similar to Fig. 3(b), with F anywhere on the vertical below H, consideration of the rigid regions determines Fig. 3(b), to represent the unique complete solution of this type. The wedge carries a false nose of the plastic material which performs the penetration. Such a nose is observed experimentally in armor penetration with blunt projectiles.

The type of solution discussed in this section attempts to determine the plastic flow for large strains without following through the complete development of the flow pattern, as the strain builds up from the elastic solution. This is a difficult requirement which may not be achievable in certain cases. Moreover, these solutions may not be unique, and we may have to make a choice between a number of possible solutions. This often can be done on general grounds. The correct physical problem is that which results from the limit of elastic-plastic work-hardening solutions, and this may determine a single solution when the foregoing theory does not. In spite of these difficulties the method gives correct solutions as checked by agreement with experiment (1, 16), but these questions emphasize the need for further experimental work, and for study of the development of plastic solutions from the initial elastic deformation. The latter type of problem has been investigated by Allen and Southwell (17) and by Jacobs (18, 19), using relaxation methods, but has been carried only to cases where plastic strains are of the order of elastic strains. These solutions cover the case where plastic regions have spread completely across a section of the body considered, but a study of the solutions indicates that considerable change must take place in the further development of the flow pattern before strains, large compared with elastic strains, can occur. Further extension of these solutions appears to be extremely tedious and may involve difficulties due to the change from predominantly elliptic to hyperbolic equations.

Discussion of Some Solutions in the Literature

In the previous section we have discussed the lack of completeness of solutions of the stress equations only, and the fact that such solutions which have appeared in the literature may not even be approximations to the corresponding complete solutions. In this section we consider some examples.

Let us consider the solution given by Prandtl (15) for the indentation of a rough cylindrical punch. The slip-line field is shown in Fig. 5. This type of solution has been used extensively by Sokolovsky (5). $GHBA$ is a false nose of the type discussed in the previous section. The slip-line field in $ABCF$ consists of tangents and involutes to the surface of the indenter. In CFE we have circular arcs and radii through C, and CED is a uniform stress field with the straight slip lines inclined at 45 deg to CD. Prandtl showed that this field satisfies the stress equations and the free surface boundary condition on CD. It determines a distribution of pressure on ABC, the indenter surface modified by the false nose, and so determines the indenting force required. The direction of the shear stresses on the slip lines determines the α, β-directions as shown.

Let us now consider the associated velocity solution. Let ψ be the inclination of the boundary ABC to the vertical. On AB $\psi = 45$ deg, and it decreases toward C. Application of the second of Equations [10], with $d\varphi$ zero since the β-lines are straight, determines constant v along each β-line, which must be zero throughout, since the rigid material below $AFED$ is at rest. The first of Equation [10] then determines u to be constant on each α-line, and the conditions of continuous normal velocity across the surface of the indenter gives $u = U_o \sin \psi$, since the stress solution requires the punch to press against the body all along ABC.

Let us now consider the magnitude of λ in Equation [6]. For simplicity we will consider the region CED and Cartesian axes along ED and EC as shown. Then the second term in Equation [6] becomes $(\partial u/\partial y)/(2k)$, since $u_x = u$, $u_y = v = 0$, and $\tau_{xy} = k$, the first term being indeterminate. Using the expression for u previously determined, Equation [6] becomes

$$\frac{U_0 \cos \psi}{2k} \frac{\partial \psi}{\partial y} = \lambda \geq 0$$

But ψ decreases with increasing y between B and C (i.e., as the curve ABC is traversed), so that $\partial\psi/\partial y$ is negative, and the inequality is violated. Along the boundary $AFED$ the discontinuity in velocity produces an infinite rate of shear strain which determines positive λ there. Thus this solution is not a satisfactory complete solution of the problem. The difficulty is clear from a kinematical standpoint as illustrated by the velocity profile for CE shown in Fig. 5. The velocity imparted to the material as it crosses the plastic-rigid boundary is sufficient to carry the material above it away from the indenter surface. To prescribe that the material remain in contact with the indenter along ABC, as does the stress solution, demands shear of the material toward the indenter, which is opposite to the direction of the shear stress. This condition indicates that the correct solution determines local pressure in the region of the nose of the indenter, with separation of the indenter and plastic material further back toward the surface of the material. The corresponding stress field would be quite different from that shown in Fig. 5. It should, perhaps, be mentioned that this difficulty with Prandtl's solution does not arise if the indenter has the form of a straight-sided wedge, as considered in the preceding section.

It was mentioned in the preceding section that there is an infinite number of velocity solutions associated with a particular stress field, and, accordingly, one can suggest many physical problems for which Fig. 5 is the correct stress field, although the rigid indenter is not among them. For example, if we consider an indenter with hinges at B and G, such that the sides BC and GJ open out as the indentation proceeds, with sufficient angular velocity to maintain positive λ, the stress field in Fig. 5 determines the satisfactory complete solution.

Van Iterson (6) considers many metal-forming problems in terms of the stress equations only. There are many examples in his work where the position of a rigid-plastic boundary prevents the determination of a satisfactory velocity field, so that the stress field given is incorrect. An example of another type of error which can arise occurs in his consideration of the stress field associated with the machining of a ductile material with a rough tool. This is shown in Fig. 6. For the initial motion problem before the surface of the work ABF has been deformed appreciably, this field determines a satisfactory complete solution. However, this initial force is of no technological interest, since, during almost the entire cut, a steady problem occurs with the chip being formed continuously and carried away up the tool face. From the standpoint of the stress field only, such a chip could be considered attached to AB, and merely carried away as an unstressed rigid body, since no surface tractions occur along AB. Presumably van Iterson considers this case, for he compares the resulting tool force with measurements made in continuous machining. However, a study of the velocity equations

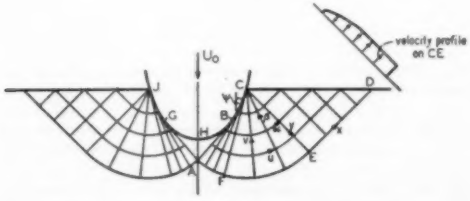

FIG. 5

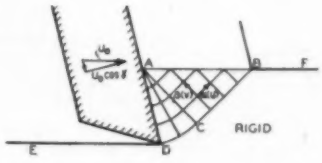

FIG. 6

shows that no satisfactory velocity solution is associated with this stress field.

The velocity solution is similar to that associated with Fig. 5 and detailed in the foregoing. Consider the tool to be moving and the work to be at rest. Then the linear β-lines and continuity across DCB determines v to be zero throughout. This, combined with the velocity condition at the tool face AD, determines u to be constant throughout and equal to the component of the tool velocity normal to the tool face. Because of the rotation of the slip lines through DAC, the velocity component of the particles of AB normal to the tool face is equal to u cos DAC, so that the chip which is carried on AB, will have a velocity component normal to the tool face less than that of the tool itself. This is incompatible with a steady-state solution; thus the stress field shown in Fig. 6 is not correct for this condition. Satisfactory complete solutions for such machining problems have been given by Lee and Shaffer (20).

A further graphic demonstration of the pitfalls to be encountered in the consideration of the metal-forming problems in terms of the stress equations only appears in a paper by Siebel (21). Siebel appreciated the difficulty and gave alternative solutions to certain problems, without being able to choose between them. These difficulties are resolved when the associated velocity solutions are examined. The consideration of his work from the standpoint of complete solutions is given in the discussion of the paper by Hill, Lee, and Orowan [see discussion of reference (21)].

From these few examples it is evident that much of the early work on stress distributions in metal-forming problems needs re-examination from the standpoint of complete solutions.

TYPES OF PROBLEMS

It was stated in the section, Complete Solutions, that metal-forming problems, in general, have mixed boundary conditions involving both surface tractions and surface velocities. This is apparent from the consideration of some common processes. For example, in rolling with rough rolls, the surfaces in contact with the rolls have prescribed velocities, and the surfaces outside the rolls are stress-free. In this case, as for most examples, the force initiating the plastic flow is transmitted through boundaries having prescribed velocities. The magnitude and distribution of this force are determined by the solution of the plastic-flow problem. This is usually the case, for, in general, it is difficult or impossible, without first obtaining a complete solution, to specify a forming problem generated by a prescribed stress distribution. A simple example will be used to emphasize this point.

Consider a parallel-sided slab of material stressed in tension or compression in plane strain, the slab surfaces being free from traction. The resulting behavior depends on the magnitude of the applied stress σ in comparison with the tensile yield stress in plane strain, $2k$.

If $|\sigma| < 2k$, the slab is strained elastically and no plastic flow occurs. If $\sigma = 2k$, tensile plastic strain can occur, and if $\sigma = -2k$, compressive plastic strain. If $|\sigma| > 2k$, no equilibrium solution is possible with the ideal plastic material which we are considering. Thus, to set this problem in terms of stress-boundary values to determine plastic flow requires a precise choice of

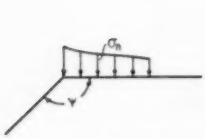

FIG. 7(a)

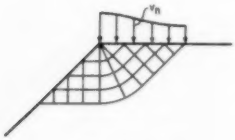

FIG. 7(b)

the stress σ. In fact, $\sigma = \pm 2k$. No such precision is required to set the problem in terms of velocity boundary conditions on the part of the surface where the force is applied. With the present rigid-plastic type of analysis, approach of the ends gives plastic flow in compression for all velocity magnitudes; and separation of the ends gives plastic flow in tension.

From consideration of this example, it might appear that one could set a plastic-flow problem in terms of stress-boundary values, by assuming proportionate increase of all boundary tractions until flow occurs. However, a study of particular examples indicates that a trivial type of solution is likely to result in which plastic flow occurs at a point only in the plane of flow, or along a line.

Consider, for example, a straight-sided wedge with pressure on one face as shown in Fig. 7(a). Plastic flow can be generated in such a wedge by prescribing a normal surface-velocity distribution, as shown in Fig. 7(b), with zero shear component of surface traction. If the distribution of normal velocity v_n is not compatible with a rigid-body motion of the surface, plastic flow must occur in the wedge material. For v_n decreasing away from the apex as shown, Fig. 7(b) shows the slip-line field which gives a satisfactory complete solution. It is determined uniquely by the unstressed surface and the zero shear traction where the velocity is prescribed. It determines uniform pressure over the top surface where the velocity is prescribed. This particular distribution of pressure is the only one which determines flow throughout the apex of the wedge, and with it acting, any monotonically decreasing distribution of normal velocity under the pressure is permissible.

If the pressure distribution shown in Fig. 7(a) is applied, with the magnitude increasing from zero proportionately at all points, flow will occur in an infinitesimal region at the apex, when the maximum pressure (which occurs at the apex) reaches the pressure determined for Fig. 7(b). Apart from local flow at the apex, the wedge will remain undeformed, for the pressure along the face will be smaller than that required to produce general flow. Thus, setting a stress-boundary-value problem with any pressure distribution which has its maximum value at the apex, gives plastic flow at one point only in the plane, the material otherwise remaining rigid. If a finite band of pressure which increases away from the apex is applied, a consideration of the interaction of the stress fields determined by the surface tractions indicates that as the pressure is increased proportionately, flow will occur along a line rather than throughout a region, with the apex of the wedge remaining rigid. Thus it appears from this example, that in general, one can only set a stress-boundary-value problem to give flow throughout a region if the corresponding complete solution is known. There are of course exceptions to this statement where the symmetry of a problem implies general flow, such as the slab considered previously, or a circular tube with uniform internal pressure.

If a wedge with curved sides is considered, the problem analogous to that shown in Fig. 7(b) determines a unique pressure distribution which is not uniform, and this particular distribution will generate flow throughout the wedge.

This difficulty of setting plastic-flow problems in terms of stress-boundary values has not been recognized generally. For example, Christianovich (22) considers closed regions with prescribed normal and shear tractions on their boundaries. His method of attack is to assume that the problems correspond to plastic-flow conditions, and to solve the corresponding stress Equations [4] and [7] with the given boundary conditions.

As is to be expected with the solution of hyperbolic equations in closed domains, difficulties arise, the characteristics forming an envelope beyond which the solution cannot be carried. At such an envelope, stress derivatives become infinite, and Christianovich termed such envelopes lines of rupture, and ascribed to them physical significance as potential regions of failure. However, such a solution can have no physical meaning, for in a satisfactory solution the body must be divided into plastic and rigid regions, and not into plastic regions and regions about which nothing can be determined.

The error in this type of analysis is clear from the example considered in the first part of this section, for the stress-boundary values may determine a purely elastic problem, an elastic-plastic problem, or no equilibrium solution for an ideal plastic material. Therefore one cannot assume a plastic region around the entire boundary and proceed to solve the stress equations of plasticity.

As a simple example, consider the slab in tension treated in the foregoing, and illustrated in Fig. 8. Assuming plastic flow throughout, the slip-line configuration determined uniquely by the boundary conditions is shown, and consists of straight lines at 45 deg to the boundaries. The boundary AD determines the field in AED, BC that in BCF, the remainder being determined by the lateral unstressed boundaries.

FIG. 8

In this case the lines of rupture take the particular form of discontinuities in the normal stress across AE, ED, BF, and FC, unless $\sigma = \pm 2k$, when the stress field is uniform. From the previous discussion the solution is purely elastic for $|\sigma| < 2k$, and none exists for $|\sigma| > 2k$. The lines of stress discontinuity AE, ED, BF, and FC have no physical significance, for the plastic stress field represents the solution only for $\sigma = \pm 2k$ when the discontinuities disappear. For $|\sigma| < 2k$, the slab is elastic, and the stress equations of plasticity do not apply.

It was emphasized in the section, Complete Solutions, that one of the main difficulties in the theoretical analysis is the determination of the plastic-rigid boundaries, and so of the regions in which the equations of plastic flow apply, and this is neglected entirely when an attempt is made merely to solve the plastic-stress equations throughout.

Conclusions

This paper emphasizes the need to study complete solutions of plane plastic-flow problems, which satisfy all the equations and conditions specified in the section Complete Solutions. In addition to the inequality on λ and the rigid-body conditions, this calls for the solution of two pairs of first-order hyperbolic equations containing derivatives of stresses and velocities, respectively. The slip lines are characteristics of both, and solutions are required in closed regions. This type of problem has not commonly occurred in other branches of applied mechanics. The extensive work on the stress equations only, although unsatisfactory when considered on its own, is required in the development of complete solutions. For example, in the wedge problem discussed in the preceding section, the stress field is built up from the unstressed surface by means of the stress equations. The velocity equations are needed only to ascertain that there is an associated satisfactory velocity solution. In many cases it may not be necessary actually to obtain the

velocity solution if the stress distribution only is required, the satisfactory form of the velocity solution being apparent by inspection.

Although general methods for handling this type of free-boundary problem are not available, many particular examples have been obtained. In addition to those already cited in the Bibliography, these include (23, 24, 25, and 26).

BIBLIOGRAPHY

1 "The Theory of Wedge Indentation of Ductile Materials," by R. Hill, E. H. Lee, and S. J. Tupper, Proceedings of the Royal Society of London, series A, vol. 188, 1947, pp. 273–289.

2 "Mechanik der festen Koerper in plastischen deformablen Zustand," by R. von Mises, *Goettinger Nachrichten, Mathematik und Physik*, vol. Kl. 1913, pp. 582–592.

3 "The Plastic Distortion of Metals," by G. I. Taylor and H. Quinney, Philosophical Transactions of the Royal Society of London, series A, vol. 230, 1931, pp. 323–362.

4 "Über einige statische bestimmte Faelle des Gleichgewichts in plastischen Koerpern," by H. Hencky, *Zeitschrift für angewandte Mathematik und Mechanik*, vol. 3, 1923, pp. 241–251.

5 "Theory of Plasticity," by W. W. Sokolovsky, Moscow, USSR, 1946 (Russian, English summaries).

6 "Plasticity in Engineering," by F. K. Th. van Iterson, Hafner Publishing Company, New York, N. Y., 1947.

7 "The Solution of Plane Strain Problems in the Plastic Flow of Metals Under Large Strains," by E. H. Lee and R. Hill, Sixth International Congress of Applied Mechanics, Paris, France, 1946.

8 "The Plastic Yielding of Notched Bars Under Tension," by R. Hill, *Quarterly Journal of Mechanics and Applied Mathematics*, vol. 2, 1949, pp. 40–51.

9 "On Stress Discontinuities in Plane Plastic Flow," by E. H. Lee, Proceedings of the Third Annual Symposium of Applied Mathematics, American Mathematical Society, Ann Arbor, Mich., 1949, pp. 213–228.

10 "A Method of Numerical Analysis of Plastic Flow in Plane Strain and Its Application to the Compression of a Ductile Material Between Rough Plates," by R. Hill, E. H. Lee, and S. J. Tupper, JOURNAL OF APPLIED MECHANICS, Trans. ASME, vol. 73, 1951, p. 46.

11 "Bemerkungen zur Formulierung des mathematischen Problems der Plastizitaetstheorie," by R. von Mises, *Zeitschrift für angewandte Mathematik und Mechanik*, vol. 5, 1925, pp. 147–149.

12 "Beitrag zum voltstaendigen ebenen Plastizitaetsproblem," by H. Polaczek-Geiringer, Proceedings of the Third International Congress of Applied Mechanics, vol. 2, 1930, pp. 185–190.

13 "Mechanik isotroper Koerper im plastischen Zustand," by H. Geiringer and W. Prager, *Ergeb. d. exact. Naturwiss*, vol. 13, 1934, pp. 310–363.

14 "Discontinuous Solutions in the Theory of Plasticity," by W. Prager, Courant Anniversary Volume, 1948, pp. 289–299.

15 "Anwendungsbeispiele zu einem Henckyschen Satz über das Plastische Gleichgewicht," by L. Prandtl, *Zeitschrift für angewandte Mathematik und Mechanik*, vol. 3, 1923, pp. 401–406.

16 "Experiments on the Compression of a Body Between Rough Plates," by J. F. Nye, British Armaments Research Department Report 39/47, 1947.

17 "Relaxation Methods Applied to Engineering Problems. XIV—Plastic Straining in Two Dimensional Stress Systems," by D. N. de G. Allen and R. V. Southwell, Philosophical Transactions of the Royal Society, vol. 242, 1950, pp. 379–414.

18 "Relaxation Methods Applied to Problems of Plastic Flow. I—Notched Bar Under Tension," by J. A. Jacobs, *Philosophical Magazine*, seventh series, vol. 41, 1950, pp. 349–361.

19 Ibid., II, *Philosophical Magazine*, seventh series, vol. 41, 1950, pp. 458–467.

20 "The Theory of Plasticity Applied to a Problem of Machining," by E. H. Lee and B. W. Shaffer, Brown University Technical Report All-43, 1949, under Contract with the Office of Naval Research. JOURNAL OF APPLIED MECHANICS, Trans. ASME, vol. 73, 1951, pp. 405–413.

21 "The Application to Shaping Processes of Hencky's Laws of Equilibrium," by E. Siebel, *Journal of the Iron and Steel Institute*, vol. 155, 1947, pp. 526–534. Discussion, vol. 156, 1947, pp. 511–522.

22 "The Plane Problem of the Mathematical Theory of Plasticity in the Case Where the External Forces Are Applied Along a Closed Contour," by S. Christianovich, *Mat. Sbornik*, vol. 1, 1936, pp. 511–534 (Russian).

23 "A Theoretical Analysis of the Stresses and Strains in Extrusion and Piercing," by R. Hill, *Journal of the Iron and Steel Institute*, vol. 158, 1948, pp. 177–185.

24 "A New Theory of the Plastic Deformation in Wire Drawing," by R. Hill and S. J. Tupper, *Journal of the Iron and Steel Institute*, vol. 159, August, 1948, pp. 353–359.

25 "Some Special Problems of Indentation and Compression in Plasticity," by R. Hill, Proceedings of the Seventh International Congress of Applied Mechanics, vol. 1, 1948, pp. 365–377.

26 "Plastic Flow in a V-Notched Bar Pulled in Tension," by E. H. Lee, Brown University Report, 1950. To be presented at the Annual Conference of the ASME Applied Mechanics Division, The Pennsylvania State College, State College, Pa., June, 19–21, 1952. Paper No. 52—APM-4.

Appendix

DETERMINATION OF PLASTIC-RIGID BOUNDARY

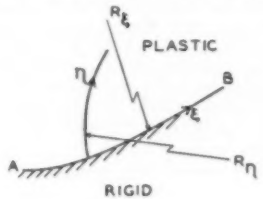

FIG. 9

In Fig. 9 consider the instantaneous position of a segment of the plastic-rigid boundary AB, and superpose velocities to bring the rigid body to rest. Let the velocity distribution in the plastic region be represented by components u_ξ, u_η in the directions of any orthogonal curvilinear co-ordinates ξ, η, for which AB is a co-ordinate curve of constant η.

Then the strain-rate components are

$$\dot{\epsilon}_{\xi\xi} = \frac{du_\xi}{ds_\xi} - \frac{u_\eta}{R_\xi}, \quad \dot{\epsilon}_{\eta\eta} = \frac{du_\eta}{ds_\eta} - \frac{u_\xi}{R_\eta}, \quad \dot{\gamma}_{\xi\eta} = \frac{du_\eta}{ds_\xi} + \frac{du_\xi}{ds_\eta} + \frac{u_\xi}{R_\xi} + \frac{u_\eta}{R_\eta}$$

where R_ξ and R_η are the radii of curvature of the co-ordinate lines, and s_ξ, s_η are are lengths along the co-ordinate lines ξ, η increasing, respectively. Continuity requires u_η to vanish on AB. Incompressibility demands that

$$\dot{\epsilon}_{\xi\xi} + \dot{\epsilon}_{\eta\eta} = 0$$

Suppose u_ξ is not zero in the plastic material adjacent to AB so that there is a velocity discontinuity across AB. Then the derivative $(du_\xi)/(ds_\eta)$ in $\dot{\gamma}_{\xi\eta}$ is not defined, since the ratio of infinitesimals increases without limit across AB. Other terms in the strain-rate components are finite, so that $\dot{\gamma}_{\xi\eta}$ approaches infinity while $\dot{\epsilon}_{\xi\xi}$ and $\dot{\epsilon}_{\eta\eta}$ remain finite. Substitution into the Mises condition, Equation [2], taking x, y parallel to ξ, η at the point in question, replacing the increments by strain-rate components, and writing $\dot{\epsilon}_z = \dot{\gamma}_{zx} = \dot{\gamma}_{zy} = 0$ for plane strain, determines $\sigma_{\xi\xi} = \sigma_{\eta\eta}$, so that AB is a slip line. It might be pointed out that the discontinuity in u_ξ does not necessarily imply separation of the material there, but only finite strain if the boundary AB is moving.

Suppose now that $u = 0$ on AB, then $(du_\xi)/(ds_\xi) = 0$, and incompressibility combined with zero u_η requires $(du_\eta)/(ds_\eta)$ to be zero. Thus, $\dot{\epsilon}_{\xi\xi} = \dot{\epsilon}_{\eta\eta} = 0$, while $\dot{\gamma}_{\xi\eta}$ will not be zero if $(du_\xi)/(ds_\eta)$ is not zero, and again Mises relation Equation [2] requires AB to be a slip line.

The conditions considered in the foregoing cover most problems encountered, for the condition that all first derivatives of velocity are zero is not common.

The Optimum Problem of the Sandwich Plate

By W. FLÜGGE,[1] STANFORD, CALIF.

While numerous papers have been published on the stability of sandwich plates in compression, Fig. 1, so far, attention has almost exclusively been focused on the problem of finding the critical load under which the plate becomes unstable, assuming that the dimensions and the materials are given. Some 7 or 8 years ago the author realized that this is not enough for practical purposes. The engineer needs some advice as to how the dimensions of a plate should be chosen in order to obtain a favorable relation between its weight and the load carried. The method used in answering this question will be explained in this paper.

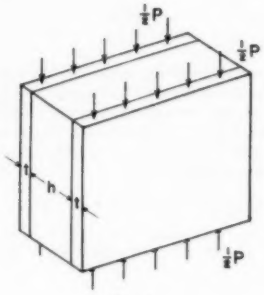

FIG. 1

INTRODUCTION

THE general result of sandwich theory is illustrated by the two curves shown in Fig. 2. They describe the critical load in terms of the length l of a buckling wave (half period) when everything else is kept constant. Both scales of these curves are logarithmic.

Curve 1 belongs to a plate having a thin core made of a rather rigid material. Its buckling load decreases monotonically with increasing l, and, therefore, a plate of any length b will always buckle with the wave length $l = b$.

Quite different and more characteristic is the curve 2. It belongs to a sandwich plate which has thin faces and a thick core of a very fluffy material. If either $b > l_1$ or $b < l_2$, the plate will again buckle with one wave only, the case $b < l_2$ being without practical interest. But when the length of the plate is such that $l_2 < b < l_1$, the plate will subdivide in many short waves of length l_2 and will become unstable at the corresponding load P_2. Following the general usage, we shall call this short-wave instability "wrinkling," reserving the word "buckling" for the instability which resembles the buckling of a solid plate.

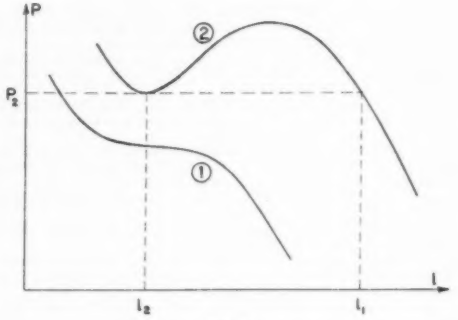

FIG. 2

BUCKLING

Curves like No. 1 are the result of an elaborate theory and of lengthy computations, but for the essential parts of curve 2, rather generous simplifications are possible which lead to simple formulas. For the descending part to the right, it is enough to introduce into the buckling theory a term which takes care of the shear deformation of the core.

When the plate is compressed transversely, Fig. 3(*a*), and when its short edges are unsupported, we have the simple Euler case[2] and find

$$P_1 = \frac{E' I \pi^2}{b^2 + \dfrac{E' I \pi^2}{G_c h}}$$

Here $E' = E/(1 - \nu^2)$ is the plate modulus of the face material, and G_c the shear modulus of the core material. I is the moment of inertia per unit width of cross section, in which we may neglect the insignificant contribution of the core and the term in t^3 writing

$$I = \frac{1}{2}\, t h^2$$

We introduce

$$\zeta = \frac{\pi^2}{2}\,\frac{E'\, t h}{G_c\, b^2}$$

[1] Associate Professor, School of Engineering, Stanford University.

Presented at the National Western Conference of the Applied Mechanics Division, Stanford, Calif., June 22–23, 1951, of THE AMERICAN SOCIETY OF MECHANICAL ENGINEERS.

Discussion of this paper should be addressed to the Secretary, ASME, 29 West 39th Street, New York, N. Y., and will be accepted until April 10, 1952, for publication at a later date. Discussion received after the closing date will be returned.

NOTE: Statements and opinions advanced in papers are to be understood as individual expressions of their authors and not those of the Society. Manuscript received by ASME Applied Mechanics Division, July 6, 1951.

[2] "Theory of Elastic Stability," by S. Timoshenko, McGraw-Hill Book Company, Inc., New York, N. Y., 1936, p. 140, equation 92.

and write the buckling formula in the following form

$$P_1 = \frac{\pi^2}{2} E' \frac{th^2}{b^2} \frac{1}{1+\zeta} \qquad [1a]$$

It is possible to introduce a similar shear term into the theory of plate buckling and thus to treat a plate strip under lengthwise compression, Fig. 3(*b*). The result is a formula which contains the wave length l

$$P_1 = 2\pi^2 E' \frac{th^2}{b^2} \frac{(b^2+l^2)^2}{4b^2[l^2+\zeta(b^2+l^2)]}$$

From this formula the curves in Fig. 4 have been plotted. They show P_1 versus l/b for $\zeta \gtrless 1$. If $\zeta < 1$, P_1 has a minimum for a certain value of l, and one easily may verify that this minimum is given by the following formula

$$P_1 = 2\pi^2 E' \frac{th^2}{b^2} \frac{1}{(1+\zeta)^2}, \qquad \zeta \leqq 1 \qquad [1b]$$

and that the corresponding wave length is

$$l = b\sqrt{\frac{1-\zeta}{1+\zeta}} \qquad [2]$$

If $\zeta > 1$, two minima and one maximum combine to a very shallow minimum at $l = 0$. It is

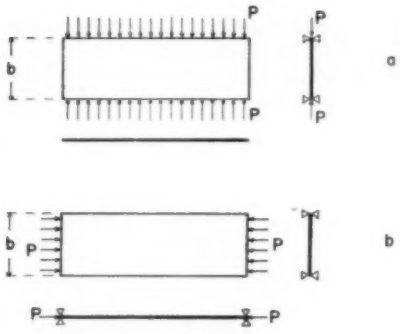

FIG. 3

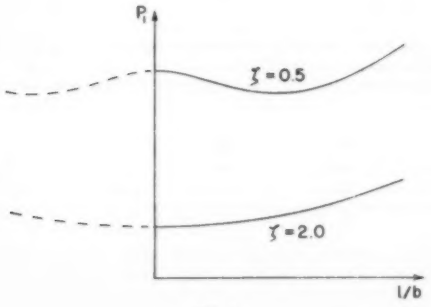

FIG. 4

$$P_1 = 2\pi^2 E' \frac{th^2}{b^2} \frac{1}{4\zeta}, \qquad \zeta \geqq 1 \qquad [1b']$$

Of course, a zero wave length does not make much sense, but what really happens is this: Our simple formulas neglect the individual bending rigidity $E't^3/12$ of each face sheet. This rigidity has a tendency to increase the wave length, but since the minimum of P_1 is so shallow, its value is not much raised by this shifting to the right. We necessarily must exclude this possible refinement of the theory from our graphs since it would introduce an additional parameter, but it may be advisable to check numerical results in the region of high values of ζ by a more elaborate theory.

WRINKLING

The other type of instability of a sandwich plate, wrinkling, is characterized by a very short wave length and is dominated by the individual flexural rigidity of the faces, the core acting as a kind of elastic bedding which opposes the lateral deflection of each face. If the critical load of a sandwich plate is represented by a curve like No. 1 in Fig. 2, the two faces influence each other across the core, but when the curve of load versus wave length looks like No. 2, the bedding stresses do not penetrate deeply. In the latter case the wrinkling load is independent of the core thickness h and just the same as if each face sheet were fixed to a half space of core material. Then the theory of a bar on elastic foundation[8] may be applied which yields the critical load

$$P_2 = 2\left(\frac{E' t^3\pi^2}{12l^2} + \frac{\beta l^2}{\pi^2}\right)$$

Here β is the modulus of foundation. In most applications of the theory of a bar on elastic foundation it is assumed that β is a constant. This would be true if the foundation were a kind of a spring mattress; but when it is an elastic body, β depends upon the wave length l, the half period of the sinusoidal load imposed on its surface

$$\beta = \frac{2\pi}{3l} E_c$$

If the core material is isotropic, E_c almost equals its elastic modulus E_c; and if it is anisotropic, E_c is a certain function of all its moduli. When we introduce the expression for β into the formula for P_2, we have

$$P_2 = 2\left(\frac{E' t^3\pi^2}{12l^2} + \frac{2}{3} E_c \frac{l}{\pi}\right)$$

and now we may choose l such as to make P_2 a minimum. The result will be

$$l = \frac{\pi t}{2}\sqrt[3]{\frac{2E'}{E_c}} \qquad [3]$$

and

$$P_2 = t\sqrt[3]{2E' E_c^2}$$

For later use we write the load in the form

$$P_2 = 2E' t\,\mu^{2/3} \quad \text{with} \quad \mu = \frac{E_c}{2E'} \qquad [4]$$

Since the wrinkles are very narrow, it is immaterial whether or not the unloaded edges of the plate are supported, and the formula applies to both cases, Figs. 3(*a*) and (*b*).

[8] Reference (2), p. 110, equation [74].

The Optimum Problem

When a sandwich plate is designed, the aim will be either to find the plate of minimum weight per unit of its surface Q for a given critical load P, or the plate with the maximum critical load P for a given weight Q. In both cases it may be supposed that the following data are fixed in advance:

Width b of panel (Fig. 3),

Material of faces, that is, its plate modulus E' and its specific gravity γ,

General type of core material so that its shear modulus G_c, its modulus E_c, as defined in the preceding section, and its specific weight γ_c are all proportional to each other, but in the whole will depend upon the degree of fluffiness which will be adopted.

The dimensions which still must be determined are the core thickness h and the face thickness t, Fig. 1. In addition, the degree of fluffiness of the core material may still be chosen within certain limits. Since G_c, E_c, γ_c are proportional, the ratios

$$m = \frac{2G_c\gamma}{E'\gamma_c} \quad \text{and} \quad \delta = \frac{E_c}{2G_c}$$

are given constants, and when we have chosen γ_c the moduli are fixed.

To get an idea of the optimum problem, let us consider a series of plates of the same width b and of the same weight

$$Q = 2t\gamma + h\gamma_c$$

and even of the same t. We may still vary γ_c and h, but $h\gamma_c$ and hence hG_c must be constant. When we plot P_1 from Equation [1a] and P_2 from Equation [4], we obtain the curves shown in Fig. 5, rising or falling monotonically from the left to the right. In the left-hand part of the diagram, $P_2 < P_1$ and the sandwich plate will fail by wrinkling; in the right-hand part $P_1 < P_2$ and the plate will fail by buckling. Therefore the critical load is given by the heavy line, and its maximum will be found where $P_1 = P_2$.

We consider another series of plates, now keeping Q and γ_c constant and varying t, and correspondingly h, within certain limits. The plot of P_1 and P_2 versus t, Fig. 6, looks quite similar to Fig. 5, and again the optimum is found where $P_1 = P_2$.

Our general problem considers both possibilities, varying t and γ_c but keeping Q constant. We may then plot P_1 and P_2 as ordinates over a t, γ_c-plane. The result will be two surfaces. The surface representing P_1 will slope down in the direction of increasing co-ordinates t and γ_c; the other one, representing P_2 will slope down toward the origin. They intersect in an edge, the divide of the P-hill. On one side of the divide P_1 will be the smaller of the two critical loads, and the plate will fail by buckling, while on the other side the wrinkling load P_2 will be the smaller one and will determine the failure of the plate. In Fig. 7 the divide is shown in a perspective drawing, and one may imagine how the two slopes of the P-hill are situated. Our Figs. 5 and 6 are profiles t = const and γ_c = const of this hill. In each profile the best P lies on the divide, and the highest point on the divide will be the summit of the P-hill and will yield the best P that can be obtained for a given set of Q, b, E, γ. Our principal task is to determine this summit.

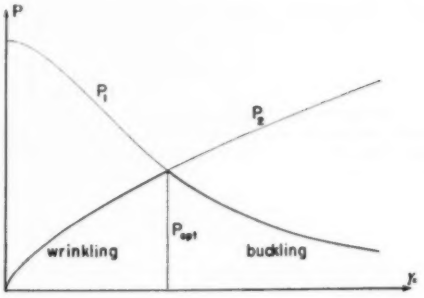

Fig. 5

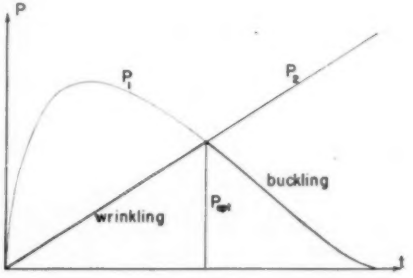

Fig. 6

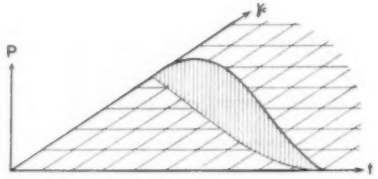

Fig. 7

Development of Diagrams

One might, of course, in any given case use Equations [1] and [4] to construct the P-hill, and then find its summit; but since this would take much time and would have to be done again and again for other sets of the given quantities, it is desirable to reduce the number of parameters of the problem so far that a general diagram may be constructed once and then kept ready for repeated use. Owing to the simple structure of the equations involved, this is really possible.

The first step is the adoption of a set of dimensionless variables. We put

$$\left.\begin{aligned} p &= \frac{\pi}{2}\frac{P}{E'b^3}, \qquad x = \frac{2t\gamma}{Q} = \frac{\pi t}{bq}, \qquad \lambda = \frac{\gamma_c}{\gamma} \\ q &= \frac{\pi}{2}\frac{Q}{\gamma b^2}, \qquad 1 - x = \frac{h\gamma_c}{Q} = \frac{\pi h\lambda}{2bq} \end{aligned}\right\} \quad \ldots\ldots [5]$$

The new variables are so chosen that an extreme of P or Q corresponds to an extreme of p or q. When we introduce Equations [5] into Equations [1a, b, b'] and [4], the latter will assume the following form:

Buckling, lateral pressure

$$p_1 = \frac{q^2 x (1-x)^2}{\lambda^2 \left[1 + \frac{2q^2}{\lambda^2 m} x (1-x)\right]} \quad \ldots\ldots [6a]$$

Buckling, lengthwise pressure

$$p_1 = \frac{4q^2 x (1-x)^2}{\lambda^2 \left[1 + \frac{2q^2}{\lambda^2 m} x (1-x)\right]^2}, \quad \text{if} \quad \frac{2q^2}{\lambda^2 m} x(1-x) < 1 \ldots [6b]$$

$$p_1 = \frac{m}{2} q (1-x), \quad \text{if} \quad \frac{2q^2}{\lambda^2 m} x (1-x) > 1 \ldots\ldots [6b']$$

Wrinkling

$$p_2 = qx \left(\frac{\delta \lambda m}{2}\right)^{2/3} \quad \ldots\ldots [7]$$

In these formulas, x and λ are the variables which must be determined. Besides p and q there are still two parameters, m and δ. When we study Equations [6] and [7] we see that we may rid them of these parameters by a second substitution

$$p' = \frac{p\delta}{m}, \; q' = \frac{q\delta}{m}, \; \lambda' = \frac{\lambda \delta}{\sqrt{m}}$$

In this notation the formulas for the critical loads will assume the following form:

Buckling, lateral pressure

$$p_1' = \frac{q'^2 x (1-x)^2}{\lambda'^2 \left[1 + \frac{2q'^2}{\lambda'^2} x (1-x)\right]} \quad \ldots\ldots [8a]$$

Buckling, lengthwise pressure

$$p_1' = \frac{4q'^2 x (1-x)^2}{\lambda'^2 \left[1 + \frac{2q'^2}{\lambda'^2} x (1-x)\right]^2}, \text{ if } \frac{2q'^2}{\lambda'^2} x (1-x) < 1 \ldots [8b]$$

$$p_1' = \frac{1}{2} q' (1-x), \text{ if } \frac{2q'^2}{\lambda'^2} x (1-x) > 1 \ldots\ldots [8b']$$

Wrinkling

$$p_2' = q' x \left(\frac{1}{2}\lambda'\right)^{2/3} \quad \ldots\ldots [9]$$

We may now get a first idea of how the final diagram will look. When we fix q', then p' depends only on x and λ' and may be plotted by drawing lines $p' = \text{const}$ in an x, λ'-plane. Of course we shall at every point consider only the smaller one of p_1' and p_2'. The result is shown in Fig. 8. The upper right is the region of buckling, the lower left the region of wrinkling. The dividing line between them is the projection of the divide of the p'-hill on the x, λ'-plane. It has the equation

$$p_1' = p_2' \quad \ldots\ldots [10a]$$

and may be determined point by point by intersecting contour lines for equal values of p_1' and p_2'. The summit of the hill is characterized by the fact that there the contour lines do not intersect but just touch each other

$$\frac{\partial p_1'/\partial x}{\partial p_1'/\partial \lambda'} = \frac{\partial p_2'/\partial x}{\partial p_2'/\partial \lambda'} \quad \ldots\ldots [10b]$$

One may determine the co-ordinates of the summit by introducing

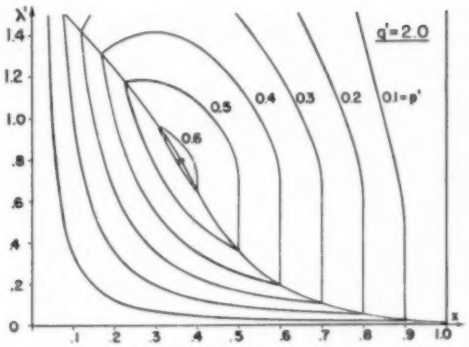

FIG. 8

p' from Equations [8] and [9] into Equations [10a, b], and solving for x and λ'. The result depends, of course, on the choice of the parameter q'. Simple formulas will be obtained when everything is expressed in terms of x. They are for lateral pressure

$$p'_{opt} = 2(1-x)^2 (2-3x)^2 x^{-1/2} (4-5x)^{-1/2}$$

$$q'_{opt} = 2(1-x)(2-3x)^2 x^{-1/2} (4-5x)^{-1/2}$$

$$\lambda'_{opt} = 2(1-x)^{1/2} (2-3x)^{1/2} x^{-1/2} (4-5x)^{-1/2}$$

and for lengthwise pressure

$$p'_{opt} = 32 (1-x)^4 (2-3x)^3 x^{-2} (4-5x)^{-3}$$

$$q'_{opt} = 8 (1-x)^3 (2-3x)^2 x^{-2} (4-5x)^{-3}$$

$$\lambda'_{opt} = 16 (1-x)^3 (2-3x)^{1/2} x^{-1/2} (4-5x)^{-2}$$

From these formulas Figs. 9(a and b) have been prepared, which for a given p' yield those values of q', λ', x which will lead to the lightest sandwich plate possible. Each time when these diagrams have been used, one should determine the wave length of wrinkling from Equation [3] and, in the case of lengthwise compression, also the wave length of buckling from Equation [2], and then decide whether our simple Equations [1] and [4] are trustworthy, or whether the result must be checked and eventually corrected by consulting a more elaborate sandwich theory.

Figs. 9(a) and (b) yield all necessary information about the optimum dimensions of the plate. However, in practical design work it may be necessary to deviate from the exact optimum, and a diagram is desirable which shows at a glance the influence of such a deviation on critical load and weight.

Such a diagram may be constructed if we can rid ourselves of one more parameter. The substitution

$$\bar{p} = p'/q', \quad \bar{\lambda} = \lambda'/q'$$

will eliminate q' from most of the formulas. When we introduce the new variables into Equations [8] and [9] we obtain for buckling, lateral pressure

$$\bar{p}_1 = \frac{x(1-x)^2}{\bar{\lambda}^2 \left[1 + \frac{2x(1-x)}{\bar{\lambda}^2}\right]} \quad \ldots\ldots [11a]$$

for buckling, lengthwise pressure

$$\bar{p}_1 = \frac{4x (1-x)^2}{\bar{\lambda}^2 \left[1 + \frac{2x (1-x)}{\bar{\lambda}^2}\right]^2}, \text{ if } \frac{2x (1-x)}{\bar{\lambda}^2} < 1 \ldots [11b]$$

$$\bar{p}_1 = \frac{1-x}{2}, \quad \text{if} \quad \frac{2x(1-x)}{\bar{\lambda}^2} > 1 \ldots\ldots\ldots [11b']$$

for wrinkling

$$\bar{p}_2 = xq'^{2/3}\left(\frac{1}{2}\bar{\lambda}\right)^{2/3} \ldots\ldots\ldots [12a]$$

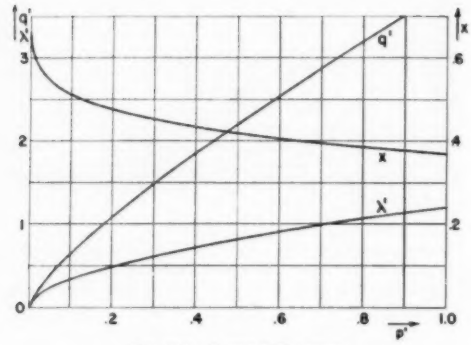

FIG. 9(a) LATERAL PRESSURE

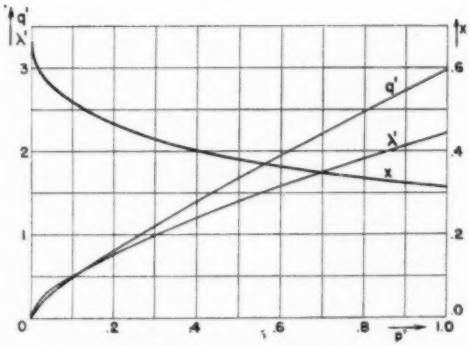

FIG. 9(b) LENGTHWISE PRESSURE

From this last equation we may eliminate q' only if we are willing to tolerate p' besides $\bar{p}$. Then we may write as well

$$\bar{p}_2 = x^{2/3}\, p'^{2/3}\left(\frac{1}{2}\bar{\lambda}\right)^{2/3} \ldots\ldots\ldots [12b]$$

When the load P is given and we aim at a minimum of the weight Q, then p' is known, but not q', and Equation [12b] must be used. In the inverse case where the weight Q and hence q' is known and P is required to be a maximum, Equation [12a] will be the wrinkling condition. We shall here restrict the discussion to the more important first case; the other one may easily be treated along the same lines.

Since $\bar{p}_1$ depends only on x and $\bar{\lambda}$ (in both cases), one may use Equation [11a] or Equations [11b, b'] to draw once and for all a set of curves $\bar{p}_1 = \text{const}$ in the x, $\bar{\lambda}$-plane. But it is not possible to handle the wrinkling load $\bar{p}_2$ in the same simple way. Because of the parameter p', Equation [12b] would yield another set of curves for every other value of p', and that is, of course, too much for one sheet of paper. But there is only one divide $\bar{p}_1 = \bar{p}_2$ for every p', and a set of divides may easily be drawn and numbered according to p'. This has been done in Fig. 10.

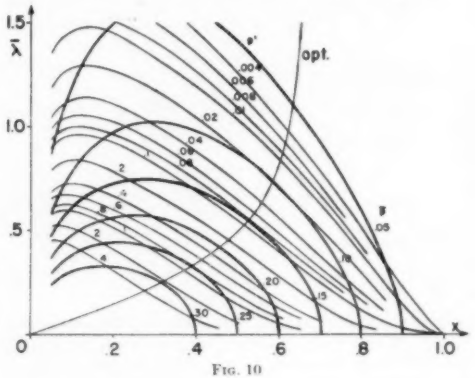

FIG. 10

This diagram may be used in the following way: From the given P we compute

$$p' = \frac{\pi}{2}\,\frac{P}{E'b}\,\frac{\delta}{m}$$

and on the divide corresponding to this value of p' we look for the point where it has a common tangent with a contour line. This is the optimum point. For greater convenience, the curve which passes through all optimum points has been drawn in the diagram and is marked "opt." If for one reason or another we want to choose other values x and $\bar{\lambda}$, it will make a difference whether the point lies toward the upper right or toward the lower left of the divide. Above and to the right of the divide is the buckling region and one may read $\bar{p}_1$ from the set of contour lines of the diagram. On the other side of the divide we are in the wrinkling region, where the contour lines $\bar{p}_1 = \text{const}$ are not applicable, and we must use Equation [12b] to compute $\bar{p}_2$. In both cases we find then $q' = p'/\bar{p}$ and from there everything we need by going back through the equations of this paper.

From the diagram it becomes evident that if a deviation from the optimum is necessary one should try to keep close to the divide because there the loss in $\bar{p}$ and hence the increase in q' will be least.

After every use of the diagram, Equation [3] and, in the case of lengthwise compression, Equation [2], should be used in order to find the wave length of buckling or wrinkling. If the result suggests that our basic formulas might not be a sufficient approximation, more elaborate formulas should be used for a check. The outcome may modify the final decision, but even in such cases the diagram will give a good hint regarding the location of the optimum in the x, $\bar{\lambda}$-plane.

ACKNOWLEDGMENT

The present paper is prepared from two extensive reports[4] which the writer published together with K. Marguerre. Many of the details represented here and in the more comprehensive papers have been worked out by the latter, and the author wishes to express his thanks to him for his co-operation.

[4] "Théorie de la stabilité en compression de la Plaque Sandwich and Les dimensions optima de la Plaque Sandwich comprimée," by W. Flügge and K. Marguerre, Reports No. 421 R 1 and 421 R 2, 1947, of the Office National d'Études et de Recherches Aéronautiques. Paris, France.

Statistical Design of Fatigue Experiments

By WALODDI WEIBULL,[1] BOFORS, SWEDEN

An analytical expression connecting fatigue lives with applied stresses, and methods for computing the values of its parameters from experimental data are given. Formulas for estimating the uncertainty of computed parameter values, caused by scatter of loads and fatigue lives, for optimum distribution of specimens, and for optimum choice of stress levels, are deduced. Testing time and costs may be reduced by more than 40 per cent by using the formulas.

IT IS quite impossible to decide experimentally whether or not the size, or any other factor, has any effect on the endurance limit, without knowing how accurately this limit has been determined. Furthermore, if such a decision is to have any significance at all, the accuracy must be sufficiently high, in proportion to the observed effect.

This self-evident condition is, in fact, not always satisfied, owing to the lack of suitable methods for estimating the accuracy, and thus it seems to be of great urgency to produce such methods, indispensable as they also are for rational designing of the experiments, sometimes with considerable savings in time and costs.

The first step in this direction should be to find an analytical equation connecting fatigue life and applied stress.

Relation Between Life and Stress

Supposing the existence of an exact relationship between life and stress, and approximating it by some mathematical expression, it will be found readily that even if the approximation is not very close, the number of tests necessary to reveal the differences between the exact and the approximate relation will be surprisingly large, owing to the side scatter of observed fatigue lives.

An improvement of the approximation, either by changing the function or by increasing its number of parameters, quite soon will bring us to a position of being unable to decide experimentally whether or not there are any divergences. Such a relation, which cannot be disproved by experimental means, may be called a true one even if it is not the exact one. As a consequence, there may exist two or more true relationships of different shapes. Facing this abundance, the only reasonable way to act seems to be to choose the one which most easily gives answers to posed questions.

The *S-N* Equation

In the course of time, many such equations have been proposed, but so far none has been founded on a convincing theoretical basis. With the foregoing pragmatical standpoint in mind, the relation between applied stress S and fatigue life N is proposed to be

$$S - E = A\,(N + B)^{-m} \qquad [1]$$

This equation includes the endurance limit E and three other parameters A, B, and m, and may also be written

$$\log A - m \log (N + B) - \log (S - E) = 0 \qquad [2]$$

Denoting

$$X = \log N,\ Y = \log (S - E),\ Z = \log (N + B),\ a = \log A \qquad [3]$$

Equation [2] takes the form

$$F = a - mZ - Y = 0 \qquad [4]$$

The slope of the $S - X$-curve may be obtained by differentiating Equation [4] giving

$$dS/dX = -2.30258\,\frac{mN}{N + B}\,(S - E) \qquad [5]$$

or

$$dX = -0.43429\,\frac{N + B}{mN}\,\frac{S}{S - E}\,\frac{dS}{S} \qquad [6]$$

The parameters may be determined either by graphical or by analytical methods.

Graphical Determination of Parameter Values

Having four applied stresses S_1, S_2, S_3, S_4, arranged in the order of decreasing magnitude where, if possible, S_3 = statical ultimate strength, and corresponding lives N_1, N_2, N_3, N_4, Equation [3] gives

$$Y_i = \log (S_i - E),\ Z_i = \log (N_i + B)\ (i = 1, 2, 3, 4) \qquad [7]$$

The parameters E and B have to be determined in such a way that the four points (Y_i, Z_i) plotted on the scale (Y, Z) will fall on a straight line.

We now start, on trial, with two values E_0 and B_0, calculate the values (Y_{i0}, Z_{i0}) and plot them on an ordinary Cartesian scale.

Knowing that a change of B affects only Z, and Z_1 considerably more than Z_4, and that a change of E affects only Y and Y_1 less than Y_4, after some trials, values of the two parameters, close to the accurate ones, may be found. Finally, the slope of the line through the four points gives the parameter m, and its intersection with the Z-axis the parameter a.

The accuracy obtained by graphical methods is not always sufficiently high, and thus analytical methods may sometimes be more useful. Another reason for this is the necessity to have analytical expressions of the derivatives of the parameters for the purpose of estimating the uncertainties of computed values, owing to the scatter of observed fatigue lives.

Computation of Parameter Values From Four (S_i, N_i)

Even now we have to start with two estimated values E_0 and B_0. The unknown deviations from the exact values E and B may be e and b, respectively; thus

$$E = E_0 - e,\ B = B_0 - b \qquad [8]$$

Denoting partial derivatives by indexes as

$$\partial X/\partial N = X_N,\ \partial Z/\partial A = Z_A, \text{ etc.} \qquad [9]$$

---

[1] Professor at the Royal Institute of Technology, Stockholm. Scientific Advisor to A. B. Bofors; Mailing Address: Bofors, Sweden.

Discussion of this paper should be addressed to the Secretary, ASME, 29 West 39th Street, New York, N. Y., and will be accepted until April 10, 1952, for publication at a later date. Discussion received after the closing date will be returned.

NOTE: Statements and opinions advanced in papers are to be understood as individual expressions of their authors and not those of the Society. Manuscript received by ASME Applied Mechanics Division, November 12, 1951.

we have

$$\left.\begin{aligned} X_N &= 0.43/N,\ Y_S = -Y_E = 0.43/(S-E) \\ Z_N &= Z_B = 0.43/(N+B),\ Z_X = N/(N+B) \end{aligned}\right\} \quad \cdots [10]$$

where 0.43 has been substituted for the more accurate value 0.43429. If e and b be small, we may have approximately

$$Y_i = Y_{i0} - e\,Y_{E i0},\ Z_i = Z_{i0} - b\,Z_{B i0} \quad \cdots [11]$$

From Equations [4] and [10] it follows that

$$\begin{aligned} F_i = a - mZ_{i0} + 0.43(mb)/(N_i + B_0) - 0.43\,e/(S_i - E_0) \\ - Y_{i0} = 0\ (i = 1, 2, 3, 4) \quad \cdots [12] \end{aligned}$$

From Equations [12] a, m, (mb), and e may be computed, as Y, Y_E, Z, Z_B are known quantities.

The values b and e will not be quite accurate, as the correct values of Z_B and Y_E are to be found somewhere between $(N_i + B_0)$ and $(N_i + B_0 - b)$, and between $(S_i - E_0)$ and $(S_i - E_0 + e)$, respectively.

If computed values of b and e turn out to be too large, the procedure may be iterated any number of times by inserting corrected values of E_0 and B_0 according to Equation [8]. Thus any degree of accuracy may be obtained.

Computation of Parameter Values From More Than Four (S_i, N_i)

If the purpose of testing is to determine the values of the parameters only, the optimum number of stress levels is four. From other reasons, there may be a necessity to have more than four stress levels. In this case it is impossible to satisfy the condition $\Sigma(F_i)^2 = 0$, which has to be modified to

$$\Sigma(F_i)^2 = \text{minimum} \quad \cdots [13]$$

By differentiating we obtain

$$\left.\begin{aligned} F\partial F/\partial a &= \Sigma(F_i) = 0 \\ F\partial F/\partial m &= \Sigma(F_i Z_i) = 0 \\ F\partial F/\partial(mb) &= \Sigma(F_i Z_{Bi}) = 0 \\ F\partial F/\partial e &= \Sigma(F_i Y_{Ei}) = 0 \end{aligned}\right\} \quad \cdots [14]$$

If the stress levels are five or six, it may sometimes be better to pick out four of the Equations [12] for computing the parameters and then to compute the values of F_i from Equation [4] for the remaining Equations [12]. The quantities $\Delta Z_i = F_i/m$ may be regarded as deviations of Z_i (supposing no scatter in S_i). Accordingly, if they are small in proportion to the standard deviations of Z_i, the procedure may be stopped at this stage.

The deviations ΔZ_i also may be dispersed over all of the Equations [12] by accepting obtained values of E and B but by computing new values of a and m, using the first two Equations [14]. If the values F_i are still too large, the more tedious way of solving the Equations [14] has to be taken.

Derivatives of the Parameters

In order to estimate the influence of the errors of the experimentally determined loads S_j and the fatigue lives N_j, or X_j, $(j = 1, 2, 3, 4)$ on computed values of the parameters a, m, B, and E, it is necessary to derive formulas for the derivatives of these parameters with respect to S_j and X_j denoted $a_{Sj} \ldots E_{Sj}$ and $a_{Xj} \ldots E_{Xj}$.

This may be accomplished by differentiating the four equations

$$F_i = a - m\,Z_i - Y_i = 0 \quad (i = 1, 2, 3, 4)$$

obtained by inserting in Equation [4] the four pairs of values (Y_i, Z_i) of Equation [7].

It may be pointed out that a variation of the load S_j does not affect either of the other loads $S_i\ (i \neq j)$ nor any one of the fatigue lives N_i. A corresponding rule applies to a variation of X_j.

By differentiating Equation [4], we thus obtain

$$\left.\begin{aligned} a_{Sj} - m_{Sj}Z_i - 0.43\,B_{Sj}m/(N_i + B) + 0.43\,E_{Sj}/(S_i - E) &= \begin{cases} 0.43/(S_i - E) & (i = j) \\ 0 & (i \neq j) \end{cases} \\ a_{Xj} - m_{Xj}Z_i - 0.43\,B_{Xj}m/(N_i + B) + 0.43\,E_{Xj}/(S_i - E) &= \begin{cases} \dfrac{mN_i}{N_i + B} & (i = j) \\ 0 & (i \neq j) \end{cases} \end{aligned}\right\} \quad \cdots [15]$$

The numerical computation will be simplified by introducing the coefficients k, defined by

$$k_{aj} - k_{mj}Z_i - k_{Bj}/(N_i + B) + k_{Ej}/(S_i - E) = \left\{\begin{matrix} 1\ (i = j) \\ 0\ (i \neq j) \end{matrix}\right\} \quad \cdots [16]$$

Comparing Equations [15] and [16] we obtain

$$\left.\begin{aligned} a_{Si} &= 0.43429\,k_{ai}/(S_i - E) \\ m_{Si} &= 0.43429\,k_{mi}/(S_i - E) \\ B_{Si} = E_{Bi}/m(S_i - E),\ E_{Si} &= k_{Ei}/(S_i - E) \end{aligned}\right\} \quad \cdots [17]$$

and

$$\left.\begin{aligned} a_{Xi} = k_{ai}mN_i/(N_i + B),\ m_{Xi} &= k_{mi}mN_i/(N_i + B) \\ B_{Xi} &= 2.30258\,k_{Bi}N_i/(N_i + B) \\ E_{Xi} &= 2.30258\,k_{Ei}mN_i/(N_i + B) \end{aligned}\right\} \quad \cdots [18]$$

By putting all the right-hand members of Equation [16] equal to 1, we find

$$\Sigma k_{ai} = 1,\ \Sigma k_{mi} = \Sigma k_{Bi} = \Sigma k_{Ei} = 0 \quad \cdots [19]$$

which may be used as a check on the computation.

Another check may be obtained by the evident fact that an error of ΔS in all of the S_i will give the same error in E but will not affect the other parameters.

Mathematically expressed

$$\Delta E = \Sigma E_{Si}\Delta S = \Delta S$$

from which it follows

$$\Sigma E_{Si} = 1 \quad \cdots [20]$$

and, in the same way

$$\Sigma a_{Si} = \Sigma m_{Si} = \Sigma B_{Si} = 0 \quad \cdots [21]$$

From Equations [17] and [18] it will be seen that

$$E_{Si}/E_{Xi} = 0.43\,(N_i + B)/mN_i(S_i - E) \quad \cdots [22]$$

or, considering Equation [6]

$$E_{Si} = -(dX/dS)_i\,E_{Xi} \quad \cdots [23]$$

Uncertainty of Computed Parameter Values

As already demonstrated, it is possible to compute these

values with any degree of accuracy for a given set (Y_i, Z_i), but it must not be forgotten that Y_i and Z_i are statistical variables which are widely scattered as a consequence of the large scatter of observed fatigue lives, in some cases, also due to the testing machine.

Denoting by $\bar{S}_i$ and $\bar{X}_i$ the (unknown) means of S_i and X_i (where i is the number of the stress level in a succession of levels) and by $\bar{E}$ a value computed from these means, we may put

$$E = \bar{E} + \Sigma E_{S_i}(S_i - \bar{S}_i) + \Sigma E_{X_i}(X_i - \bar{X}_i) \quad [24]$$

on the conditions that the differences $(S_i - \bar{S}_i)$ and $(X_i - \bar{X}_i)$ are sufficiently small which may be the case, if the numbers n_i are sufficiently large.

The variance of E may be calculated (see for instance, Cramér[2]) as

$$\sigma_E^2 = D^2(E) = \Sigma E_{S_i}^2 D^2(S_i) + \Sigma E_{X_i}^2 D^2(X_i) \quad [25]$$

Let σ_{Si} and σ_{Xi} denote the standard deviations of S and X, respectively, and n_i the number of observations at the ith stress level; the

$$\left.\begin{aligned} D^2(S_i) &= \sigma_{S_i}^2/n_i,\ D^2(X_i) = \sigma_{X_i}^2/n_i \\ \sigma_E^2 &= (\Sigma E_{S_i}^2\sigma_{S_i}^2 + \Sigma E_{X_i}^2\sigma_{X_i}^2)/n_i \end{aligned}\right\} \quad [26]$$

or considering Equation [23]

$$\sigma_E^2 = \Sigma[E_{X_i}^2\,(\sigma_{X_i}^2 + (dX/dS)_i^2\sigma_{S_i}^2)/n_i] \quad [27]$$

If we denote by s^2 the total variance of X, it follows that

$$s_i^2 = \sigma_{X_i}^2 + (dX/dS)_i^2\sigma_{S_i}^2 \quad [28]$$

and

$$\sigma_E^2 = \Sigma[E_{X_i}^2 s_i^2/n_i] \quad [29]$$

The scatter measured by s depends not only upon the material and the size and shape of the specimens but includes also the scatter due to the testing machine.

If S_1 is a statical load, there is, of course, no scatter in N_1. The first term of Equation [29], $E_{X_1}^2 s_1^2/n_1$, should then be replaced by the term $E_{S1}^2\,\sigma_{S1}^2/n_1$, whence

$$\sigma_E^2 = E_{S1}^2\sigma_{S1}^2/n_1 + \Sigma[E_{X_i}^2 s_i^2/n_i]\ (i = 2, 3, 4) \quad [30]$$

Scatter Values s_i

The standard deviation s_i of X at a given stress level may be computed (see, for instance, Snedecor[3]) as

$$s_i^2 = D^2(X) = [\Sigma X^2 - (\Sigma X)^2/n]/(n-1) \quad [31]$$

This value is an estimate of the exact value and independent of the number n, though the accuracy of the estimate increases with the number of observations.

From Equation [28] it may be seen that the scatter in fatigue lives consists of two parts, the first caused by the specimen, its material, surface conditions, and so forth, the other caused by errors in the nominal loads of the testing machine. As these errors have to be multiplied by the slope dX/dS of the $X-S$-curve in order to have their influence on X, and as this slope may take values of 20 or more, the scattering influence of the machine often may be much greater than anticipated.

For instance, when studying the size effect, which statistically depends entirely upon the scatter, it is absolutely necessary to separate the two parts of the scatter, as the second part does not have any influence on the size effect. On the contrary, for the statistical designing of the fatigue test, it is not necessary to separate the two parts.

If S_1 is a static load, the scatter σ_{S1} also may consist of two parts, one depending upon the specimen, the other on the machine.

It is evident that s_i is independent of all stresses but S_i, and thus there may exist a unique relation between s and S. This relation has to satisfy the obvious condition that s increases infinitely as soon as one single specimen of the population does not fail, i.e., when $S \to E_h$, where E_h is the upper endurance limit (somewhere above 34.5 in Fig. 2)

As a first attempt, we put

$$s = H(S - E_h)^{-k} \quad [32]$$

or

$$\log s = \log H - k\log(S - E_h) \quad [33]$$

It is apparent that instead of taking s as a function of S, it is just as possible to take it as a function of X. We then obtain the advantage that s is everywhere finite, but its value has to be computed from the $S-N$-curves. For this reason it is easier to use, as a measure of the scatter, the range, which is identical to the difference between the two extreme $S-N$-curves, the numbers n_i being equal. The only objection against this modification is that the standard deviation is much less dependent upon the extreme values than the range, and therefore is more accurate.

Optimum Distribution of Specimens Among Given Stress Levels

The foregoing formulas will make it possible to estimate the uncertainty of parameter values, computed from given observations. They also may be used to decide how the specimens have to be distributed in order to have the most favorable relation between information and costs.

The optimum distribution depends upon the premises. There may be three cases as follows:

1 We have a given number of specimens at our disposal.
2 We have a given amount of time.
3 We have a given amount of costs.

In case (1), we start from Equation [29] or [30], supposing the number $n = \Sigma n_i = \text{const}$. It may be proved that σ_E takes a minimum value on the condition that

$$n_i/n = (E_X s)_i/\Sigma(E_X s) \quad [34]$$

all E_X taken with positive signs.

Introducing Equation [34] in [29] the minimum value is found to be

$$\sigma_E = \Sigma(E_X s)/\sqrt{n} \quad [35]$$

In cases (2) and (3) the time or cost needed for a single specimen consists of one part t_1, independent of the fatigue life, and another part t_2, dependent upon the fatigue life. At each stress level the mean of time or cost per specimen will be $t_i = t_1 + t_2$ and the total amount for each stress level

$$T_i = t_i n_i \quad [36]$$

Introducing $n_i = T_i/t_i$ in Equation [29] and keeping $T = \Sigma T_i = \text{const}$, the optimum distribution will be

$$T_i/T = (E_X s t^{1/2})_i/\Sigma(E_X s t^{1/2}) \quad [37]$$

or

$$n_i/n = (E_X s t^{-1/2})_i/\Sigma(E_X s t^{-1/2}) \quad [38]$$

with the minimum value

[2] "Mathematical Methods of Statistics," by H. Cramér, Princeton Mathematical Series, 1946, p. 180.

[3] "Statistical Methods," by G. W. Snedecor, fourth edition, The Iowa State College Press, Ames, Iowa, 1950, pp. 91-92.

$$\sigma_E = \Sigma(E_X s t^{1/2})/\sqrt{T} = \Sigma(E_X s t^{-1/2})/\sqrt{n} \quad [39]$$

The same formulas will apply to other parameters by substituting B, a, or m for E.

Optimum Choice of Stress Levels

Any change of a stress level S_i may affect the uncertainty of computed parameter values. Accordingly, there will exist an optimum combination of stress levels, but this problem is much more difficult to solve than in the previous case, since a change of S_i will have an influence on N_i and s_i as well as on all of the coefficients k.

It may be pointed out that in this case the changing of S_i is supposed to have no effect on the values of the parameters, which have been computed from the observations obtained.

For the moment, the most practicable procedure seems to be to compute the minimum value by changing successively one stress level at a time. The most influential of these stresses is S_4 as the corresponding value of s may be very large when $S \to E_h$. For this reason S_4 gives a very definite minimum.

Application of Formulas to Pulsating Tensile Fatigue Tests on Aluminum Alloy 75 S

Tests have been run at the Aeronautical Research Institute of Sweden on a 10-ton Amsler high-frequency pulsator. Specimens were turned from 23-mm bars, supplied by the Svenska Metallverken, and finished with a sharp tool and light cuts (0.25 mm deep). Test section diameter 6 mm, length 20.4 mm.

The data obtained are given in Table 1 from which it may be seen that there is no significant difference between mean $\bar{X}$ and median X of X at a given stress level. Standard deviations s, of X are computed by Equation [31]. Standard deviation of $\bar{X}$ is $s/\sqrt{n}$ and of X_m about 25 per cent larger. The ratio, range/s, is remarkably constant for stress levels 53, 47, and 35. The too high value 5.55 for $S = 47$, after inspection, was found to be due to a bad surface condition of the specimen with the shortest fatigue life, which was not the case at the other stress levels (see Fig. 2).

TABLE 1 STATICAL TENSILE TESTS AND PULSATING TENSILE FATIGUE TESTS MINIMUM STRESS = 0. MATERIAL: 75 S

S	n	X_1	X_m	X_{24}	$\bar{X}$	s	$s/\sqrt{n}$	Range	Range/s
67[a]	24	—	—	—	—	0.697	0.146	3.2	4.59
53	24	4.0086	4.3222	4.6628	4.3431	0.175	0.036	65.42	3.74
47	24	4.0453	4.6826	5.0792	4.6777	0.186	0.038	(1.0339)	(5.55)
41	24	4.7324	5.2028	5.5821	5.1630	0.227	0.047	0.8487	3.74
35	24	5.3802	6.4088	7.4597	6.4396	0.551	0.112	2.0795	3.78

[a] Ultimate tensile strength, mean. Minimum value = 65.7; Maximum value = 68.9 kg per sq mm.
S = maximum stress in kg per sq mm; n = number of tests; X = log N.
s = estimated standard deviation; Range = difference between maximum and minimum values at 24 observations.

TABLE 2 PARAMETERS, COMPUTED FROM STATICAL LOAD AND FATIGUE MAXIMUM STRESSES 53, 41, AND 35 KG PER SQ MM

P	E	$B \times 10^{-4}$	a	m
0.04	31.6	1.139	1.578	0.743
0.50	33.5	1.432	1.618	0.600
0.96	34.5	2.450	1.768	0.593

Parameter values given in Table 2 have been computed by Equation [12] inserting values of X_1, X_m, and X_{24} at $S = 67$, 53, 41, and 35, from Table 1. The value of X_m for $S = 47$ was then computed with these parameters, which gave an error $\Delta Z = F_z/m = 0.020$. This value is about 50 per cent of corresponding $s/\sqrt{n}$ and thus insignificant. The $Y - Z$-curve for $P = 0.50$ is shown in Fig. 1, and $S - X$-curves for $P = 0.04$ and 0.96 in Fig. 2.

The coefficients k and derivatives of the parameters with respect to S and X have been computed for $P = 0.50$ and are given in Tables 3, 4, and 5.

These values make it possible to calculate the uncertainty of computed parameter values. Using Equation [30] and values from Tables 1, 4, and 5, we have

$$24\,\sigma_E^2 = (0.091 \times 0.697)^2 + (7.643 \times 0.175)^2 + (11.315 \times 0.227)^2 + (3.673 \times 0.551)^2 = 12.481$$

whence

$$\sigma_E = 1.25 \times 0.72 = 0.90$$

The reason for the introduction of the coefficient 1.25 is that the medians and not the means of X have been used.

It has been possible to obtain the same precision with a smaller number of specimens, better distributed on the given stress levels. From Equation [35] it is easily found that $\sigma_E = 0.72$ and $[E_{31}a_1 + \Sigma(E_X s)] = 5.991$ gives a number $n = 69$. Equation [34] leaves the optimum distribution 1:15:30:23. In this way the same precision of E may be obtained by running 69 specimens only instead of $4 \times 24 = 96$.

Taking as distribution basis the cost, instead of the number of specimens, Equation [39] and specified costs t_i from the Aeronautical Research Institute, it has been found that the total cost of this series, having been 5.442 Swedish Crowns, may come down to 3.864 Sw. Cr. with unchanged precision of E, by choosing a more favorable distribution of the number of specimens.

The influence of changing the stress levels will be demonstrated by changing S_i only. The corresponding variation in s may be found from Equation [33] which seems to be quite usable, as illustrated in Fig. 3. Values of $\sigma_E\sqrt{n}$, according to Equation [30] have been computed and plotted in Fig. 4. The

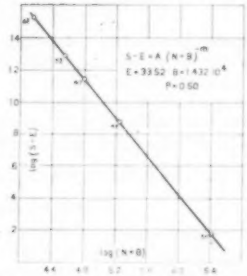

Fig. 1 Relationship of Stress S and Fatigue Life N for a Probability of Failure $P = 0.50$
(Al-alloy 75 S. Pulsating tensile stress.)

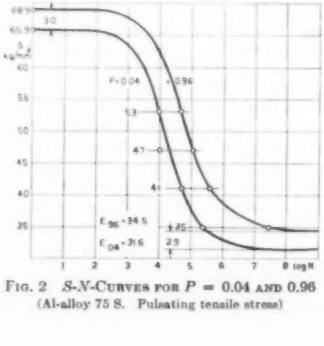

Fig. 2 S-N-Curves for $P = 0.04$ and 0.96
(Al-alloy 75 S. Pulsating tensile stress)

TABLE 3 COMPUTED k-VALUES FOR $P = 0.50$

S	k_a	k_m	k_B	k_E	k_E $S_4 = 36$
67	−1.771	−1.583	−3.745	−3.056	−4.723
53	+4.808	+4.587	+6.259	+9.309	+14.780
41	−2.182	−3.398	−2.748	−8.928	−16.463
35	+0.145	+0.394	+0.234	+2.675	+6.406
Σ	+1.000	0.000	0.000	0.000	0.000

$E = 33.52$; $B = 1.432 \times 10^4$; $a = 1.6182$; $m = 0.5997$

TABLE 4 COMPUTED VALUES OF a_s, m_s, mB_S, AND E_S FOR $P = 0.50$

S	a_s	m_s	mB_S	E_S	E_S $S_4 = 36$
67	−0.023	−0.021	−0.112	−0.091	−0.141
53	+0.107	+0.102	+0.321	+0.478	+0.759
41	−0.127	−0.197	−0.367	−1.194	−2.201
35	+0.043	+0.116	+0.158	+1.807	+2.583
Σ	0.000	0.000	0.000	+1.000	+1.000

$E = 33.52$; $B = 1.432 \times 10^4$; $a = 1.6182$; $m = 0.5997$

TABLE 5 COMPUTED VALUES OF a_x, m_x, mB_X, AND E_X FOR $P = 0.50$

S	a_X	m_X	mB_X	E_X	E_X $S_4 = 36$
67	−0.000	−0.000	−0.000	−0.000	−0.000
53	+1.714	+1.635	+5.139	+7.643	+12.135
41	−1.201	−1.870	−3.482	−11.315	−20.864
35	+0.086	−0.235	+0.321	+3.673	+8.711

$E = 33.52$; $B = 1.432 \times 10^4$; $a = 1.6182$; $m = 0.5997$

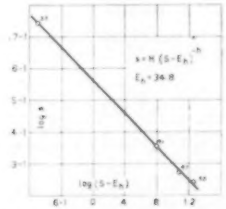

FIG. 3 RELATIONSHIP OF SCATTER s AND STRESS S
(Al-alloy 75 S. Pulsating tensile stress.)

values for $S_4 = 36$, keeping other stresses unchanged, are given in Tables 3, 4, and 5. As seen from Fig. 4, a change of S_4 from 35 to 36.4 will about double the value of $\sigma_E\sqrt{n}$, which means that the number of specimens has to be quadrupled in order to have the same σ_E.

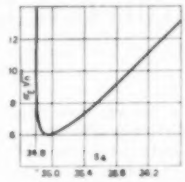

FIG. 4 RELATIONSHIP OF STANDARD DEVIATION $\sigma_E\sqrt{n}$ AND STRESSES S_4 FOR CONSTANT S_1, S_2, AND S_3
(Al-alloy 75 S. Pulsating tensile stress.)

Using the values from Tables 4 and 5, it is found that $\sigma_E = 1.23$ for $S_4 = 36$, compared with the value 0.72 for $S_4 = 35$. The small change from 35 to 36 requires 2.9 times as many tests to obtain the same precision of E. Probably substantial gains would be possible by changing the other stress levels also, but the computations are time-absorbing and the use of modern computing machines seems desirable.

INFLUENCE OF THE TESTING MACHINE

It seems worth while to analyze to what extent the machine is responsible for the scatter in fatigue lives.

The load of the Amsler machine is measured by an elastic bar, acting as a dynamometer. The indication on the scale, being 1 cm per ton, may be read with an accuracy not better than ±0.1 mm or ±10 kg at each stress limit. For a 6-mm specimen this gives an uncertainty of the range of stress = ±0.707 kg per sq mm.

Taking as a preliminary value $\sigma_S = 0.70$, the variances of fatigue lives have been split up into two parts, one depending on the machine, the other on the specimens. The figures are computed by Equations [26] to [30] and given in Table 6, from which it may be seen that the scatter in life is not greatly dependent on the machine at high stresses, but that about 40 per cent of the variance of fatigue life at stress level 35 is caused by the testing machine.

TABLE 6 ANALYSIS OF VARIANCES; $\sigma_S = 0.70$ KG PER SQ MM

S	$\frac{dX}{dS}$ mm²/kg	s^2	$\left(\frac{dX}{dS}\sigma_S\right)^2$	σ_X^2	$(E_S\sigma_S)^2$	$(E_X\sigma_X)^2$	$(E_X s)^2$
67	3.110	0.4858	—	—	0.004	—	0.004[a]
53	0.0625	0.0306	0.0019	0.0287	0.112	1.676	1.788
41	0.1055	0.0515	0.0055	0.0460	0.698	5.895	6.593
35	0.4920	0.3036	0.1186	0.1850	1.600	2.496	4.096
		0.3857	0.1260	0.2597	2.414	10.067	12.481
				0.1260		2.414	
				$\Sigma s^2 = 0.3857$		$n_i\sigma_E^2 = 12.481$	

[a] Equals $(E_S\sigma_S)^2$

An Electrical Method for Determining Journal-Bearing Characteristics[1]

By D. S. CARTER,[2] PRINCETON, N. J.

More than half a century has passed since Osborne Reynolds employed hydrodynamic principles to derive his well-known differential equation for the pressure distribution in a thin film of viscous fluid under shear. During that time many ingenious methods have been put forward for the solution of Reynolds equation in cases of engineering interest. These methods have been found useful in the few cases to which they have been applied; but none is adaptable to the production, in quantity, of much-needed data. Any future program for the preparation of a comprehensive set of bearing data will surely be carried out with the help of the large, modern, rapid-calculating machines. Until these machines become more readily available, however, the need will remain for improved calculational techniques which require only modest financial and material resources. It was with this need in mind that the work described in the present paper was undertaken.

Section 1

THE problem under discussion is the solution of Reynolds equation for the pressure distribution in the oil film of a journal bearing

$$\frac{\partial}{\partial x}\left(h^3\frac{\partial p}{\partial x}\right)+\frac{\partial}{\partial y}\left(h^3\frac{\partial p}{\partial y}\right)=6\mu U\frac{dh}{dx} \quad \ldots\ldots [1]$$

Here, p is the pressure, h the film thickness, μ the lubricant viscosity, U the relative speed of journal and bearing surfaces, x the co-ordinate measured along the bearing surface in the direction of motion, and y the co-ordinate measured across the surface (perpendicular to the direction of motion, see Fig. 1). Term h depends on x alone; μ will be taken as constant, although the generalization of this method to cases of variable μ is easily carried out.

The boundary condition which p must satisfy is one of the two types:

Type 1, p vanishes at the edge of the bearing surface, see Fig. 1(*a*).

Type 2, p vanishes around a curve of the form shown in Fig. 1(*b*). The curved portion of the boundary lies within the bearing surface, and is determined by the additional condition that $\partial p/\partial x = 0$ on the curve.

The Type 1 boundary condition is to be used whenever the resulting pressure distribution has no negative pressures; and the Type 2 condition is to be used when negative pressures are encountered with the Type 1 condition.

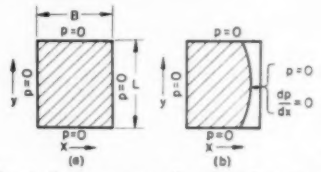

FIG. 1 ILLUSTRATION OF BOUNDARY CONDITIONS
(Bearing surface is developed.)

Section 2

Equation [1] may be transformed to a more convenient form by working the substitution[3]

$$q=\frac{h^{3/2}p}{6\mu U} \quad \ldots\ldots [2]$$

Setting $p = 6\mu U h^{-3/2} q$ in Equation [1] we obtain the equation

$$\frac{\partial^2 q}{\partial x^2}+\frac{\partial^2 q}{\partial y^2}-\frac{\ddot{H}}{H}q-\frac{\dot{h}}{H}=0 \quad \ldots\ldots [3]$$

where

$$H = h^{3/2}$$

and dots denote differentiation with respect to x. The advantage of the substitution Equation [2] is that the derivatives of q enter Equation [3] only through the Laplacian operation

$$\frac{\partial^2}{\partial x^2}+\frac{\partial^2}{\partial y^2}$$

This has the effect that the basic electrical network used to solve Equation [3] may be constructed from constant rather than variable impedance elements (see section 4).

The boundary conditions for q are the same as those for p. Thus p and q have the same sign, and since

$$\frac{\partial q}{\partial x}=\frac{3}{2}h^{1/2}\frac{dh}{dx}\frac{p}{6\mu U}+\frac{h^{3/2}}{6\mu U}\frac{\partial p}{\partial x}$$

it is clear that the condition $p = (\partial p/\partial x) = 0$ implies $q = (\partial q/\partial x) = 0$.

For the electrical analogy, we shall divide the bearing surface by a network of $n + 1$ equally spaced lines along the surface, and $m + 1$ equally spaced lines across the surface. Accordingly, we set

$$\xi=\frac{n}{B}x \quad \ldots\ldots [4a]$$

---

[1] The work described in this paper was done during the summer of 1949, while the author was attached to the Mechanics Department of the Westinghouse Research Laboratories, East Pittsburgh, Pa.

[2] Research Assistant, Princeton University.

Contributed by the Applied Mechanics Division and presented at the Annual Meeting, Atlantic City, N. J., November 25–30, 1951, of THE AMERICAN SOCIETY OF MECHANICAL ENGINEERS.

Discussion of this paper should be addressed to the Secretary, ASME, 29 West 39th Street, New York, N. Y., and will be accepted until April 10, 1952, for publication at a later date. Discussion received after the closing date will be returned.

NOTE: Statements and opinions advanced in papers are to be understood as individual expressions of their authors and not those of the Society. Manuscript received by ASME Applied Mechanics Division, August 28, 1950. Paper No. 51—A-27.

[3] In case of variable viscosity, the factor $1/\mu$ is left out of this substitution.

$$\zeta = \frac{m}{L}\, y \qquad [4b]$$

where B is the linear extent of the bearing arc, and L is the bearing length. The lines $\xi = 0, 1, 2, \ldots, n$; and $\zeta = -m/2, -m/2 + 1, \ldots, +m/2$ form the required network (see Fig. 2). We take m to be an even integer, so that the center line $\zeta = 0$ is included.

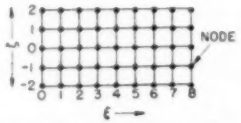

FIG. 2 NETWORK DRAWN ON DEVELOPED BEARING SURFACE

In terms of ξ and ζ, Equation [3] reads

$$\frac{\partial^2 q}{\partial \xi^2} + \left(\frac{m}{n}\,\frac{B}{L}\right)^2 \frac{\partial^2 q}{\partial \zeta^2} - \frac{H'}{H}\, q - \frac{B}{n}\,\frac{h'}{H} = 0 \qquad [5]$$

where primes denote differentiation with respect to ξ.

For the journal bearing, h has the well-known form

$$h = C(1 + \epsilon \cos \theta) \qquad [6]$$

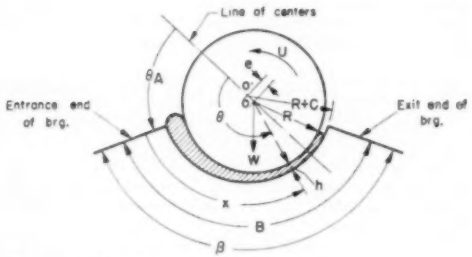

R = radius of shaft
C = radial clearance (not shown in figure)
ϵ = eccentricity = distance as measured on line of centers between shaft center o and bearing center o'
ϵ = eccentricity ratio = e/C
h = oil-film thickness at any value of θ
θ = angular distance from line of centers to any point on bearing arc, measured in direction of rotation
x = linear distance from entrance end of bearing to any point on bearing arc, measured in direction of rotation
θ_A = angular distance from line of centers to "entrance end"
β = angular length of bearing
B = linear length of bearing arc = βR
W = total bearing load

FIG. 3 JOURNAL BEARING NOMENCLATURE

where (see Fig. 3)

$$C = \text{radial clearance}$$
$$\epsilon = \text{eccentricity ratio}$$
$$\theta = \frac{x}{R} + \theta_A$$
$$R = \text{bearing radius}$$

In terms of the bearing arc $\beta = B/R$, it is clear that

$$\theta = \frac{\beta}{n}\,\xi + \theta_A \qquad [7]$$

Substituting into Equation [5], dividing by

$$RC^{-1/2}\,\epsilon \left(\frac{\beta}{n}\right)^2$$

and setting q proportional to the new function u

$$q = RC^{-1/2}\,\epsilon\,(\beta/n)^2 u \qquad [8]$$

we obtain the equation

$$\frac{\partial^2 u}{\partial \xi^2} + \left(\frac{m}{n}\,\frac{B}{L}\right)^2 \frac{\partial^2 u}{\partial \zeta^2} - f(\xi)u + g(\xi) = 0 \qquad [9]$$

where

$$f(\xi) = \frac{3}{4}\,\epsilon \left(\frac{\beta}{n}\right)^2 \left[\frac{\epsilon \sin^2\theta}{(1 + \epsilon \cos\theta)^2} - \frac{2\cos\theta}{1 + \epsilon\cos\theta}\right] \qquad [10a]$$

$$g(\xi) = \frac{\sin\theta}{(1 + \epsilon\cos\theta)^{1/2}} \qquad [10b]$$

According to Equations [2] and [8]

$$p = 6\mu U R \epsilon h^{-2/3} C^{-1/2} (\beta/n)^2 u \qquad [11]$$

The boundary conditions for u are, again, the same as those for p.

SECTION 3

When we speak of an approximate solution of Equation [9] we mean a set of values which approximate an exact solution at the nodes of the network of Fig. 2. Thus, for points on a line in the ξ direction (say, at $\zeta = \zeta_0$), a plot of the solution would appear as shown in Fig. 4.

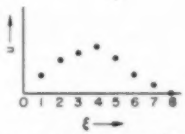

FIG. 4 PLOT OF SOLUTION OF PRESSURE FUNCTION u AT $\zeta = \zeta_0$

If the network is chosen sufficiently fine, i.e., if m and n are sufficiently large, a good approximation to the exact solution would be obtained by drawing a parabola through each set of three successive points in Fig. 4. If ξ_0, $\xi_1 = \xi_0 - 1$, and $\xi_2 = \xi_0 + 1$ are the abscissas of three such points, and if u_0, u_1, and u_2 are the respective ordinates of these points, the equation of the corresponding parabola[4] is

$$u = \frac{1}{2}\,[u_1 - 2u_0 + u_2]\xi^2 - \frac{1}{2}\,[(\xi_0 + \xi_2)u_1 - 2(\xi_1 + \xi_2)u_0 + (\xi_1 + \xi_0)u_2]\xi + \frac{1}{2}\,(\xi_0\xi_1 u_1 - 2\xi_1\xi_2 u_0 + \xi_1\xi_0 u_2) \qquad [12]$$

Taking the second derivative of Equation [12], we find that in so far as this approximation is valid, the value of $(\partial^2 u)/(\partial \xi^2)$ at the center node (ξ_0, ζ_0) is

$$\frac{\partial^2 u}{\partial \xi^2} = u_1 + u_2 - 2u_0 \qquad [13a]$$

[4] It can be shown by the use of Lagrange's interpolation formula that the equation of a parabola which passes through three successive points will have the foregoing form when the distance between each point equals unity.

Exactly the same argument, applied to points along the line $\xi = \xi_0$ across the surface, yield the approximate value

$$\frac{\partial^2 u}{\partial \zeta^2} = u_3 + u_4 - 2u_0 \quad [13b]$$

for $(\partial^2 u)/(\partial \zeta^2)$ at (ξ_0, ζ_0). Here u_3 and u_4 are the values of u at $\zeta = \zeta_0 - 1$ and $\zeta = \zeta + 1$, respectively (see Fig. 5).

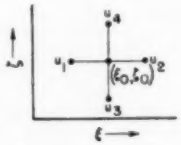

FIG. 5 INTERIOR NODE OF BEARING NETWORK, ENLARGED

Substituting Equations [13] into Equation [9], we obtain a set of algebraic equations, one for each interior node of the network

$$u_1 + u_2 - 2u_0 + \left(\frac{m}{n}\frac{B}{L}\right)^2 (u_3 + u_4 - 2u_0) - f(\xi_0)u_0 + g(\xi_0) = 0 \quad [14]$$

The boundary conditions furnish one additional equation for each boundary node, so that the total number of equations is equal to the number of unknowns. For Type 1 boundary conditions we set

$$u_0 = 0 \quad [15]$$

at each boundary node. Boundary conditions of Type 2 are more complicated: (*a*) The curved portion of the boundary where $(\partial p)/(\partial x) = 0$ is unknown, and (*b*) this curve need not pass through nodes of our network. In applying this condition, the boundary should first be located roughly by a method such as the following: Choose an arbitrary boundary through nodes of the network, set $u_0 = 0$ at each boundary point, and solve for the pressure distribution. If this initial boundary has been chosen beyond the correct one (toward the "exit end" of the bearing surface), the solution will be negative near the boundary. If so, move the trial boundary back, and repeat this procedure until no negative pressures occur. The true boundary will lie near the final trial boundary. With the electrical method to be described, this procedure should not be tedious.

In many cases the approximate boundary, determined as in the foregoing, should yield a sufficiently accurate pressure distribution for purposes of determining bearing characteristics. There are two reasons why this is expected: (*a*) The pressure gradient $(\partial p)/(\partial x)$ vanishes at the boundary, so the error obtained by setting $p = 0$ at adjacent nodal points, instead of on the true boundary, should not be large. (*b*) A small error in the pressure distribution near the boundary would result in a much smaller relative error at distant points, where the pressures are large. Since the chief contribution to the resultant load comes from the high-pressure region, the effect of an error in the distribution in the low-pressure region near the boundary should be small.

In cases where the arguments of the last paragraph are invalid, or where a more accurate determination of the boundary is required, the following method may be applied: Consider a line of nodes in the ξ-direction, and let ξ_0 be that node nearest which the true boundary passes. If the solution is carried one node beyond ξ_0, to $\xi_2 = \xi_0 + 1$, the true solution might be drawn as in Fig. 6. If u_2, u_0, and u_1 are the values of u at ξ_2, ξ_0, and

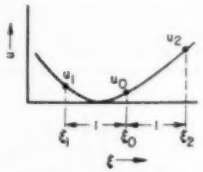

FIG. 6 PARABOLIC METHOD OF APPLYING TYPE 2 BOUNDARY CONDITION

$\xi_1 = \xi_0 - 1$, respectively, the parabolic approximation to u near ξ_0 has the form

$$u = \frac{1}{2}(u_1 + u_2 - 2u_0)z^2 - \frac{1}{2}(u_1 + 3u_2 - 4u_0)z + u_2 \quad [16]$$

where z is the distance measured back along the ξ-axis from ξ_2. The minimum point, where $(du)/(dz) = 0$, occurs for

$$z = \frac{1}{2}\frac{u_1 + 3u_2 - 4u_0}{u_1 + u_2 - 2u_0} \quad [17]$$

Since the boundary condition requires that u shall vanish at this point, we substitute Equation [17] in Equation [16], and set $u = 0$, to obtain the condition for boundary nodes

$$u_2 - \frac{(u_1 + 3u_2 - 4u_0)^2}{8(u_1 + u_2 - 2u_0)} = 0 \quad [18]$$

SECTION 4

The electrical method proposed for the solution of the algebraic Equations [14] and [15], is based on an analogy between the various terms in Equation [14] and the currents which flow in an electrical network.[5]

Consider a network of electrical resistances (see Fig. 7) of precisely the same form as the network introduced in section 2. The resistances connecting nodes on lines in the ξ-direction all have the same value R_1, while those parallel with the ζ-direction all have the value R_2. Let e_0 be the potential at one of the interior nodes of this network, and let e_1, e_2, e_3, e_4 be the potentials of the surrounding nodes (see Fig. 8). The currents i_1, i_2, i_3, i_4, flowing into the center nodes through the network resistors, are

[5] Analogies for the solution of similar equations have been known and used for some time. The author is indebted to Dr. R. Bott, formerly of the Electronics Department, Westinghouse Research Laboratories, for pointing out the general method, including the method of dealing with symmetry.

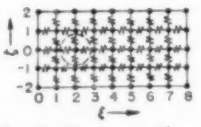

FIG. 7 RESISTANCE NETWORK REPLACING GRAPHICAL NETWORK OF FIG. 2

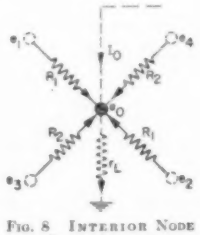

FIG. 8 INTERIOR NODE WITH INPUT CURRENT AND LEAK RESISTOR ADDED

$$i_1 = \frac{e_1 - e_0}{R_1}, \quad i_2 = \frac{e_2 - e_0}{R_1}, \quad i_3 = \frac{e_3 - e_0}{R_2}, \quad i_4 = \frac{e_4 - e_0}{R_2} \quad \ldots\ldots\ldots [19]$$

Let there be a wire leading current into each node of the network and let the strength of the current flowing into the center node above be I_0. Finally, let there be a resistor connecting each node to "ground" (the point of zero potential), and let the size of the resistor connected to the center node be r_L. By continuity of charge flow, the algebraic sum of the currents flowing into the center node is zero; and we obtain the equation

$$\frac{e_1 + e_2 - 2e_0}{R_1} + \frac{e_3 + e_4 - 2e_0}{R_2} - \frac{e_0}{r_L} + I_0 = 0 \quad \ldots [20]$$

Let I_0 for each node be proportional to the last term in Equation [14] for the corresponding point

$$I_0 = \lambda\varphi(\xi_0), \lambda > 0 \ldots\ldots\ldots\ldots\ldots [21a]$$

and let r_L be inversely proportional to the coefficient of the third term in Equation [14]

$$r_L = \frac{1}{\gamma\lambda f(\xi_0)}, \quad \gamma \neq 0 \ldots\ldots\ldots\ldots [21b]$$

where γ and λ are constants for the network. Let R_1 and R_2 have the values

$$R_1 = 1/\gamma\lambda \ldots\ldots\ldots\ldots\ldots [21c]$$

$$R_2 = n^2L^2/m^2B^2\gamma\lambda \ldots\ldots\ldots [21d]$$

Substitution of Equations [21] into [20] yields an equation which is clearly equivalent to Equation [14] provided u is set proportional to e

$$u = \gamma e \ldots\ldots\ldots\ldots\ldots [22]$$

In terms of potentials, the boundary conditions, Equations [15] and [18], take the form

$$e_0 = 0 \ldots\ldots\ldots\ldots\ldots [23]$$

and

$$e_2 - \frac{(e_1 + 3e_2 - 4e_0)^2}{8(e_1 + e_2 - 2e_0)} = 0 \ldots\ldots\ldots [24]$$

respectively. Equation [23] is imposed simply by grounding the boundary nodes. Equation [24] might be imposed automatically with the use of an electronic device, but a "trial-and-interpolation" method, in which the potentials (e_2) of nodes just beyond the boundary are adjusted until the expressions in Equation [24] vanish, may also be used. The latter method was applied in the example to be described.

In some cases the expression H^*/H, i.e., the term $f(\xi_0)$, is negative for nodes near the entering edge of the bearing, and the analogy requires negative leak resistances r_L. This effect may be obtained by electronic means, or by increasing the currents I_0 by the amounts that would flow in through the negative leaks. This may be done in the following manner: Set up the circuit at all nodes as shown in Fig. 8 except at those where negative leaks are called for. Use no leak (infinite resistance) at these points. Determine the potentials of these nodes, and calculate the amounts of current which would have flowed in from ground if negative resistors had been used. Add this to the currents I_0 for these points, reset the currents to these new values, and repeat the process until a point is reached when the current to be added becomes negligible. The potentials will then be the same as those if negative resistors had been used. Preliminary tests show that this process converges rapidly so that two or three trials should be sufficient.

A simplifying feature arises from the symmetry of the pressure distribution about the center line of the bearing surface. In the network previously described, the potential at each node is equal to that of its image node across the center line. Hence no change would occur if the network were folded about the center line, until opposite pairs of nodes were brought in contact. Accordingly, the original network is equivalent to one of half its size. In the "new" network, the resistances R_1, r_L, and the currents I_0 are the same as those in the "old" network only along the line of nodes which corresponds to the center line. All other new resistances have half their old values, and all other new currents have twice their old values.

Section 5

In order to illustrate the electrical method, an initial test was carried out for a case requiring the application of Type 2 boundary conditions, and the simulation of negative leak resistance. Since only a few accurate resistors were available when the test was made, the bearing length was taken to be infinite; for then the pressures do not vary across the bearing, no current flows across the network, and the network may be replaced by a single line of resistors.

The example chosen was the 180-deg bearing ($\beta = 180$ deg), with eccentricity $\epsilon = 0.5$, and $\theta_A = 43°14'$. The number $n = 8$ was chosen, so the bearing arc was divided into eight segments (a rather coarse network), represented by eight 1000 Ω wire-wound resistors. Having chosen $R_1 = 1000$ Ω, the values $\lambda = 10^{-3}$, $\gamma = 1$ were found suitable. The currents I_0 were furnished from a 135-volt battery, through regulating resistances of the order of 1 megohm. The large ratio of regulating resistance to network resistance was used in order that the currents I_0 would be insensitive to network potentials. Fig. 9 shows the basic circuit for each interior node.

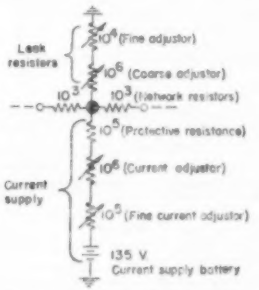

Fig. 9 Basic Circuit for Each Interior Node of Infinite Bearing Network

The current settings, leak-resistance settings, and potential readings were all made with a portable potentiometer, using a special switching circuit.

The preliminary calculations are shown in Tables 1 and 2. According to Table 2, the first leak resistance is negative. This effect was achieved by the method mentioned in section 4. Only two trials were necessary before the final current setting was obtained; and this setting was not affected by later adjustment of the potential at the opposite end when the Type 2 boundary condition was applied. The method mentioned in section 4 was used to apply the boundary condition.

The network potentials, converted into pressure readings in

TABLE 1 CALCULATION OF INPUT CURRENT (I_0) FOR 180-DEG INFINITELY LONG BEARING WITH $\epsilon = 0.5$ AND $\theta_A = 43°14'$

ξ	θ	① $\sin\theta$	$\cos\theta$	$1+\epsilon\cos\theta$	$(1+\epsilon\cos\theta)^{\frac{1}{2}}$	② $(1+\cos\theta)^{\frac{3}{2}}$	$g(\xi_0)=①\times②$ (Eq. 10b)	λ	$I_0=\lambda g(\xi_0)$ (Eq 21a)
0	43°14'							10^{-3}	
1	65°44'	0.91164	0.41098	1.20549	1.09795	0.75554	0.68878	"	0.68878×10^{-3}
2	88°14'	0.99952	0.03083	1.01542	1.00768	0.97730	0.97683	"	0.97683×10^{-3}
3	110°44'	0.93524	-0.35402	0.82299	0.90719	1.33939	1.25265	"	1.25265×10^{-3}
4	133°14'	0.72857	-0.68497	0.65752	0.81088	1.87558	1.36649	"	1.36649×10^{-3}
5	155°44'	0.41098	-0.91164	0.54418	0.73769	2.49106	1.02378	"	1.02378×10^{-3}
6	178°14'	0.03083	-0.99952	0.50024	0.70728	2.82638	0.08714	"	0.08714×10^{-3}
7	200°44'	-0.35402	-0.93524	0.53238	0.72964	2.57437	-0.91138	"	-0.91138×10^{-3}
8	223°14'							"	

TABLE 2 CALCULATION OF LEAK RESISTANCE (r_L) FOR 180-DEG INFINITELY LONG BEARING WITH $\epsilon = 0.5$ AND $\theta_A = 43°14'$

ξ	① $\frac{\sin^2\theta}{(1+\epsilon\cos\theta)^2}\cdot\frac{3}{4}\left(\frac{\pi}{\beta}\right)^2$	② $\frac{\cos\theta}{1+\epsilon\cos\theta}+\frac{3}{2}\epsilon\left(\frac{\pi}{\beta}\right)^2$	③ ①-②$=f(\xi_0)$ (Eq. 10a)	$\frac{1}{k\gamma}$	$r_L=\frac{1}{k\gamma f(\xi_0)}$ (Eq 21b)
0				1000	
1	0.016536	0.039431	-0.022895	"	-4.368×10^{4}
2	0.028016	0.003511	0.024505	"	4.081×10^{4}
3	0.037339	-0.049753	0.087092	"	1.148×10^{4}
4	0.035501	-0.12049	0.15599	"	0.6411×10^{4}
5	0.016492	-0.19376	0.21025	"	0.4756×10^{4}
6	0.000098	-0.23109	0.23120	"	0.4325×10^{4}
7	-0.012786	-0.20318	0.19039	"	0.5252×10^{4}
8				"	

TABLE 3 COMPARISON OF RESULTS OF ELECTRICAL METHOD WITH EXACT RESULTS OF VOGELPOHL

Quantity	Our Value	Vogelpohl's Value
Maximum pressure variable	3.47	3.486
Length of oil film	174° 13'	173° 6'
Resultant load variable	4.56	—
Position of load as measured from line of centers in direction of rotation	132°	133° 14'

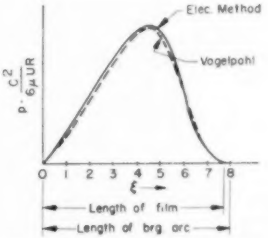

FIG. 10 COMPARISON OF RESULTS FOR PRESSURE DISTRIBUTION BETWEEN ELECTRICAL METHOD AND VOGELPOHL'S METHOD

accordance with Equations [11] and [22], are plotted in Fig. 10. The position of the end of the oil film was found from Equation [17]. The dotted curve was taken from a small-scale printed graph by Vogelpohl.[6] This curve represents his "exact" results for the same bearing. Table 3 gives a comparison of the results of the electrical method with the exact results of Vogelpohl.

ACKNOWLEDGMENT

The author wishes to thank Mr. J. Boyd and Mr. A. A. Raimondi of the Mechanics Department, Westinghouse Research Laboratories, who edited this report and prepared the figures. He also wishes to thank the Westinghouse Research Laboratories under whose summer student program this work was done.

[6] "On the Integration of Reynolds' Equation for Journal Bearings of Finite Width" (in German), by G. Vogelpohl, *Ingenieur Archiv*, vol. 14, 1943, pp. 192–212.

Design Data and Methods

It is important that the data contained in technical papers be made readily available to designing engineers. In order to satisfy these needs of industry, this section of the Journal includes a concise presentation of data and information drawn chiefly from papers previously published by the Applied Mechanics Division of The American Society of Mechanical Engineers.

The Calculation of Rectangular Bar Helical Springs

By A. M. WAHL,[1] EAST PITTSBURGH, PA.

Formulas and charts are given for calculating deflection and stress in helical compression or tension springs of rectangular cross section taking curvature effects into account. Such curvature effects are of importance particularly in small index springs in calculating stress (where fatigue is involved) and in calculating deflections for springs coiled flatwise.

HELICAL springs of square or rectangular bar section are sometimes used for cases where a large amount of energy must be stored within a given space. Particularly if the spring is coiled flatwise (Fig. 1) it is clear that a larger amount of material may be provided within a given outside diameter and compressed length than if a circular section were used. Consequently, other things being equal, a larger amount of energy may be stored within a given space for such a design than would be the case if a circular bar section were used. Although theoretically the rectangular bar section does not have as favorable an elastic stress distribution as does the round bar section, for static loading or loads repeated only a few times, this disadvantage is of no particular importance since local yielding of the most highly stressed portions can occur without affecting the performance of the spring appreciably or the capacity for storing energy. However, where fatigue or repeated loading of the spring is present, this nonuniformity of stress distribution will be a disadvantage.

In general, when bar stock of rectangular section is coiled to a helical form, a keystone shape of cross section finally results (Fig. 2). The formulas given herein, however, are based on the assumption of a true square or rectangular shape. It is believed that these formulas are sufficiently accurate for most practical purposes.

In contrast to the round wire helical compression or tension spring where curvature effects can be neglected in calculating deflections, such effects are particularly important for small index helical springs coiled flatwise (Fig. 1). In such cases, neglecting curvature may result in errors of 15 per cent or more. To facilitate the calculation in such cases the charts given herein may be used.

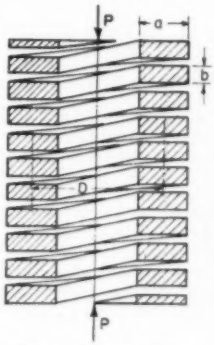

FIG. 1 HELICAL SPRING COILED FLATWISE

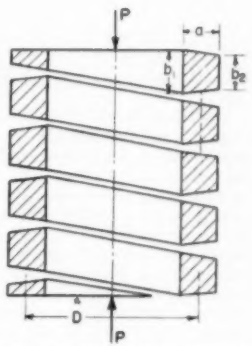

FIG. 2 KEYSTONE SHAPE ASSUMED BY SQUARE WIRE AFTER COILING

The formulas given also neglect the effects of pitch angle which are small for most practical springs. For taking such effects into account, the reader is referred to other published works.[2,3]

STRESS FORMULAS

(*a*) *Uncorrected Stress.* Where static loads are involved, the so-called "uncorrected" stress S_s (which neglects effects of bar curvature and direct shear) is generally considered to afford a better indication of load-carrying ability of the spring than does the "corrected" stress which takes these factors into account. The uncorrected stress is calculated from elastic theory by assuming the spring to behave essentially as a prismatical bar of rectangular cross section acted on by a torsion moment.[2] For a spring coiled flatwise as in Fig. 1, the uncorrected stress is

$$S_s = \frac{PD}{kab^2} \quad (a > b) \qquad [1]$$

In this case, P = load, a = long side, b = short side, D = mean

[1] Advisory Engineer, Westinghouse Electric Corporation. Mem. ASME.

Discussion of this paper should be addressed to the Secretary, ASME, 29 West 39th Street, New York, N. Y., and will be accepted until April 10, 1952, for publication at a later date. Discussion received after the closing date will be returned.

NOTE: Statements and opinions advanced in papers are to be understood as individual expressions of their authors and not those of the Society. Manuscript received by ASME Applied Mechanics Division, June 19, 1951.

[2] "Mechanical Springs," by A. M. Wahl, The Penton Publishing Company, Cleveland, Ohio, 1944.

[3] "Berechnung Zylindrischer Schraubenfedern," by O. Göhner, *Zeitschrift des Vereines deutscher Ingenieure*, vol. 76, 1932, pp. 269–272; correction, p. 352; appendix, 735.

diameter, k = a factor depending upon the ratio (long side)/(short side) = a/b and which may be taken from Table 1.

TABLE 1 SPRING DATA

Ratio $\frac{a}{b}$ or $\frac{b}{a}$	k	C_1
1.0	0.416	0.179
1.2	0.438	0.212
1.5	0.462	0.250
2	0.492	0.292
2.5	0.516	0.317
3.0	0.534	0.335
5	0.582	0.371
10	0.624	0.398
∞	0.666	0.424

For a square bar section the formula becomes

$$S_s = \frac{2.4\,PD}{a^3} \quad \ldots\ldots [2]$$

It should be noted that for a keystone section as in Fig. 2 an average length of side should be used, i.e., average of sides b_1, b_2, a (Fig. 2) should be used for a in Equation [2].

The uncorrected stress for the case shown in Fig. 3 where the long side of the bar section is parallel to the spring axis ($a < b$) is

$$S_s = \frac{PD}{kba^2} \quad (a < b) \quad \ldots\ldots [3]$$

In this case the ratio b/a is to be used to obtain the value of k from Table 1.

(*b*) *Corrected Stress.* This stress takes into account both effects of direct shear and bar curvature and should be used for calculating stress range where the spring is subjected to fatigue or repeated loading.

For the spring coiled with the long side parallel to the spring axis (Fig. 3) the maximum corrected stress occurs at a localized region near the inside of the coil at the middle of the long side. However, for a spring coiled flatwise (Fig. 1) the maximum stress may occur either at the inside of the coil or at some point on the long sides. Hence the calculation of corrected stress in rectangular bar springs is, in general, more complicated than that in round bar springs.[3] To simplify this calculation, the following formula due to Liesecke[4] may be used: The corrected stress S_s' is

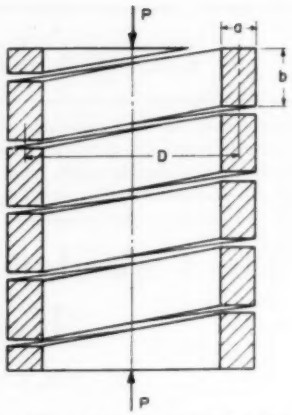

FIG. 3 HELICAL SPRING WITH LONG SIDE OF BAR PARALLEL WITH AXIS

$$S_s' = \beta \frac{PD}{ab\sqrt{ab}} \quad \ldots\ldots [4]$$

where β is a factor taken from the chart in Fig. 4 for the given value of a/b or b/a and of the index $c = D/a$. It should be noted that for the spring coiled flatwise (Fig. 1) a/b is used; for the spring in Fig. 3, b/a is used.

For square bar springs (where $a/b = 1$) the corrected stress is given by[3]

[4] "Berechnung Zylindrischer Schraubenfedern mit rechteckigen Drahtquerschnitt," by G. Liesecke, *Zeitschrift des Vereines deutscher Ingenieure*, vol. 77, 1933, pp. 425–426.

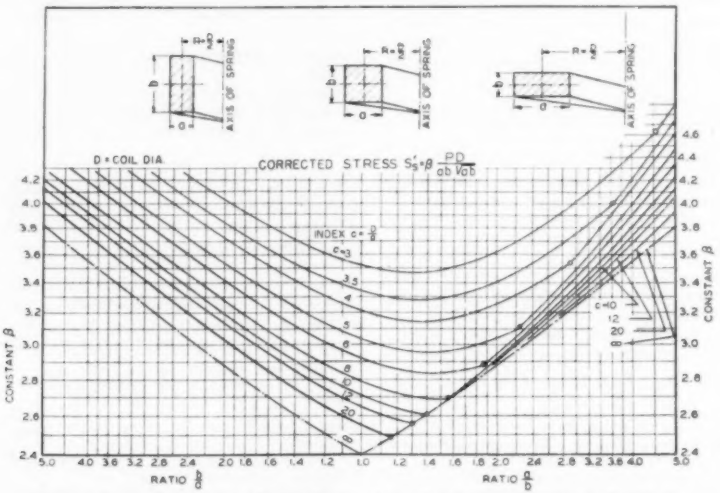

FIG. 4 CURVES FOR FINDING STRESS FACTOR β FOR CALCULATING CORRECTED STRESS IN RECTANGULAR BAR SPRINGS
(Based on charts by Liesecke, footnote 4.)

$$S_s' = K'S_s \quad \ldots\ldots [5]$$

where S_s = uncorrected stress for square bar springs (Equation [2]) and K' is a stress-multiplication factor, depending upon spring index $c = D/a$

$$K' = 1 + \frac{1.2}{c} + \frac{0.56}{c^2} + \frac{0.5}{c^3} \quad \ldots\ldots [6]$$

A curve of K' versus index c is given in Fig. 5. Incidentally, this curve gives slightly lower values than the corresponding curve for round bar springs.[5]

Deflection Formulas

The deflections of rectangular bar springs are frequently calcu-

[5] Footnote 2, p. 37.

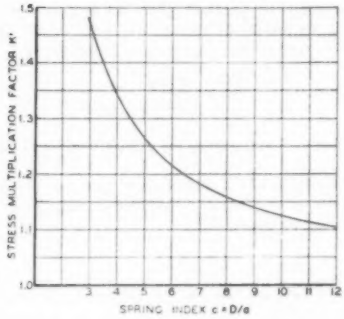

Fig. 5 Stress Multiplication Factor K' for Square Bar Helical Springs; Spring Index ≥ 3

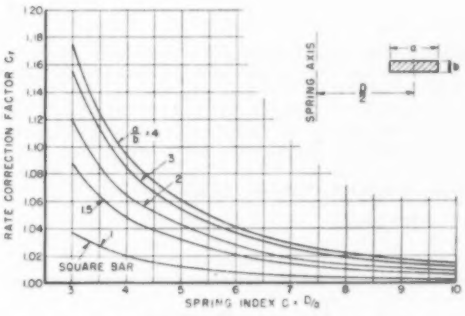

Fig. 7 Curves for Finding Rate Correction Factor C_r
(Spring coiled flatwise.)

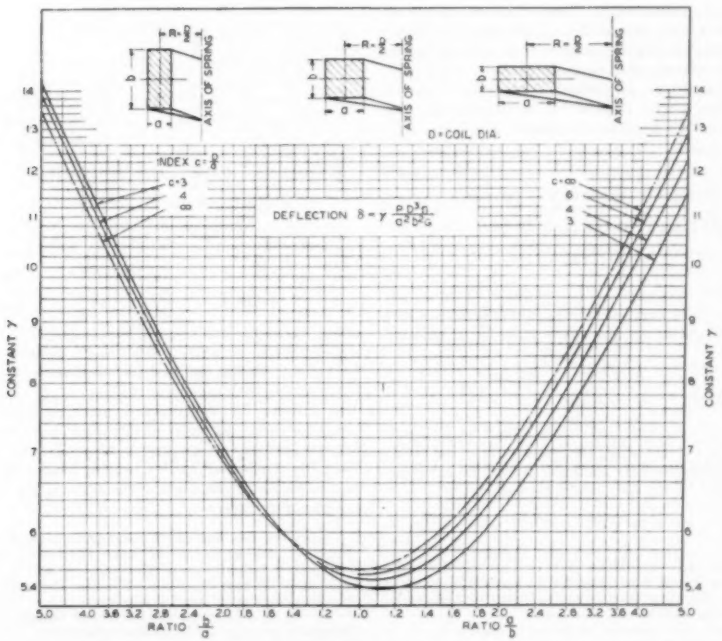

Fig. 6 Curves for Finding Deflection Factor γ for Calculating Rectangular Bar Springs
(Based on charts by Liesecke, footnote 6.)

lated in a simple manner by assuming the spring to act essentially like a rectangular bar under a torsion moment $PD/2$. However, since this method neglects the effects of bar curvature and direct shear, the calculated deflections may be in error by as much as 15 per cent or so, particularly for springs coiled flatwise and having small indexes and ratios a/b over 2. To take curvature effects into account, the deflection δ may be calculated from the following formulas[6]

$$\delta = \gamma \frac{PD^3 n}{a^2 b^2 G} \quad [7]$$

In this, n = number of active coils, G = modulus of rigidity, and γ is a factor depending on the spring index c and on the ratio a/b or b/a. The factor γ may be taken from the chart in Fig. 6 which is based on that given by Liesecke.[6] Note that if the spring is coiled flatwise, the ratio a/b is used (right side of chart) while if coiled lengthwise the ratio b/a is taken (left side). Interpolation for intermediate values of the spring index c may be carried out with enough accuracy for most purposes.

[6] Footnote 4, p. 892.

For springs coiled flatwise as in Fig. 1, the deflection δ also may be calculated by

$$\delta = \frac{\delta_0}{C_r} \quad [8]$$

where δ_0 is the deflection calculated in the usual way by assuming the bar section to be in torsion and neglecting curvature effects. The factor C_r (Fig. 7) is a rate-correction factor which depends on the index c and on the ratio a/b of the lengths of the sides. Values given are based on formulas due to Göhner.[7] The deflection δ_0 for a spring coiled flatwise (Fig. 1) is given by

$$\delta_0 = \frac{PD^3 n}{C_1 a b^3 G} \quad [9]$$

where the factor C_1 depends on the ratio a/b and may be taken from Table 1.

Further discussion of the calculation of elastic stresses and deflections in square or rectangular bar helical compression or tension springs is given elsewhere.[2,3]

Brief Notes

On the recommendations of the Executive Committee of the ASME Applied Mechanics Division, it has been decided to initiate a section devoted to brief notes on technical matters in mechanics. These notes must not be longer than 750 words (about 2½ double-spaced typewritten pages, including figures) and will be subject to the usual review procedure prior to publication. After approval such notes will be published in the next issue of the Journal. The notes should be submitted to the Secretary of the ASME Applied Mechanics Division.

Bending of Honeycombs and of Perforated Plates

By G. HORVAY,[1] SCHENECTADY, N. Y.

A HONEYCOMB structure, or a perforated sheet of triangular layout with long, slender ligaments can be treated in bending calculations as an isotropic solid plate of effective constants

$$\left.\begin{aligned} \mu_b &= (1-K)/(1+3K), \quad E_b = (1-\mu_b)Eh/R \\ \mu_a &= \mu, \quad E_a = 2Eh/R, \quad G_a = Gh/R \end{aligned}\right\} \quad [1a, b, c, d, e]$$

where μ_b, E_b are Poisson's ratio and Young's modulus for bending, μ_a, E_a for axial stretching, G_a the modulus for axial shear; μ, E, G are the ordinary moduli; $2R$, $2h$, H denote the hole spacing, average ligament width, and plate thickness, and

$$K = C/B \quad [2]$$

is the ratio of torsional rigidity C to the bending stiffness $B = EI$ of a ligament.[2]

I. Malkin, who first considered the problem of determining μ_b, E_b in an important paper,[3] represented the perforated sheet by an array of hexagons, as indicated in Fig. 1, and compared the (bending and torsional) energy of the three beams $\overline{01}$, $\overline{12}$, $\overline{13}$

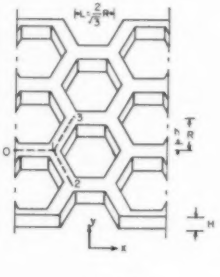

FIG. 1

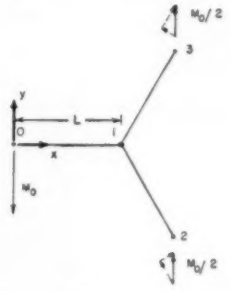

FIG. 2

in Fig. 2 (expressed in terms of curvatures), with the corresponding expression for plates. Due to an unfortunate slip in the derivations, Malkin obtained the value $\mu_b = (1-K)/(3+K)$. His E_b agrees with Equation [1b].

In deriving the formulas it is much more convenient to express the energy in terms of moments, or to use the moment-balance method, as adopted in the author's Congress paper. From Fig. 2 it is seen that if a bending moment M_x per inch acts on the left and right edges of the plate in Fig. 1, beam $\overline{01}$ will experience a moment

[1] General Electric Company, Knolls Atomic Power Laboratory.

Discussion of this paper should be addressed to the Secretary, ASME, 29 West 39th Street, New York, N. Y., and will be accepted until April 10, 1952, for publication at a later date. Discussion received after the closing date will be returned.

NOTE: Statements and opinions advanced in papers are to be understood as individual expressions of their authors and not those of the Society. Manuscript received by ASME Applied Mechanics Division, August 10, 1951.

[2] The sheet also has effective stretching constants μ^* and E^* to be used in plane stress calculations. The latter constants were derived in the author's unclassified Report KAPL P-456, January, 1951, and will also be published in the Proceedings of the First National Congress of Applied Mechanics.

[3] "Notes on a Theoretical Basis for the Design of Tube Sheets of Triangular Layout," by I. Malkin, presented at the Annual Meeting, New York, N. Y., November 26–December 1, 1950, of THE AMERICAN SOCIETY OF MECHANICAL ENGINEERS; to be published in 1952 Transactions.

$$M_0 = 2RM_x \quad \ldots [3]$$

while beams 12, 13 will experience moments $M_0/2$ each, of which $\sqrt{3}M_0/4$ is a twisting moment, $M_0/4$ a bending moment. They cause bending (φ) and twisting (ψ) of beams 01, 12 of amount

$$\varphi_{01} = M_x L/B,\ \psi_{01} = 0,\ \varphi_{12} = M_0 L/4B,\ \psi_{12} = \sqrt{3}M_0 L/4C \quad [4]$$

Consequently, the curvatures are

$$\left.\begin{aligned} \kappa_x &= \frac{\varphi_{01} + \varphi_{12}/2 + \sqrt{3}\psi_{12}/2}{3L/2} = \left(\frac{3/4}{B} + \frac{1/4}{C}\right) 2RM_x \\ \kappa_y &= \frac{\sqrt{3}\varphi_{12}/2 - \psi_{12}/2}{\sqrt{3}L/2} = \left(\frac{1/4}{B} - \frac{1/4}{C}\right) 2RM_x \end{aligned}\right\} \quad \ldots [5]$$

From the defining equations

$$\mu_h = -\kappa_y/\kappa_x,\quad \frac{E_h I_{\text{solid}}}{I_{\text{solid}}} = \frac{M_x/\kappa_x}{H^3/12} = \frac{(1-\mu_h)B/2R}{I/2h} \quad \ldots [6]$$

Equations [1*a*, *b*] follow at once.

Similarly, if V_x per inch shear force acts on the left and right edges of the plate in Fig. 1, beam 01 will experience a shear force

$$V_0 = 2RV_x \quad \ldots [7]$$

while beams 12 and 13 will experience shear forces $V_0/2$ each. The resultant shear deflection

$$\frac{3}{2} V_x L/2\bar{h}HG$$

divided by the distance $3L/2$ of edge 23 from the y-axis yields the shear strain

$$\gamma = V_0/2\bar{h}HG \quad \ldots [8]$$

and the effective axial shear modulus assumes the value $G_a = V_x/H\gamma$ given in Equation [1*e*]. The relation, Equation [1*c*], is obvious, while Equation [1*d*] expresses the amount of material in the tube sheet in terms of the material in the solid plate.

Bending of Rectangular Beams

By L. H. DONNELL,[1] CHICAGO, ILL.

THE stresses in a rectangular beam with axis in the x-direction under unit pressure $T(x)$ on the top surface ($z = -c$) and $B(x)$ on the bottom surface ($z = c$), are expressed as infinite series, in which the first terms correspond to elementary theory and later terms to increasingly minor refinements. Let $M(x)$ and $V(x)$ represent the conventional bending moment and transverse shear (per unit width); let $T - B = D(x)$, $T + B = S(x)$; then $D = -V_x$, $V = M_x$, and

$$c^3\sigma_x = 3Mz/2 + D(5z^3 - 3c^2z)/10 - D_{xx}(105z^5 + 70c^2z^3 - 87c^4z)/2800 + c^3S_{xx}(3z^2 - c^2)/12 \ldots\ldots$$

$$c^3\sigma_z = -D(z^3 - 3c^2z)/4 - c^3S/2 + D_{xx}(z^5 - 2c^2z^3 + c^4z)/40 \ldots\ldots$$

$$c^3\tau_{xz} = -3V(z^2 - c^2)/4 - D_x(5z^4 - 6c^2z^2 + c^4)/40 + D_{xxx}(35z^6 + 35c^2z^4 - 87c^4z^2 + 17c^6)/5600 - c^3S_{xxx}(z^3 - c^2z)/12 \ldots\ldots$$

These series satisfy equilibrium and continuity conditions of two-dimensional elasticity theory and the boundary conditions on the top and bottom surfaces, $z = -c, c$: $\tau_{xz} = 0$, $\sigma_z = -T$, $-B$. End conditions can be satisfied approximately in the same way as in elementary beam theory; more exact satisfaction could be achieved by superposition of self-balancing load systems on the ends. A few basic solutions for such loads could be developed for this purpose; these would be local and hence substantially independent of beam length as long as this exceeded the depth.

The first terms in σ_x and τ_{xz} represent elementary beam theory; the next terms in σ_x and σ_z, involving D and S, have been suggested by Seewald.[2] The first term in σ_z and in τ_{xz} and the first two in σ_x together constitute a good approximate solution for the complete load system. All other terms give zero stresses on the top and bottom and zero resultants on all cross sections, and represent increasingly minor corrections to the internal stress distribution. The present solution thus differs fundamentally from, and, in general, converges much faster than series solutions such as the well-known Fourier solution in which each term takes care of only one load component.

The foregoing solution may be found step by step as follows: The coefficients of terms involving D, S, D_x, S_x, are found from the elementary beam-theory terms by substituting all these terms in the general equilibrium and continuity conditions and $-c\int^c \sigma_x dz = 0$, $-c\int^c \sigma_x z\, dz = M$, $-c\int^c \tau_{xz} dz = V$, $\tau_{xz}(z = \mp c) = 0$, $\sigma_z(z = \mp c) = -T, -B$, neglecting terms involving derivatives higher than the first. Coefficients of terms involving second and third derivatives are then found from the terms just neglected by substituting all these terms in the equilibrium and continuity conditions and $-c\int^c \sigma_x dz = -c\int^c \sigma_x z\, dz = -c\int^c \tau_{xz} dz = \tau_{xz}(z = \mp c) = \sigma_z(z = \mp c) = 0$, neglecting derivatives higher than the third; subsequent terms are found similarly.

Displacements can be found from the stresses as usual. The deflection w of the middle surface is given by $Ewc_{xx} = -3M/2c^3 - 3(8 + 5\mu)D/20c \ldots$ for plane stress (for plane strain substitute $E/[1-\mu^2]$ and $\mu/[1-\mu]$ for E and μ).

The present solution of course applies directly only when there are no discontinuities in D, S, and their derivatives. However, if there are discontinuities the solution can be applied as usual to all sections except those where the discontinuities lie; then it can be shown that each type of discontinuity produces a characteristic "local distribution" of stresses and displacements which can be calculated for unit magnitude of the discontinuity, multiplied by the magnitude present, and superposed on the foregoing solution to give the complete solution.

The most serious such discontinuity is that caused by a concentrated load. For such a load alone at a certain section, D and S would be zero at other sections and the present solution would give the same results as the elementary solution. Seewald[2] has determined the characteristic local distribution for this case, that is, the difference between the exact and elementary solutions. Similar local distributions for unit discontinuities in magnitude, slope, and so forth of distributed load could be developed; they would be much less important. Separate local distributions would not have to be developed for discontinuities occurring near an end of the beam (except perhaps for a concentrated load at the end, involving a singular point on the end cross section). The local distributions for discontinuities merely should be added before satisfying the beam end conditions; the presence of some added stresses on the end cross sections would not make this any more difficult.

---

[1] Research Professor of Mechanics, Illinois Institute of Technology. Mem. ASME.

Discussion of this paper should be addressed to the Secretary, ASME, 29 West 39th Street, New York, N. Y., and will be accepted until April 10, 1952, for publication at a later date. Discussion received after the closing date will be returned.

NOTE: Statements and opinions advanced in papers are to be understood as individual expressions of their authors and not those of the Society. Manuscript received by ASME Applied Mechanics Division, December 29, 1951.

[2] "Theory of Elasticity," by S. Timoshenko, McGraw-Hill Book Company, Inc., New York, N. Y., 1934, p. 44.

[3] Ibid., pp. 99–103.

A Photoelastic Re-Examination of Notched Tension Bars

By M. M. FROCHT,[1] R. GUERNSEY, JR.,[2] and D. LANDSBERG[3]

IN 1937 Neuber[4] published factors of stress concentration for tension bars with semicircular grooves based on an interpolation between limiting theoretical values. In 1947 Chih-Bing Ling[5] published similar factors based on a purely theoretical solution. In 1948, R. E. Peterson[6] pointed out that Chih-Bing Ling's results differed substantially from the available photoelastic data. However, Ling considered the experimental evidence inconclusive.

We have recently re-examined this problem photoelastically employing the latest refinements of technique.[7] In order to demonstrate the accuracy of the latest photoelastic results, factors of stress concentration were determined for a tension bar having a central circular hole, for which Howland[8] gives a theoretical solution. Values of k were computed for nine different ratios of r/d within the range of Howland's solution.

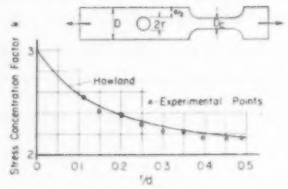

FIG. 1

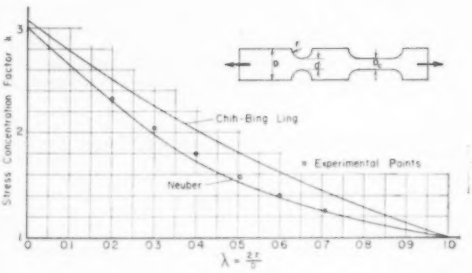

FIG. 2

The results are shown in Fig. 1 along with the theoretical curve. The maximum deviation of any experimental point from the theoretical value is 1.8 per cent and most of the results are much closer

Fig. 2 gives the latest photoelastic results for the grooved bar as well as the two theoretical curves. It is seen that all of the experimental values lie considerably below the curve given by Ling. The differences, which are as much as 13 per cent, are too large to be ascribed soley to experimental error. In view of the demonstrated accuracy of the photoelastic results in the case of the Howland solution a re-examination of the mathematical solution for the grooves is perhaps indicated.

[1] Research Professor of Mechanics, Illinois Institute of Technology, Chicago, Ill. Mem. ASME.

[2] Research Corporation Fellow, Laboratory of Experimental Stress Analysis, Mechanics Department, Illinois Institute of Technology; now Associate Professor of Mechanics, University of Texas, Austin, Texas.

[3] Assistant Research Engineer, Laboratory of Experimental Stress Analysis, Mechanics Department, Illinois Institute of Technology.

[4] "Kerbspannungslehre-Grundlagen für Genaue Spannungsrechnung," by H. Neuber, Julius Springer, Berlin, Germany, 1937; or "Theory of Notch Stresses; Principles for Exact Stress Calculation," Translation 74, David Taylor Model Basin, 1945.

[5] "Stresses in a Notched Strip Under Tension," by Chih-Bing Ling, JOURNAL OF APPLIED MECHANICS, Trans. ASME, vol. 69, 1947, pp. A-275–280.

[6] Reference 5, discussion by R. E. Peterson, JOURNAL OF APPLIED MECHANICS, Trans. ASME, vol. 70, 1948, p. A-176.

[7] "Photoelasticity—A Precision Instrument of Stress Analysis," by M. M. Frocht, R. Guernsey, Jr., and D. Landsberg, to be presented at the spring, 1952, meeting of the Society for Experimental Stress Analysis.

[8] "On the Stresses in the Neighborhood of a Circular Hole in a Strip Under Tension," by R. C. J. Howland, Philosophical Transactions of the Royal Society, vol. A-229, 1930, pp. 49–86.

Discussion of this paper should be addressed to the Secretary, ASME, 29 West 39th Street, New York, N. Y., and will be accepted until April 10, 1952, for publication at a later date. Discussion received after the closing date will be returned.

NOTE: Statements and opinions advanced in papers are to be understood as individual expressions of their authors and not those of the Society. Manuscript received by ASME Applied Mechanics Division, December 10, 1951.

Discussion

Stability of Flow in a Rocket Motor[1]

S. Sherman.[2] Recently D. F. Gunder and D. R. Friant analyzed the chugging of liquid-fuel rocket motors.[1] In the bipropellant case, their analysis results in the following: The rocket motor is stable (chug-free) if and only if none of the roots of

$$z^2 + Mz + N + e^{-z}(Sz + T) = 0 \quad \ldots\ldots\ldots [1]$$

has positive real parts where M, N, S, and T are positive rocket parameters defined in the paper.[1] For simplicity the borderline case where Equation [1] has pure imaginary roots is ignored. Equation [1] is identical with the authors' Equation [28].

The locations of the roots of equations such as Equation [1] have been studied in references (1, 2, 3, 4, 5),[3] and particularly in connection with the stability of dynamical systems with time lag. An efficient method for stability calculations in these cases has been given in references (1, 2). The method given there as well as the method given in reference (5) has the advantage over the method given in the paper in that the full Nyquist diagram need not be plotted but merely the intersection of the diagram with certain simple critical contours must be computed. The contours in references (1, 2) have the advantage over the contours of reference (5) in so far as they lead to very simple calculations such as the solution of a quadratic equation with real coefficients and the determination of a small number of angles. While the purpose of this discussion is to show how the methods of references (1, 2) can be applied to the location of the roots of Equation [1], the method can be applied to the roots of $z^2 + Mz + N + e^{-z}(Rz^2 + Sz + T) = 0$, where no assumption need be made about the sign of the real coefficients M, N, R, S, T.

Because of the assumptions on M and N, the roots of Equation [1] have positive real parts if and only if the roots of

$$1 + \frac{(Sz + T)e^{-z}}{z^2 + Mz + N} = 0 \quad \ldots\ldots\ldots [2]$$

have positive real parts. Applying the Cauchy-Nyquist method of references (1, 2) we see that none of the roots has positive real parts if and only if the curve, defined by

$$f(p) = \frac{(Sp + T)e^{-p}}{p^2 + Mp + N} \quad \ldots\ldots\ldots [3]$$

as p traverses the imaginary axis from $-i\infty$ to $+i\infty$, encloses the point $-1 + 0i$, zero times (measured algebraically). If we let $p = i\alpha$ for real α, $\arg f(i\alpha)$ is no longer a monotone function for positive α unlike the situation in references (1, 2). It continues to be true that as $|\alpha| \to \infty$, $f(i\alpha) \to 0$.

Following references (1) and (2), we seek first to determine when $|f(i\alpha)| = 1$ which yields

$$\alpha^2 = \frac{-M^2 + S^2 + 2N \pm \sqrt{(M^2 - S^2 - 2N)^2 + 4(T^2 - N^2)}}{2} \quad \ldots\ldots [4]$$

We thus get four roots for α (counting multiple roots multiply).

If all of these are not real then for all real α, $|f(i\alpha)| < 1$ and the graph of $f(i\alpha)$ for real α does not encircle $(-1,0)$. In this case we have a stable system.

If some of the roots are real, arrange them in descending size. Let the largest α be γ_1. Further, count multiple roots the appropriate multiple number of times. For convenience of notation, if there are less than 4 real roots, repeat the last root until there is a sequence $\gamma_1 \geq \gamma_2 \geq \gamma_3 \geq \gamma_4$, and the case where there are no real roots could be included in the subsequent analyses by letting $\gamma_1 = \gamma_2 = \gamma_3 = \gamma_4 = \infty$. In the intervals $\infty > \alpha > \gamma_1$, and $\gamma_2 > \alpha > \gamma_3$, we have $|f(i\alpha)| < 1$ and the contour does not encircle $-1 + 0i$. In the intervals $\gamma_1 > \alpha > \gamma_2$ and $\gamma_3 > \alpha > \gamma_4$, we have $|f(i\alpha)| > 1$.

Let N_{jk} = number of integer values of n such that

$$\arg f(i\gamma_j) > (2n + 1)\pi > \arg f(i\gamma_k) \quad \ldots\ldots\ldots [5]$$

From the foregoing definition $N_{jk} + N_{kj}$ gives the net number of times the appropriate contour encircles $(-1 + 0i)$ in a clockwise direction.

Theorem. The system is stable if and only if

$$N_{12} + N_{21} + N_{34} + N_{43} = 0 \quad \ldots\ldots\ldots [6]$$

This means that the curve does not encircle $(-1 + 0i)$.

Note that if either $N_{12} \geq 2$ or $N_{34} \geq 2$ then the system is necessarily unstable. The situation differs from the reference (1) and (2) cases in so far as theoretically one "unstable" interval (γ_1, γ_2) may be saved by a possibly stabilizing interval (γ_3, γ_4) so that both intervals have to be considered as well as the N_{jk} terms, while, in the reference (1, 2) cases, the existence of one unstable interval immediately implies that the system is unstable. Thus in the reference (1, 2) cases the N_{jk} terms need not be introduced.

The foregoing yields sufficient conditions for stability such as

$$(a) \quad \text{if } M^2 - S^2 - 2N > 0 \text{ and } |T| < |N|, \quad \ldots\ldots [7]$$

or

$$(b) \quad \text{if } (M^2 - S^2 - 2N)^2 + 4(T^2 - N^2) < 0 \quad \ldots\ldots [8]$$

then the system is stable.

After the current discussion was written, but before it was submitted for publication, the writer had the opportunity to read a discussion of the paper[4] by H. I. Ansoff. The discussion proceeds in the spirit of the current discussion and derives "a sufficient condition for stability" of a bipropellant rocket motor, whereas the current discussion derives a "necessary and sufficient condition." By the methods of the current discussion, the sufficient condition for stability of a monopropellant rocket motor derived in Ansoff's discussion can be weakened to give a necessary and sufficient condition which is the following: A monopropellant system is stable if and only if $B \geq H$ or

$$\sqrt{H^2 - B^2} + \arctan\left(\frac{\sqrt{H^2 - B^2}}{B}\right) \leq \pi$$

with $H > B$. The critical equality

$$\sqrt{H^2 - B^2} + \arctan\left(\frac{\sqrt{H^2 - B^2}}{B}\right) = \pi$$

[1] By D. F. Gunder and D. R. Friant, published in the September 1950, issue of the Journal of Applied Mechanics, Trans. ASME, vol. 72, pp. 327–333.

[2] Staff Engineer, Lockheed Aircraft Corporation, Burbank, Calif.

[3] Numbers in parentheses refer to the Bibliography at the end of this discussion.

[4] Journal of Applied Mechanics, March, 1951, p. 114.

implies Equation [12] of the paper,[1] when a trivial typographical error is corrected in the latter. There is also a typographical error in Equation [18] of the paper.[1]

BIBLIOGRAPHY

1 "Stability of Linear Oscillating Systems With Constant Time Lag," by H. I. Ansoff, JOURNAL OF APPLIED MECHANICS, Trans. ASME, vol. 71, 1949, pp. 158–164.

2 "A General Stability Criterion for Linear Oscillating Systems With Constant Time Lag," by H. I. Ansoff and J. A. Krumhansl, *Quarterly of Applied Mathematics*, vol. 6, 1948, pp. 337–341.

3 "On a Problem of Hurwitz for Transcendental Equations," by W. N. Capyrin, Akademi Nauk, SSSR Prikl, Mat. Mch., vol. 12, 1948, pp. 301–328. (Russian.)

4 "The Routh-Hurwitz Problem for Polynomials and Entire Functions," by N. G. Cebotarev and N. N. Meiman, with Appendix by G. S. Barhin and A. N. Hovansky, *Trudy Mat. Institut Steklov*, vol. 26, 1949, 333 pp. (Russian.)

5 "A Note on Stability Calculations and Time Lag," by S. Sherman, *Quarterly of Applied Mathematics*, vol. 5, 1947, pp. 92–96.

6 "Stability of a Class of Systems of Automatic Regulation With Distributed Parameters," *Avtomatika i Telemehanika*, vol. 9, 1948, pp. 176–189. (Russian.)

Sinusoidal Torsional Buckling of Bars of Angle Section Under Bending Loads, as a Problem of Plate Theory[1]

P. P. BIJLAARD.[2] The discrepancies found by the author between his calculations from plate theory and from bar theory (theory of torsional and flexural buckling) must be due to incorrect assumptions. In 1939 the writer derived the exact buckling condition for an angle with equal legs subjected to pure compression according to the plate theory. He took account of the fact that the intersection line of the middle planes of the flanges does not remain straight.[3] It is a special case of the writer's theory on the elastic and plastic stability of plate assemblies.[4] Later he discussed the buckling condition of an angle in an English paper.[5] The results differ only 0.5 per cent from those of the theory of torsional and flexural buckling.[6]

Discrepancies between a calculation from plate and bar theory occur only if one of the plates is significantly rotationally restrained by the other(s) so that its cross section will bend, which distortion is not taken into account in the formulas for torsional and flexural buckling. This occurs, for example, with the web of a T-section with a relatively rigid flange. For the latter case simple explicit formulas for the critical stress were derived by the writer's method of split rigidities.

From the speaker's calculation according to the plate theory, it follows that one reason for the discrepancy is that in Equation [2] of the paper he assumes that $w = 0$ for $y = 0$. Actually for $y = 0$ the "buckling" leg is supported elastically by the other leg. The latter is bent in its own plane by the pressures exerted on it by the buckling leg and vice versa. Hence, one of the conditions for $y = 0$ is not $w = 0$ but[7]

$$EI\frac{\partial^4 w}{\partial x^4} + D\left[\frac{\partial^4 w}{\partial y^4} + (2 - \nu)\frac{\partial^4 w}{\partial x^2 \partial y}\right] + A\sigma_x\frac{\partial^2 w}{\partial x^2} = 0$$

Since by the torsional buckling of the flanges the center of gravity of the angle displaces in the direction of the minor axis of inertia, the angle will bend about its major axis so that the neutral plane in bending comprises the intersection line of the middle planes of the flanges. Hence in the foregoing boundary condition the moment of inertia I of the supporting flange has to be taken about its upper boundary and $I = tb^3/3$, where t and b are the thickness and width of a flange.[8,9] Furthermore, $A = bt$.

The foregoing explains the discrepancy for long columns (small α). The writer appreciates the fact that for short columns (large α) the discrepancy is caused by the author's assumption that the warping constant Γ is zero.

G. HERRMANN.[8] In this paper the author undoubtedly has presented an important contribution in the field of elastic stability, combining in his method of attack exact and approximate procedures and having succeeded in determining exact buckling values for such a complicated case as that considered. In obtaining approximate load factors, which were used as a guide to limit the amount of calculation needed for the exact eigenvalues, the author should be aware of the fact that in applying the Rayleigh-Ritz method, the deflection function has to satisfy only the so-called "artificial boundary conditions," but need not satisfy any "natural boundary conditions."[9] Much avoidable computation work would have been saved in taking advantage of the theorem mentioned.

The plate-buckling problem of the paper was considered before by C. F. Kollbrunner and the writer[10] on the basis of the Rayleigh-Ritz method. The deflection function was assumed to be of the very simple form

$$w = cy \sin\frac{\pi x}{a} \qquad [1]$$

For the free edge $y = b$, of the plate the artificial boundary conditions are

$$\frac{\partial^2 w}{\partial y^2} = 0, \quad \frac{\partial^3 w}{\partial y^3} = 0 \qquad [2]$$

which might be called, in this case, "beam boundary conditions," since they are the same as at the free end of a beam. The "Ansatz" Equation [1] satisfies Equation [2] herewith.

The deflection function does not need, however, to satisfy the plate-boundary conditions for the free edge, as postulated by the author, which are formulated by Equation [3] of the paper.

---

[1] By H. J. Plass, Jr., published in the September, 1951, issue of the JOURNAL OF APPLIED MECHANICS, Trans. ASME, vol. 73, pp. 285–292.

[2] Cornell University, Ithaca, N. Y.

[3] "Nauwkeurige berekening van de Plooispanning van hoekstalen, zoowel voor het elastische als voor het plastische Gebied," by P. P. Bijlaard, De Ingenieur in Ned. Indie, 1939, pp. I.35–I.45.

[4] "Theory of the Plastic Stability of Thin Plates," by P. P. Bijlaard, Public International Association of Bridge and Structural Engineering, vol. 6, 1940–1941, pp. 45–69.

[5] "Some Contributions to the Theory of Elastic and Plastic Stability," by P. P. Bijlaard, Public International Association of Bridge and Structural Engineering, vol. 8, 1947, pp. 17–80.

[6] "On the Torsional and Flexural Stability of Thin Walled Open Sections," by P. P. Bijlaard, Proc. Kon. Akad. v. Wetensch, Amsterdam, Holland, vol. 51, 1948, pp. 314–321.

[7] "Theory of Elastic Stability," by S. Timoshenko, McGraw-Hill Book Company, Inc., New York, N. Y., 1936, p. 346.

[8] Assistant Professor of Civil Engineering, Columbia University, Department of Civil Engineering, New York, N. Y.

[9] See, for example: "Problems of Equilibrium and Vibrations," by R. Courant, Bulletin, American Mathematical Society, vol. 49, 1943, pp. 1–23.

"Stabilitätsprobleme der Elastostatik," by A. Pflüger, J. Springer, Berlin, Germany, 1950, p. 169.

[10] Reine Biegungsbeulung rechteckiger Platten im elastischen Bereich," by C. F. Kollbrunner and G. Herrmann, Mitteilungen der TKVSB, No. 2, Verlag Leemann, Zürich, Switzerland, 1949.

See also: Stabilität rechteckiger, durch linear verteilte Randkräfte beanspruchter Platten in elastischen Bereich," by C. F. Kollbrunner and G. Herrmann, Schweizerische Bauzeitung, vol. 67, May 28, 1949, No. 22.

Using the deflection function Equation [1] of this discussion, the Rayleigh-Ritz method yields a short formula for approximate value of the critical-load factor k_a

$$k_a = \frac{2b^2}{a^2} + \frac{12}{\pi^2}(1 - \nu) \quad [3][11]$$

The simplicity of this formula for k_a, in comparison with the corresponding Equation [32] of the paper where the introduction of auxiliary functions requires almost a printed page, is striking indeed.

In Fig. 1 of this discussion k_a is plotted versus $\pi b/a$, for

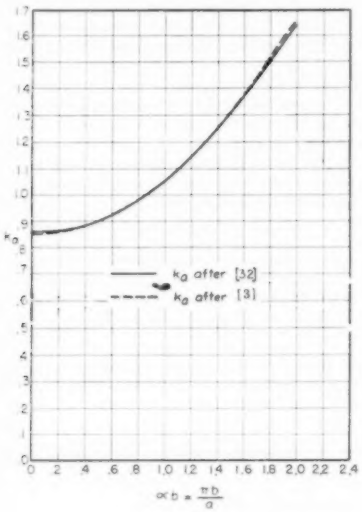

FIG. 1

$\nu = 0.30$, as obtained by Formula [32] of the paper, and taken from Fig. 3 of the paper (full curve), and as obtained by Equation [3], herewith, (dashed curve).

In the range where the exact buckling values have been computed ($0.5 < \pi b/a < 1.5$) the two formulas yield practically the same results. Since the Rayleigh-Ritz method gives always approximate eigenvalues which are too high, the simple formula, Equation [3] of this discussion, gives a better value in the range $0 < \pi b/a < 0.5$ than Equation [32]. In the range $1.5 < \pi b/a < 2.0$, Equation [3] is slightly worse than Equation [32] of the paper. Had an "admissible"[12] deflection function been chosen, involving more adjustable parameters than the single one (c) used in Equation [1] herewith, all the parameters should be determined by minimizing the energy expression, as required by the Rayleigh-Ritz procedure. If some of them would be determined by means of the natural boundary conditions, the resulting eigenvalue obviously would be larger and hence worse.

AUTHOR'S CLOSURE

The author wishes to express his thanks to Professors Bijlaard and Herrmann for their interest in his paper and for their helpful comments. In addition, he adds to these a brief summary of a letter written to the chairman of the session at which the paper was presented at the 1950 ASME Annual Meeting. The letter was from Dr. H. L. Engel of the Hughes Aircraft Company. He pointed out that an error was made in using bar theory when it was assumed that Γ was zero. The correct value of Γ is $^1/_{15}$ b^3t^2 for the entire section, where b is the width of one flange and t is the thickness. With this correction it turns out that for short columns the agreement between bar and plate-theory calculations is very good, that is, within a few per cent.

[11] This is equation [99] in the first item of reference 10.

[12] One satisfying the artificial boundary conditions.

Transverse Vibrations of a Free Circular Plate Carrying Concentrated Mass[1]

J. E. BROCK.[2] It is unfortunate that the author felt impelled to condense his paper to the extent he did. The writer had the opportunity of examining the analysis in an earlier and more extended stage and found the motivation much more evident there. While the first sentence of the section titled "Solution" tells what is done, the second contains either an error or such obscure notation that the reader comes to a full stop. In these two equations a symbol other than ξ should appear on the left side. The situation appears to be this: transforming Equations [4] leads to a differential equation for $W(\xi, s)$. This can be solved by transform methods; transforming with respect to ξ, one is led to examine a function $W(x, s)$ and it is with the inversion of this function to obtain $W(\xi, s)$ that the formulas in question are concerned.

The use of impulse functions $\delta(r)$ seems to be a convenient way of accounting for the concentrated central mass and the fact that the exciting blow is struck at the center. The principal conclusions (natural frequencies and the significant observation that for small mass ratios these depend critically upon mass ratio) are, of course, independent of the fact that an impulsive loading is used.

AUTHOR'S CLOSURE

The difficulties at the beginning of the Solution to which Dr. Brock refers were due to some misprints in the preprint upon which his discussion was based. These misprints have been corrected in the paper as it appears in the JOURNAL. It is still a matter of rather tedious manipulation to proceed from Equation [4] to [5]. The rationale of the procedure was felt to be obvious, but in any case is correctly inferred by Dr. Brock.

On Elastic Continua With Hereditary Characteristics[1]

KARL KLOTTER.[2] The question of damping in materials already has been given considerable thought and has been attacked in various ways. The author in a previous paper[3] takes a new approach to this problem by linking it up in a rational way with the

[1] By R. E. Roberson, published in the September, 1951, issue of the JOURNAL OF APPLIED MECHANICS, Trans. ASME, vol. 73, pp. 280–284.

[2] Director of Research, Midwest Piping and Supply Co., Inc., St. Louis, Mo. Mem. ASME.

[1] By Enrico Volterra, published in the September, 1951, issue of the JOURNAL OF APPLIED MECHANICS, Trans. ASME, vol. 73, pp. 273–279.

[2] Acting Associate Professor of Engineering Mechanics, Stanford University, Stanford, Calif.

[3] "Vibrations of Elastic Systems Having Hereditary Characteristics," by E. Volterra, JOURNAL OF APPLIED MECHANICS, Trans. ASME, vol. 72, 1950, pp. 363–371.

so-called dynamic stress-strain relationship, which he assumes can be expressed as follows

$$\sigma = E\epsilon + \int_0^t \phi(t-\tau)\frac{d\epsilon(\tau)}{d\tau}d\tau \quad [1]$$

Experiments which are mentioned suggest for the "hereditary function" $\phi(t)$ the use of

$$\phi(t) = A_0 + A_1 e^{-\alpha t} \quad [2a]$$

or

$$\phi(t) = A_1 e^{-\alpha_1 t} + A_2 e^{-\alpha_2 t} \quad [2b]$$

generally

$$\phi(t) = \sum_{i=1}^{m} A_i e^{-\alpha_i t} \quad [2]$$

Making use of the first two of these functions ϕ, the author calculated (in the previous paper) the response curves (magnification factor versus frequency ratio) for a vibrating system having a single degree of freedom, that means satisfying the equation of motion

$$M\frac{d^2q(t)}{dt^2} + a^2q(t) + \int_0^t \phi(t-\tau)\dot{q}(\tau)d\tau = 0 \quad [3]$$

The present paper contributes to the solution of the problem in two ways: (*a*) It is shown how one can set up a mechanical analog (with linear dashpots) for a system governed by Equation [3] combined with the Assumption [2]. These results coincide with those by J. M. Burgers.[4] (*b*) The paper deals with continuous systems (systems having an infinite number of degrees of freedom) such as a sphere, a string, a bar, a membrane. The author treats all of these cases rather explicitly, even assuming various boundary conditions. The common feature of all these cases, however, may be summarized quickly as follows: The equation of motion of any such damped system admits a separation of variables

$$q(x, y, z, t) = Q(x, y, x)f(t) \quad [4]$$

thus leading for the space-depending factor Q to exactly the same differential equation which governs the corresponding undamped system, and for the time-depending factor f to a common differential equation, Equation [3], which is that one governing the single-degree-of-freedom system, and which was dealt with in the previous paper.[3]

Thus it is shown that the elaborate results of the previous paper have a meaning also for continuous systems in dealing with the time-depending factor, whereas the purely elastic side of the problem is not affected at all.

The significance of all the results, neat and rational as they are, hinges, of course, on the ease with which the experimental results fit into the Assumptions [1] and [2].

Author's Closure

The author wishes to thank Professor Klotter for his comments. As far as the experimental verification of the results obtained in the paper is concerned, such experimental work is now in progress under the sponsorship of the Office of Naval Research, Washington, D. C.

[4] "First Report on Viscosity and Plasticity," by J. M. Burgers, Academy of Sciences, Amsterdam, Holland, 1935, chapt. 1, p. 22 et seq.

Book Reviews

Advanced Fluid Dynamics and Fluid Machinery

Advanced Fluid Dynamics and Fluid Machinery. By R. C. Binder. Prentice-Hall, Inc., New York, N. Y., 1951. Cloth, 5½ × 8½ in., figs., tables, references, problems, index, x and 426 pp., appendix, $8.

Reviewed by George F. Wislicenus[1] and Hsuan Yeh[2]

As THE application of the science of fluid mechanics in engineering problems in recent years requires more fundamental analysis instead of empirical rules, the engineer working in this field becomes keenly aware that an elementary course in fluid mechanics is often not enough for him to handle his problems. Many problems nowadays require an understanding of the effects due to compressibility or viscosity; and often a two- or three-dimensional flow analysis is necessary. Such topics are only briefly treated, if treated at all, in a first-year course in fluid mechanics. There is a continuous demand, therefore, for a book that will lead the engineer to an understanding of the more advanced topics in fluid mechanics, while at the same time not overburdening him with too much mathematical details and theoretical refinements. Professor Binder has written just such a book.

As in the author's earlier book "Fluid Mechanics," this book covers a surprisingly large number of topics in a volume of its size. At a time of ever-increasing refinements in detail considerations the very concise form of treatment of the author is as refreshing as it is desirable in spite of the fact that one cannot help but wish in some places for greater completeness and rigor. In the hand of a competent teacher the book should prove most valuable and instructive, summing up important facts from a very large field. Ample use is made of physical intuition in developing the essential aspects of a problem. The numerous illustrations skillfully drawn and explained are a valuable feature of this book.

Although the book is titled "Advanced Fluid Mechanics," a considerable portion of the material can be very profitably incorporated in a first-year course on the subject. As a textbook for a graduate course, the book gives adequate coverage on some topics but appears to be somewhat too sketchy in the treatment of others. While there is much to be said for stating important facts in simple and forceful language which Professor Binder so excellently does in both of his books, one wonders if it is not proper, especially in a book of advanced level, to present also the more complex aspects of certain topics. For example, if the topic of radial equilibrium in axial-flow turbomachinery is treated at all then one should hardly avoid the issue of departures

[1] Chairman, Mechanical Engineering Department, The Johns Hopkins University, Baltimore, Md. Mem. ASME.

[2] Mechanical Engineering Department, The Johns Hopkins University, Baltimore, Md.

of the tangential and axial velocities from the irrotational flow pattern.

This book is divided into sixteen chapters. Chapter 1 groups together the basic terminology and equations. The latter includes equations of continuity, momentum, and energy, all expressed in one-dimensional form. Chapter 2 treats steady one-dimensional compressible flow, covering essentially the same ground as given in chapter 12 of the author's earlier book "Fluid Mechanics," but with the addition of a qualitative discussion on the effect of compressibility on lift and drag forces and a brief but lucid introduction to supersonic flow along a wall (Prandtl-Meyer flow). Chapter 3 treats one-dimensional compressible flow with friction and heat transfer. Here again the part dealing with isothermal flow and adiabatic flow with friction is essentially the same as given in chapter 13 of the earlier book. The addition of the general case with both friction and heat transfer makes the topic more complete. Chapter 4 treats boundary layer and turbulence, with strong emphasis on the physical aspect of the problem.

Chapters 5 to 10 deal with fluid machinery. Chapter 5 introduces general features of turbomachinery, such as the energy equation, the velocity diagram, and the various nondimensional parameters used in the analysis of performance. An inaccuracy worth mentioning appears in the proof of the free-vortex type of flow. On page 150 it is stated that if no torque is applied the angular momentum does not change with respect to time, or $\frac{d}{dt}(Rq) = 0$ where q is the velocity and R is the radius. From this one can only conclude that Rq is constant with respect to time. One cannot conclude from this alone, as the book does, that Rq is constant along the radius.

Chapters 6 to 10 treat various kinds of fluid machinery, including axial and centrifugal fans, pumps and compressors, turbines, jet compressors and jet pumps, and fluid couplings and torque converters. Ample illustrations showing contemporary practice should prove to be both valuable and stimulating to the students.

Chapter 11 on unsteady one-dimensional flows is a unique feature of this book, as this subject is seldom covered in a book on fluid mechanics. In connection with the solution of the one-dimensional wave equation, some mathematical tools such as complex numbers and Fourier series are introduced in a nonrigorous but convincing manner.

Chapter 12 develops the classical equation of continuity and momentum. Chapter 13 treats steady two-dimensional incompressible flow. The material covered in these two chapters is very much the same as given in chapter 19 of the author's earlier book. However, with the addition of stream function to the velocity potential and the brief introduction of complex variables, a deeper insight into classical hydrodynamics is achieved than in the earlier book. In chapter 14 on two-dimensional compressible flows, the Prandtl-Glauert and the Kármán-Tsien approximations are explained in a manner that can be readily understood by undergraduate students. Chapter 15 derives the Navier-Stokes equations, but gives no applications after they are derived. It would be more natural if the connection between these equations and the boundary-layer theory of chapter 4 were explained, at least to a limited degree. The last chapter, or chapter 16, presents the fundamentals of vector analysis and the continuity and momentum equation in vector form. Although the subject is ably presented, one doubts if the average student without previous training in vector analysis can understand this material given in the short space of eight pages.

On the whole, Professor Binder's book has achieved the objective as stated in its preface, namely, that of bridging the gap between the first treatment of fluid mechanics and the advanced problems and reference material in current literature.

Thermodynamics of Fluid Flow

THERMODYNAMICS OF FLUID FLOW. By Newman A. Hall. Prentice-Hall, Inc., New York, N. Y., 1951. Cloth, 5½ × 8½ in., x and 278 pp., illus., tables, problems, appendixes, index, $5.50.

REVIEWED BY WALTON FORSTALL, JR.[1]

ANOTHER title for this book might have been "Steady, One-Dimensional Flow of Fluids," for these conditions, stated clearly at the outset, apply throughout. This is an extremely important field for chemical, civil, and mechanical engineers, among others, and it is good to have a book which assembles and organizes the relations pertaining to it from mechanics and thermodynamics.

An introductory chapter sets forth the author's choice of definitions, units, and thermodynamic nomenclature. The second chapter deals with frictional flow of fluids in pipes, as it affects pressure loss, with emphasis on the local action.

Chapters 3 and 4 introduce the fundamental physical principles commonly known as continuity, energy, and momentum. With these tools at hand, specialized cases are treated in the succeeding chapters on incompressible fluids, perfect gases, constant-area adiabatic flow, varying-area adiabatic flow, shock regions, flow measurement and control, and diabatic flow. A final chapter deals with propulsive ducts.

One of the many useful features of this book is the inclusion in the appendix of the tables for Fanno line flow, isentropic flow, Rayleigh line flow, and normal shock which were computed by Shapiro, Hawthorne, and Edelman for the U. S. Navy Department, Bureau of Ordnance, Project Meteor (Meteor Report No. 14, December, 1947). While the tables are, of course, also available in a few other publications, it is certainly convenient to have these important aids to problem solution in the same text that presents the theory.

Each author has his own style in the presentation of thermodynamic argument, so that each new book differs somewhat from earlier ones. If a student should read them all, however, he might be perplexed by the diversity and come to the conclusion that in any one of them the reasoning used in the development of, for example, the general energy equation for steady flow, does not matter so long as the familiar terms come out in their accustomed places.

In this book the kinetic energy and gravity-potential terms are introduced as the result of "kinetic work" and "gravitational work" which are added to displacement work and external work to get total work. The purpose of this approach is probably to avoid the thermodynamic sleight-of-hand that so many books use to go from the first-law system of fixed identity to the control surface for steady flow.

In Professor Hall's presentation of the second law of thermodynamics, entropy changes are divided into "external" and "internal" parts, thus reducing the need to make algebraic statements as inequalities. This concept of the dual nature of entropy change is then employed at various places later in the text to analyze the performance of fluid-flow processes.

A careful distinction is made between incompressible fluids (density unaffected by pressure) and constant-density fluids. Perfect gases are treated with the importance they deserve, but other fluids are dealt with also, and a proper balance of emphasis is preserved.

The principles of continuity, energy, momentum, the second-law requirements, equations of state, and so on, when applied to various flow conditions and to various fluids, inevitably lead to

---

[1] Associate Professor of Mechanical Engineering, Carnegie Institute of Technology, Pittsburgh, Pa. Mem. ASME.

numerous relationships among the properties. Thus the reader will find over five hundred numbered equations in the course of the text, many, of course, being algebraic steps to an end result. More than two hundred of these equations are emphasized by a special mark. As each development proceeds, the author is always careful to explain the restrictions and assumptions which apply. Where needed throughout the text, there are many useful tables and charts embodying recent information.

This important new book should be in the library of every teacher and worker in the field of fluid flow. It is suitable as a text for either a one or two-semester course at the first-year graduate level. For students with a proper background in thermodynamics and elementary fluid mechanics, it could serve as the basis for a valuable course in the senior year. At the end of each chapter there are appropriate problems.

Aircraft Jet Power Plants

AIRCRAFT JET POWERPLANTS. By Franklin P. Durham. Prentice-Hall, Inc., New York, N. Y., 1951. Cloth, 5½ × 8½ in., ix and 326 pp., illus., problems, tables, chart, index, $5.

REVIEWED BY V. V. SCHLOESSER[4]

AS STATED by the author, this book is intended primarily as a text for junior and senior undergraduate courses in jet power plants. It seems well suited for this purpose. A generous number of photographs, illustrations, and sample problems are included which aids in giving purpose to the underlying principles and theories presented. The need for understanding the basic theory presented is emphasized to the student by showing its application throughout the book.

An introductory chapter provides general engine descriptions and points out the approximate applicational spectrum for the turbojet, turboprop, ramjet, and rocket. The next five chapters are devoted to basic thermodynamics, turbojet and turboprop thermodynamic processes, and application of Newton's third law to define thrust and drag. The concept of dimensional analysis is employed to derive useful gas-turbine performance parameters. This material on basic fundamentals is presented in a clear and interesting fashion.

Chapters seven through eleven deal with the principal gas-turbine components; inlet diffuser, compressor, combustion chamber, turbine, and jet nozzle. Elementary fluid-flow considerations applicable to inlet diffuser and duct performance are presented. A good discussion of elementary compressor, both axial and centrifugal, and turbine fluid-flow principles is given. Velocity triangles for various-stage types are analyzed. The chapter on flow in nozzles develops basic nozzle-flow relationships covering both converging and converging-diverging nozzles.

Chapter twelve treats fundamentals of ramjets. Equations of flow through oblique and normal shocks are developed. The supersonic inlet diffuser and the over-all ramjet-engine thermodynamic process are analyzed.

The last chapter of the book gives a brief description of the rocket power plant and presents elementary rocket-propulsion principles.

It is this reviewer's opinion that the book combines a good balance between fundamental theory and aircraft jet power-plant descriptive material. It is recommended as a text for junior and for senior undergraduate courses in aircraft jet power plants.

[4] Section Engineer, Preliminary Design Section, Aviation Gas Turbine Engineering, Westinghouse Electric Corporation, Lester Branch P. O., Philadelphia, Pa.

Fluid and Particle Mechanics

FLUID AND PARTICLE MECHANICS. By C. E. Lapple (with the assistance of G. E. Alves, O. P. Bergelin, D. F. Boucher, H. L. Bunker, M. G. Kershaw, M. S. Maleson, and R. D. Morse). (Based on a graduate chemical-engineering course given at the University of Delaware.) University of Delaware, Newark, Del., 1951. Paper, 8½ × 11 in., references, 182 figs., tables, v and 353 pp., $6.

REVIEWED BY H. L. LANGHAAR[5]

THE name "particle mechanics" in the title of this publication refers to particles that are suspended or immersed in fluids. The authors have undertaken to compile classroom notes and published articles on fluid mechanics that will serve both academic and industrial needs of chemical engineers.

The first four chapters deal with standard material—the energy equation, the momentum principle, the mixing-length theory of turbulence, boundary layers, turbulent flow in pipes, head losses in pipes, and one-dimensional compressible flow. There are five chapters treating the design and performance of ejectors and pumps, the design of pipe lines, valves, and fittings, the design of ventilating systems, and the use of flow metering devices. There is a chapter on two-phase flow in pipes and a chapter on topics in rheology. The last four chapters deal principally with the technology of measurement of sizes and distributions of solid particles in fluids, rates of settling of particles, methods for collecting mist and dust, and rising flow through granular beds.

The work will be valuable to engineers who encounter certain types of flow problems. However, it is, in some respects, a handbook rather than a textbook. The concepts, assumptions, and analysis that are the vital parts of hydrodynamics and gas dynamics have been subordinated to the practical objectives of the work. Consequently, the reader requires a background in some phases of theoretical fluid mechanics.

Elasticity

THEORY OF ELASTICITY. By S. Timoshenko and J. N. Goodier. Second edition. Engineering Societies Monographs. McGraw-Hill Book Company, Inc., New York, N. Y., 1951. Cloth, 6 × 9 in., xviii and 506 pp., illus., problems, appendix, author and subject indexes, $9.50.

REVIEWED BY D. L. HOLL[6]

THIS revised edition enlarges the original edition of 1934 by the senior author from 416 pages to 506 pages, adds 90 new problems, increases the numbered chapters from 12 to 15, and concludes with an appendix on finite-difference methods. The notation remains unchanged. Some 125 references which are new since 1934 are cited.

The general arrangement of this new edition is similar to the original; nevertheless the revision reflects the many developments which have occurred since the publication of the first edition. Major changes have been made by according the treatment of photoelasticity a new and separate chapter in which a brief account of the frozen stress method for three-dimensional stress is made. The chapter on the use of complex variables set up in fine print (may be omitted on first reading) in the first edition is replaced by a new one stressing general orthogonal-plane co-ordinate systems and the function theoretic methods. Plane-stress problems involving elliptical, circular, and hyperbolic notches are treated and emphasis is given to those regions of high stress concentration. A new chapter on thermal stresses has been added. Stress distributions are determined in plane

[5] Professor, Theoretical and Applied Mechanics Department, University of Illinois, Urbana, Ill. Mem. ASME.

[6] Head, Department of Mathematics, Iowa State College, Ames Iowa.

disks, long cylinders, and spheres when variable temperatures are present. New sections have been added to cover topics on plane strain and rotation components, strain-gage rosettes and their graphical reduction, shear lag in box beams, the reciprocal theorem of Betti, shear center and center of twist, and the approximate character of plane-stress solutions. The appendix gives a satisfactory introduction to the method of finite differences and the application of the relaxation method of solving them. Rectangular, triangular, and hexagonal nets are considered and block or group relaxations illustrated. Examples include torsion of the square section, hollow square section, equilateral-triangle section, and circular shafts of variable diameter.

In making such a general revision, the authors made no changes in the notation, retaining the stress notations (σ_x, σ_y, σ_z, τ_{xy}, τ_{yz}, τ_{zx}) for stresses in rectangular co-ordinates and (ϵ_x, ϵ_y, ϵ_z, γ_{xy}, γ_{yz}, γ_{zx}) for strains, and ν for Poisson's ratio. Why should they avoid the tensor notation τ_{ij} and e_{ij}? The factor 2 prevents one from writing the composite form of the laws of stress and strain transformation, and also the compatibility conditions. One may also inquire whether the general three-dimensional theory should be postponed until chapter 8 on page 213. This might imply that to the average student reader, strain-energy methods, photoelastic methods, and all plane-stress problems including the heavier methods of general curvilinear co-ordinates are more important in his case than the three-dimensional theory. It is the reviewer's opinion that if only a one-semester course is available to the engineering graduate student he should have some knowledge of the three-dimensional analysis. No mention is made of finite strain theory where one includes quadratic terms in space derivatives of the displacement vector.

The format of the text is commendable. There are many figures to assist the reader. The selected problems are a challenge to the student. The authors are to be complimented in their revision.

Theory of Perfectly Plastic Solids

THEORY OF PERFECTLY PLASTIC SOLIDS. By William Prager and Philip G. Hodge, Jr. John Wiley & Sons, Inc., New York, N. Y.; Chapman and Hall, Ltd., London, England, 1951. Cloth, 6 × 9½ in., 90 figs., x and 264 pp., references, problems, author, and subject index, $5.50.

REVIEWED BY C. W. MACGREGOR[7]

THIS book forms one of the Wiley Applied Mathematics Series under the editorship of I. S. Sokolnikoff. It deals exclusively with ideally plastic materials which exhibit no strain hardening, and for this reason many engineers may feel that its application to practical engineering problems is distinctly limited. The utility, however, of solutions based upon ideally plastic conditions with no strain hardening has often been unduly minimized, since they frequently throw considerable light on the general flow problem and in certain instances, such as in limit-design of structural members, provide results of definite pragmatic value. As the authors have stated, this branch of the subject has most nearly taken definitive form.

Topics include a brief introduction to the geometrics of stress and strain, yield conditions, the Prandtl-Reuss and the Mises stress-strain rate relations, simple trusses and beams, elastic and plastic torsion, plane-strain solutions of the thick-walled tube under internal pressure, an extended discussion of shear lines, problems of incipient plastic flow in frictionless extrusion and indentation, limit analysis in plain strain with a discussion of specific problems such as notched bars in tension and hollow square prisms under internal pressure, Cartesian tensors and extremum principles for the Mises and Prandtl-Reuss theories. At the end of each chapter a collection of suggested problems is included together with a bibliography for further study.

In general, the book is well-written, lucid, and shows evidence of much thought having been given to the organization of subject matter. It will be a welcome addition to the rapidly growing number of books in the field of plasticity. Certain features will be criticized by engineers. For a book of its size, perhaps undue attention has been focused upon mathematical proofs and theorems to the exclusion of concrete problems. The powerful, simple, and useful stress-strain relations of Hencky have been ignored entirely save for two suggested problems at the end of chapters 1 and 3. The bibliographies appear to be somewhat incomplete and in the text too much is often left to the reader to fill in. On the other hand, this book contains one of the best discussions of limit analysis which has come to the reviewer's attention.

[7] Professor of Applied Mechanics, Head of Materials Division, Massachusetts Institute of Technology, Cambridge, Mass. Mem. ASME.

Metals

THE STRUCTURE AND MECHANICAL PROPERTIES OF METALS. By Bruce Chalmers. A Series of Monographs on Metallic Materials published under the authority of The Royal Aeronautical Society. Volume 2. John Wiley & Sons, Inc., New York, N. Y., 1951. Cloth, 5½ × 8½ in., ix and 131 pp., 89 figs., $3.50.

REVIEWED BY E. OROWAN[8]

THE chapter titles are: (1) The Structure of Pure Metals. (2) The Structure of Alloys. (3) The Effect of Distortion on Structure. (4) The Effect of Heat Treatment on Structure. (5) The Determination of Structure. (6) The Mechanical Properties and Their Dependence on Structure.

The field covered by this book is the same as that treated in Boas' "Physics of Metals and Alloys"; the type of the reader to which it is addressed, however, is entirely different. The author writes in the preface: "The object of this monograph is to provide the simplest possible picture of the structure of metals and alloys and its relations to the mechanical properties. In avoiding any resort to mathematical considerations, the author has necessarily glossed over many of the finer points and has had to be content with a rather superficial approach to some aspects of the subject. The result of this has, perhaps, been oversimplification, which will be recognized by the serious student of the physics of metals; he may even recognize inaccuracies that have resulted from the effort to avoid unnecessary complexity. No apology is made for such inadequacies, as the reader who is conscious of them is not the reader to whom the book is offered."

That the book cannot lead the reader to a thorough understanding of the phenomena described is obvious from the fact that the material treated in its 123 text pages would require at least 400 or 500 pages in order to be explained in a manner that would satisfy the student or the interested layman. It will be, however, an excellent source of information for those professionals, executives, and businessmen who want to obtain some general orientation in this field but have neither the time and interest nor the fundamental training necessary for a study that leads to a real understanding. For these the book is a rich storehouse of information, much of it up to the minute. There are some signs that it was written in a hurry; these will no doubt disappear in the next edition. On page 1, e.g., the electric charge of the proton is given as 4.7×10^{-10} esu instead of 4.8×10^{-10} esu; its mass as 1.6×10^{-24} gram, instead of 1.67×10^{-24}

[8] George Westinghouse Professor of Mechanical Engineering, Massachusetts Institute of Technology, Cambridge, Mass.

$\approx 1.7 \times 10^{-24}$ gram; the conventional symbols for atomic number and relative atomic mass are given as N and Z, instead of Z and A, respectively. On page 17 dendritic crystallization is said to occur when the temperature gradient in the melt is small, and to be "due to the fact that it is easier for atoms to freeze on to some types of planes of atoms on the crystals than on others." Some of the figures, e.g., fig. 39 and fig. 83, show similar shortcomings.

Steam Turbines

STEAM TURBINES AND THEIR CYCLES. By J. Kenneth Salisbury. John Wiley and Sons, Inc., New York, N. Y., Chapman and Hall, Ltd., London, England, 1950. Cloth, 5¾ × 9 in., illus., figs., tables, exercises, appendix, bibliography, index, xvi and 645 pp., $9.

REVIEWED BY ADOLF EGLI[9]

THIS book is unique among works on steam turbines inasmuch as it gives a thorough, complete, and up-to-date exposition of the regenerative or feedwater-heating power cycle. In this respect it fills a long existing gap in power-plant literature. In the reviewer's opinion it is unfortunate that this particular feature of the book is not better emphasized in the title.

Salisbury's book belongs into the working library of every power-plant engineer, turbine designer, and steam-application engineer.

The text is organized in four parts. Part one, approximately 250 pages, entitled "Fundamentals of Turbine Design," covers the fundamentals of steam flow through turbines with emphasis on the characteristic properties needed in cycle analysis. The author here is attempting to explain fundamental thermodynamic concepts in elementary language. One might argue about the value of a philosophically rigid presentation of thermodynamics to practicing power-plant engineers and accept a "practical" treatment avoiding formal mathematics. A little more liberal use of clean-cut mathematical equations, however, would have made the explanation of some of the turbine characteristics less cumbersome and the text would be easier to use as a reference in practical work.

Parts two, "The Regenerative Cycle," 90 pages, and three, "Cycle Analysis," 200 pages, are those which make the book outstandingly valuable to the power-plant engineer. Here the modern regenerative steam-power cycle is analysed in detail. After explaining the conventional method of heat-balance calculation, the author presents a useful short-cut method which allows a rapid evaluation of feed-heating cycles. The method is based on the concept of an "ideal" cycle containing an infinite number of heaters, each with zero terminal temperature difference and no pressure losses, which heat the feedwater to the saturation enthalpy corresponding to the turbine throttle pressure. Performance curves are given of the ideal cycle for all steam conditions of practical interest. The correction to be applied to the theoretical performance values to obtain the performance of the actual cycle is rationally analyzed, taking into account the individual effects of the finite number of heaters, heater spacing, extraction-line pressure drops, terminal temperature differences, types of heaters, heater arrangement, turbine exhaust loss. Of particular value in the author's calculation method is the fact that the relatively small, but economically important, over-all effect from a change in a single-cycle component can be determined directly and accurately while in the conventional heat balance this effect must be found with great labor and as the difference of two large quantities.

Separately analyzed are the effects of evaporation make-up generator coolers in the condensate circuit, introduction of external steam and water, boiler feed-pump power, liquid compression. The reader will greatly welcome the many well-presented numerical examples demonstrating the application of the calculation methods to the most widely used cycle arrangements.

Part four, "Application Engineering," 60 pages, gives a brief description of the construction details of modern steam turbines, illustrated by photographs and cross sections, all of designs by the General Electric Company. Of considerable value is a set of curves on steam rates and heat rates of medium size to large size, 500 to 100,000 kw, central-station turbines and industrial turbines. While all these data refer specifically to turbines of General Electric design they are representative of modern practice.

There is an appendix containing an abridged reproduction of the "Theoretical Steam Rate Tables," by Keenan and Keyes; a reproduction of selected portions of the large Mollier steam chart of the ASME; an abridged reproduction of the Keenan-Keyes Steam Tables, 1936, of the properties of superheated and saturated steam.

The reviewer feels obliged to call particular attention to some 115 curves and 25 tables, besides those of the appendix, containing an enormous amount of useful data which to produce required thousands of man-hours of work and the background of an expert's lifetime of practical experience in the steam-power field.

Physics of Lubrication

PHYSICS OF LUBRICATION. British Journal of Applied Physics. Supplement No. 1. The Institute of Physics, London, England, 1951. Cardboard, 8 × 10¾ in., viii and 96 pp., illus., 15s.

REVIEWED BY L. M. TICHVINSKY[10]

THIS book contains papers with discussions which were presented at a symposium held jointly by the British Rheologists' Club and the Manchester and District Branch of the Institute of Physics in Manchester from June 29 to July 1, 1950.

The book consists of two parts and is arranged as follows: four papers are in the first group, "Hydrodynamic Lubrication and the Rheology of Lubricants," and fourteen papers are in the second group, "Boundary Layer and Extreme Pressure Lubrication." The first part begins with a short survey of the hydrodynamic lubrication followed by the rheology of lubricant films, viscosity of lubricating oils at high rates of shear, and lubircation of textiles. Of particular interest is the article pertaining to the decrease of the viscosity at rates of shear up to 4×10^6 units per second.

An article on boundary and extreme-pressure lubrication serves as an introduction to the second part of the booklet. Some of the titles of articles presented below indicate the scope and general content of that part of the symposium. Boundary layer, scuffing temperatures of boundary lubricant films, lubrication with materials in the solid state, with metallic soaps, and with long-chain organic compounds, study of boundary lubrication by means of electron diffraction and electrostatic component of the force of friction. Of particular interest are the two articles in which adsorption and surface damage are investigated with the aid of radioactive tracers and radioactive metals. There is also an article on the spreading behavior and lubricating properties of mixed liquids. The closing paper of this part is an article on the effect of lubrication on friction, wear, and abrasion.

The booklet is well illustrated by numerous photographs, sketches, and graphs. It undoubtedly will be of great interest to those engaged in theoretical and practical problems of lubrication.

[9] Professor of Mechanical Engineering, Towne Scientific School, University of Pennsylvania, Philadelphia, Pa. Mem. ASME.

[10] Professor of Mechanical Engineering, University of California, Berkeley, Calif. Mem. ASME.